Universidade de Aveiro
2022

NEHA CHAUDHARY

SISTEMAS DE POSICIONAMENTO BASEADOS EM COMUNICAÇÃO POR LUZ PARA AMBIENTES INTERIORES

VISIBLE LIGHT COMMUNICATION BASED INDOOR LOCALIZATION

Universidade de Aveiro
2022

NEHA CHAUDHARY

SISTEMAS DE POSICIONAMENTO BASEADOS EM COMUNICAÇÃO POR LUZ PARA AMBIENTES INTERIORES

Tese apresentada à Universidade de Aveiro para cumprimento dos requisitos necessários à obtenção do grau de Doutor em Engenharia Eletrotécnica, realizada sob a orientação científica do Doutor Luis Nero Alves, Professor (Professor auxiliar) do Departamento de Eletrónica, Telecomunicações e Informática da Universidade de Aveiro e sob a co-orientação do Professor Zabih Ghassemlooy, Professor do Departamento de Matemática, Física, e Engenharia Elétrica da Universidade de Northumbria.

VISIBLE LIGHT COMMUNICATION BASED INDOOR LOCALIZATION

Thesis presented to the University of Aveiro to fulfil the necessary requirement to obtain the degree of Doctor of Philosophy in Electro-technical Engineering, conducted under the scientific guidance of Dr. Luis Nero Alves, Professor (Assistant Professor) of the Department of Electronics, Telecommunications and Informatics of the University of Aveiro and under the co-guidance of Prof. Zabih Ghassemlooy, Professor at Department of Mathematics, Physics, and Electrical Engineering at Northumbria University, UK.

Apoio financeiro dos projectos — Projeto financiado pelo Acordo de Subvenção nº. H2020-MSCA-ITN-2016-764461 com a União Europeia

This Thesis is dedicated to my parents and grandparents: Mrs. Nirmala Devi, Mr. Harmesh Lal, Mrs. Krishna Devi, and Mr. Amar Singh.

o júri

Presidente

Doutor Tito da Silva Trindade
Professor Catedrático da Universidade de Aveiro

Vogais

Doutor Nobby Stevens
Professor Associado, Ku Leuven

Doutor Mohammad-Ali Khalighi
Professor Associado, École Centrale de Marseille

Doutora Pétia Georgieva Georgieva
Professora Associada, Universidade de Aveiro

Doutor Luis Filipe Mesquita Nero Moreira Alves (Orientador)
Professor Auxiliar, Universidade de Aveiro

Doutora Anna Maria Vegni
Professora Auxiliar, Roma Tre University

Acknowledgement

Firstly, I would like to express my sincere thanks to my supervisor Dr. Luis Nero Alves, who supported and guided me during my studies and gave me the opportunity to be a part of a great team of people. Without his unlimited support, this work would not have been accomplished on time. My sincere gratitude goes to my co-supervisor Prof. Zabih Ghassemlooy for the excellent supervision, guidance and the invaluable time invested into my work, which made this work possible.

I would like to thank Prof. Rafael Perez-Jimenez for the opportunity at Universidad de Las Palmas de Gran Canaria and for his support and inputs to my research activities. I also extend my thanks to Prof. Stanislav Zvanovec, Dr. Pedro Fonseca, Dr. Hoa Le-Minh, Prof. Ali Khalighi, Prof. Murat Usyal, for their consistent guidance throughout my PhD programme.

I would like to express my appreciation to my colleagues from circuits and system integration lab, Luis Rodrigues, Miguel Rego, Shusmitha Kyatam, Latifah Almaghrabi, Patricia Martins, Joao Pandeirada, and Miguel Soares for their innovative discussions and feedback. They gave me so much help both in research and everyday life in Portugal. Thank you, Celso Pereira and Pedro Rodrigues for your help in developing the testbed for VLP. I also want to thank the colleagues from Las Palmas, Behnaz Majlesein, Cristo Jurado, Edmundo Torrez, Vicente Matus, Victor Alonso and Dr. Victor Guerra and for helping me out.

I would like to thank OCRG group including, Othman Younus, Zun Htay, and Nithin Mohan for their collaboration and hard time during pandemic. This period has taught us that working from home has many advantages, but also it was incredibly lonely. I am therefore very grateful that I had the opportunity to work together with such wonderful colleagues. We had many stimulating discussions during office hours and shared many good times outside of office hours as well.

I am indeed very grateful to the European Union H2020, under the Marie Sklodowska Curie Actions for sponsoring my PhD programme through the Visible light-based Interoperability and Networking (VISION) project, which was a joint doctoral and innovative training programme.

I am also grateful to my dearest friends Neha Gupta, Raja Dharmateja, Deepak Kumar, Bharat Surisetti, and Uday Kukadiya for the motivation and fun filled conversations. They brought me so much happiness in the past years and encouraged a lot throughout my journey. I am grateful to my brother, Dr. Sushank Chaudhary and sister-in-Law, Dr. Dipima Buragohain for their unconditional support in this journey. Finally, special thanks go to my parents, Mrs. Nirmala Devi and Mr. Harmesh Lal for their never-ending support and patience. To all those who have contributed in one way or the other, whose names are not mentioned here, you are very much important. Thanks for all your immeasurable contributions and advice.

palavras-chave

Comunicações por luz visível, posicionamento por luz visível, sistemas de localização em ambientes interiores, redes neuronais artificiais, aprendizagem automática, reflexões multipercurso

Resumo

A procura por sistemas de posicionamento interior (IPSs) de alta precisão tem crescido rapidamente devido ao seu interesse nas técnicas cada vez mais populares da Internet das Coisas, dispositivos móveis inteligentes e inteligência artificial. O IPS tornou-se um domínio de pesquisa promissor que tem atraído grande atenção devido aos seus benefícios em vários cenários de trabalho, como indústrias, locais públicos e navegação autónoma. Além disso, o IPS tem uma contribuição destacada no dia a dia de organizações, como, centros de saúde, aeroportos, supermercados, fábricas, locais subterrâneos, etc. As tecnologias baseadas em radiofrequência (RF) e comunicação óptica sem fio (OWC) podem ser adotadas para localização em ambientes interiores. Embora o sistema de posicionamento global (GPS) baseado em RF ofereça taxas de penetração mais altas com precisão reduzida (ou seja, na faixa de alguns metros), não funciona bem em ambientes interiores (e não funciona bem em certos casos como túneis, minas, etc.) devido ao sinal muito fraco e falta de acesso direto aos satélites. Por outro lado, o sistema baseado em luz conhecido como sistema de posicionamento de luz visível (VLP), como parte dos sistemas OWC, usa a infraestrutura de iluminação baseada em díodos emissores de luz (LEDs) pré-existentes, é um sistemas de baixo custo e alta precisão quando comprado com os sistemas baseados em RF. O VLP é uma tecnologia emergente que promete alta precisão, alta segurança, baixo custo de implantação, menor tempo de resposta e baixa complexidade relativa quando comparado ao posicionamento baseado em RF.

No entanto, os sistemas VLP interiores, exibem algumas limitações, como, a reflexão multicaminho, inclinação do transmissor, posição do transmissor e incerteza de orientação, sombra/bloqueio humano e ruído, que têm como consequência o aumento do erro de posicionamento, e consequente redução da precisão do sistema. Portanto, é imperativo estudar as características dos diferentes canais VLP e modelá-los adequadamente para o duplo propósito de iluminação e localização. Esta tesa aborda, primeiramente, o impacto dos ângulos de inclinação do transmissor e reflexões multipercurso no desempenho do sistema de posicionamento. Demonstra-se que a inclinação do transmissor pode ser benéfica em sistemas VLP considerando tanto a linha de vista (LOS) como as reflexões. Com os transmissores orientados para o centro do plano recetor, o nível de potência recebido é maximizado devido aos componentes LOS. Também é mostrado que o esquema proposto oferece uma melhoria significativa de precisão de até ~66% em comparação com um sistema VLP de transmissor não inclinado típico. O efeito da inclinação do transmissor na uniformidade da iluminação também é investigado e os resultados comprovam que a uniformidade alcançada está de acordo com a Norma Europeia EN 12464-1.

O impacto da posição do transmissor e incerteza de orientação na precisão do sistema VLP com base na intensidade do sinal recebido (RSS) foi também

investigado. Os resultados da simulação mostram que as incertezas do transmissor têm um impacto severo no erro de posicionamento, que pode ser atenuado com o uso de mais transmissores. Para incertezas de posicionamento dos transmissores menores que 5 cm, os erros médios de posicionamento são 23.3, 15.1 e 13.2 cm para conjuntos de 4, 9 e 16 transmissores, respetivamente. Enquanto que, para a incerteza de orientação de um transmissor menor de 5°, os erros médios de posicionamento são 31.9, 20.6 e 17 cm para conjuntos de 4, 9 e 16 transmissores, respetivamente.

O trabalho da tese abordou a investigação dos aspetos de projeto de um sistema VLP indoor no qual uma rede neuronal artificial (ANN) é utilizada para estimativa de posicionamento considerando um canal multipercurso. O estudo considerou a influência do ruído como indicador de desempenho para a comparação entre diferentes abordagens de projeto. Três algoritmos de treino de ANNs diferentes foram considerados, a saber, Levenberg-Marquardt, regularização Bayesiana e algoritmos de gradiente conjugado escalonado, para minimizar o erro de posicionamento no sistema VLP. O projeto da ANN foi otimizado com base no número de neurónios nas camadas ocultas, no número de épocas de treino e no tamanho do conjunto de treino. Mostrou-se que, a ANN com regularização Bayesiana superou a técnica RSS tradicional usando a estimação não linear dos mínimos quadrados para todos os valores da relação sinal-ruído.

Foi proposto um novo sistema VLP indoor baseado em máquinas de vetores de suporte (SVM) e regressão polinomial considerando dois ambientes interiores diferentes: uma sala vazia e uma sala mobiliada. Os resultados mostraram que, numa sala vazia, a melhoria da precisão de posicionamento para o erro de posicionamento de 2.5 cm são 36.1, 58.3 e 72.2% para três cenários diferentes de acordo com a distribuição das regiões na sala. Para a sala mobiliada, uma melhoria de precisão relativa de posicionamento de 214, 170 e 100% é observada para erro de posicionamento de 0.1, 0.2 e 0.3 m, respetivamente.

Finalmente, foi proposto um sistema VLP indoor baseado em redes neurais convolucionais (CNN). O sistema foi demonstrado experimentalmente usando luminárias LED como transmissores e uma camara com obturador rotativo como recetor. O algoritmo de detecção usou um detector de disparo único (SSD) baseado numa CNN pré configurada (ou seja, MobileNet ou ResNet) para classificação. O sistema foi validado usando uma configuração de teste de tamanho real contendo oito luminárias LED. Os resultados obtidos mostraram que o erro de posicionamento quadrático médio alcançado é de 4.67 e 5.27 cm com os modelos SSD MobileNet e SSD ResNet, respetivamente. Os resultados da validação mostram que o sistema pode processar 67 imagens por segundo, permitindo o posicionamento em tempo real.

keywords

Visible light communication, visible light positioning, indoor localisation, artificial neural networks, machine learning, multipath reflections.

abstract

The demand for highly precise indoor positioning systems (IPSs) is growing rapidly due to its potential in the increasingly popular techniques of the Internet of Things, smart mobile devices, and artificial intelligence. IPS becomes a promising research domain that is getting wide attention due to its benefits in several working scenarios, such as, industries, indoor public locations, and autonomous navigation. Moreover, IPS has a prominent contribution in day-to-day activities in organizations such as health care centers, airports, shopping malls, manufacturing, underground locations, etc., for safe operating environments. In indoor environments, both radio frequency (RF) and optical wireless communication (OWC) based technologies could be adopted for localization. Although the RF-based global positioning system, such as, Global positioning system offers higher penetration rates with reduced accuracy (i.e., in the range of a few meters), it does not work well in indoor environments (and not at all in certain cases such as tunnels, mines, etc.) due to the very weak signal and no direct access to the satellites. On the other hand, the light-based system known as a visible light positioning (VLP) system, as part of the OWC systems, uses the pre-existing light-emitting diodes (LEDs)-based lighting infrastructure, could be used at low cost and high accuracy compared with the RF-based systems. VLP is an emerging technology promising high accuracy, high security, low deployment cost, shorter time response, and low relative complexity when compared with RF-based positioning.

However, in indoor VLP systems, there are some concerns such as, multipath reflection, transmitter tilting, transmitter's position, and orientation uncertainty, human shadowing/blocking, and noise causing the increase in the positioning error, thereby reducing the positioning accuracy of the system. Therefore, it is imperative to capture the characteristics of different VLP channel and properly model them for the dual purpose of illumination and localization. In this thesis, firstly, the impact of transmitter tilting angles and multipath reflections are studied and for the first time, it is demonstrated that tilting the transmitter can be beneficial in VLP systems considering both line of sight (LOS) and non-line of sight transmission paths. With the transmitters oriented towards the center of the receiving plane, the received power level is maximized due to the LOS components. It is also shown that the proposed scheme offers a significant accuracy improvement of up to ~66% compared with a typical non-tilted transmitter VLP. The effect of tilting the transmitter on the lighting uniformity is also investigated and results proved that the uniformity achieved complies with the European Standard EN 12464-1.

After that, the impact of transmitter position and orientation uncertainty on the accuracy of the VLP system based on the received signal strength (RSS) is investigated. Simulation results show that the transmitter uncertainties have a severe impact on the positioning error, which can be leveraged through the usage of more transmitters. Concerning a smaller transmitter's position

uncertainty of 5 cm, the average positioning errors are 23.3, 15.1, and 13.2 cm for 4-, 9-, and 16- transmitter cases, respectively. While for a smaller transmitter' orientation uncertainty of 5°, the average positioning errors are 31.9, 20.6, and 17 cm for 4-, 9-, and 16- transmitter cases, respectively. Next, an investigation of the design aspects of an indoor VLP system is performed in which an artificial neural network (ANN) is used for positioning estimation by considering a multipath channel. The study considers the influence of noise as a performance indicator for the comparison between different design approaches. Three different ANN algorithms are considered, namely, Levenberg-Marquardt, Bayesian regularization, and scaled conjugate gradient algorithms, to minimize the positioning error in the VLP system. The ANN design is optimized based on the number of neurons in the hidden layers, the number of training epochs, and the size of the training set. It is shown that, the ANN with Bayesian regularization outperforms the traditional RSS technique using the non-linear least square estimation for all values of signal to noise ratio.

Furthermore, a novel indoor VLP system is proposed based on support vector machines and polynomial regression considering two different multipath environments of an empty room and a furnished room. The results show that, in an empty room, the positioning accuracy improvement for the positioning error of 2.5 cm are 36.1, 58.3, and 72.2 % for three different scenarios according to the regions' distribution in the room. For the furnished room, a positioning relative accuracy improvement of 214, 170, and 100 % is observed for positioning error of 0.1, 0.2, and 0.3 m, respectively. Ultimately, an indoor VLP system based on convolutional neural networks (CNN) is proposed and demonstrated experimentally in which LEDs are used as transmitters and a rolling shutter camera is used as receiver. A detection algorithm named single shot detector (SSD) is used which relies on CNN (i.e., MobileNet or ResNet) for classification as well as position estimation of each LED in the image. The system is validated using a real-world size test setup containing eight LED luminaries. The obtained results show that the maximum average root mean square positioning error achieved is 4.67 and 5.27 cm with SSD MobileNet and SSD ResNet models, respectively. The validation results show that the system can process 67 images per second, allowing real-time positioning.

Table of Contents

List of Figures

Glossary of Abbreviations

ANN	Artificial neural network
AOA	Angle of arrival
BR	Bayesian regularization
CCD	Charge coupled devices
CCS	Camera coordinate system
CDF	Cumulative distribution function
CMOS	Complementary metal oxide semiconductors
CNN	Convolutional neural networks
CRLB	Cramer rao lower bound
DPDOA	Differential pdoa
FLCs	Fuzzy logic controllers
FOV	Field of view
FSK	Frequency shift keying
GPS	Global positioning system
GS	Global shutter
HLs	Hidden layers
HPA	Half-power angle
ICS	Image coordinate system
ID	Identification
IMU	Inertial measurement unit
IoU	Intersection over Union
IPSs	Indoor positioning systems
ISs	Image sensors
LEDs	Light emitting diodes
LLS	Linear least square
LM	Levenberg-marquardt
LOS	Line of sight
MIMO	Multi-input, multi-output
MSE	Mean square error
NLLS	Non-linear least square
NLOS	Non-line of sight
OCC	Optical camera communication
PASS	Particle-assisted stochastic search
PDOA	Phase difference of arrival
PDs	Photodetectors
PnP	Perspective-n-point
R-CNNs	Region-based CNNs
RF	Radio-frequency
RFID	Radio frequency identification
RMS	Root-mean-square
RS	Rolling shutter
RSS	Received signal strength
SCG	Scaled conjugate gradient
SNR	Signal to noise ratio
SPAO	Simultaneous positioning and orientation
SSD	Single shot detector

SVM	Support vector machines
TDOA	Time difference of arrival
TOA	Time of arrival
UWB	Ultra-wideband
VLC	Visible light communication
VLP	Visible light positioning
WCS	World coordinate system

Glossary of Symbols

$(x_k, y_{k)}$	The position of k^{th} transmitter
(u, v)	2D positions in image coordinates
J_i	Jacobian matrix
$(f_x\ ,\ f_y)$	Focal lengths in pixels
(x_r, y_r)	The position of the receiver
$\bar{p}_1, \bar{p}_2, \ldots . \bar{p}_i$	The set of non-zero weight vectors
$\bar{s}_i$	Second-order information
Δ_i	Comparison parameter
A_{ref}	Reflectance area
A_r	Area of the photodetector
$D_{k,k+1}$	The difference between the ranges r_{k+1} and r_k
E_D	Squared error
E_W	Sum of squared weights
$E'_{qw}(p_i)$	Quadratic approximation of the error function, $F(p_i)$
$\hat{F}(p_i^m)$	Least mean square error function
L_{conf}	Confidence loss
L_i	Lagrange multiplier
L_{loc}	Localization loss
N_P	The number of positive matches
N_c	Number of classifiers
N_{wb}	Total number of parameters (weights and biases) of the network
$N_x\ ,\ N_y$	The total number of pixels in both axes
$P_{R,k}$	Total received power from the k^{th} transmitter
$P_{r,k(\text{LOS})}$	Received power from the k^{th} transmitter due to the path loss
$P_{r,k(\text{NLOS})}$	Received power from k^{h} transmitter due to NLOS path
$P_{t,k}$	Transmitted power from the k^{th} transmitter
$\tilde{Q}$	Cost function
W_{in}^m	Weight
$a_0 \ldots a_j$	Coefficients of the polynomial model for the j^{Th} Order polynomial
a_{ratio}	Aspect ratio
a_i	The network output for the i^{th} neuron
c_x	Principal point in x direction
c_y	Principal point in y direction
$d_{k,w}$	The distance between the k^{h} transmitter and the reflective area
d_k	Distance between the k^{th} transmitter and the receiver
$d_{w,r}$	The distance between the reflective area and the receiver
e_i	Error matrix
p_i	The vector containing all the network weights and biases for the i^{th} neuron, i.e., $p_i = [W_i, b_i]$
r_k	The horizontal distance from the transmitter to the receiver
t_i	The target output of the network for the i^{th} neuron
u_j	A point in the sample
x_{ij}^p	An indicator for matching the i^{th} default box to the j^{th} ground box of the category p
α_k	AOA measurement with respect to the k^{th} transmitter
γ_e	Effective number of parameters
θ_x	Euler angle in x direction

θ_y	Euler angle in *y* direction
θ_z	Euler angle in *z* direction
λ_i	A scalar
μ_i	A scalar
ξ_i	Step size
$\varphi_{k,w}$	The receiving incident angle between the k^{h} transmitter and the reflective area
$\varphi_{w,r}$	The receiving incident angle between the reflective area and the receiver
$\omega_{k,w}$	The irradiance angle between the k^{h} transmitter and the reflective area
ω_k	The irradiance angle from the k^{th} transmitter to the receiver
$\omega_{w,r}$	The irradiance angle between the reflective area and the receiver
b	Bias term
c	Constant
F	Focal length in meters
f	Feature maps
$F(p_i^m)$	Mean square error
F_c	Focal center
g	Ground truth box
$g(\varphi)$	Concentrator gain of the receiver
h	The vertical distance between the transmitter and receiver
H	The height of the image sensor
$h\nu$	Incident photon energy
i	Number of neurons
I	Identity matrix
K	Total number of transmitters
l	Predicted box
m	Number of layers
N	Total number of inputs
R	Rotational matrix
$\mathcal{R}$	Photodiode responsivity
s	Arbitrary scaling of projective transformation
S	Sensitivity matrix
$\text{tr}(H^{-1})$	The trace of the inverse of Hessian matrix
$T_s(\varphi)$	Transmittance function
W	The width of the image sensor
γ	Input vector,
ρ	The reflectance factor depending on the material of the reflective surface
φ	Incident angle
G	Learning rate
H	Hessian matrix
M	Maximum number of layers
n	Number of inputs
q	Electron charge
t	Translation vector
v	Lambertian mode
α, β	Regularization parameters
δ	Number of classes
η	Quantum efficiency
ϵ	The weight for the localization loss

Chapter 1: Introduction

1.1 Background

Indoor positioning systems (IPSs) have gained increasing attention from the academic and industrial communities with numerous applications, including pedestrian navigation, asset tracking, inventory management, automatic driving, autonomous robot movement, etc [1]. Many broad and essential applications, such as surveillance, object, and navigation tracking services, can be provided by indoor localization that can be utilized in different areas (i.e., museums, warehouses, parking facilities, shopping malls, and supermarkets). Global positioning system (GPS) is a well-known system used for outdoor localization, though it is not suitable for indoor localization for the following reasons. Firstly, there is a severe attenuation of GPS signals when electromagnetic waves penetrate through walls. Therefore, these GPS signals are not detectable in most indoor locations, which results in compromised performance. Secondly, the GPS uses the information of the traveling time of the signal to estimate the coordinates of the user. However, multipath reflections severely affect signals where the precision of time information is mainly affected, and indoor positioning performance is degraded for indoor environments.

Earlier, several technologies (e.g., ultrasounds [2], radio waves [3]–[5], ultra-wideband (UWB), Wi-Fi, and Bluetooth) have been investigated for indoor localization. However, these positioning systems have drawbacks that restrict their pervasive usage. The ultrasound wavelength is generally enormous as well as its velocity is influenced by environment temperature, which may bring about huge-ranging and localization errors. Radio frequency (RF)-based systems face several problems including electromagnetic radiations and multipath fading effects in the indoor environment. These multipath fading effects increase localization errors and electromagnetic radiations limit the application in RF-sensitive areas (e.g., medical). In general, Bluetooth- and Wi-Fi-based systems have a limited range of issues and need network access authorization. The UWB technology transmits short RF pulses with a low-duty cycle (less than 0.5 percent), which provides precise localization and tracking for mobile devices in indoor environments [6]. Despite the advantage of precise localization, the UWB technology is still not perfect for IPSs. It has not been embraced widely because of its cost, complexity, and need for synchronization between transmitters and the targets [7].

In ancient times, light has been used to find or locate for a long period; for instance, stars have been used to navigate around the globe [8]. The astrolabe quadrant uses the position of stars and

sun to determine the time and their latitude based on the angles [9]. In recent years, visible light communication (VLC) has gained much attention from researchers due to the significant progress in the manufacture of light-emitting diodes (LEDs). VLC, which is license-free, and free from RF-induced electromagnetic interference, is ideal in many applications, including hospitals. In addition, VLC uses the pre-existing LEDs infrastructure as a transmitters that can provide illuminance and communication simultaneously [10]. The rapid development of VLC networks has encouraged researchers to propose positioning solutions based on this technology. Visible light positioning (VLP) using LEDs is an emerging optical wireless technology, considered as an integrated or alternative technology to RF. The LEDs offer high bandwidth, high security, high-speed data transmission, low implementation cost, and low power consumption. In indoor environments, the VLP technology provides high accuracy from millimetre to meter levels in the localization since the effect of multipath optical signals is significantly lower than with RF signals [10]; and typically, the reflected optical signals have significantly lower power than the line of sight (LOS) signals [10]. The RF spectrum is becoming congested and overcrowded; on the contrary, the VLC spectrum is widely available and free from regulations.

In VLP systems, photodetectors (PDs) or image sensors (ISs) are commonly used as receivers. The formers promise a high data-rate and low-cost optical wireless links. In contrast, the latter offers higher positioning accuracy, but at the cost of a complex positioning algorithm and limited positioning speed. Currently, VLP technologies, are based on the triangulation techniques where the distance or angle between the transmitter and the receiver needs to be estimated. The distance or the angle can be determined in several ways, including received signal strength (RSS), angle of arrival (AOA), time of arrival (TOA), and time difference of arrival (TDOA). These methods present their intricacies. The major drawback of AOA is that the system needs expensive sensor arrays or ISs to measure the incident angle with high accuracy [11]. TOA needs accurate synchronization between the transmitter (i.e., LED) and the receiver, which increases the deployment cost [12]. On the other hand, RSS requires a precise determination of the incident signal power, thus being strongly dependent on the signal-to-noise ratio (SNR) [13]. Simple approaches rely on proximity-based and scene analysis, which trades simplicity with accuracy. These are suitable for low accuracy systems, not demanding high location precision. A positioning system must consider many factors when selecting an IPS, such as, positioning accuracy, availability, cost, complexity, system integration, and scalability.

1.2 Motivation

As of now, researchers have explored many possibilities when designing VLP systems and algorithms. The indoor positioning market has already generated revenues of USD 6.54 billion in 2020 and has a target to hit USD 35.65 Billion by 2028, as depicted in Fig. 1.1 [1]. Many potential approaches have been investigated exploring an accurate positioning system. Since the 1970s, the GPS has evolved to the point where precise location data is available via satellite infrastructure. Since then, IPS has been rapidly proposed and developed. From the late 1990s, technologies involving IPS began to evolve after mobile network services entered a prosperous era. IPS is always a concern since technologies for outdoor positioning provide inadequate performance inside the buildings. Even with a reasonable solution to the problem of outdoor positioning with systems such as GPS, these systems are not suitable for indoor positioning.

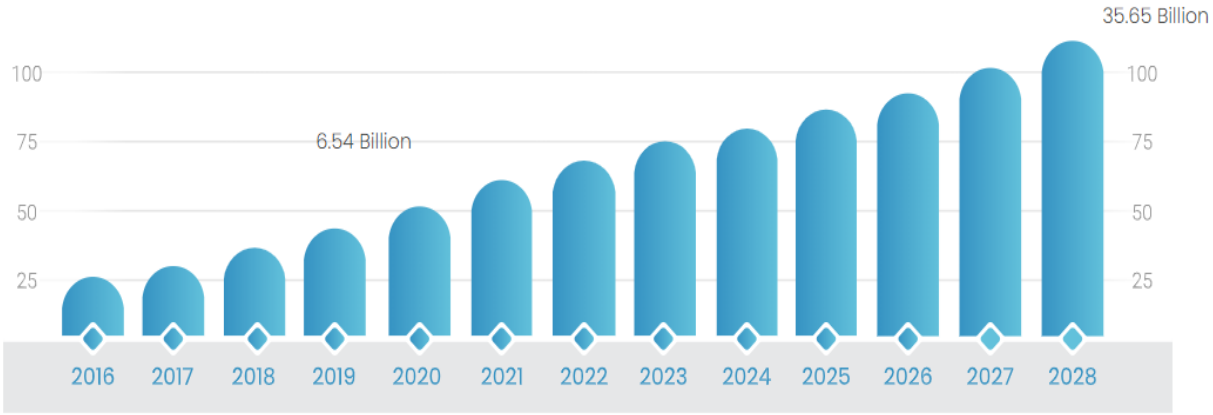

Fig. 1.1. Market revenue of indoor positioning ([1]).

The use of VLP is one approach with a lot of potential where white LEDs are used for indoor lighting and high-speed data transmission. VLP can benefit from this technology by using LED lighting as positioning beacons that send their location via VLC. LEDs are quickly becoming the standard choice for indoor lighting because of their energy efficiency and longer lifespan, and they may be found in all buildings in the future. Therefore, VLP has become an attractive technology because of its low infrastructure costs and ability to achieve precise positioning accuracy.

1.3 Problem Statement and Objectives

VLP systems face many challenges that should be addressed, such as the VLP system error performance, optimized positioning algorithms for different scenarios, implementation, and validation in live scenarios.

This Ph.D. work aims to achieve high-precision indoor localization techniques for indoor scenarios. The particularity of this work is the possible presence of objects and/or obstacles in the environment. The simplicity of infrastructure deployment and its cost-effectiveness are among other requirements that will be considered. In addition, the transmitted signal through LEDs will be adapted appropriately to offer both indoor localization and illumination. The design of reconfigurable light source emission parameters will also be considered to optimize the positioning accuracy or transmission quality. The theoretical work will be complemented with simulation and experimental work that includes the development of a comprehensive experimental testbed for the proposed indoor VLC system. A comprehensive system performance measurement including SNR, accuracy, positioning error amongst others, will be carried out and compared with the predicted and simulated results.

There are four identified objectives which are as follows:

1. To achieve multi-precision in indoor localization. Solutions should tackle an application-oriented approach, where precision can be adapted to multiple contexts.
2. To develop a theoretical model for simulation and performance evaluation, which is suitable for VLP systems.
3. To design, develop and evaluate a low complexity system and compare results with the predicted data. The achieved solution will search for appropriate methodologies able to leverage system complexity.
4. To analyze system performance under realistic conditions.

1.4 Thesis Contributions

The original contribution of this research is summarized in Chapter 5 in the following manner:

1. In section 5.3, it has been demonstrated that tilting the transmitter and multipath reflections can have a significant effect on the performance of indoor VLP systems, and a novel system is proposed where tilting the transmitter is proven to be beneficial when considering both LOS and NLOS paths for transmissions. This analysis is done by employing a low complex linear least square algorithm with polynomial regression. It is revealed that the proposed scheme significantly improves accuracy by ~66% compared with a typical non-tilted transmitter VLP system.
2. In section 5.4, the impact of transmitter position and orientation uncertainty on the accuracy of the VLP system based on the RSS is investigated. It is inferred from the

simulation results that transmitter uncertainties have a severe impact on the positioning error, which can be mitigated through the usage of more transmitters.

3. In section 5.5, a theoretical analysis is conducted to study various artificial neural network (ANN) design aspects to estimate the positioning of an indoor VLP system by considering multipath transmission. This study compares different design approaches based on the influence of noise as a performance indicator. In comparison, the ANN with Bayesian regularization outperforms the traditional RSS technique using the non-linear least square estimation.
4. In section 5.6, a novel indoor VLP system is presented based on support vector machines and polynomial regression. Two different multipath environments of an empty room and a furnished room are compared in this work.
5. In section 5.7, an experimental demonstration of an indoor VLP system based on convolutional neural networks (CNN) is done by employing LEDs as transmitters and a rolling shutter camera as a receiver. This system is validated using a practical test setup containing eight LED luminaries. The results reveal that this system can process 67 images per second, allowing real-time positioning and the maximum average root mean square positioning error achieved is 4.67 and 5.27 cm using single shot detector (SSD) MobileNet and SSD ResNet models, respectively.

1.5 Thesis Structure

This dissertation is organized as follows: After the introduction and stating the objectives of this work in Chapter 1, a detailed review of the state of the art in VLP is presented in Chapter 2, highlighting the recent research and recent techniques employed in this research field. Chapter 3 comprises the fundamentals of the VLC system including system modeling employed in this thesis. The classification of VLP systems is also detailed in this chapter. Next, the methodology explored in the work including different traditional and machine learning algorithms is detailed in Chapter 4. The results of this work are discussed in Chapter 5, utilizing a compendium of publications. Finally, an overview of the conclusions reached from this study and future research directions are presented in Chapter 6.

1.6 List of Publications

1.6.1 Journal articles

- **N. Chaudhary**, O. I. Younus, L. N. Alves, Z. Ghassemlooy, S. Zvanovec, and H. Le-Minh, 'An Indoor Visible Light Positioning System Using Tilted LEDs with High Accuracy', *Sensors*, vol. 21, no. 3, p. 920, Jan. 2021.
- **N. Chaudhary**, L. N. Alves, and Z. Ghassemlooy, 'Impact of Transmitter Positioning and Orientation Uncertainty on RSS-based Visible Light Positioning Accuracy', Sensors, vol. 21, no. 9, p. 3044, April 2021.
- **N. Chaudhary,** O. I. Younus, L. N. Alves, Z. Ghassemlooy, and S. Zvanovec, 'Usage of ANNs for Regression Analysis in Visible Light Positioning Systems', Sensors, submitted.
- **N. Chaudhary**, C. J. Verdu, P. Fonseca, L. N. Alves, R. P. Jimenez, and Z. Ghassemlooy, 'A Convolutional Neural Network-based Visible Light Positioning System using Rolling Shutter Cameras', Optics Express, submitted.

1.6.2 Conference proceedings

- **N. Chaudhary**, L. N. Alves, and Z. Ghassemlooy, 'Current Trends on Visible Light Positioning Techniques', in *2019 2nd West Asian Colloquium on Optical Wireless Communications (WACOWC)*, Tehran, Iran, Apr. 2019, pp. 100–105.
- **N. Chaudhary**, L. N. Alves, and Z. Ghassemlooy, 'Feasibility Study of Reverse Trilateration Strategy with a Single Tx for VLP', in *2019 2nd West Asian Colloquium on Optical Wireless Communications (WACOWC)*, Tehran, Iran, Apr. 2019, pp. 121–126.
- **N. Chaudhary**, L. N. Alves, and Z. Ghassemlooy, 'Impact of Transmitter Positioning Uncertainty on RSS-based Visible Light Positioning Accuracy', in *2020 12th International Symposium on Communication Systems, Networks and Digital Signal Processing (CSNDSP)*, Porto, Portugal, Jul. 2020, pp. 1–6.
- **N. Chaudhary**, O. I. Younus, Z. N. Chaleshtori, L. N. Alves, Z. Ghassemlooy, and S. Zvanovec, 'A Visible Light Positioning System based on Support Vector Machines', in *2021 IEEE 32nd Annual International Symposium on Personal, Indoor and Mobile Radio Communications (PIMRC)*, Helsinki, Finland, Sep. 2021, pp. 1–6.

1.6.3 Collaborations

- O. I. Younus, **N. Chaudhary**, Z. N. Chaleshtori, L. N. Alves, Z. Ghassemlooy, and S. Zvanovec, 'The Impact of Blocking and Shadowing on the Indoor Visible Light Positioning System', in *2021 IEEE 32nd Annual International Symposium on Personal, Indoor and Mobile Radio Communications (PIMRC)*, Helsinki, Finland, Sep. 2021, pp. 1–6.
- M. R. Soares, **N. Chaudhary**, E. Eso, O. I. Younus, L. Nero Alves, and Z. Ghassemlooy, 'Optical Camera Communications with Convolutional Neural Network for Vehicle-to Vehicle Links', in *2020 12th International Symposium on Communication Systems, Networks and Digital Signal Processing (CSNDSP)*, Porto, Portugal, Jul. 2020, pp. 1–6.

- O. I. Younus, **N. Chaudhary**, Z. Ghassemlooy, N. B. Hassan, L. N. Alves, and S. Zvanovec, ‘Unilateral 3D Indoor Positioning System Employing Optical Camera Communications’, Optics Express, submitted.

Chapter 2: State of the Art

In this chapter, a detailed literature survey on the major techniques used in the VLP systems is performed.

The positioning system provides the location coordinates of an object or a person in a given environment. There can be two types of positioning: indoor and outdoor. There are many reliable solutions for outdoor positioning, for instance, GPS is a famous example of outdoor positioning. It is popular all over the world. It provides reliable positioning with an error in the order of meters. On the other hand, GPS does not work well for indoor positioning. The radio waves do not penetrate through the walls. It results in high inaccuracy in indoor positioning. Other IPS have been proposed in recent years, for instance, ultrasound, Wi-Fi, Bluetooth, ZigBee, RF-identification (ID), and UWB. However, these systems face many issues. For instance, ultrasound-based positioning systems require additional hardware, and it is sensitive to the environment. Although Bluetooth and Wi-Fi provide low installation costs, these methods are highly susceptible to interference from walls, buildings, therefore they do not provide high accuracy in case of indoor positioning. RF-ID and ZigBee require dedicated beacons to perform positioning, which increases the cost. UWB uses electromagnetic waves that consist of a sequence of very short pulses. This method is more precise and expensive, but cannot be used in some areas, such as hospitals and airports.

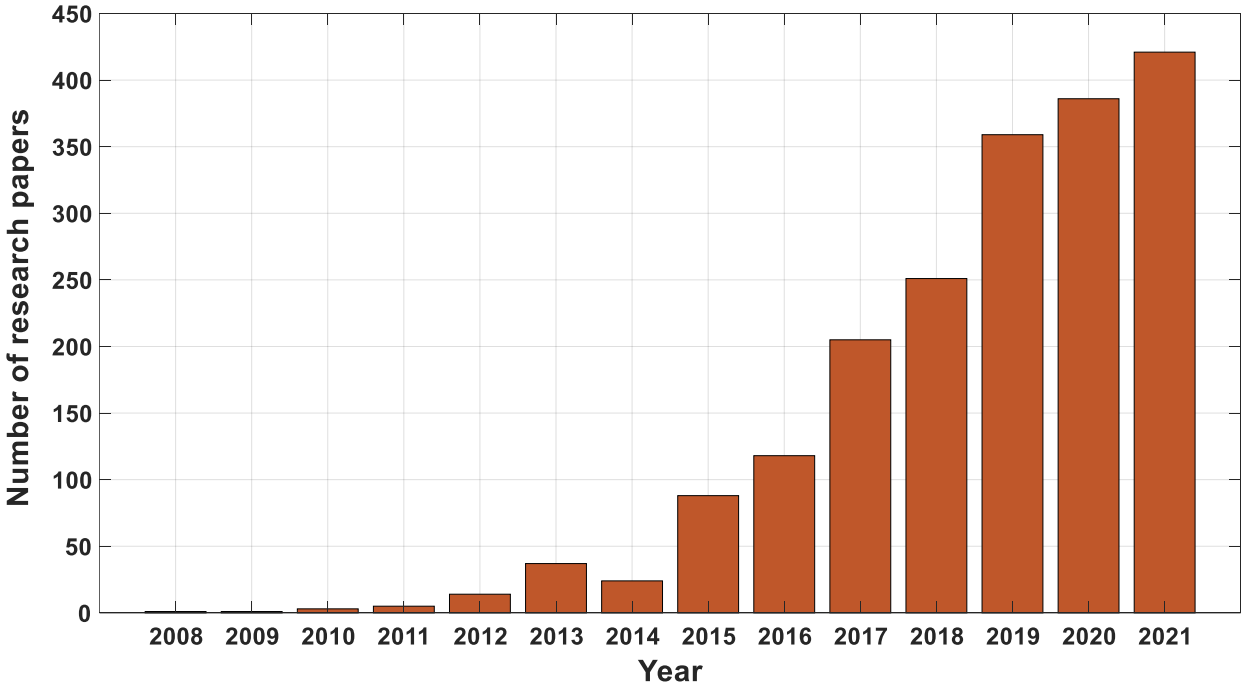

Fig. 2.1.Trend of VLP in years [14].

On the other hand, VLP systems provide high accuracy at a low cost and complexity as compared to other existing technologies. One of the main advantages of VLP systems is using LEDs as a transmitter that are already installed in almost every place. In recent years, VLP has become an interesting research topic due to the tremendous advantages of LEDs, as evident in Fig. 2.1.

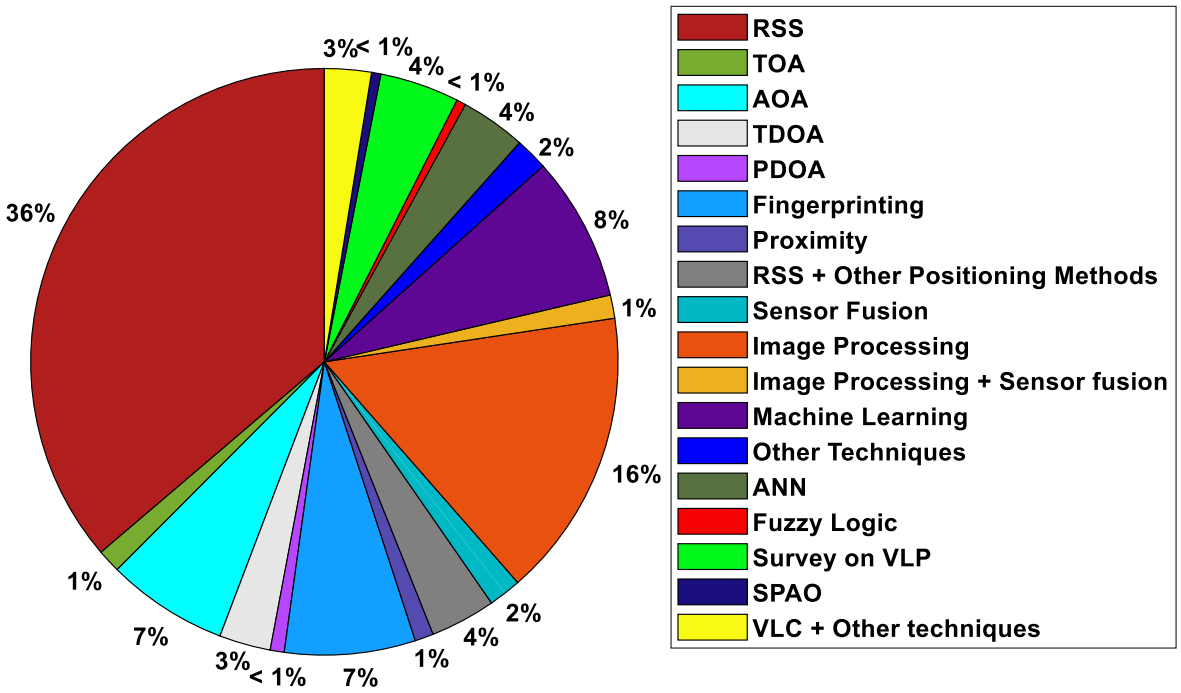

Fig. 2.2. Different techniques used in VLP [15]–[18].

Fig. 2.2 summarizes the state of the art focusing on different positioning methods till now. In the following sections, each of these techniques is discussed one by one:

***RSS*:** Is one of the triangulation techniques, which has been extensively utilized in IPSs and VLP systems because of its simplicity, that determine the received signal strength and measure the propagation loss of the emitted signal. A path loss model is employed to measure the position estimation. There is no requirement of any other additional devices to determine the RSS values, as it uses only a single PD. In [19], an IPS based on VLC was proposed with a carrier allocation modulation method. This system is able to provide accurate estimates with an average positioning error of 6 cm by utilizing the normalization method. In [20], a new regression-based approach was used to investigate an RSS-based VLP system along with linear least square (LLS)- and non-linear least square (NLLS)-based estimations. The results revealed that, the minimum error is around 0.6 m utilizing the polynomial regression approach compared with the other traditional approaches. An efficient RSS-based VLP algorithm was proposed in [21] to estimate the three-dimensional

location of a receiver, by combining two-dimensional trilateration with the NLLS. The computational time for NLLS is limited to approximately 17 millisecond (ms), which is further reduced to less than 2 ms using a fast search algorithm. As we can see in Fig. 2.2, RSS is the most exploited technique for the VLP system (nearly 36 %) [16], [18], [22].

***TOA and TDOA*:** Are two important positioning methods, which have been employed from earlier years. In fact, the well-known GPS also uses TOA to determine the location all over the world. TOA implies the absolute travel time of a signal from the transmitter to the receiver. However, it requires accurate synchronization between transmitter and receiver [23], [24]. TDOA computes the difference in propagation time between the transmitter and the receiver for estimation. Therefore, IPS uses TDOA rather than TOA in order to avoid synchronization. However, time synchronization is required between the transmitters. TDOA is more used than TOA, see Fig. 2 [12], [25]–[33]. In [34], a novel TOA positioning system was analyzed where TOA based distance estimation was employed. Cramer-Rao bounds was derived to calculate the theoretical limits on estimation accuracy for the intensity-modulated sinusoidal signals. The results showed that, it is possible to achieve an accuracy of about 5 cm by assuming the perfect synchronization between the transmitter and the receiver. A 3-D indoor positioning algorithm was proposed [35], where the positioning accuracy was ensured by taking the transmitter shapes into consideration. The results revealed that the average error of 1.8 cm was achieved.

***AOA*:** AOA-based positioning systems determine the angle of arrival of the detected signals from several transmitters. The intersection of direction lines is a measure of the target position. The advantage of using AOA-based systems is that no synchronization is required between the transmitter and the receiver [36]–[59]. In [60], a switching estimated receiver position scheme has been proposed where 6 axes sensor was employed. The positioning accuracy was improved by optimizing error distance estimation. This system was capable to improve more than 30% of accuracy as compared to conventional positioning schemes. It is easy to compute the AOA of the incoming signal by utilizing imaging sensors as receivers. Nevertheless, the imaging receiver has limited resolution, which can downgrade the accuracy of positioning when the target moves away from transmitters. A further drawback of AOA techniques includes high complexity and the additional cost of the imaging receivers.

***Fingerprinting*:** Is a positioning algorithm where, at first fingerprints are collected for a sample of positions in a room. Then, the location of the target is estimated by comparing the real-time measurement with these collected fingerprints. It is also known as scene analysis. Fingerprint

includes all positioning techniques, that are stated prior, such as RSS, AOA, TOA, and TDOA. RSS-based fingerprinting is the most commonly used fingerprinting method due to its low complexity. In [61], the performance limits of fingerprinting-based localization were investigated which includes multipath reflection as a source of information (i.e., fingerprinting map). Accuracy limitations were determined by Cramer Rao lower bound (CRLB) for various numbers of PDs employed in the proposed system. The results showed that the root mean square (RMS) positioning accuracy achieved were 45, and 5 cm for one and four PDs, respectively. The main advantage of using this technique is time and power-saving since it requires less time to match fingerprints. Conversely, there is a drawback also. For a particular environment, it needs precise pre-calibration. Therefore, it can only be used for a specific scenarios [16].

***Proximity*:** Is a positioning technique that depends on a dense grid of different reference points, where each reference points have a known position. If a target receives the signal with the strongest intensity, then it is assumed to be close to that transmitter. Also, if the target receives multiple signals with the same intensity, it is supposed to be in the center of transmitters (one with the same intensity). This technique is simple and straightforward to implement in comparison with other positioning techniques. But it does not provide precise estimation as it relies on the density of receivers distributions [10], [16].

***PDOA*:** The phase difference of arrival (PDOA) is the positioning technique where distance differences are computed by the phase difference of arriving signals. In [62], an improved PDOA scheme was proposed for indoor VLP that precluded the use of local oscillators (LOs) at the receiver. There was no need for synchronization between transmitters and receivers. This scheme could reduce the complexity of the system and provided relaxation to the frequency allocation constraints and conclusively improved the positioning accuracy. In [63], differential PDOA (DPDOA) was experimentally demonstrated for the first time. This algorithm also did not require any LOs. Additionally, a Kalman filter was used for reducing the variation of the estimation of distance difference and a neural network was adopted for reducing positioning shifting error respectively. This error was induced by the non-uniform initial time delay of off-the-shelf white LEDs. The experimental results showed that the proposed system was capable of achieving an average RMS and maximum RMS errors of 1.8 and 0.08 m, respectively, with a 1×1.2 m^2 coverage and a 2 m height. This system was the first system based on DPDOA to provide sub-decimeter accuracy.

***Image Processing*:** Is a technique where an IS or a camera is used as a receiver. A lot of research has been developed in recent years. For instance, the effects of camera parameters were investigated in [64] on the performance of an indoor VLP system based on an IS or a camera. The results revealed that the error can be improved by increasing the number of LED transmitters and increasing the field of view (FOV) of the camera. In [65], a new 2-D ANN-based VLP system was proposed, where the LEDs were grouped into blocks. The block coordinates were encoded using under-sampled modulation. A camera was used as the receiver to decode the block coordinate, and the system achieved a mean error of 1.49 cm. A novel VLP system was proposed in [66], based on the features of the receiver signal and the relative position of the two LEDs images on the camera sensor, which reduced the dependency on the LEDs' brightness level and the higher pixel resolution. It was revealed that, the system was able to determine the receiver's position with an error of less than 5 cm for a height of 170 cm. In [67], a camera-assisted RSS for VLP systems was proposed, where the simultaneous visual and strength information of visible light was used with LLS method to achieve the precise positioning at a low computational cost. Simulation results revealed that the proposed system achieved an average three-dimensional (3D) positioning error of ~12.5 cm.

***Sensor fusion*:** Is a method where different types of sensors are combined together to provide better performance of the system. Magnetic compass, gyroscopes, and accelerometer are the famous sensors, which are being used in positioning. For instance, magnetometers, proximity sensors, gyroscopes, and many other sensors are inbuilt under mobile devices which can be used for positioning and orientation purposes. For instance, in [68], a tightly coupled visible light and inertial positioning system were presented where the inertial measurement unit (IMU) and VLC information were fused together to make the system capable of providing continually location service. The results showed that the proposed method increases the percentage of image frame utilization from 51.4% to 100 % in the same dataset. A new loosely-coupled VLP-inertial fusion method was proposed in [69] for VLP, where the robustness was improved by using IMU and a rolling shutter camera. The results showed that the average accuracy achieved was 2.1 cm for stationary localization and the average computational time was around 33 ms. Different sensor fusion-based VLP systems have been investigated in [70]–[75], which have shown higher positioning accuracy.

Machine learning: Is an ensemble of techniques, such as, ANNs and CNN that gives the system the capability to automatically learn and improve from the experience without being

explicitly programmed. VLP systems can use this technology in terms of data cleaning classification and regression. There is a lot of research on VLP systems based on machine learning techniques that have been reported in the literature. For instance, in [76], machine learning was introduced for VLP for the first time. The system is capable of reaching 0.31 m of average accuracy in an indoor environment of a dimension of $4.3 \times 4 \times 4$ m^3. In [77], a pointwise reinforcement learning (PWRL) algorithm was proposed for a VLP system based on the multi-detector. The experimental results showed an improvement of around 70 % positioning accuracy. In [78], an enhanced machine learning-based IPS was proposed using LED lights. This solution improved positioning accuracy as well as reduced computational time. A novel dual-function machine learning and signal preprocessing were employed to achieve highly precise positioning. In addition, [79]–[82] are some research that has improved the accuracy of the VLP system.

ANN: Is a machine learning method that is biologically inspired. ANNs are inspired by the human brain and replicate the way that humans learn. For instance, in [83], both RSS and ANN methods were proposed to achieve an accurate indoor VLP system with a diffuse optical channel. An accuracy of 6.39 cm was achieved with the averaged error being ~13 times smaller than the RSS-based positioning system. In addition, a low-cost indoor VLP system was proposed using a machine learning algorithm in [84], which was achieved an error of 3.65 cm with a height tolerance of 15 cm. In [85], a VLP system based on the RSS and a deep ANN-based Bayesian regularization VLP system was proposed (the study considered only LoS signal transmission). The results showed that, only 20 training points were used to achieve the minimum error of 3.4 cm. In [86], an ANN-based approach was proposed exploiting the distortions caused by inaccurate modeling (phase and intensity models) in both the PDOA and RSS-based positioning systems. The pre-trained models were applied to the ANN-based VLP system for reduced complexity and enhanced robustness, showing an error of 12 cm.

Deep Learning: Is an another prominent technology, which is also a machine learning approach that outperforms traditional methods in a wide range of applications and has been extensively employed in estimating the receiver position [87]. For instance, in [88], two deep ANN models based on multilayer perceptron and CNN were used to efficiently map the instantaneous received SNR with user 3D position and user equipment orientation. The results revealed that the average positioning errors were 10.53 and 13.04 cm for CNN and multilayer perceptron, respectively. [89] describes a new VLP indoor localization technique based on a CNN-based algorithm with handover probability analysis. The algorithm was categorized into two modes:

offline and online. Firstly, the algorithm was trained utilizing a dataset of received VLC signal and data generated from the smart device in the offline mode. Secondly, users assessed their position in the online mode based on the received VLC signal. The simulation results revealed that the average positioning error achieved was 4.31 cm for the proposed algorithm.

***Fuzzy logic*:** Is an extension of binary logic to multilevel logic. Fuzzy logic techniques can proficiently manage the linguistic rules, thus becoming an attractive technique for various range of applications, for instance, indoor localization. In [90], a novel fuzzy-based positioning system has been introduced by using VLCs. transmitters are used to process data and deliver the computed position of a receiver to the system. A particle swarm optimization technique has been used to get the optimal configuration of the proposed fuzzy logic controllers (FLCs). The proposed system shows better results with the optimization of the membership function of FLCs. Moreover, optimal localization reliability has been produced by adjusting the range of FLCs. The results revealed that the average error achieved was 0.75 m with the proposed system.

SPAO: Simultaneous positioning and orientation (SPAO) is a scheme where both positioning and orientation can be achieved at the same time. It does not require prior knowledge of the target height and orientation angle. In [91], a novel successive LLS algorithm was proposed to get a simple LiFi localization solution. This system does not require precise orientation alignment of the transceiver or any earlier information about the user height. The proposed algorithm is capable of attaining a precise solution with a fast convergence rate by providing a proficient closed-form update equation for both user location and orientation angle. It is remarked that in the case of LOS-only, a localization error of 0.48 cm has been achieved with an SNR of 40 dB. Besides, the LLS algorithm can achieve 0.1 to 0.5 m error for a general scenario with the 10% non-line of sight (NLOS) signal power over the total RSS. RSS-based SPAO is a non-convex optimization problem for VLCs because of the nonlinear RSS model. A new multi-scale particle-assisted stochastic search (PASS) algorithm has been proposed in [92] with a problem-specific update rule design in order to solve the non-convex SPAO problem. A closed-form CRLB has also been derived for localization error and VLC based SPAO performance limits are revealed. The proposed PASS algorithm investigated the diverse update information to handle the non-convex optimization problem, therefore enhancing the evolution efficiency. It is presented from the results that user position and orientation accuracies are linear to SNR and direction information. Moreover, the orientation and positioning accuracies decay with four and six powers of the transmission distance respectively.

***RSS and Other positioning techniques*:** RSS can be used with a combination of other techniques (AOA, TDOA, TOA) in order to improve the positioning estimation, for instance, in [93], a quasi-synchronous VLP system has been investigated where TDOA technique is employed to estimate positioning. It is a hybrid TDOA-RSS localization system where TDOA information is utilized with channel attenuation information. Moreover, position estimation based CRLB has been derived in a typical 3D scenario to specify the accuracy limits for this system. After that, a direct positioning technique was adopted to compute the maximum likelihood position estimator. Also, the author proposed a two-step position estimator, where TDOA and RSS estimates were computed in the first step and then the estimation of position is implemented in the second step. The mean square error (MSE) of both approaches was closely matched at high SNRs. Additionally, time information (TDOA) was erroneous at low SNR, so as to result in distortion of the overall performance of the two-step approach in comparison with direct approach. It was analyzed that the two-step approach was more appropriate at high SNRs while the direct approach was more convenient at low SNRs due to its improved performance.

***Other techniques*:** There are some other optimization models that have been used for VLP systems. For example, in [94], a 3D high precise IPS was proposed by using Tabu search. Tabu search is a dominant global optimization algorithm. This was the first time that the Tabu search algorithm was applied to the VLP system. The localized ID information is sent by each LED, Tabu search algorithm was used to locate the photodiode after the receiver detected ID information (optical signal) from different LEDs. The experiment results revealed that the positioning effect was superior to the existing indoor 3D positioning. Some other techniques, such as, area-based optimization models, fine-grained indoor localizations have been reported in the literature in [71], [95]–[99].

Chapter 3: Fundamentals of Visible Light Positioning Systems

This chapter compiles the basic technical knowledge needed for the development of the VLP systems used in this thesis. The principles described include the fundamentals of VLC technology and optical wireless channel modelling. The main aspects of optical camera communication (OCC) and VLP technology are also detailed. Moreover, VLP systems are categorized based on the receiver detector.

3.1 Visible Light Communication Systems

The carrier frequency of RF lies between 30 MHz and 5 GHz, while the band of VLC is within the THz range, as depicted in Fig. 3.1. RF communication systems operate at wavelengths between centimeters and kilometers, while VLC operates at wavelengths around several hundred nanometers [100].

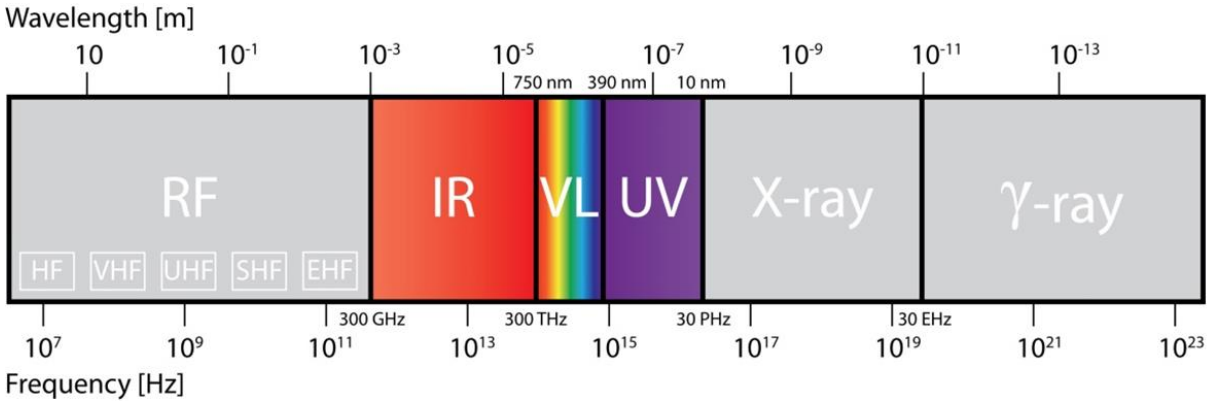

Fig. 3.1. Wavelengths and frequencies of radio and optical carriers.

In general, VLC is a subset of the optical wireless communication (OWC) technology defined in IEEE 802.15.7 in order to complement the ubiquitous RF-based mobile communications and is designed to be incorporated with high capacity mobile data networks [101]–[104]. The VLC technology became more prominent due to its efficiency in utilizing pre-existing LEDs-based lighting infrastructure as the transmitter to provide significant improvements in luminous efficiency, data communication, and indoor localization [102]. LEDs can be switched at high speeds as compared to other lighting sources, which allows data transmission that can be detected by PDs or ISs. Figure 3.2 illustrates the physical layer architecture of a unidirectional VLC system [105].

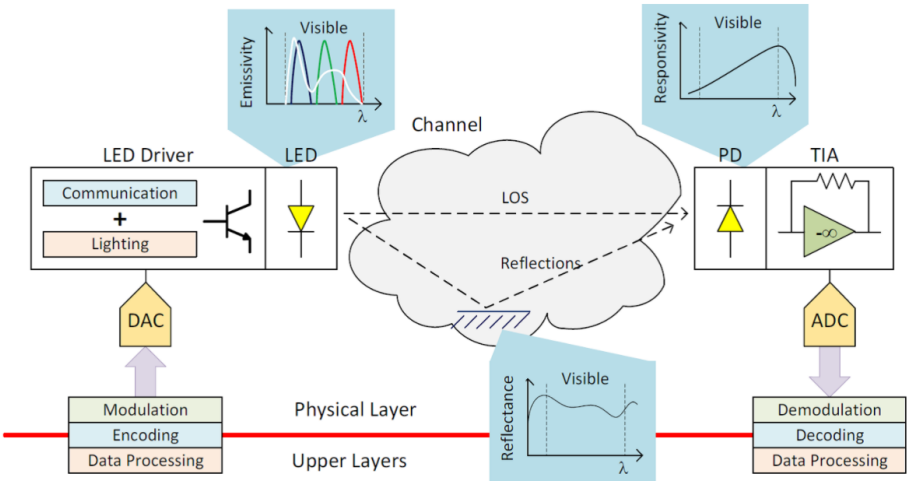

Fig. 3.2. The physical layer architecture of a VLC system [105].

VLC systems consist of an LED driving circuit front end and receiving front end. A major reason for the synergy between VLC systems and lighting systems is the use of the same lighting devices, namely LEDs. VLC systems utilize pre-installed LEDs as a transmitter. Therefore, an LED driver is used on the transmitter side to combine signal transmission with lighting requirements. Another feature of the transmitter is the light modulation. The VLC technology uses an intensity modulation/direct detection scheme, in which the electrical signal modulates the light produced by the LED. On the receiver side, the basic elements consist of a PD or IS array, amplifier, and analog-to-digital converter. Other tasks pertaining to signal demodulation are typically done by digital signal processors or field-programmable gate arrays. The transmitter, receiver, and channel characteristics are detailed in the following subsections.

3.1.1 VLC Transmitters

VLC systems will have synergy with lighting systems since they both utilize the same lighting devices, i.e., LEDs, which are also used in lighting systems. An LED bulb is composed of several LED chips that act as transmitters, as illustrated in Fig. 3.3. Since LEDs are not monochromatic, they radiate light in a wide spectral range. Considering that LEDs are also used as an illumination source, the luminance should be considered between 300 and 1500 lx (1 lx = 1 lm/m^2), which is standardized by International Organization for Standardization (ISO) for the typical working environment [106]. LEDs are usually cost-effective, power-efficient, illumination-efficient, compact, and low maintenance. In contrast to traditional light sources such as compact fluorescent light and incandescent bulbs, LEDs can switch on and off at high speeds, making them an ideal option for communication. A LED source has a specific radiation pattern usually modelled by a Lambertian law [100], and its bandwidth ranges between 20 MHz and 100 MHz [105]. On

the transmitter side, the LED driver provides the transmission of the signal as well as lighting requirements.

Fig. 3.3. VLC transmitter.

Mathematical representation of spatial power distribution of LED is given as:

$$I_\theta = I_0 \cos^m \theta, \tag{3.1}$$

where I_θ represents the intensity in the direction specified by the angle of θ with the normal direction, and I_0 represents the intensity in direction of the LED symmetrical axis, i.e., the normal direction. Parameter *v* is Lambertian order which is given by:

$$v = -\frac{\ln(2)}{\ln\left(\cos\left(\Theta_{\frac{1}{2}}\right)\right)}, \tag{3.2}$$

where $\Theta_{\frac{1}{2}}$ is the light source irradiance half-power angle (HPA).

3.1.2 VLC Channel Modelling

VLC systems use a white LED with transmitted power $P_{t,k}$ as the light source and the signal is modulated and transmitted using an optical wireless channel. The received power $P_{r,k}$ at the receiver from the k^{th} transmitter will be a combination of power from both LOS and NLOS paths and can be expressed as:

$$P_{r,k} = \sum P_{r,k(\text{LOS})} + \sum P_{r,k(\text{NLOS})}, \tag{3.3}$$

where $P_{r,k(\text{LOS})}$ and $P_{r,k(\text{NLOS})}$ represents the received power for LOS and NLOS at the k^{th} transmitter, respectively. The received power from LOS path can be expressed as [107]:

$$\sum P_{r,k(\mathrm{LOS})} = \sum_{k=1}^{K} P_{t,k}\, A_r \mathcal{R} \left(\frac{v+1}{2\pi}\right) \frac{\cos^v(\omega_k)\cos(\varphi)}{\|d_k\|^2} T_s(\varphi) g(\varphi), \tag{3.4}$$

where $P_{t,k}$ is the transmit power, d_k is the distance between k^{th} transmitter and the receiver, K is the total number of transmitters [107]. ω_k and φ are the irradiance angle from the k^{th} transmitter to the receiver and the receiving incident angle, respectively. A_r and $\mathcal{R}$ are the PD's active area and responsivity, respectively. $T_s(\varphi)$ and $g(\varphi)$ are the gains of the optical filter and the concentrator at the receiver, respectively.

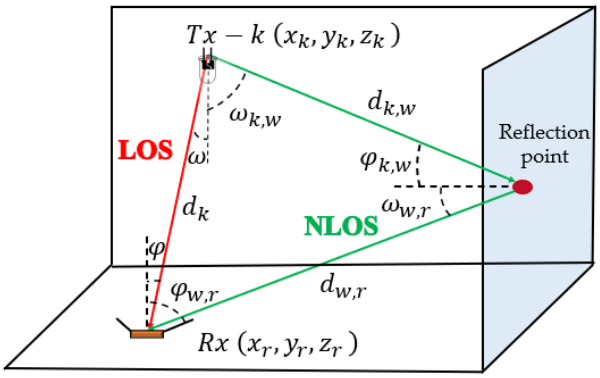

Fig. 3.4. A typical indoor VLC system [108].

Considering the NLOS path, the total received power can be expressed as [109]:

$$\sum P_{r,k(\mathrm{NLOS})} = \sum_{k=1}^{K} \sum_{\text{wall}} \rho P_{t,k}\, A_r \mathcal{R} \left(\frac{v+1}{2\pi}\right) A_{\text{ref}} \frac{\cos^v(\omega_{k,w})\, cos(\varphi_{k,w})}{\pi\left(\|d_{k,w}\|\|d_{w,r}\|\right)^2} \times T_s(\varphi_{w,r})\, g(\varphi_{w,r}) \cos(\omega_{w,r}) \cos(\varphi_{w,r}), \tag{3.5}$$

where $d_{k,w}$, $\varphi_{k,w}$, and $\omega_{k,w}$ are the distances, receiving incident angle, and the irradiance angle between the k^{th} transmitter and the reflective area, respectively. $d_{w,r}$, $\varphi_{w,r}$, and $\omega_{w,r}$ are the distances, receiving incident angle, and the irradiance angle between the reflective area and the receiver, respectively. ρ is the reflection coefficient that relies on the reflective surface material, and A_{ref} is the reflection area [109].

3.1.3 VLC Receivers

A VLC system commonly utilizes two types of detectors: (i) PDs; and (ii) ISs, i.e., multi-array PDs like those used in cameras. The former is a low-cost device and provides a larger detection area (or higher bandwidth). This latter camera, which consists of multiple PDs (i.e., pixels) in orthogonal alignment, can provide large detection areas as well as multi-input, multi-output

(MIMO) capabilities but requires complex processing. A brief overview of each detector is provided in the following subsections.

3.1.3.1 Photodiode

A semiconductor LED produces state-solid lighting by combining electrons and holes in order to release light, which is released as photons of a specified wavelength. It is also possible to induce current over the semiconductor device from incident photons, which is the reverse process. The conduction path is created because of travelling photons providing electrons in the valence band. These devices are referred to as PDs. It is an electronic device that can detect the presence of light by converting light energy into electrical energy. PDs with large surfaces are recommended for optimal VLC reception. The common PD is illustrated in Fig. 3.5.

Fig. 3.5. A typical photodiode.

The output current or voltage of the PD is proportional to the amount of received optical power. In addition, PD has a limited bandwidth ranging from several MHz to several GHz. Larger bandwidths lead to a smaller detection area [46]. The responsivity *R* of PD is considered as one of the most important factors that determine the efficiency of the PD, which is given by:

$$R = \frac{\eta q}{h\nu}, \tag{3.6}$$

where η is the quantum efficiency, $h\nu$ is the incident photon energy and q is the electron charge.

3.1.3.2 Image sensor

ISs create a two-dimensional (2D) representation of a scene using an array of PDs and lenses. In recent years, their widespread availability in consumer electronics, as well as urban infrastructures, has been characterized as a promising alternative for optical wireless communications systems. The general IS array is illustrated in Fig. 3.6.

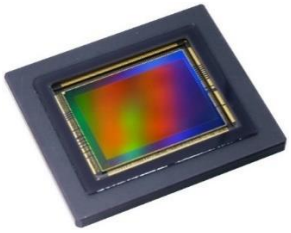

Fig. 3.6. An image sensor array.

An electronic camera consists of a lens, a color filter, a 2D array of PDs, and a post-processing unit [110]. The main purpose of the ISs is to convert light into electrons using either charge-coupled devices (CCDs) or complementary metal-oxide semiconductors (CMOS) PD arrays. In CMOS ISs, there are two modes of capturing: global shutter (GS) and rolling shutter (RS). In the GS, the entire image is exposed at the same time to light, while in the RS system, pixels are exposed sequentially in a row-by-row manner, with a small time delay between rows (see Fig. 3.7) [111].

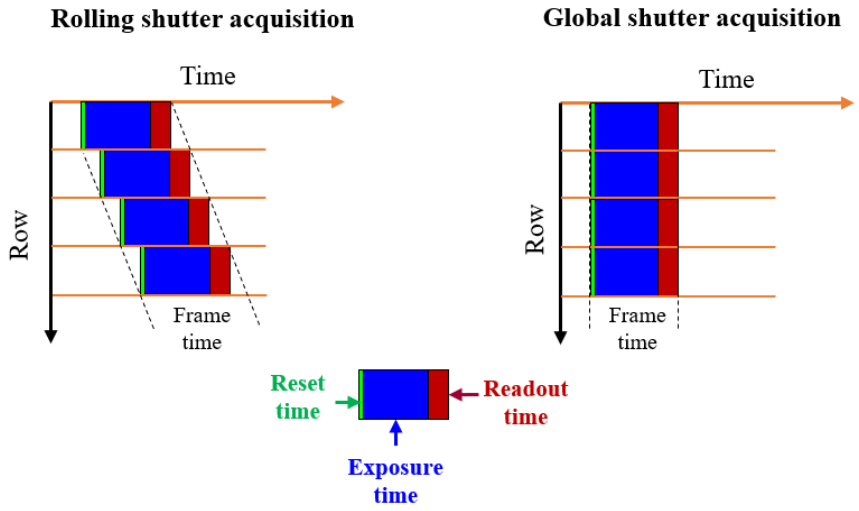

Fig. 3.7. Row-by-row and simultaneous frame exposure in RS and GS acquisition mechanisms [111].

The RS technique consists of exposing each row of pixels at once, which results in an image of an LED that produces pulsed light showing white and dark stripes. The number of stripes and their width depend on the frequency of the blinking light and the distance between the sensor and LED. Furthermore, in the case of RS-based IS, when a square wave with different frequencies is received, the captured width of the stripes will be inversely proportional to the frequency of the receiving signals (i.e., the higher frequency will provide smaller stipes width). This allows for frequency modulation of data symbols, also known as frequency-shift keying (FSK). In addition, different ISs may capture stripes of varying widths with the same fixed-frequency light source

since the analog-to-digital conversion time (light to 2D image conversion) is affected by the manufacturer.

3.2 OCC Systems

According to the standards, a VLC system that uses an IS as a receiver is known as an OCC system since it does not need any hardware modifications [112]–[114]. As explained earlier, the IS present in the camera consists of many individual micro-scale PDs, that are stacked together to make a matrix, when paired with a lens, can be utilized to provide a MIMO system, i.e., enabling spatial separation of light sources on the IS. Furthermore, the SNR in IS-based VLC systems is independent of transmission distance [115]. It is important to note that the incident light power level per pixel remains the same if the projected image of the transmitting LEDs covers a number of pixels.

In recent years, CMOS ISs are widely available in current smartphones [111], [116], since OCC technology takes advantage of a CMOS IS and RS for receiving information from an LED light source, at a higher frequency than the maximum frames per second of the device. This technology is an attractive alternative to PDs. ISs offer many advantages over PDs, such as, a larger field of view, spatial separation of light, and the ability to process various wavelengths provided by color filters [110]. On the other hand, CMOS RS-based ISs are only capable of low frame rates (between 30 and 60 frames per second), with OCC being limited to a data rate of range between 0.01 and 100 kbit/s [117].

3.3 Visible light Positioning Systems

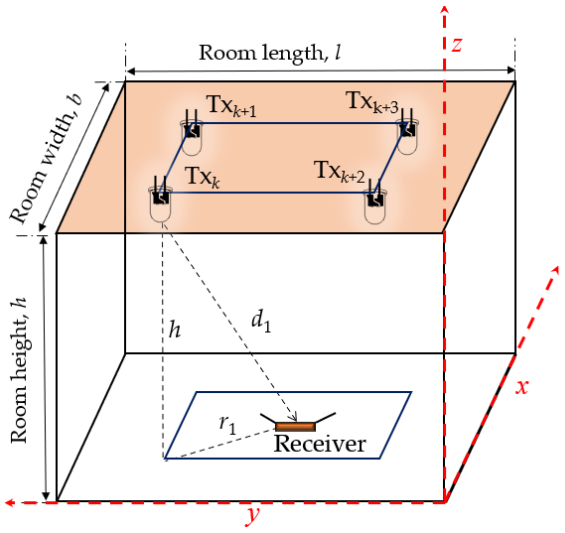

Fig. 3.8. A generalized model of indoor VLP.

VLP is a technology of determining the location of a receiver using the visible light signal transmitted from a base station. Usually, LEDs are used as the transmitters whereas the PDs or IS array are used to receive the positioning signal, which could contain information such as, the location of the LED or the LED-ID, or any other information relevant to the positioning process.

A generalized indoor VLP system is illustrated in Fig. 3.8, which utilizes pre-installed LEDs to transmit a positioning signal. Note that, in order to determine the location of the mobile device, it is always necessary to determine the information about the location of the LED lamps. The transmitter establishes world coordinates in the room using the Cartesian coordinate system. A unique coordinate is assigned to each LED. The implementation principle of the VLP system is illustrated in Fig. 3.9.

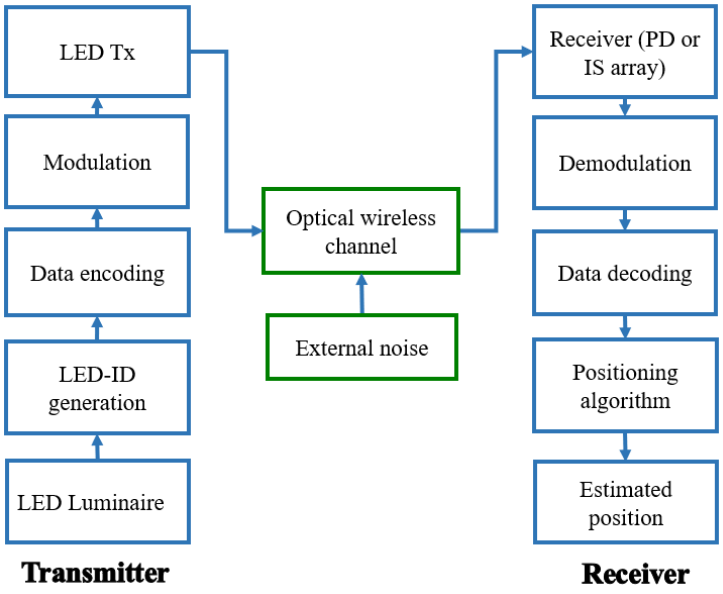

Fig. 3.9. The implementation principle of the VLP system.

In VLP systems, each LED transmits information on its unique landmark, (i.e., LED-ID, which can be either modulated signals or light characteristics of LEDs) through the optical wireless channels. The unique LED-ID creates a high-level and low-level voltage using the LED driver, that subsequently transmits the light intensity signal through fast on-off switching. Generally, indoor positioning systems include more than one LED in a room. As a result, it is necessary for the receiver to simultaneously receive LED-ID information from all the LEDs within the room. There are different multiplexing techniques, such as, frequency division multiplexing [118], time-division multiplexing [119], for avoiding the conflicts between different LED-ID signals. The signal is then transmitted through the optical wireless channel. At the receiver side, the receiver

receives the LED-ID information transmitted by each LED using a light-sensing device (IS array or PDs). Then, the received signals are demodulated, decoded in order to determine the world coordinates of each LED. After that, the receiver estimates the position by adopting an appropriate positioning algorithm, such as, RSS, TOA, or AOA.

The VLP system can be classified into two categories based on the receiver used, i.e., PD-based VLP and OCC-based VLP, which is depicted in Fig. 3.10. In PD-based VLP, the PDs are used as a receiver while in the latter one, an IS array is used as a receiver.

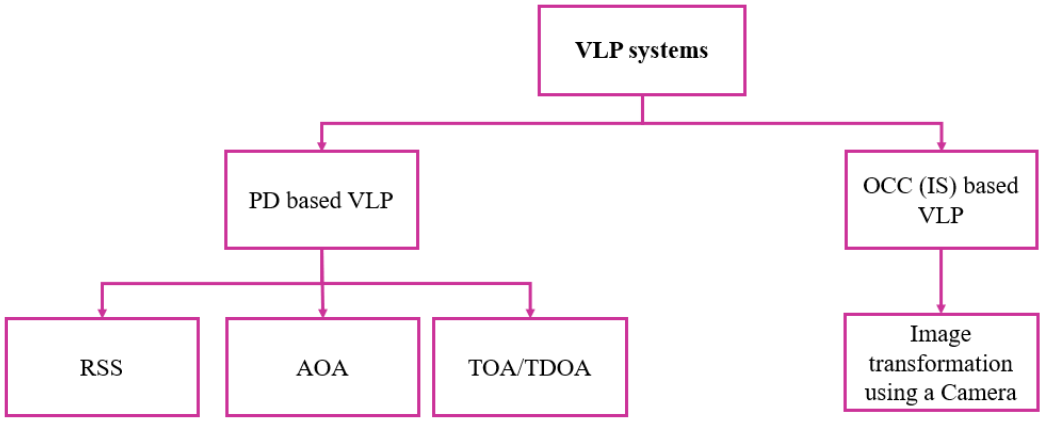

Fig. 3.10. A broad classification of the VLP system.

3.3.1 PD-based VLP

When an LED transmitter emits light, it propagates via an optical wireless channel, which results in intensity and phase variations. A PD is a solid-state device that detects incident light and converts it into an electric current that is directly proportional to the incident optical power. The signals received from each LED (whereby each LED has its own code and multiplexing protocol allowing differentiation between them) are then further processed. Most PD-based VLP systems rely on RSS, AOA, or TDOA information of received optical signals. These positioning algorithms are detailed in the following subsections.

3.3.1.1 Receiver Signal Strength

As described earlier in Chapter 2, RSS is one of the widely adopted triangulation techniques used in indoor positioning systems and VLP systems [16]. As the name implies, RSS is the strength of a received signal measured at the receiver. This is the simplest technique for realization and does not need any synchronization requirement between transmitter and receiver. In this technique, firstly received signal strength is determined and then, the propagation loss of the emitted signal is measured.

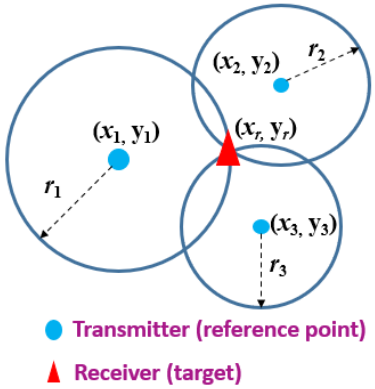

Fig. 3.11. Positioning based on RSS.

According to geometric properties, it is necessary to have a minimum of three transmitters at the center of the circle, where the estimated distance is regarded as the radius of the circle, see Fig. 3.11. Let (x_k, y_k) and (x_r, y_r) represent the position of k^{th} transmitter and the position of the receiver (target), respectively. The transmitter coordinates and the receiver coordinates are related with measured distance, r_k using the following equations:

$$(x_r - x_k)^2 + (y_r - y_k)^2 = {r_k}^2, \tag{3.7}$$

where $k = 1, 2, \ldots, K$ and K is the total number of transmitters involved in the measurement.

An important aspect of RSS is the measurement of r_k, i.e., the projection of the distance vector d_k on the *x*-*y* plane, see Fig. 3.8. The distance can also be computed as:

$$\|d_k\|^2 = \|r_k\|^2 + h^2, \tag{3.8}$$

where h is the vertical distance between the transmitter and the receiver planes. Therefore, the estimated distance between the receiver and the k^{th} transmitter can be estimated by solving (3.4) and (3.8), which is given by:

$$r_k = \sqrt{\left(\left(\frac{v+1}{2\pi}\right)\frac{P_{t,k}\, A_r \mathcal{R} h^{v+1}}{P_{r,k(\text{LOS})}}\right)^{\frac{2}{v+3}} - h^2}, \tag{3.9}$$

After estimating the horizontal distance, r_k LLS estimation algorithm is applied for position estimation.

3.3.1.1.1 Linear Least Square estimation

LLS is a general estimation method introduced by A. Legendre in the early 1800's. By considering the estimated distances of LOS paths, LLS is used to analyse the performance of the

VLP system in our work, which has a low complexity compared to NLLS. As mentioned earlier, (3.7) can be further re-written as:

$$\begin{cases} (x_r - x_1)^2 + (y_r - y_1)^2 = {r_1}^2 \\ (x_r - x_2)^2 + (y_r - y_2)^2 = {r_2}^2 \\ \vdots \\ (x_r - x_K)^2 + (y_r - y_K)^2 = {r_K}^2 \end{cases}, \tag{3.10}$$

A closed-form solution using the LLS estimation method is used to estimate the position of the receiver which is given by:

$$X = (A^T A)^{-1} A^T B, \tag{3.11}$$

$$A = \begin{bmatrix} x_2 - x_1 & y_2 - y_1 \\ x_3 - x_1 & y_3 - y_1 \\ x_4 - x_1 & y_4 - y_1 \end{bmatrix}, \quad B = 0.5 \times \begin{bmatrix} ({r_1}^2 - {r_2}^2) + ({x_2}^2 + {y_2}^2) - ({x_1}^2 + {y_1}^2) \\ ({r_1}^2 - {r_3}^2) + ({x_3}^2 + {y_3}^2) - ({x_1}^2 + {y_1}^2) \\ ({r_1}^2 - {r_4}^2) + ({x_4}^2 + {y_4}^2) - ({x_1}^2 + {y_1}^2) \end{bmatrix}. \tag{3.12}$$

where $X = \begin{bmatrix} x_r \\ y_r \end{bmatrix}$, which is the estimated receiver position.

3.3.1.2 Angle of Arrival

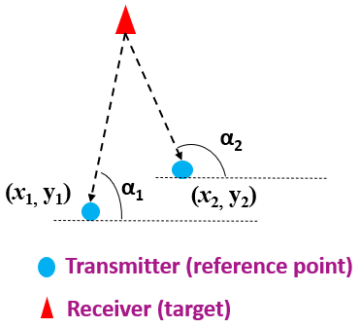

Fig. 3.12. Positioning based on the AOA.

As the name suggests, AOA is a technique that measures the angle of arriving signals from different reference points to the receiver. Fig. 3.12. depicts the mechanism of AOA. One of the main advantages of AOA-based VLP systems is that they do not require any time synchronization between the transmitter and receiver. They do not need a precise measurement of signal strength. Furthermore, ISs (i.e., cameras) are easier to use for finding the AOA of the signals than complex antenna arrays, RF-based positioning systems. For mathematical expression, let α_k denote the AOA measurement with respect to the k^{th} transmitter, which is given as:

$$\tan \alpha_k = \frac{y_r - y_k}{x_r - x_k} \tag{3.13}$$

LLS solution of AOA-based system is solved by the matrix form represented in the general expression, where *A* and *B* matrices are given by:

$$A = \begin{bmatrix} -\sin\alpha_1 & \cos\alpha_1 \\ \vdots & \vdots \\ -\sin\alpha_K & \cos\alpha_K \end{bmatrix}, \qquad B = \begin{bmatrix} y_1\cos\alpha_1 - x_1\sin\alpha_1 \\ \vdots \\ y_K\cos\alpha_K - x_K\sin\alpha_K \end{bmatrix}. \tag{3.14}$$

3.3.1.3 Time of Arrival/ Time difference of arrival

One of the most prevailing methods for positioning is TOA used in GPS. TOA is the absolute travel time of a wireless signal from the transmitter to the receiver. GPS precision is achieved through very tight synchronization conditions between all satellites within the network, often relying on atomic clocks. Thus, IPSs normally adopt TDOA instead of TOA to avoid the requirement of precise synchronization. Although, time synchronization is still required between the transmitters. Fig. 3.13. shows the intersection of hyperbolas which determine the location of the target.

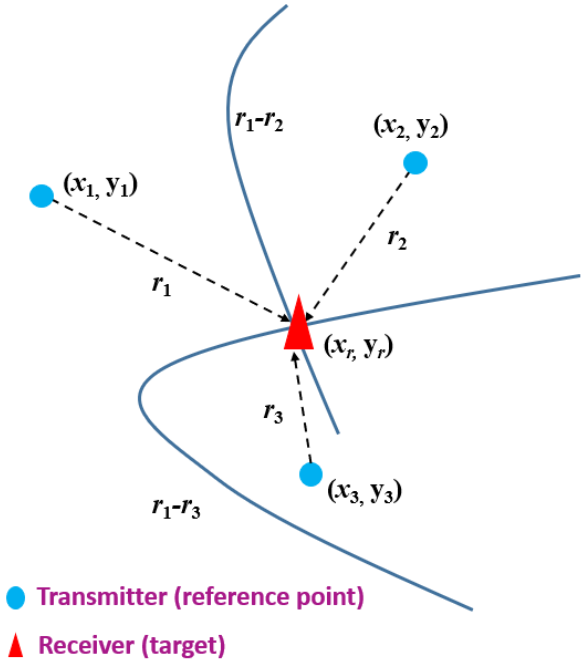

Fig. 3.13. Positioning based on the TDOA.

Each hyperbola in Fig. 3.13 represents a set of possible positions of the receiver which are determined by single measurement of the differences in range. Each hyperbola is represented as:

$$D_{k,k+1} = r_{k+1} - r_k = \sqrt{(x_{k+1} - x_r)^2 + (y_{k+1} - y_r)^2} - \sqrt{(x_k - x_r)^2 + (y_k - y_r)^2} \tag{3.15}$$

where $D_{k,k+1}$ is the difference between the ranges $r_{k+1}$and r_k. For the TDOA technique, LLS solution is solved by the matrix form represented in the general expression, where *A* and *B* matrices are given by:

$$A = \begin{bmatrix} x_2 - x_1 & y_2 - y_1 & D_{2,1} \\ \vdots & \vdots & \vdots \\ x_K - x_1 & y_K - y_1 & D_{K,1} \end{bmatrix}, B = \begin{bmatrix} (x_2^2 + y_2^2) - (x_1^2 + y_1^2) - D_{2,1}^2 \\ \vdots \\ (x_K^2 + y_K^2) - (x_1^2 + y_1^2) - D_{K,1}^2 \end{bmatrix}. \quad (3.16)$$

3.3.2 OCC based VLP

OCC-based VLP systems utilize IS arrays or cameras as a receiver. Cameras are optical devices that enable incident light to capture an image on a light-sensitive surface (image sensor) which translates the 3D world into a 2D projection in front of them. In general, it consists of an image sensor and a lens, which focus and direct light rays into the image sensor. Ideally, a pinhole camera model can be used to describe this 2D-to-3D mathematical relationship. According to this model, the incident light passes through the lens (i.e., an infinitely small hole) of the camera during the illumination process and creates an inverted image on the image plane. An image plane can be defined as an infinite plane with an infinite sampling resolution. A pinhole camera is therefore considered to have infinite depth of field, because everything in the image is projected in focus. It has a focal length (*F*) similar to the real camera that corresponds to the distance between the image plane and the focal center (F_c). This focal length impacts the FOV and the amount of distortion caused by perspective. For instance, a longer focal length provides a narrower FOV with less perspective distortion while a shorter focal length leads to a wider FOV with more perspective distortion. In the end, the image of the scene is projected onto the image plane which has been flipped onto both axes by the passing of light rays through the pinhole [120]. Figure 3.14 illustrates the geometrical model for the pinhole camera.

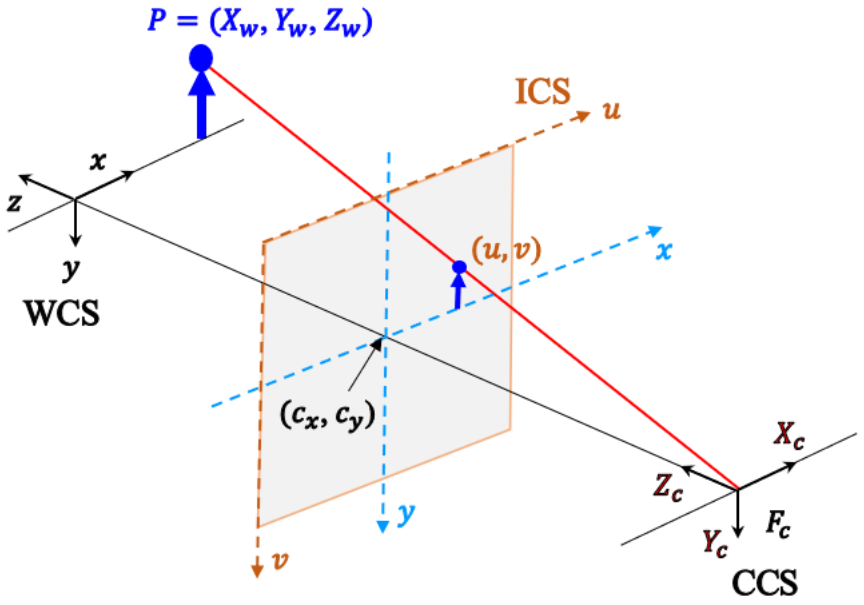

Fig. 3.14. A geometrical model for the pinhole camera.

According to the standard camera coordinate system (CCS), the X_c axis points to the right, the Y_c axis points downwards, and the Z_c axis points to the front. As shown in Figure 3.14, an arbitrarily selected point P is projected onto the image plane at (u,v) in the image coordinate system (ICS). Note that, matrix representations are used for all operations in this subsection, and homogeneous coordinates are also utilized to represent multiple points in both 2D and 3D space. In the pinhole camera model, a distortion-free projective transformation that translates 3D points in world coordinates (X_w, Y_w, Z_w) into 2D positions in image coordinates (u,v) is given by [121]:

$$s\begin{bmatrix} u \\ v \\ 1 \end{bmatrix} = \begin{bmatrix} f_x & 0 & c_x \\ 0 & f_y & c_y \\ 0 & 0 & 1 \end{bmatrix} \begin{bmatrix} r_{11} & r_{12} & r_{13} & t_x \\ r_{21} & r_{22} & r_{23} & t_y \\ r_{31} & r_{32} & r_{33} & t_z \end{bmatrix} \begin{bmatrix} X_w \\ Y_w \\ Z_w \\ 1 \end{bmatrix}, \tag{3.17}$$

which is equivalent to:

$$s\begin{bmatrix} u \\ v \\ 1 \end{bmatrix} = A[R|t] \begin{bmatrix} X_w \\ Y_w \\ Z_w \\ 1 \end{bmatrix}, \tag{3.18}$$

where

$$A = \begin{bmatrix} f_x & 0 & c_x \\ 0 & f_y & c_y \\ 0 & 0 & 1 \end{bmatrix}, \tag{3.19}$$

$$R = \begin{bmatrix} r_{11} & r_{12} & r_{13} & t_x \\ r_{21} & r_{22} & r_{23} & t_y \\ r_{31} & r_{32} & r_{33} & t_z \end{bmatrix}, \tag{3.20}$$

$$t = \begin{bmatrix} t_x \\ t_y \\ t_z \end{bmatrix}, \tag{3.21}$$

where *s* is the projective transformation's arbitrary scaling, *A* is the camera intrinsic matrix composed of the focal lengths f_x and f_y which are expressed in pixels, and the principal point (c_x, c_y), *R* and *t* are the rotation matrix and translation vector, respectively. With the following expressions, focal lengths are converted from meters to pixels:

$$f_x = F\frac{N_x}{W}, \tag{3.22}$$

$$f_y = F\frac{N_y}{W}, \tag{3.23}$$

where *F* is the focal length in meters, *W* and *H* are the width and height of the image sensor, which is also in meters, N_x and N_y are the total number of pixels in both axes. The translation vector (t_x, t_y, t_z) corresponds directly to the position of the camera in the world coordinate system (WCS). In order to determine the camera's orientation, *R* is represented by three rotation matrices signifying rotations around each angle, which is given by:

$$R = R_z R_y R_x\,, \tag{3.24}$$

$$R_x = \begin{bmatrix} 1 & 0 & 0 \\ 0 & \cos(\theta_x) & -\sin(\theta_x) \\ 0 & \sin(\theta_x) & \cos(\theta_x) \end{bmatrix}, \tag{3.25}$$

$$R_y = \begin{bmatrix} \cos(\theta_y) & 0 & \sin(\theta_y) \\ 0 & 1 & 0 \\ -\sin(\theta_y) & 0 & \cos(\theta_y) \end{bmatrix}, \tag{3.26}$$

$$R_{xz} = \begin{bmatrix} \cos(\theta_z) & -\sin(\theta_z) & 0 \\ \sin(\theta_z) & \cos(\theta_z) & 0 \\ 0 & 0 & 1 \end{bmatrix}. \tag{3.27}$$

The angles $(\theta_x, \theta_y, \theta_z)$ are the Euler angles which represent the orientation of the camera in the WCS, in radians. Note that, lens distortion is not considered in our work.

Chapter 4: Methodology

This chapter focuses on the methods developed and employed in this thesis which include the estimation methods, ANNs, CNNs, required for positioning. Both PD-based VLP systems using RSS algorithm as well as OCC-based VLP systems using a camera as a receiver are employed in our work. Note that each publication covered in Chapter 5 provides a detailed description of the precise method by which the experiments or simulations were carried out.

4.1 Non-Linear Least Square Estimation

LLS estimation can be extended for use with a much larger and more general class of functions with NLLS estimation. An NLLS model can incorporate almost any function that can be written in closed form. Nevertheless, the process of estimating the unknown parameters in the function is conceptually similar to that of LLS. However, the LLS estimation solution may not offer a high positioning accuracy [122]. This is especially true for situations where the received signal strength cannot be modelled precisely by the LOS model, this happens in regions close to walls or corners of a room, or due to the presence of furniture or users in the environment. NLLS estimation can be used to estimate the target location, in which the solution can be estimated by attaining $\tilde{X} = [\tilde{x}, \tilde{y}]$ that minimizes a cost function given by:

$$\tilde{Q} = \sum_{k=1}^{K} \left(\sqrt{(x_r - x_k)^2 + (y_r - y_k)^2} - r_k \right)^2 . \tag{4.1}$$

An iterative procedure is utilized to estimate $\tilde{X}$ by employing the trust-region reflective algorithm [123]. In this algorithm, first, an estimate is introduced as $\tilde{X}_0$, followed by computing the corresponding cost function $\tilde{Q}_0$. Next, several points about $\tilde{X}_0$ are replaced in (4.1), and the one that minimizes the cost $\tilde{Q}_1$ is selected as $\tilde{X}_1$. The receiver coordinates $\tilde{X}$ will eventually be obtained following several iterative steps to ensure convergence of $\tilde{Q}$. In our work, the initial value for $\tilde{X}_0$ is estimated using an LLS approach.

4.2 Polynomial Regression

Polynomial regression is a type of regression. When there is a non-linear relationship between the dependent and independent variables, then some polynomial terms are added to the linear regression in order to convert it into polynomial regression. In the case of NLOS links, high errors are introduced in the channel due to the presence of reflections [35,36], therefore the distance estimation approach using (3.9) is no longer valid. Therefore, it is possible to use polynomial

regression to generate a polynomial fitted model for the power and distance relationship defined by:

$$d_k = a_0 + a_1 P_{R,k} + a_2 \left(P_{R,k}\right)^2 + \cdots + a_j \left(P_{R,k}\right)^j, \tag{4.2}$$

where a_j is the coefficient of the fitted polynomial at j^{th} degree polynomial and $P_{R,k}$ is the total received power at the receiver from k^{th} transmitter. Note, d_k is computed using (4.2), which is then substituted into (3.8) to determine r_k. After that, LLS estimation or NLLS estimation is used for estimating the receiver position. The polynomial regression has a huge impact on the positioning error. For instance, Fig 4.1 shows the cumulative distribution function (CDF) against the positioning errors for NLLS estimation with and without polynomial regression. It is realized that, there is an evident improvement in the positioning accuracy by using NLLS estimation with polynomial regression for power-distance modeling. Therefore, the polynomial regression can improve the accuracy of position estimation without the inclusion of high complexity algorithms. However, there are some limitations of the polynomial regression; for instance, the coefficients of the polynomial model must be provided along with the transmitter's positions in practical scenarios.

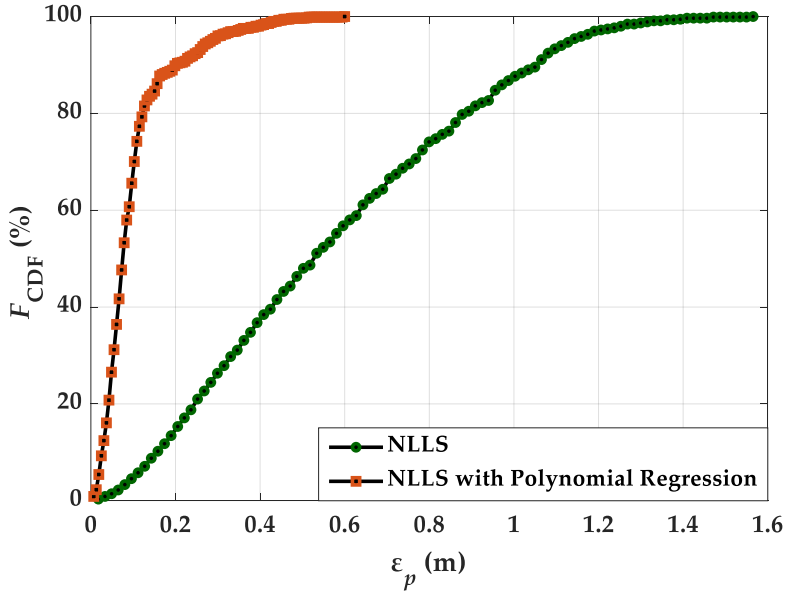

Fig. 4.1. CDF of the positioning error computed by NLLS and NLLS with polynomial regression estimation [108].

4.3 Support Vector Machines

Support vector machines (SVM) is a supervised machine learning algorithm used for solving classification and regression problems. SVM classifies data by achieving the best hyperplane that distinguishes all data points of one class from those of another class. The best hyperplane is the one with the largest margin between two (different) classes. Although SVMs were originally developed for binary class classification, they can be extended to multiclass classification. The multiclass problem is split into multiple binary classification cases, also known as one-vs-one classification, as depicted in Fig. 4.2.

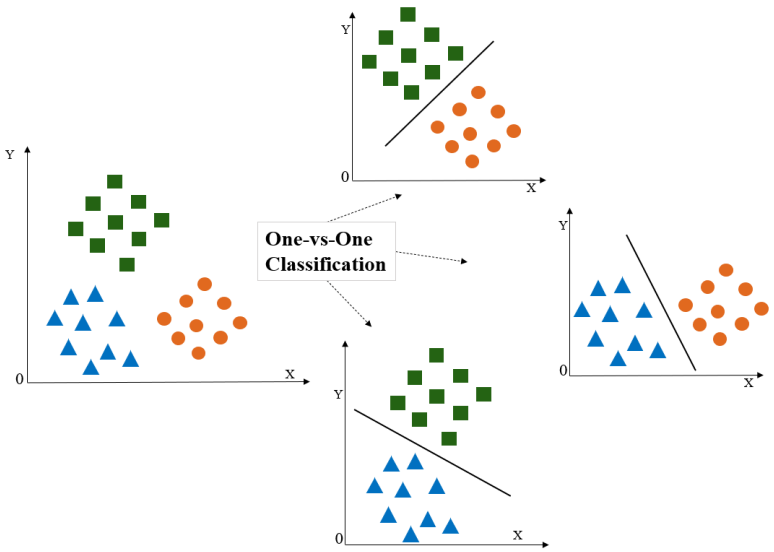

Fig. 4.2. The schematic diagram of one-vs-one multiclass SVM.

In one-vs-one classification, a series of classifiers are employed to each pair of classes, with the most frequent class identifier [124]. SVMs also need the training of different classifiers using the data from each pair of classes. The number of classifiers N_c required for one-vs-one multiclass classification can be retrieved by [124]:

$$N_c = \frac{\delta \times (\delta - 1)}{2}, \tag{4.3}$$

where δ represents the number of classes. In this work, the SVM is used to classify the minimum positioning error based on different regions, so the number of classes is given by the number of regions.

For non-linear problems, the training data is not linearly separable in the original input space. Therefore, mapping of the original input space into a high-dimensional space is done using a concept called kernel trick [124]. In this algorithm, *N* training samples are considered. Each

sample is indicated by (u_i, p_i), where u_i corresponds to the attribute set for the i^{th} sample (i = 1, 2, …, N), and p_i correspond to the i^{th} label. The SVM classifier can be defined as:

$$f(u) = \sum_{i,j=1}^{N} L_i\, p_i\, G\left(u_i, u_j\right) + b, \tag{4.4}$$

where L_i is the Lagrange multiplier, and b is the bias term. $G\left(u_i, u_j\right)$ is the kernel function, and u_j is any data point in the sample. In this work, the 3rd order polynomial kernel is used, which is given by:

$$G\left(u_i, u_j\right) = \left(u_i^{\mathrm{T}}.u_j + c\right)^d, \tag{4.5}$$

where c is the constant, T represents the transpose, and d is the degree of the polynomial [124]. Lagrange multipliers are obtained using convex quadratic optimization algorithms [123].

4.4 Artificial Neural Networks

The artificial neural network is inspired by the process of the human brain and therefore, is composed of neurons that work in parallel. Each neuron is capable of performing a simple mathematical operation individually [125]. Collectively, the neurons can evaluate complex problems, emulating most of the functions and providing precise solutions. The ANN is an interconnected network of processing elements (neurons) and it includes two different phases: (*i*) the training phase - where the ANN estimates an input-output map based on the training data set. During this training phase, the neuron weights are continuously adapted to minimize the error between the estimated output and the training data vectors. The process terminates when the required performance is achieved, or the complete training set is used; and (*ii*) the operation phase - where the ANN is employed to perform estimates based on the input data alone. The ANN structure consists of at least three layers; a single input layer, one or several hidden layers (HL), and a single output layer, see Fig. 4.3(a). These layers are linked together based on a collection of connected units or nodes, called the artificial neurons. The importance of these neurons is defined based on their weights and the learning process. The weight W_{in}^{m} has the capability to acquire and store experimental knowledge, where *i*, *n*, and *m* represent the number of neurons, inputs, and layers, respectively. These are also known as the synaptic weights because their working principle is similar to the synapses present in biological brains. It relates the n^{th} input to the j^{th} neuron.

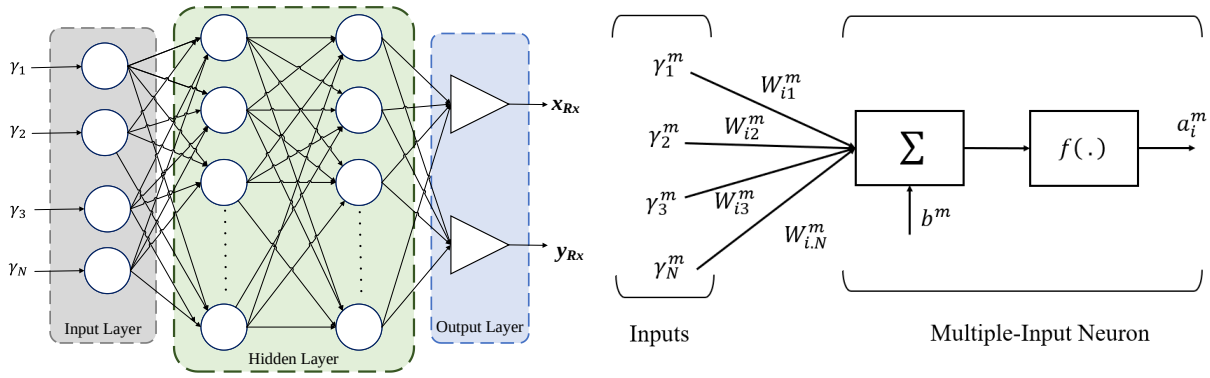

(a) (b)

Fig. 4.3. The artificial neural network with: (a) basic structure, and (b) a structure of i^{th} neuron with N inputs in the layer m.

Note, the number of neurons in the hidden layer controls the weights and the bias in the network. Each neuron can be biased with a value b^m as depicted in Fig. 4.3(b). Since Sigmoid and linear activation functions have been shown to perform well in regression tasks [126], they were selected for the hidden and output layers, respectively. The performance of an ANN algorithm is measured by the mean square error, which can be expressed as a function of $F(p_i^m)$ as:

$$F(p_i^m) = e_i^m = \|t_i^m - a_i^m\|_2, \tag{4.6}$$

where p_i is the vector containing all network weights and biases for the i^{th} neuron (i.e., $p_i = [W_i, b_i]$), and a_i^m is the network output of the i^{th} neuron for the m^{th} layer and t_i^m is the target output of the i^{th} neuron for the m^{th} layer. The weights and the bias are updated by the backpropagation method [125] as:

$$W_{i,n+1}^m = W_{i,n}^m - GS^m(a_i^{m-1})^T, \tag{4.7}$$

$$b_{i,n+1}^m = b_{i,n}^m - GS^m, \tag{4.8}$$

where G is the learning rate, $m = 0,1,\dots,M-1$, M is the number of layers in the network, and $(.)^T$ is the transposed. $b_{i,n}^m$ is the bias vector. S^m is the sensitivity matrix, which is evaluated from the least mean square error function, $\hat{F}(p_i^m)$ for various values of j, wherein j is defined in the matrix form as $\gamma_i W_i + b_i$. γ_i is the input vector of i^{th} neuron.

The aim of this work is to investigate the utilization of ANN for regression analysis in the VLP system. A comprehensive study is done about the optimization of an ANN for VLP systems and a complete assessment of its performance. The error performance of the proposed system is evaluated under a noisy channel by considering noise over a wide range of SNR. For that, three different ANN algorithms, including Levenberg-Marquardt (LM), Bayesian regularization (BR), and scaled conjugate gradient (SCG) algorithms, are explored to minimize positioning error of the proposed VLP system. The error performance is analyzed and compared with the traditional RSS technique, which uses an NLLS algorithm along with a polynomial regression model [127]. Firstly, the proposed ANN is optimized based on the number of neurons in the hidden layers (HLs) and the number of training epochs. Finally, the noise performance of the proposed system is analyzed in comparison with the traditional approaches. In addition, the ANN structure in the proposed study is composed of four layers: an input layer, two HLs, and an output layer. Each layer has a different number of neurons, with the input and output layers having four and two neurons, respectively. The estimated x and y position coordinates are represented by the output neurons. The estimated distances from each transmitter are applied to the input layer with the help of (4.5).

In our work, the number of HLs are investigated and have determined that a simple ANN with only one hidden layer would not provide the desired results i.e., high positioning errors. Using two hidden layers provided a more effective framework for achieving improved performance. Therefore, based on our preliminary research, the number of hidden layers are limited to two. The neurons in the HLs are activated using a Sigmoid transfer function, which thresholds the input data and outputs a continuous value between zero and one. A linear transfer function is used in the output layer.

Following that, a few well-known training algorithms are adopted and used to analyze the positioning error of the proposed system. For our investigation, the default values of Matlab's fitnet tool are used to fix the parameters such as the learning rate. Note that, other parameters such as the number of neurons in HLs or the activation functions could also be optimized based on the topology of the HLs.

The network records the trained information in W_{in}^{m} and b^{m}. Note, the ANN can be trained in supervised and unsupervised modes, where the former offers higher reliability compared with the latter; thus, it is adopted in this work as explained in the following subsections.

4.4.1 Levenberg-Marquardt Algorithm

LM algorithm is employed to solve the NLLS problems. By leveraging the most used optimization algorithms (i.e., Gauss-Newton algorithm, and the steepest descent algorithm), the LM algorithm can avoid some problems, such as over-parameterization, local minima, and non-existence of the inverse matrix [128]. Moreover, it inherits the speed advantage of Gauss-Newton algorithm and the stability of the steepest descent algorithm. The updated rule of weights and biases, i.e., p_i is given by:

$$p_{i+1} = p_i - [J_i^T J_i + \mu_i \mathrm{I}]^{-1}. J_i e_i, \tag{4.9}$$

where J_i is Jacobian matrix of the function, $F(p_i)$, and $\mu_i \geq 0$ is a scalar, and I is the identity matrix.

4.4.2 Bayesian Regularization Algorithm

BR is an algorithm that updates the values of weight and bias in accordance with LM optimization. In this algorithm, firstly, a linear combination of the squared errors and the weights are minimized and then, the linear combination is modified with the aim of obtaining a network with good generalization qualities [125]. In BR, the mean squared error function can be defined as:

$$F(p_i) = \beta E_D + \alpha E_W, \tag{4.10}$$

where E_D is the squared error, E_W is the sum of squared weights, which penalizes large weights in reaching a better generalization and smoother mapping, α, and β are the regularization parameters (or objective functions), which are given as:

$$\alpha = \frac{\gamma_e}{2E_W(p_i)}, \beta = \frac{N_{wb} - \gamma_e}{2E_D(p_i).}, \tag{4.11}$$

where $\gamma_e = N - 2\alpha \mathrm{tr}(H^{-1})$ is called the effective number of parameters, $H = \nabla^2 F(p_i)$ is the Hessian matrix, N_{wb} is the total number of parameters (weights and biases) of the network, $\mathrm{tr}(H^{-1})$ is the trace of the inverse of Hessian matrix. Note, the 2nd term in (4.11) is known as the weight decay, and therefore small values of W would reduce the overfitting of the model.

4.4.3 Scaled Conjugate Gradient Algorithm

Most of the conjugate gradient algorithms use line search for each iteration, thus making them computationally complex. Therefore, to address this the SCG algorithm is adopted developed by Moller [129]. SCG is based on conjugate directions without performing line search, with

reduced computational complexity. The SCG algorithm, which is a scaled conjugate gradient method for updating the weight and bias values, is robust and does not depend on the user-defined parameters given that the step size is a function of quadratic approximation of the error [129]. Different approaches are used for estimating the step size, which is given by:

$$\xi_i = \frac{\mu_i}{\delta_i} = \frac{-\bar{p}_i^T E'_{qw}(p_i)}{\bar{p}_i^T \bar{s}_i + \lambda_k |\bar{p}_i|^2}, \tag{4.12}$$

where $E'_{qw}(p_i)$ is the quadratic approximation of the error function, $F(p_i)$. $\bar{p}_1, \bar{p}_2, \ldots . \bar{p}_i$ is the set of non-zero weight vectors, and $\bar{s}_k$ is the second-order information. λ_i is the scaler to be updated such that:

$$\lambda_i = 2\left(\lambda_i - \frac{\delta_i}{|\bar{p}_i|^2}\right). \tag{4.13}$$

If $\Delta_i > 0.75$, then $\lambda_i = \frac{\lambda_i}{4}$, and if $\Delta_i < 0.25$ then $\lambda_i = \lambda_i + \frac{\delta_i(1-\Delta_i)}{|\bar{p}_i|^2}$.

Δ_i is a comparison parameter given by:

$$\Delta_i = \frac{2\delta_i[F(p_i) - F(p_i + \xi_i \bar{p}_i)]}{\mu_i^2}. \tag{4.14}$$

4.5 Single-Shot Detector

SSD is an object detection model that uses feed-forward convolutional networks to generate a set of fixed-size bounding boxes and scores that indicate the presence of an object class instance in each box. Following this, an additional non-maximum suppression step is performed to detect final objects [130]. In SSD, only a single shot is required to detect multiple objects within the image. As illustrated in Fig. 4.4, the SSD object detection model comprises of two main blocks: *i*) feature extractor block and *ii*) extra feature block in which convolutional filters are applied for object detection. The model adopted in our work is the pre-trained *SSD_MobileNet_v2_COCO* and *SSD_ResNet50_v1_COCO*, which embeds all the enumerated features.

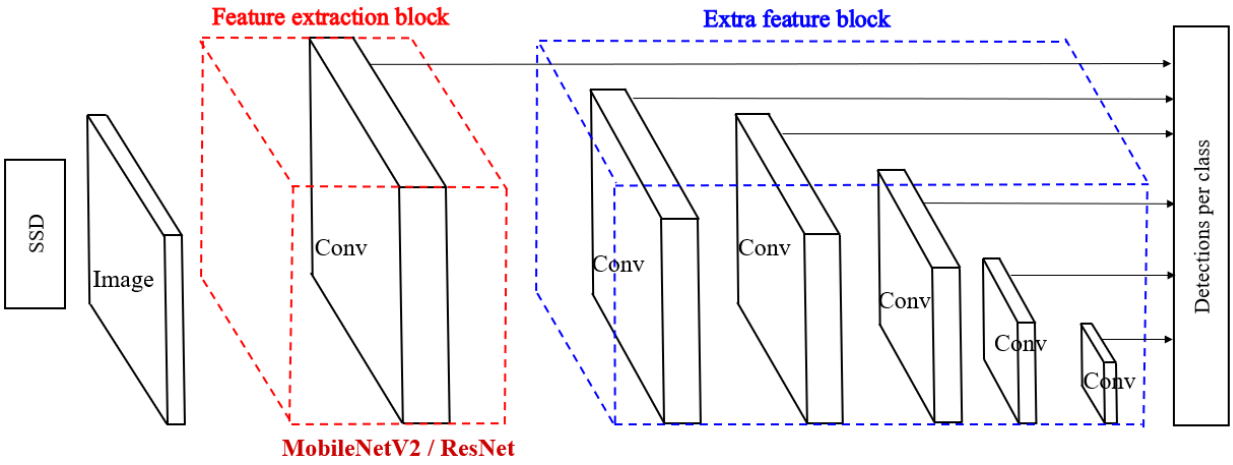

Fig. 4.4. SSD network structure of the indoor VLP system.

In our work, two different methods are used for feature maps extraction, i.e., MobileNetV2 [131] and ResNet [132] for high-quality image classification, which is named as the feature extractor network (in our case, it is either MobileNetV2 or ResNet) which will be explained later in this subsection. Following that, an auxiliary structure with the following key features is added to the network for object detection:

Multi-scale feature maps for detection: The convolutional feature layers are added to the end of the feature extractor network. Each layer of this model decreases in size gradually and allows predictions of detections on multiple scales. Each feature layer has a different convolutional model for predicting detections. These multi-scale feature maps improve the accuracy of the model significantly.

Convolutional predictors for object detection: SSD does not have any delegated region proposal network, rather it uses a very simple method. It utilizes small convolution filters to calculate both the location and class scores. For a feature layer of size m × n with p channels, the basic component for predicting parameters is a 3 × 3 × p small kernel, which produces a score for each category or an offset for each shape in relation to the default box coordinates. Every time the kernel is applied at one of the m × n locations, an output value is produced. The bounding box offset output value is determined relative to a default box position for each corresponding feature map location.

4.5.1 SSD Training

The most significant difference between training an SSD and a traditional detector (such as, region-based CNNs, i.e., R-CNNs), is that the ground truth information must be assigned to specific outputs in a fixed set of detector outputs. After the assignment, the loss function and

backpropagation are employed end-to-end [133]–[135]. In addition to selecting a set of default boxes and scales for detection, the training also includes hard negative mining which is explained below in detail:

Matching strategy: The predictions of SSD are categorized as positive matches or negative matches. SSD considers the positive matches only for the calculation of localization cost (the boundary box mismatch). It is measured by Intersection over Union (IoU) parameter which is the ratio between the intersected area over the joined area for two regions. The match is positive if the corresponding default boundary box (not the predicted boundary box) has an IoU > 0.5 with the ground truth, otherwise, it is negative. Once the positive matches have been identified, the cost is calculated using the predicted boundary boxes. This matching strategy encourages each prediction to predict shapes closer to the corresponding default box. As a result, our training predictions are more stable and diverse.

Training objective: The objective of SSD training is derived from the MultiBox objective [135], but is extended to process multiple object categories. Let $x_{ij}^{p} = \{1,0\}$ be an indicator for matching the i^{th} default box to the j^{th} ground box of the category p. In the matching strategy above, there is $\sum_i x_{ij}^{p} \geq 1$. The overall objective loss function is defined as a weighted sum of both localization loss L_{loc} and confidence loss L_{conf}, which is defined as:

$$L(x, c, l, g) = \frac{1}{N_P}\Big(L_{conf}(x, c) + \epsilon L_{loc}(x, l, g)\Big). \tag{4.15}$$

where N_P is the number of positive matches and ϵ is the weight for the localization loss. For N_P = 0, the loss is set to 0. The localization loss is the mismatch between the ground truth and the predicted boundary boxes. Smooth L1 loss is used between the predicted box l and the ground truth box g parameters [136]. As mentioned earlier, SSD only considers predictions from the positive matches, and therefore, negative matches can be ignored. Similar to Faster R-CNN [134], offsets are regressed for the center (cx; cy) of the default bounding box d and for its width w and height h. The L_{loc} and L_{conf} are computed as [137]:

$$\begin{gathered} L_{loc}(x, l, g) = \sum_{i \in Pos}^{N} \sum_{m \in \{cx,cy,w,h\}} x_{ij}^{k} \text{smooth}_{\text{L1}}\left(l_i^m - \hat{g}_j^m\right) \\ \hat{g}_j^{cx} = \frac{\left(g_j^{cx} - d_i^{cx}\right)}{d_i^w} \qquad\qquad \hat{g}_j^{cy} = \frac{\left(g_j^{cy} - d_i^{cy}\right)}{d_i^h} \end{gathered} \tag{4.16}$$

$$\hat{g}_j^w = log\left(\frac{(g_j^w)}{d_i^w}\right) \qquad\qquad \hat{g}_j^h = log\left(\frac{(g_j^h)}{d_i^h}\right).$$

The confidence loss is the loss of making a class prediction. Note, for the matching with (*i*) positive prediction, a loss is incurred according to the confidence score of the class corresponding to the prediction; and (*ii*) negative prediction, the loss is incurred according to the confidence score of the class "0" (i.e., the class "0" indicates that no object being detected). The confidence loss is computed as the Softmax loss over multiple classes confidences, *c* (class score). The Softmax loss consists of Softmax activation combined with a cross-entropy loss. The Softmax activation function provides a probability for each class, and the summation of these probabilities adds up to unity. The Cross entropy loss is the result of summing the negative logarithm of probabilities as given by:

$$L_{conf}(x,c) = -\sum_{i\in Pos}^{N} x_{ij}^p log\left(\hat{c}_i^p\right) - \sum_{i\in Neg} log(\hat{c}_i^0), \tag{4.17}$$

where $\hat{c}_i^p = \frac{exp(c_i^p)}{\sum_p exp(c_i^p)}$ and the weight term ϵ is set to 1 by cross-validation.

Choosing scales and aspect ratios for default boxes: The default boundary boxes are selected manually. For that, SSD specifies a scale value for each layer of feature maps. For example, if *f* feature maps are to be used for prediction. The scale, s_k of the default boundary boxes for each feature map is then calculated as:

$$s_f = s_{\min} + \frac{s_{\max} - s_{\min}}{f-1}(k-1), \qquad k \in [1,f] \tag{4.18}$$

where $s_{\min}$ and $s_{\max}$ are 0.2 and 0.9, respectively. It implies that the lowest layer has a scale value of 0.2 and the highest layer has a scale value of 0.9, and all layers are regularly spaced between them. The width and height of the default box can be computed by combining the scale value with the target aspect ratios. For instance, for the layers making 6 predictions, SSD start with different aspect ratios that are imposed on the default boxes and donate them as $a_{\text{ratio}} \in \left\{1,2,3,\frac{1}{2},\frac{1}{3}\right\}$. Then the width and the height of the default boxes are computed as:

$$w_f^a = s_f.\sqrt{a_{\text{ratio}}},$$
$$h_f^a = \frac{s_f}{\sqrt{a_{\text{ratio}}}}. \tag{4.19}$$

A default box is also added for the aspect ratio of 1, whose scale is $\acute{s_f} = \sqrt{s_f s_{f+1}}$, resulting in 6 default boxes per feature map location.

Hard negative mining: However, SSD makes a lot more predictions than there are objects, so there are more negative matches than positive matches, creating a class imbalance during training. The model is trained to learn background space instead of detecting objects. Although SSD still requires negative sampling in order to learn what is a bad prediction. Therefore, the negatives are sorted based on their highest confidence loss instead of using all the negatives. SSD selects the negatives that have the highest loss and ensures the ratio between selected negatives and positives is at most 3:1. This enables faster and more stable training performance.

4.5.2 ResNet

A ResNet is a type of neural network that consists of sequences of convolutions bypassed by skip connections, thus allowing the model to learn residual values within the convolutional layers [138]. The ResNet-50 model presented in [132], incorporates 16 bottleneck blocks and 50 layers with trainable parameters, including a convolutional layer following the input and output layer.

4.5.3 MobileNetV2

MobileNetV2 uses a depthwise convolutional layer [131]. The number of input channels in the depthwise convolution layer equals the number of filter channels. This layer reduces the total number of parameters to a minimum. MobileNet v2 introduces a new layer called 1 × 1 convolution layer, whose purpose is to increase the number of channels in the data prior to depthwise convolution is applied. There is a depthwise convolution layer followed by a 1 × 1 convolution layer is referred to as the pointwise/projection layer. The projection layer projects data with a high number of channels into the output with a much lower number of channels. The residual connection works similarly to ResNet to add gradients in MobileNetV2. ReLU6 is used to prevent too many activations.

4.6 SolvePnP Function

The perspective-n-point (PnP) is a well-known problem, in which the position of a camera is determined based on a set of correspondences between points in an image and their locations in the real world. In order to determine the position of the receiver (i.e., camera) in OCC-based VLP systems, the solvePnP function is used. This function can be found in OpenCV library, which produces a set of six coordinates corresponding to the position and orientation of the camera in the

real world [121]. The most important inputs that should be considered are object points; image points; camera matrix and solving method. The object points are corresponding to an array with the world coordinates for each point. In our work, the coordinates of each LED in the WCS are considered as object points. The image points are the coordinates of the LED in the ICS. The camera matrix defines the intrinsic parameters of the camera, which can be computed based on the camera specification. The method of solving the problem can be classified as one of two methods: P3P, and ITERATIVE. With the P3P method, it requires specifically four points, which is not suitable for our work, since we want to be able to make the position estimation from as many transmitters as possible, whenever possible, and not be restricted to four. While the iterative method require at least four points to estimate the position and permit the inclusion of a larger number of points. The iterative method is based on the Levenberg-Marquardt optimization. This algorithm works on the premise that identifies a pose that minimizes the reprojection error, which is a measure of the sum of the squares of the distances between the initial coordinates of each image point and the reprojected coordinates resulting from each guessed pose. Therefore, the iterative method is utilized in our work. The position of receiver can be determined if these four inputs are known.

Chapter 5: Research Outcomes

This chapter presents the outcomes as published and submitted research articles, including three published conference papers and two published peer-reviewed journal papers. The full and original papers with bibliographic citations and individual contributions to the report are provided in the following sections.

Firstly, a detailed survey on the VLP techniques has been done in section 5.1, where all traditional positioning algorithms used for indoor positioning are described in detail. The current trends in the VLP are also explained. In section 5.2, a VLP system relying on a single transmitter is proposed to infer position information. The system adopts a reverse trilateration scheme, where a set of three photodiodes is employed to estimate the position. The reverse trilateration scheme adopted for this system yields to a very simple mathematical framework, suitable for low power and low complexity systems. The position information is inferred through the received signal strength, without the need for sophisticated angle measurements or precise synchronization as is the case in AOA and time difference of arrival systems.

Following our previous research, it is realized that the accuracy of the RSS-based VLP system in indoor applications is constrained by the tilt angles of transmitters and receivers as well as multipath reflections. Therefore, for the first time, it is shown that tilting the transmitter can be beneficial in VLP systems considering both LOS and NLOS transmission paths as described in section 5.3. With the transmitters oriented towards the center of the receiving plane (i.e., the pointing center F), the received power level is maximized due to the LOS components on F. It revealed that the proposed scheme offers a significant accuracy improvement of up to ~66% compared with a typical non-tilted transmitter VLP at a dedicated location within a room using a low complex linear least square algorithm with polynomial regression. The effect of tilting the transmitter on the lighting uniformity is also investigated and results proved that the uniformity achieved complies with the European Standard EN 12464-1. Furthermore, it also demonstrated that the accuracy of VLP can be further enhanced with a minimum positioning error of 8 mm by changing the height of F.

In the previous studies, it is realized that LED-based indoor VLP system where the transmitter's positions are usually known, which is an advantage provided they have not been altered. However, when replacing the LEDs and carrying out regular maintenance ensuring uniform position and orientation of all light sources might not be practical. Therefore, the

transmitters will have some random placement and orientations, which will manifest as position and orientation errors. These errors can affect substantially the positioning accuracy of the system in applications where high accuracy is the main requirement e.g., in medical, manufacturing, etc. Therefore, it is believed that the approach adopted in the paper is valuable and significant. Thus, the impact of transmitter's position and orientation uncertainty on the RSS-based VLP accuracy is studied in section 5.4.

ANN has attracted much attention for solving regression problems. Therefore, an indoor VLP system that uses ANN for positioning estimation in the presence of both LOS and NLOS multipath signals is proposed in section 5.5. The aim of this work is to investigate the utilization of ANN for regression analysis in VLP systems. The error performance of the proposed system is evaluated under a noisy channel by adding noise over a wide range of SNR. For that, three different ANN algorithms including Levenberg-Marquardt, Bayesian regularization, and scaled conjugate gradient algorithms are explored to minimize the positioning error of our proposed VLP system. The error performance is analysed and compared with the traditional RSS technique which uses an NLLS algorithm along with a polynomial regression model.

Following our previous research based on the polynomial regression approach, the results from that research suggest that, the accuracy of the polynomial regression model depends on the specific area within the room. Therefore, section 5.6, focuses on the new indoor VLP system that is proposed based on the polynomial regression and SVM. In order to analyze it, two different environments are considered an empty room and a furnished room, where multipath channels are considered and estimated using OpticStudio® software. In both environments, the total room area is divided into different regions, such as, corners, the middle area of the room, regions near the walls, or depending on furniture layout, thus creating four different scenarios. At a second stage, polynomial fitting is carried out for these different regions and the position is estimated for the entire room using the polynomial regression approach. Finally, SVM is employed to perform the classification and select the best region based on the lowest positioning error.

Another prominent technology, i.e., Deep learning (DL) is a subfield of machine learning that outperforms traditional methods in a wide range of applications and has been extensively employed in estimating position. Therefore, a new visible light positioning system based on CNNs is proposed in which LEDs are used as transmitters and a rolling shutter camera is used as a receiver. A detection algorithm named SSD is used which relies on CNN (i.e, MobileNet or ResNet) for classification as well as position estimation of each LED in the image. Additionally,

a PnP problem algorithm is employed to estimate the receiver position. The system is validated using a real-world size test setup containing eight LED luminaries.

5.1 Current Trends on Visible Light Positioning Techniques

This section is a version of the published manuscript:

> **N. Chaudhary**, L. N. Alves, and Z. Ghassemlooy, 'Current Trends on Visible Light Positioning Techniques', in *2019 2nd West Asian Colloquium on Optical Wireless Communications (WACOWC)*, Tehran, Iran, Apr. 2019, pp. 100–105.

Connection to my Ph.D. thesis:

Firstly, a thorough review of the literature on visible light positioning techniques was conducted. This section briefly reviewed conventional positioning methods based on RSS, TDOA, and AOA. Then, it focused on the current research trends, relying on machine learning techniques, sensor fusion and communication requirements.

Current Trends on Visible Light Positioning Techniques

Neha Chaudhary
Instituto de Telecomunicações
University of Aveiro
Aveiro, Portugal
neha.chaudhary@ua.pt

Luis Nero Alves
Instituto de Telecomunicações
University of Aveiro
Aveiro, Portugal
nero@ua.pt

Zabih Ghassemblooy
Optical Comm. Research Group
Northumbria University
Newcastle-upon-Tyne, UK
z.ghassemlooy@northumbria.ac.uk

***Abstract*— This paper presents a survey on visible light positioning techniques. The paper briefly reviews conventional positioning methods based on Rx signal strength (RSS), time difference of arrival (TDOA) and angle of arrival (AOA). Then it focus on the current research trends, relying on the machine learning techniques, sensor fusion and communication requirements.**

Keywords—Visible light positioning (VLP), Machine learning, Neural networks, Modulation schemes.

I. INTRODUCTION

The need for accurate indoor positioning systems (IPSs) and location-based applications are developing day by day. IPS offer surveillance, navigation and object tracking services, which have an increasing number of applications in numerous areas, for example, indoor parking facilities, shopping malls, manufacturing, supermarkets, big warehouses, and autonomous navigation, to mention a few. Even though, global positioning system (GPS) has become one of the most popular example for outdoor positioning systems, it is unable to provide high precision in indoor environments, because the GPS signals (i.e., radio frequency (RF)) do not penetrate well through the building walls, which results in disruptive errors and cannot be used in mines and underground environments [1-3]. Already, a few different technologies, for example, ultrasound [4], radio waves [5], [6], radio frequency identification (RFID) [7], [8], Zigbee, Bluetooth [9] and ultra wide band (UWB) [10] have been investigated for IPSs. Indoor positioning systems (IPS) based on ultrasounds have large ranging and localization errors (the accuracy is 10 cm range) because of the fact that its wavelength is generally large, and the speed of sound is influenced by the temperature of environment [11]. RF based localization faces several problems including electromagnetic (EM) radiation, which restrict the use of RF based systems in some areas (i.e., medical, etc.). Moreover, RF signals are (*i*) affected by multipath effects in the indoor environment which increase localization errors; and (*ii*) constrained by the available spectrum, which is highly congested. RFID and UWB recognize signals for positioning with the help of dedicated infrastructure and special devices. Other positioning methods, such Zigbee and Bluetooth based systems are vulnerable to fluctuations in signal sources.

On a different edge, light has been used to infer location for a long time. Our ancestors used the stars to navigate the globe. The astrolabe and the quadrant are perhaps within the first tools to measure angles based on the light from the stars – a precursor of angle of arrival. More recently, the light intensity and pulsation of distant stars, widened our perception of how immense is the universe we live in. This was accomplished with the discovery of Cepheid stars, by Henrietta Leavitt, and used by Edwin Hubble, to reveal that the universe is much larger than our local galaxy [12-13].

Light emitting diodes (LEDs) based visible light positioning (VLP) techniques become more prominent for indoor positioning systems compared to other positioning systems because of advantages offered by the LED technology such as [14-17]: (*i*) free from EM interference; (*ii*) compliance with RoHs recommendations; (*iii*) longer lifetimes when compared with other light sources; (*iv*) energy efficient; and (*v*) low cost and allow fast switching – a feature which enables data transmission. In VLP systems, photodetectors (PDs) or camera (i.e., image sensors (ISs)) are commonly used at the Rx [18–22]. The formers are widely reported in the literature, whereas the latter offers higher positioning accuracy, but at the cost of complex positioning algorithm and the limited positioning speed. Currently, VLP technologies, are based on the triangulation technique where the distance or angle between transmitter (Tx) and receiver (Rx) needs to be estimated. The distance or the angle can be determined in a number of ways including received signal strength (RSS), angle of arrival (AOA), time of arrival (TOA) and time difference of arrival (TDOA) [20], [23]. These methods present their intricacies. The major drawback of AOA is that the system need expensive sensor arrays or ISs to measure the incident angle with high accuracy, which is needed in indoor environments [24]. TOA need accurate synchronization between Tx (LED) and Rx, which increases the deployment cost [25]. On the other hand, RSS needs accurate determination of the incident signal power, thus being strongly dependent on signal to noise ratio (SNR) [16]. Simple approaches, rely on proximity based and scene analysis, which trades simplicity with the accuracy [23]. These are suitable for low accuracy systems, not demanding high location precision.

Machine learning has been widely used for position estimation of RF-based IPSs, for example Wi-Fi, ZigBee and UWB. In [26], machine learning has been introduced for VLP for the first time. The system is capable of reaching 0.31 m of average accuracy in an indoor environment of dimension of 4.3×4×4 m. In [27], a VLP algorithm based on artificial neural network (ANN) was considered where positioning was achieved by a trained ANN in a diffuse channel. The sensor fusion and multi-technology approaches are also reported in the literature [34]. Additional sensors like compass or gyroscopes, are useful to provide attitude correction and heading of the sensor. Hybrid technologies are also a means to achieve higher positioning accuracies [37].

978-1-7281-3767-4/19/$31.00 ©2019 IEEE

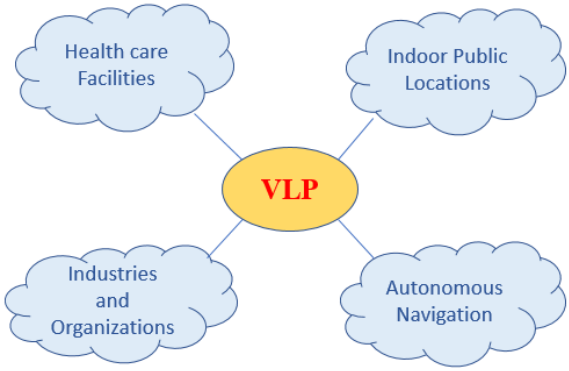

Fig. 1. Indoor VLP system applications.

The rest of the paper is organized as follows: Section II explains the VLP applications. In Section III, conventional positioning techniques are introduced for IPSs. Section IV explains the current research implied on VLP systems. In Section V, communication constraints are considered. Finally, we make a conclusion/discussion of our review in section VI.

II. VLP Applications

The VLP systems will have a large number of applications. As the creators of the GPS system, would never have considered the immense scope of GPS applications as of now being used, it is difficult to predict all the future development of VLP. However, it is clear that there will be a wide range of applications, with various limitations. Some of the applications of VLP systems in indoor environments are shown in Fig. 1. VLP is particularly suited for various working scenarios, such as health care (hospitals), indoor public locations (shopping malls, train stations, airports, amongst others), tunnels, autonomous vehicles industrial facilities (fabrics of the future), manufacturing for robots, etc.

III. Conventional Positioning Techniques

Figure 2 displays the conventional positioning techniques, which can be adopted in VLP systems. Wireless indoor positioning techniques can be classified in three types: triangulation, scene analysis (also known as fingerprinting) and proximity, which are described below.

A. Triangulation

Positioning algorithms, which use the geometric properties of triangles, are known as triangulation. It includes two methods of lateration and angulation. In lateration methods, the target location is evaluated by estimating its distance from various reference points. In VLP, the reference points are light sources and the target is an optical Rx. It is relatively difficult to measure the distance directly. Still it is possible to estimate distance based on different models, e.g., RSS, TOA or TDOA. Angulation estimates the angles with respect to few reference points (AOA) and location estimation can be completed by discovering intersection points of direction lines, which are radii from reference points [28].

Mathematical modelling for triangulation methods can be generalized. Assume (X_i, Y_i) is the position of the i-th reference point (i.e., Tx) in a two-dimensional space and (x, y) represents the position of target (i.e., Rx). R_i can be distance from the i-th Tx to the Rx as shown in Fig. 2(a) (in case of RSS) or it can be the range with respect to the i-th reference point, see Fig. 2(c) (in case of TOA and TDOA).

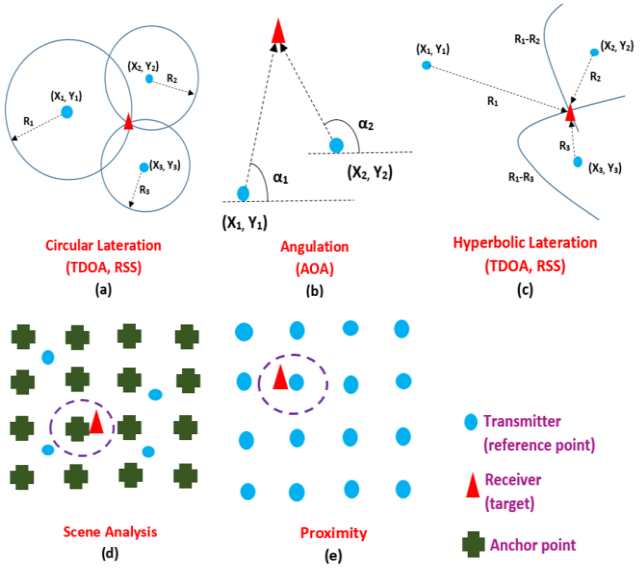

Fig. 2. Different positioning algorithms.

The system is described as:

$$AX = B, \tag{1}$$

where

$$X = [x\ y]^T, \tag{2}$$

$$A = \begin{bmatrix} X_2 - X_1 & Y_2 - Y_1 \\ \vdots & \vdots \\ X_n - X_1 & Y_n - Y_1 \end{bmatrix}, \tag{3}$$

$$B = \frac{1}{2}\begin{bmatrix} \left(R_1{}^2 - R_2{}^2\right) + \left(X_2{}^2 + Y_2{}^2\right) - \left(X_1{}^2 + Y_1{}^2\right) \\ \vdots \\ \left(R_1{}^2 - R_n{}^2\right) + \left(X_n{}^2 + Y_n{}^2\right) - \left(X_1{}^2 + Y_1{}^2\right) \end{bmatrix}. \tag{4}$$

And the least mean squares solution of the system is given by:

$$X = (A^T A)^{-1} A^T B\ , \tag{5}$$

where the matrix $(A^TA)^{-1}A^T$ is the More-Penrose pseudo inverse.

RSS: This have been broadly utilized in indoor positioning systems and VLP. RSS values are easy to measure. The DC channel gain for generalized Lambert emitter is given by:

$$H(0) = \begin{cases} \frac{m+1}{2\pi d^2}\cos^m\phi\cos\psi\frac{A_r}{d^2}T_s(\psi)g(\psi), & 0 \le \psi < \Psi_c \\ 0, & \text{otherwise} \end{cases}, \tag{6}$$

where $m = \frac{-ln(2)}{ln(\cos(HPA))}$, (7)

where HPA is the half power angle for the light source, ψ is the angle of between the light source and the PD normal, ϕ is the angle between the PD and the light source normal, A_r is the PD active area and d is the distance between the Rx and the light source, $T_s(\psi)$ is the Rx filter gain, $g(\psi)$ is the optical filter gain and Ψ_c is the Rx's field-of-view. When the Rx has estimated the intensity of transmitted signals, each distance can be evaluated from the corresponding Tx and circles can be drawn with the radii of computed distances. The Rx's location is then computed by the intersection point of the circles. We can use the generalized expression to estimate the user location [29].

TOA and TDOA: One of the most prevailing methods for positioning is TOA used in GPS. TOA is the absolute travel time of a wireless signal from the Tx to the Rx. GPS

precision is achieved through very tight synchronization conditions between all satellites within the network, often relying on atomic clocks. Thus, IPSs normally adopt TDOA instead of TOA to avoid the requirement of precise synchronization. Although, time synchronization is still required between the Txs. For the TOA technique, the mathematical expression will be same as the generalized expression except for the matrix A, which is represented as:

$$A = \begin{bmatrix} X_2 - X_1 & Y_2 - Y_1 & R_2 - R_1 \\ \vdots & \vdots & \vdots \\ X_n - X_1 & Y_n - Y_1 & R_n - R_1 \end{bmatrix}. \quad (8)$$

AOA: Is a technique where the angle of arriving signals is measured from different reference points to the Rx. The location of the target is then determined as the intersection of hyperbolas as shown in Fig. 2(b). The main benefit of AOA-based systems is that there is no time synchronization required between the Tx and the Rx. AOA does not require precise signal strength measurements. In addition, it is easier to find the AOA of the signals in the optical field by using the imaging Rx (i.e., cameras) as compared to utilizing complex antenna arrays, which are often used in RD systems. For mathematical expression, let α_i denote the AOA measurement with respect to the i-th Tx, which is given as:

$$\tan\alpha_i = \frac{y - Y_i}{x - X_i}. \quad (9)$$

Least square solution of AOA-based system is solved by the matrix form represented in the general expression, where A and B matrices are given by:

$$A = \begin{bmatrix} -\sin\alpha_1 & \cos\alpha_1 \\ \vdots & \vdots \\ -\sin\alpha_n & \cos\alpha_n \end{bmatrix}, \quad (10)$$

$$B = \begin{bmatrix} Y_1\cos\alpha_1 - X_1\sin\alpha_1 \\ \vdots \\ Y_n\cos\alpha_n - X_n\sin\alpha_n \end{bmatrix}. \quad (11)$$

B. Scene Analysis

This refers to the positioning algorithms, which make use of fingerprints related to all anchor points in a scene, see Fig. 2(d). Fingerprint measurement includes all measurement methods, which are mentioned previous, namely TOA, TDOA, RSS and AOA. Firstly, the real time measurements are calculated and then matched with the fingerprints to find the target location. The most common used fingerprinting technique relies on RSS. The benefit of this technique is power and time saving as it takes less time to match fingerprints as compared to perform a triangulation technique and computing. On the other hand, there is also a disadvantage. Fingerprinting requires a pre-calibration step, as the fingerprints may change with the system settings.

C. Proximity

Generally, when the Txs transmit signals with known locations, it is presumed that, the target, which receives the signal, is close by. One can determine the closest location to the target by comparing the RSS values of the transmitted signals. However, this location provides the rough estimation of the target location. In addition, if there are multiple signals having the same intensity, the target is intended to be in middle of these Txs. This positioning technique is relatively simple to implement as compared to other positioning methods; though, it is not extremely accurate compared to techniques that depend on the density of Tx distributions.

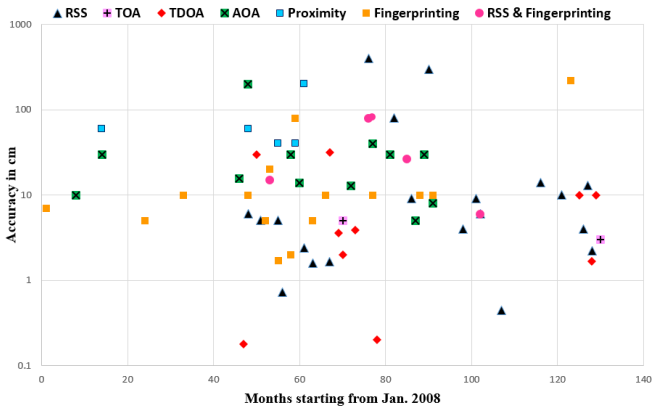

Fig. 3. Comparison of different conventional positioning techniques.

Typically, indoor LED lamps are located 2 or 3 m from each other, thus, this technique might be appropriate in situations where coarse estimations are acceptable.

D. Accuracy comparison

The accuracy of several conventional positioning techniques is shown in Fig. 3. Accuracy results reported in the literature reflect different system settings and conditions. Results were achieved either experimentally or by simulation. As it can be seen, no global trend emerges from this comparison. The average accuracy lies in the range of tenths of centimeters, with lowest achievements being reported for RSS and TDOA based systems.

IV. Current Research Techniques

Current research on VLP system performance is focusing on approaches able to enhance system performance. Machine learning offers several possibilities for performance improvement in VLP, either through the usage of data cleaning methods (for instance, using clustering algorithms) or ANNs. Sensor fusion, is another approach for performance improvement. In this case, additional sensors are used to extend the capabilities of VLP. These section reviews, current results on machine learning and sensor fusion VLP enhanced systems.

A. Machine learning

Machine learning provide systems the ability to learn automatically and improve from the experience without being explicitly programmed. In the case of VLP, one of the first used platforms for machine learning is based on data cleaning. Conventional least squares estimates are affected by the presence of outliers. Outliers, are data points, which lead to incorrect estimates. Amongst several possible data cleaning algorithms, clustering is one of the best option that can be used in VLP for position estimation improvement. Clustering algorithms, such as K-means and KNN (K nearest neighbors) seek to find data sets, which satisfy some distance criteria, and thus form clusters. In [29], DBSCAN (density-based spatial clustering of applications with noise), which is a clustering algorithm, was used to classify data into clusters and noise. Fig. 4 shows how clusters are formed with a set of points. The system comprises multiple Txs. It was found that, the position estimation using all Txs and least square approach can be biased by outliers (it produce high errors near walls and corners).

The proposed approach, starts by producing a set of estimates for sets of 3 Txs, which in turn produces a set of

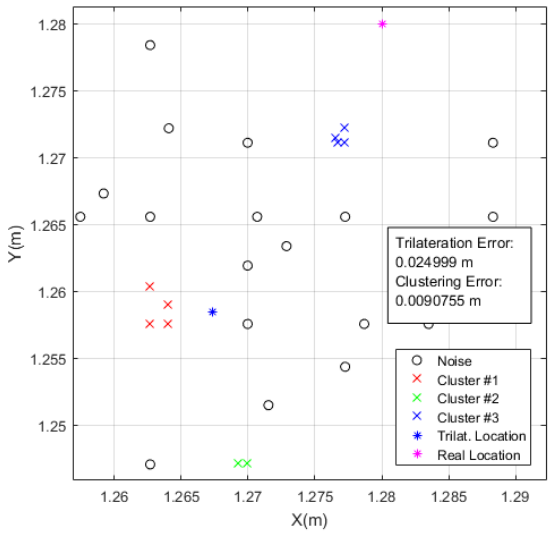

Fig.4 Formation of cluster using machine learning algorithm (reprint with permission from [29]).

disperse estimated positions, see Fig. 4. Some of these estimates are close to each other and form clusters, whereas others are disregarded as outliers. Then a learning procedure is applied to infer from the clusters, which is the estimated position. This approach improves the accuracy near walls and corners compared to the least squares approach.

Other machine learning examples reported in the literature has focused on the usage of multiple classifiers. In [30], a new localization technique was proposed based on RSS of visible light and fusion of multiple classifiers. This technique is different from other RSS based algorithms. Multiple classifiers based on RSS fingerprinting are trained by RSS fingerprints offline. In the online stage, two robust fusion algorithms, namely, grid-dependent least square (GD-LS) and grid-independent least square (GI-LS) are designed based on these multiple classifiers outputs. The mean square position error probability is lower than 5 cm, which is improved by 63.03% and 93.15% by mesh-independent mean squares and grid-dependent least squares, respectively. In [31], an indoor VLP was proposed where a ANN model was trained by constructing data features using time difference of arrival. The positioning error ε of about 1.6 cm was reported for this work.

B. ANNs

ANNs are mathematical models, which aspires to identify correlations in a data set processing in the same manner as the human brain. ANN consists of multiple layers of connected neurons. Each neuron is stimulated by neurons from previous layers, through connections that mimic the biological synapses. The weights of the synapses are adjusted by a training procedure. The neuron action consists off accumulation and activation – it accumulates the signals fed from different synapses, and produces an outgoing signal through the activation function. ANNs are able to develop meaning from complex and uncertain information data sets. Traditional application examples consist pattern and feature extraction in images. The ANN has the ability to learn how to perform a task that is dependent on the information given for training or early experience and Self-Organization.

An ANN model using back propagation is given by:

$$y = \sum_{i=1}^{n} w_i x_i + w_0, \quad (12)$$

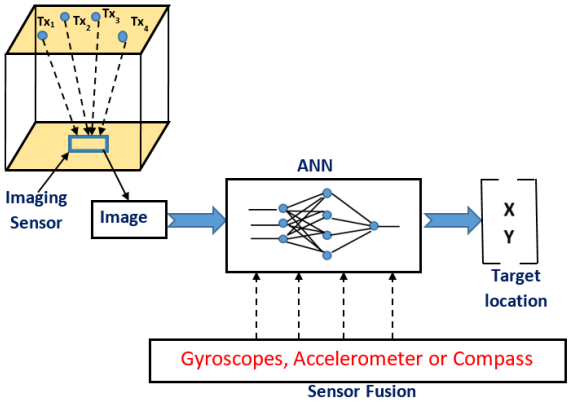

Fig 5. Setup for ANN and sensor fusion.

where x_i is the input, w_i is the weight parameter and y is the output. In the training stage of an ANN w_i are determined. E.g., an ANN algorithm with back propagation includes these steps: (*i*) hidden layer nodes values are calculated and used to compute the values of the output layer; and (*ii*) the errors are measured at the output layer and transmitted back to the hidden layer. The errors are then retransmitted from hidden layer to the input layer. The weights are updated after a single iteration of forward pass and back transmission. Finally, the algorithm is stopped when error function value become negligible.

Figure 5 depicts the usage of an ANN in a VLP system. This approach is suitable for systems employing an image sensor, where multiple features of the acquired image can be explored for positioning. The ANN input can rely on other sensors, such as compass or gyroscopes. In [32], a VLP system was proposed where an ANN based position estimator was used to precisely map the calculated RSS ratios to the measured 3D coordinates. A high accuracy was achieved with a ε of < 10 cm irrespective of arrangement and irradiation pattern of LED. The work in [27] proposed an ANN based VLP algorithm where positioning is achieved by a trained ANN in a diffuse channel. The positioning time was reduced about two orders of magnitude and the average ε was decreased about 13 times when compared to typical RSS-based positioning algorithm. Additionally, the proposed algorithm is suitable for several positioning algorithms due to its robustness with a different field-of-view of the Rx and wall's reflectivity.

C. Sensor Fusion

This is a technique that combines several sensors to improve better results. The size of the sensors became considerably smaller and less expensive with the enhancements of micro-electromechanical systems (MEMS), therefore, their usage in terminal devices, such as smartphones follows an increasing trend.

Magnetometer (magnetic compass), accelerometer and gyroscopes are the popular sensors, which can be used for positioning. A gyroscope measures the angular velocity of the sensor. An accelerometer determines the external exact force acting on the sensor. Orientation information of sensor can be determined by the integration of gyroscope measurements. E.g., suppose the coordinate system is rotating around sensor axes x, y and z with angular velocities α, γ and ρ, respectively as shown in Fig. 6 where the output of gyroscope can be taken to generate a composite rotation matrix as given by:

$$R(\alpha,\gamma,\rho) = R(\alpha)R(\gamma)R(\rho), \quad (13)$$

where $R(\alpha)$, $R(\gamma)$ and $R(\rho)$ are the rotation matrices in x, y and z directions, respectively.

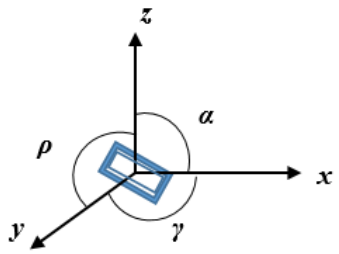

Fig 6. Gyroscope for attitude correction

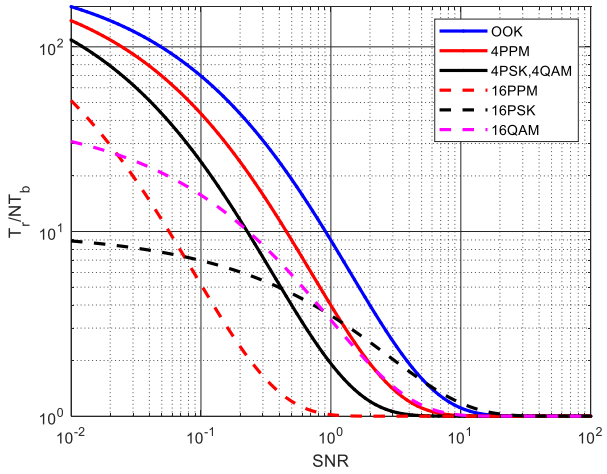

Fig. 7. Normalized time of different modulation schemes with 8 (N) bits.

In [33], a novel indoor VLP system was proposed based on the sensor fusion technique. The data is collected from the motion sensors and built-in image sensor and then combined to improve the accuracy. A singular value decomposition based sensor fusion (SVD-SF) algorithm was proposed, which is less complex. The positioning accuracy with this algorithm is around 44% compared to the one that utilize a single image sensor. A fusion positioning system based on extended Kalman filters was proposed in [34] where VLC position was fused with the inertial navigation data. This system achieved ε in centimeters. In [35], a novel IPS was proposed where sensor fusion and LED beacons were utilized to determine the position of target sensor. The sensor fusion includes a camera, an inclinometer and a magnetometer. High frequency beacon identifiers were transmitted by LED beacons and the detected code was under-sampled by using a camera over a long distance. In this scheme, novel geometric and consensus-based methods were used to perform localization. This system achieved an accuracy in the low decimeter range.

V. Communication Constraints

An important part of the VLP system is the communications with the infrastructure. This is generally accomplished using the same light sources, which act as reference points for positioning. A typical room has several light sources on the ceiling for illumination. These poses both advantages and disadvantages to the VLP system performance. More light sources are useful from a positioning perspective, as more sources imply accurate positioning information and reduced ε. On the other hand, multiple Txs (i.e., LEDs) imply increased levels of interference at the Rx. Methods to solve these interference problems, usually resort to Multiple-Input Multiple-Output (MIMO) techniques, equalization and advanced multilevel and multicarrier modulation formats (such as Orthogonal Frequency Division Multiplexing (OFDM), multiband carrier less amplitude and phase (m-CAP) modulation [36]. Using ISs as the Rxs is another possibility, which enables natural separation of the multiple Txs.

These approaches have in general a high cost in terms of system complexity and time to receive data. Here, we concentrate on the time cost. It is of paramount importance for VLP systems to generate position estimates in real time. For the generality of the applications, the user is moving with the VLP sensor, as a consequence, if the estimate takes a longer time to be achieved, there will be a large uncertainty in the position. Here we propose a method to measure how fast positioning information can be retrieved from the network.

The first thing to consider is the SNR, which is proportional to the signal strength and is inversely proportional to noise as given by:

$$SNR = \frac{R^2 P_{\text{rSignal}}^2}{\sigma^2}, \quad (14)$$

where R is the Rx's responsivity, P_{rSignal} is the received signal power and σ is the total noise variance. Moreover, SNR depend on the distance between the Tx and the Rx. If the Rx is too far, the distance will be large and the SNR degrades with the distance. The second ingredient is the bit error rate (BER), which is given by:

$$BER = f(SNR). \quad (15)$$

Since, the received information may contain errors; a single packet transmission may not be enough. We may assume that, the network is continuously transmitting data to ensure that the Rx will receive the data. The packet delivery ratio (PDR), which is a measure the effective of the process, is defined as the ratio of received number of packets without errors to the total number of transmitted packets. For N-bits long packets PDR can be defined in terms of BER as:

$$PDR = (1 - BER)^N. \quad (16)$$

Finally, the time to receive position information from the network can be evaluated by:

$$T_r = \frac{NT_b}{PDR}. \quad (17)$$

where T_b is the bit duration.

Equation (16) allows to measure how effective a given modulation format can be in terms of time to retrieve information from the network. Figure 7 depicts some examples of how the normalized time varies for different SNRs and the modulation formats. As can be seen, as the complexity of the modulation format increases, the normalized time decreases, showing that, higher order modulation formats are more robust against errors.

VI. Conclusions

This paper presented a survey on visible light positioning systems, with special focus on current research trends. The paper covered VLP applications, conventional positioning methods, current trends resorting to machine learning and

sensor fusion, and terminated with communication system constraints. Major observation states that, combining positioning and communication demands for higher complexity, or image sensor based systems, which are able to infer position and separate transmitting sources. Under these circumstances, usage of ANNs and neuromorphic computing architectures, present suitable frameworks VLP system development.

ACKNOWLEDGMENT

This work is supported by H2020/MSCA-ITN funding program under the framework of European Training Network on Visible Light Based Interoperability and Networking, project (VisIoN) grant agreement no 764461.

REFERENCES

[1] E. D. Kaplan and C. J. Hegarty, Understanding GPS: Principles and Applications. Boston, MA, USA: Artech House, 2006.

[2] H. Lan, C. Yu, Y. Zhuang, Y. Li, and N. El-Sheimy, "A novel Kalman filter with state constraint approach for the integration of multiple pedestrian navigation systems," Micromachines, vol. 6, no. 7, pp. 926–952, 2015.

[3] Y. Zhuang and N. El-Sheimy, "Tightly-coupled integration of WiFi and MEMS sensors on handheld devices for indoor pedestrian navigation," IEEE Sensors J., vol. 16, no. 1, pp. 224–234, Jan. 2016.

[4] N. Priyantha, A. Miu, H. Balakrishnan, and S. Teller, "The cricket compass for context-aware mobile applications," 6th ACM Mobicom, July 2001, Rome, Italy.

[5] P. Bahl and V. N. Padmanabhan, "RADAR: An in-building RF-based user location and tracking system," in Proc. IEEE Infocom, 2000, Mar., vol. 2, pp. 775-784.

[6] S. Gezici, Z. Tian, G. B. Giannakis, H. Kobaysahi, A. F. Molisch, H. V. Poor, and Z. Sahinoglu, "Localization via ultra-wideband radios: A look at positioning aspects for future sensor networks," IEEE Signal Process. Mag., vol. 22, no. 4, pp. 77-84, Jul. 2005.

[7] D. J. Ruiz, F. S. Granja, J. C. P. Honorato, and J. I. G. Rosas, Accurate pedestrian indoor navigation by tightly coupling footmounted IMU and RFID measurements," IEEE Trans. Instrum. Meas., vol. 61, no. 1, pp. 178–189, Jan. 2012.

[8] Y. Po and W. Wenyan, "Efficient particle filter localization algorithm in dense passive RFID tag environment," IEEE Trans. Ind. Electron., vol. 61, no. 10, pp. 5641–5651, Oct. 2014.

[9] J. Nieminen et al., "Networking solutions for connecting bluetooth low energy enabled machines to the Internet of Things," IEEE Netw., vol. 28, no. 6, pp. 8390, Nov. 2014.

[10] H. Liu, H. Darabi, P. Banerjee, and J. Liu, "Survey of wireless indoor positioning techniques and systems", IEEE Trans. on Systems, Man, and Cybernetics, Part C: Applications and Reviews, 37(6):1067–1080, 2007.

[11] S. Holm, "Ultrasound positioning based on time -of-flight and signal strength", 2012 International Conference on Indoor Positioning and Indoor Navigation, 13-15 th November, 2012.

[12] L. Tyahla,"Edwin Powell Hubble (1889-1953)", [Available on]: http://hubble.nasa.gov/overview/hubble_bio.php [Accessed on Decc. 7, 2018]

[13] Madore, F. Barry, Rigby, Jane, Freedman, L. Wendy, S. E. Persson., Sturch. Laura, Mager and Violet, "The Cepheid Period–Luminosity Relation (The Leavitt Law) at Mid-Infrared Wavelengths. III. Cepheids in NGC 6822", The Astrophysical J. vol. 693, no.1, pp. 936–939, 2009.

[14] Z. Ghassemlooy, L. N. Alves, S. Zvanovec and M. A. Khalighi: Visible Light Communications: Theory and Applications, CRC June 2017.

[15] H. Haas, L. Yin, Y. Wang, and C. Chen, "What is LiFi?" J. Lightw. Technol., vol. 34, no. 6, pp. 1533–1544, Mar. 15, 2016.

[16] D. Karunatilaka, F. Zafar, V. Kalavally, and R. Parthiban, "LED based indoor visible light communications: State of the art," IEEE Commun. Surveys Tuts., vol. 17, no. 3, pp. 1649–1678, 3rd Quart., 2015.

[17] A. Sevincer, A. Bhattarai, M. Bilgi, M. Yuksel, and N. Pala, "LIGHTNETs: Smart lighting and mobile optical wireless networks-A survey,"IEEE Commun. Surveys Tuts., vol. 15, no. 4, pp. 1620–1641, 4th Quart., 2013.

[18] M. Yoshino, S. Haruyama, and M. Nakagawa, "High-accuracy positioning system using visible light and image sensor,"in Proc. IEEE Radio Wireless Symp., 2008, pp. 439–442.

[19] Y. Liu, C. Hsu, and H. Chen, "Visible-light communication multiple-input multiple-output technology for indoor lighting,communication, and positioning," *Opt. Eng.*, vol. 52, pp. 1322–1328, 2015.

[20] S. H. Yang, H.-S. Kim, and Y.-H. Son, "Three-dimensional visible light indoor localization using AOA and RSS with multiple optical receivers," J. Lightw. Technol., vol. 34, no. 14, pp. 2482–2485, Jul. 2014.

[21] Y. Li, Z. Ghassemlooy, X. Tang, B. Lin and Y, Zhang, "A VLC smartphone camera based indoor positioning system," IEEE Photonics Technol. Letters 30 (13), pp. 1171-1174, May 2018.

[22] P. H. Pathak, X. Feng, P. Hu, and P. Mohapatra, "Visible light communication, networking, and sensing: A survey, potential and challenges," IEEE Commun. Surveys Tuts., vol. 17, no. 4, pp. 2047–2077, 4th Quart., 2015.

[23] J. Luo, L. Fan, and H. Li, "Indoor positioning systems based on visible light communication: state of the art," IEEE Commun. Surveys Tuts., vol. 19, no. 4, pp. 2871-2893, 2017.

[24] A. Arafa, S. Dalmiya, R. Klukas, and J. F. Holzman, "Angle-of-arrival reception for optical wireless location technology," Opt. express, vol. 23, no. 6, pp. 7755-7766, 2015.

[25] D. Trong-Hop and Y. Myungsik, "TDOA-based indoor positioning using visible light," Photon . Netw. Commun., vol. 27, no. 2, pp. 80-88, 2014.

[26] M. Saadi, T. Ahmad, Y. Zhao and L. Wuttisttikul, "An LED based Indoor Localization System using k-means Clustering," IEEE International Conference on Machine Learning and Applications.2016:246-252.

[27] H. Huang, A. Yang, L. Feng, G. Ni and P. Guo, "Artificial neural-network-based visible light positioning algorithm with a diffuse optical channed," Chinese Optics Letters, 15(5):1-5, 2017.

[28] S. Arnon, "Visible Light Communication" Chapter 4, Cambridge University Press, U.K., 2015.

[29] A. Gradim, P. Fonseca, L. N. Alves and R. E. Mohamed, "On the usage of machine learning techniques to improve position accuracy in visible light positioning systems," 2018 11th International Symposium on Communication Systems, Networks & Digital Signal Processing (CSNDSP), Budapest, pp. 1-6, 2018.

[30] X. Guo, S. Shao, N. Ansari, and A. Khreishah, "Indoor localization using visible light via fusion of multiple classifiers," IEEE Photon. J., Indoor Localization Using Visible Light, 12(6), 2017.

[31] X. Li, Y. Cao and C. Chen, "Machine learning based high accuracy indoor visible light location algorithm," 2018 IEEE International Conference on Smart Internet of Things (SmartIoT), Xi'an, China, 2018, pp. 198-203

[32] S. Zhang, P. Du, C. Chen and W. D. Zhong, "3D Indoor visible light positioning system using RSS ratio with neural network," OECC 2018, July,2018.

[33] R. Zhang, W. D. Zhong, D. Wu and K. Qian. "A Novel Sensor Fusion Based Indoor Visible Light Positioning System." IEEE Globecom Workshops (GC Wkshps), 1-6, 2016.

[34] Z. Li, F. Lihui and A. Yang, "Fusion based on visible light positioning and inertial navigation using extended Kalman filters" Sensors (Basel, Switzerland), vol. 17,5 1093. 11 May. 2017.

[35] G. Simon, G. Zachár and G. Vakulya, "Lookup: Robust and Accurate Indoor Localization Using Visible Light Communication", IEEE Transactions on Instrumentation and Measurement, vol. 66, no. 9, pp. 2337-2348, Sep. 2017.

[36] W. O. Popoola, Z. Ghassemlooy, and B. G. Stewart, "Pilot-assisted PAPR reduction technique for optical OFDM communication systems," Lightwave Techn., J., 32 (7), pp. 1374-1382, 2014.

[37] W. Qu, H. Luo, A. Men, F. Zhao1, X. Gao , J. Wei1, Y. Zhang and Y. Huang, "Light positioning A high-accuracy visible light indoor positioning system based on attitude identification and propagation model", International Journal of Distributed Sensor Networks, vol. 14, no. 2, 2018.

5.2 Feasibility Study of Reverse Trilateration Strategy with a single Tx for VLP

This section is a version of the published manuscript:

> **N. Chaudhary**, L. N. Alves, and Z. Ghassemlooy, 'Feasibility Study of Reverse Trilateration Strategy with a single Tx for VLP', in *2019 2nd West Asian Colloquium on Optical Wireless Communications (WACOWC)*, Tehran, Iran, Apr. 2019, pp. 121–126.

Connection to my Ph.D. thesis:

A study of visible light positioning system that rely on a single transmitter to infer position information was conducted. The system adopted a reverse trilateration scheme, where a set of three photodiodes is employed to estimate the position. The reverse trilateration scheme adopted for this system, yields to a very simple mathematical framework, suitable for low power and low complexity systems. The position information was inferred through the received signal strength, without the need for sophisticated angle measurements or precise synchronization as is the case in angle of arrival and time difference of arrival systems. In this work, the results revealed that the proposed system showed high susceptibility to noise, thus requiring high signal to noise ratios in order to achieve low positioning errors.

Feasibility Study of Reverse Trilateration Strategy with a single Tx for VLP

Neha Chaudhary
Instituto de Telecomunicações
University of Aveiro
Aveiro, Portugal
neha.chaudhary@ua.pt

Luis Nero Alves
Instituto de Telecomunicações
University of Aveiro
Aveiro, Portugal
nero@ua.pt

Zabih Ghassemblooy
Optical Comm. Research Group
Northumbria University
Newcastle-upon-Tyne, UK
z.ghassemlooy@northumbria.ac.uk

***Abstract*— This paper describes a visible light position system relying on a single transmitter to infer position information. The system adopts a reverse trilateration scheme, where a set of three photodiodes is employed to estimate the position. The reverse trilateration scheme adopted for this system, yields to a very simple mathematical framework, suitable for low power and low complexity systems. The position information is inferred through Rx signal strength, without the need for sophisticated angle measurements or precise synchronization as is the case in angle of arrival and time difference of arrival systems. Simulation results show that the proposed system shows high susceptibility to noise, thus requiring high signal to noise ratios in order to achieve low positioning errors.**

Keywords—Visible light positioning, Photodiode, RSS, Reverse Trilateration.

I INTRODUCTION

The global positioning system (GPS) is an unquestionable reference when discussing positioning systems, which is widely and effectively used in outdoor environments. However, it lacks accuracy in indoor environments, mostly due to poor coverage and high signal attenuation of the radio waves propagating through solid objects. Thus, the need for a more reliable and accurate positioning technologies for indoor applications, which has seen a grown of research activity in recent years [1], [2]. Several positioning systems based on different technologies have been proposed, such as, wireless local area networks (WLAN), ultrasounds, ultra wide band (UWB), radio frequency identification (RFID) and Bluetooth. However, most of these systems have limited positioning accuracies [3-8]. System based on radio waves are affected by multipath fading [9], whereas ultrasound based systems are influenced by the ambient temperature [10]. UWB and RFID schemes have a limited range of action [11]. Finally, Bluetooth demands user association, a feature which is not always desirable [12].

Recently, visible light communications (VLC) has become an interesting and complementary communications technology to the radio frequency wireless systems [13]. Motivated by the availability of solid-state lighting devices, VLC systems explore synergies between illumination and data communications, using the same light emitting diode (LED) based lights. Visible light positioning (VLP), has emerged quite obviously as a special application of VLC, which is more suited for indoor scenarios. Given that, lighting systems come with a spatial distribution feature, using these sources as beacons (or base-stations) for positioning provides a fertile ground for research. Traditional indoor positioning techniques using LED includes, received signal strength (RSS), angle of arrival (AOA), time of arrival (TOA) and time difference of arrival (TDOA), as well as proximity and fingerprinting [14]. TOA is a well-known method for localization, which is complex requiring accurate synchronization between the transmitter (Tx) and the receiver (Rx) [15]. In TDOA systems the requirement for synchronization is not so stringent as for TOA, but still requires an accurate clock reference at the Tx side. AOA systems require Rx diversity in order to extract the angle information [16]. Image based systems use image sensors as a means to achieve the Rx diversity [17]. RSS systems estimate the position based on the received signal power, thus being sensitive to the noise. Nevertheless, RSS systems have higher accuracy compared to proximity and fingerprinting techniques [18], as well as being simpler and cost-effective.

One common requirement for these methods is the need to have measurements based on 3 different sources, which is a mathematical imposition, where each measurement produces a locus of possible positions. Note that, the ambiguity is removed using other measurements. Therefore, considering these constraints, a minimal set up could be achieved using a single photosensitive sensor (e.g., a photodiode (PD)), and at least three reference Txs. There have been several contributions exploring minimal configurations, which are based on different set of configurations, or combination of multiple schemes. In [19], the authors described a VLP system using two LEDs. The proposed approach carried out two RSS measurements, which were sufficient to estimate the position to the right (or left) of the line defined by the Txs. The system achieved a positioning accuracy lower 20 cm under moderate SNR of 13 dB, despite having lower system complexity. In [20], a three dimensional (3D) indoor VLP system was proposed based on single Tx and a single tilted Rx as well as using RSS and AOA to improve positioning accuracy. The tilted Rx was mounted on a spinning platform, and the 3D space representation was distributed into several two-dimensional (2D) planes, which were handled by lifting the Rx's platform. The proposed VLP system offered an average position error (PE) of < 35mm. In [21], a compact VLP system with a single Tx and single tilted Rx was proposed for an indoor environment of 0.6×0.6×1.1 m with an average PE of < 25 mm. In [22], a reverse trilateration scheme employing three Rxs in the ceiling and one Tx in the ground was reported with a PE of < 0.2 m. The proposed system was relevant for applications where the network needs to know the position of the user.

This paper focuses on the reverse trilateration scheme where the position sensor uses three PDs and relies on a single

978-1-7281-3767-4/19/$31.00 ©2019 IEEE

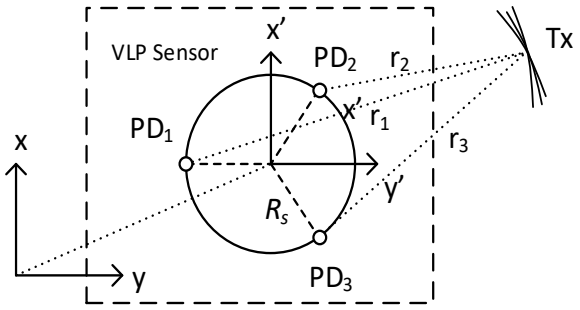

Fig.1. Reverse trilateration concept

Tx to determine the location. The system employs RSS, which makes this approach suitable for low power and low complexity applications. The paper shows theoretical analysis supported by simulation to investigate the system performance. We show that, the system's performance is highly influenced by noise. We show also, that, performance improvements can be achieved using averaging techniques.

The rest of the paper is organized as follows: Section II details the system design and modeling. Section III develops the system error performance analysis. Section IV presents the simulation set up and the achieved results. Finally section V gives the concluding remarks.

II System Design And Modeling

The schematic of the proposed reversed trilateration strategy is illustrated in Fig. 1. The VLP sensor comprises 3 PDs positioned on a circle of radius R_s. The projection of the distances between each PDs and the Tx are given by r_k, where k = 1, 2 and 3. Using r_k it is possible to form a well posed system of two equations for the center position of the sensor. These three distances provide the radius of three circles, centered at each PD, with common intercept at the Tx's position.

Let the positions of k^{th} PD be $\boldsymbol{X^o_k} = (x^o_k, y^o_k)^T$ with $\boldsymbol{X^o_1} = (-R_s, 0)^T$, $\boldsymbol{X^o_2} = (R_s/2, R_s\sqrt{3}/2)^T$ and $\boldsymbol{X^o_3} = (R_s/2, -R_s\sqrt{3}/2)^T$. The Tx projection on the x-y plane is $\boldsymbol{X_T} = (x_T, y_T)^T$. The position of the VLP sensor in the x-y plane as a function of an arbitrary translation $\boldsymbol{X} = (x, y)^T$ and an arbitrary rotation $\boldsymbol{R}(\theta)$ is given by:

$$\boldsymbol{X_k} = \boldsymbol{X} + \boldsymbol{R}(\theta)\boldsymbol{X^o_k} \tag{1}$$

The translation vector $\boldsymbol{X}$ is the center position of the sensor and the objective of the estimation procedure. r_k defines a circle with the center $\boldsymbol{X}$ and passing through $\boldsymbol{X_T}$, which form a set of three quadratic equations in standard form as given by:

$$(\boldsymbol{X_T} - \boldsymbol{X_k})^T(\boldsymbol{X_T} - \boldsymbol{X_k}) = r_k^2 \tag{2}$$

Note r_k is estimated using RSS. Developing equation (2) gives:

$$\boldsymbol{X_T^T X_T} + R_S^2 + \boldsymbol{X^T X} - 2(\boldsymbol{X^o_k})^T\boldsymbol{R}(\theta)^T(\boldsymbol{X_T} - \boldsymbol{X}) = r_k^2 \tag{3}$$

From (1) and (2) we know that $(\boldsymbol{X^o_k})^T\boldsymbol{X^o_k} = R_s^2$ and $\boldsymbol{R}^{-1}(\theta) = \boldsymbol{R}^T(\theta)$. The quadratic terms on the left hand-side of (3) can be removed by subtraction, thus yielding a system of two linear equations, which in the matrix form is given by:

$$-2R_s\boldsymbol{A_s}\boldsymbol{R}(\theta)^T(\boldsymbol{X_T} - \boldsymbol{X}) = \Delta\boldsymbol{r} \tag{4}$$

with

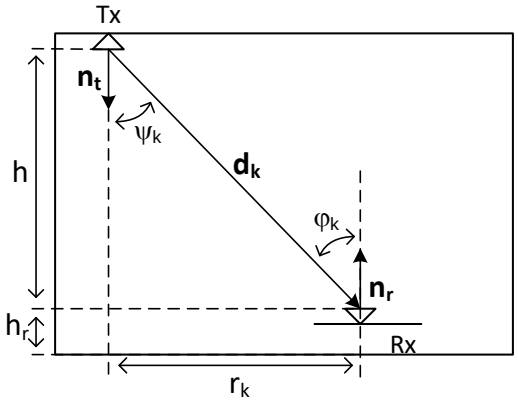

Fig. 2. System model of a single LED-based Tx and the Rx sensor with three PDs

$$\boldsymbol{A_s} = \frac{1}{R_s}\begin{bmatrix}(\boldsymbol{X^o_2})^T - (\boldsymbol{X^o_1})^T\\(\boldsymbol{X^o_3})^T - (\boldsymbol{X^o_2})^T\end{bmatrix} = \frac{1}{R_s}\begin{bmatrix}3/2 & \sqrt{3}/2\\0 & -\sqrt{3}\end{bmatrix} \tag{5}$$

$$\Delta\boldsymbol{r} = \begin{bmatrix}r_2^2 - r_1^2\\r_3^2 - r_2^2\end{bmatrix} \tag{6}$$

The estimated position is directly given by:

$$\boldsymbol{X} = \boldsymbol{X_T} + \frac{1}{2R_s}\boldsymbol{R}(\theta)\boldsymbol{A_s}^{-1}\Delta\boldsymbol{r} \tag{7}$$

Equation (7) exhibits some interesting features. (i) most terms in (7) are fixed vectors and matrix except from $\Delta\boldsymbol{r}$ and $\boldsymbol{R}(\theta)$. The sensor matrix $\boldsymbol{A_s}$, is fixed by the standard PD's positions, see Fig. 1. The arbitrary rotation of the sensor can be dealt with using a compass or a gyroscope. Here, we assume that θ = 0º (i.e., no rotation). Furthermore, as it will be demonstrated, the error performance is not affected by the sensor's rotation.

A The Rx Signal Strength

Figure 2 depicts the set up conditions for signal transmission, between the Tx and the k^{th} Rx. The objective of RSS is to measure r_k, i.e., the projection of the distance vector $\boldsymbol{d_k}$ on the x-y plane. These estimations are based on the DC channel gain of the communications link. The received signal for Lambertian emitter for a line of sight (LoS) path is given by:

$$S_k = H_o T_s(\varphi_k) g(\varphi_k) \frac{cos^m(\psi_k) cos(\varphi_k)}{\|\boldsymbol{d_k}\|^2} \tag{8}$$

where

$$H_o = \frac{m+1}{2\pi} G_o \mathcal{R} A_r P_t \tag{9}$$

$$m = -\frac{\ln(2)}{ln\big(cos(HPA)\big)} \tag{10}$$

where HPA is the half power angle for the light source, ψ_k is the angle between $\boldsymbol{d_k}$ and the LED normal, φ_k is the angle between $\boldsymbol{d_k}$ and the PD normal, A_r is the PD active area, G_o is the transimpedance gain of the Rx, $\mathcal{R}$ is the PD responsivity and P_t is the transmit power. $T_s(\varphi_k)$ is the Rx filter and $g(\varphi_k)$ is the optical concentrator [23]. For the forgoing analysis, we will assume that, $T_s(\varphi_k)$ and $g(\varphi_k)$ are both unity. Knowing that $\|\boldsymbol{d_k}^2\| = r_k^2 + h^2$ we can solve (8) to find r_k^2 as given by:

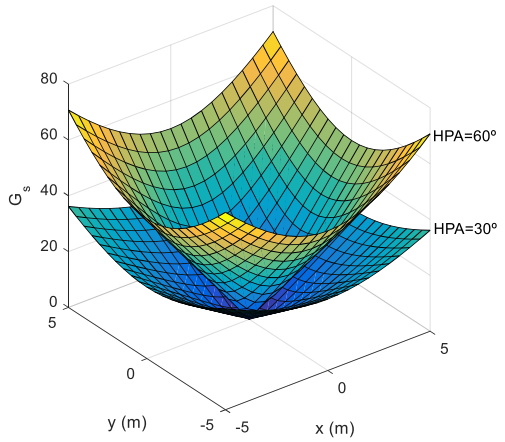

Fig. 3. The distance error geometrical factor G_s for two different HPA values.

$$r_k^2 = \left(\frac{H_o h^{m+1}}{S_k}\right)^{\frac{2}{m+3}} - h^2 \tag{11}$$

where h is the vertical distance between the Tx and the Rx. Using (11), the $\boldsymbol{\Delta r}$ vector can be expressed as a function of the received signals on the 3 PDs by:

$$\Delta \boldsymbol{r} = (H_o h^{m+1})^{\frac{2}{m+3}} \Delta_{\boldsymbol{S}} \tag{12}$$

$$\Delta_{\boldsymbol{S}} = \begin{bmatrix} S_2^{-\frac{2}{m+3}} - S_1^{-\frac{2}{m+3}} \\ S_3^{-\frac{2}{m+3}} - S_2^{-\frac{2}{m+3}} \end{bmatrix} \tag{13}$$

III ERROR PERFORMANCE ANALYSIS

The error performance analysis can be assessed using (7). The reasoning is very simple. If the detected signal is affected by noise, the measured signal power will contain errors, which are defined by small changes in $\boldsymbol{\Delta r}$, i.e., $\boldsymbol{\Delta r} \rightarrow \boldsymbol{\Delta r} + \boldsymbol{\delta r}$. Using (7) we have $\boldsymbol{\Delta X} \rightarrow \boldsymbol{\Delta X} + \boldsymbol{\delta X}$, where $\boldsymbol{\delta X}$ is the coordinate displacement due to $\boldsymbol{\delta r}$, which is given by:

$$\boldsymbol{\delta X} = \frac{1}{2R_s} \boldsymbol{R}(\theta) \boldsymbol{A_s^{-1}} \boldsymbol{\delta r} \tag{14}$$

We may transform this into a distance error, as given by:

$$\delta X = \sqrt{\boldsymbol{\delta X^T \delta X}} = \frac{1}{2R_s} \sqrt{\boldsymbol{\delta r^T \Lambda_s \delta r}} \tag{15}$$

where $\boldsymbol{\Lambda_s} = \boldsymbol{(A_s^{-1})^T A_s^{-1}}$. Equation (15) shows that, the distance error does not depend explicitly on the sensor's rotation.

A The Effect of Noise on δX

Noise can be incorporated into the error model in a very simple way. The effect of noise on the detected signal, by the k^{th} PD is expressed by $S_k \rightarrow S_k + n_k$., where n_k is the additive white Gaussian noise. Using the signal to noise ratio (SNR), γ, we find a simple transformation rule, which states $S_k \rightarrow S_k(1 + 1/\sqrt{\gamma})$. Now, using (12) and (13), and re-working (15) we have:

Table.1 Default value of the system's parameters.

Tx-Rx parameter		
A_r	100 mm^2	Area of the PD
$\mathcal{R}$	1 A/W	Responsivity
P_t	1 W	Transmit power
G_o	1 MΩ	Rx's gain
HPA	60º	Half power angle
Geometrical Parameter		
dx	0.5 m	x grid resolution
dy	0.5 m	y grid resolution
$\boldsymbol{n_t}$	$(0, 0, -1)^T$	TX heading vector
$\boldsymbol{n_r}$	$(0, 0, 1)^T$	RX heading vector
$\boldsymbol{X_T}$	$(0, 0, h + h_r)^T$	TX position
R_s	0.1 m	Sensor radius
h	2.2 m	Ceiling height
h_r	0.2 m	Sensor height
θ	0º	Sensor rotation angle

$$\delta X = G_S \frac{(H_o h^{m+1})^{\frac{2}{m+3}}}{2R_s} \left(\left(1 + \frac{1}{\sqrt{\gamma}}\right)^{-\frac{2}{m+3}} - 1 \right) \tag{16}$$

where $G_s = (\boldsymbol{\Delta s}^T \boldsymbol{\Lambda_s} \boldsymbol{\Delta s})^{1/2}$. Equation (16) exhibits the distance error dependency on all the system's parameters. It is noticeable that, the geometrical factor G_s depends on the sensor geometry (i.e., via $\boldsymbol{\Lambda_s}$) and the detected signal power. Figure 3 depicts G_s for two different values of *HPA* (i.e., 60º and 30º), in a room of size 10×10×2.4 m^3, with one Tx positioned in the center. As it can be seen, G_s has a circular symmetry, showing that the distance error is indeed independent of sensor's rotation.

IV SIMULATION RESULTS

This section outlines the system set-up conditions and present the simulation results. The simulation set-up default parameter' values are given in Table 1.

A General Error Performance Assessment

The effect of noise on the estimated position can be assessed through simulation, using Matlab. This is accomplished by adopting the following steps: (*i*) simulating the signal reception for a grid of possible Rx's positions; (*ii*) using (11) to calculate r_k for each PD; (*iii*) estimate the position using (7); and (*iv*) finally, calculate the PE as the difference between the estimated and real positions. This procedure is repeated for different SNR values.

Figures 4 and 5, depicted the PE spatial distributions in a room of 10×10×2.4 m^3, for SNRs of 50 and 60 dB, respectively. The unusually high SNR values are a clear indication of the susceptibility of the sensor to noise. RSS relies on detected signal power, as sensor PDs are closer together, where the received signal power by the three PDs do not change much. Noise effects become of paramount importance under these circumstances. As it can be seen from Figs. 4 and 5, the error increases as we move to the periphery of the room, which is in agreement with the geometrical error dependence embedded in G_s, see Fig. 3.

Statistically speaking, it is not very relevant to compare performance in terms of extreme error achievements, since the error changes randomly for different simulations. In addition,

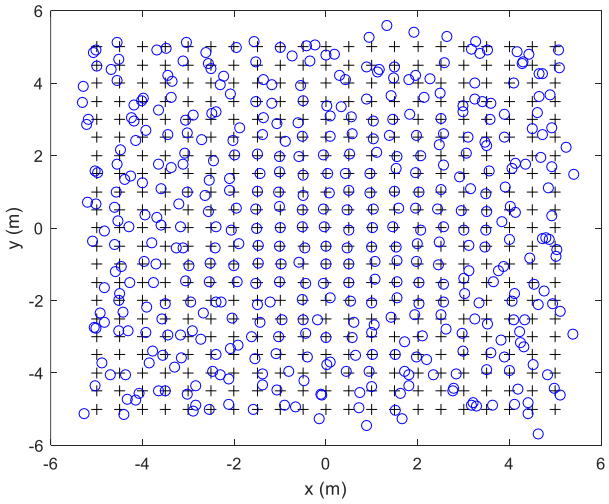

Fig. 4. The positioning error spatial distribution with *SNR*=50 *dB*.

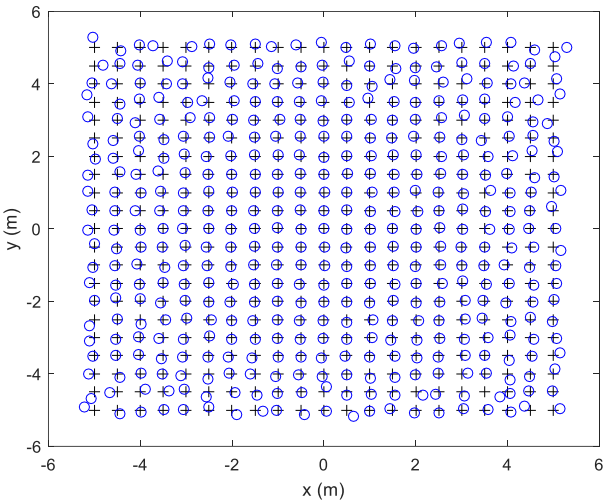

Fig. 5. The positioning error spatial distribution with SNR=60 dB.

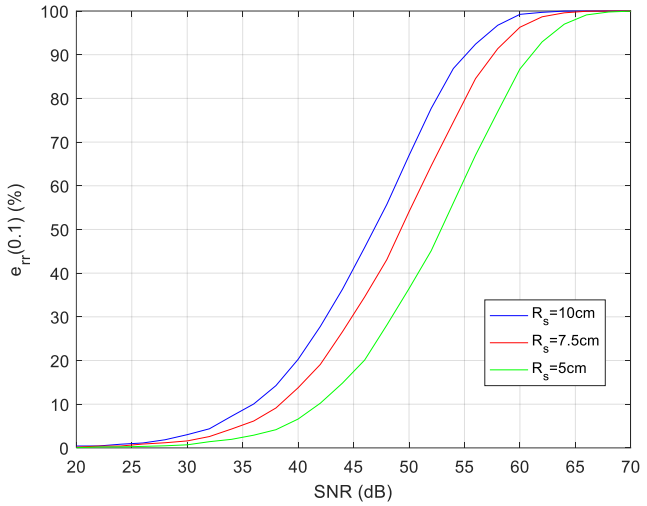

Fig. 6. The positioning error performance as function of SNR, for fixed values of R_s.

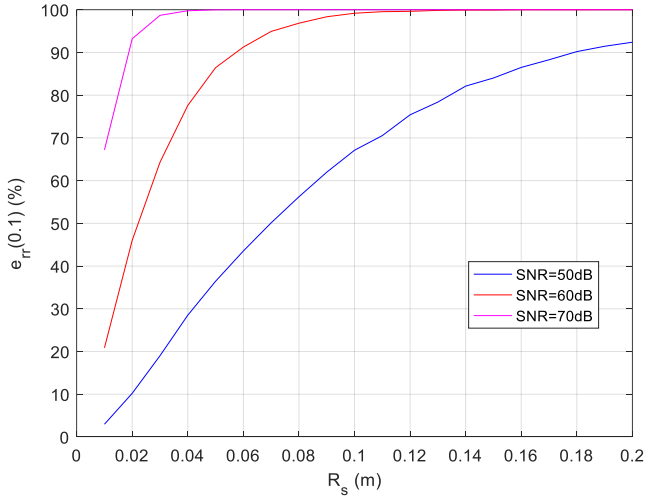

Fig. 7. The positioning error performance as function of R_s, for fixed values of SNR.

the average errors are not good performance indicators, as both high and low measured errors are taken into consideration with the equal weight. Instead, we propose a different error measure, which is more aligned with the probability theory. This measure, computes the percentage of estimates that fall below a certain distance criterion. In a total of N estimates, let $\#(e_{rr} < \varepsilon)$ represent the number of estimates with the positioning error below ε, the PE is defined by:

$$e_{rr}(\varepsilon) = \frac{\#(e_{rr} < \varepsilon)}{N} \qquad (17)$$

It is readily apparent that, as N tends towards infinity, $e_{rr}(\varepsilon)$ tends to the probability of having error estimates below ε. In Figs. 4 and 5, the achieved indicators for ε=10 cm, were, 31.5% and 79.1% for 50 and 60 dB, respectively.

B Error Performance R_s Dependency

Figures 6 and 7 depict the PE dependency on SNR and R_s. As before ε=10 cm. Fig. 6, depicts the percentage of estimates with the error below 10 cm, for different values of R_s (5, 7.5 and 10 cm) for variable SNR values (20 to 70 dB). The simulation considered a room size of 10×10×2.4 m^3 with a grid resolution of 5 cm (corresponding to N = 40401 position estimates). As it can be seen, the number of estimates with the error below 10 cm tends to increase with SNR, which is in agreement with (16). Lower values of R_s require higher *SNRs* to achieve the same performance. Equation (16) seems to suggest that, the error is monotonic with R_s - higher R_s values mean less error. In order to further explore the error dependency on R_s, we repeated the simulation for fixed values of SNR (50, *60* and 70 dB) and for range of R_s (i.e., 1 to 20 cm, as shown in Fig. 7. For each SNR value error performance increases monotonically with R_s. This behavior can be understood by recalling that $\mathbf{\Lambda_s}$ depends on the norm of the distance vectors $\boldsymbol{d_k}$. Since the PDs positions are function of R_s, $\boldsymbol{d_k}$ depends on R_s as well.

C Error Performance HPA Dependency

Figures 8 and 9 depicts the PE dependency on both *SNR* and *HPA*. For this study, we followed a similar approach as described in section IV-B. Figure 8 depicts the percentage of errors below 10 cm, for fixed values of *HPA* (45º, 30º and 15º) and a range of SNR. Here too, the PE increases with the SNR and decreasing values of HPA. Note, lower *HPA*, means transmitting sources with higher directivity and thus higher values for *m*, which translate to less geometrical dependence – G_s becomes flatter. Figure 9 shows the PE as a function of HPA for range of SNRs. Here we see that, the PE reduces with increasing values of *HPA* as predicted from G_s.

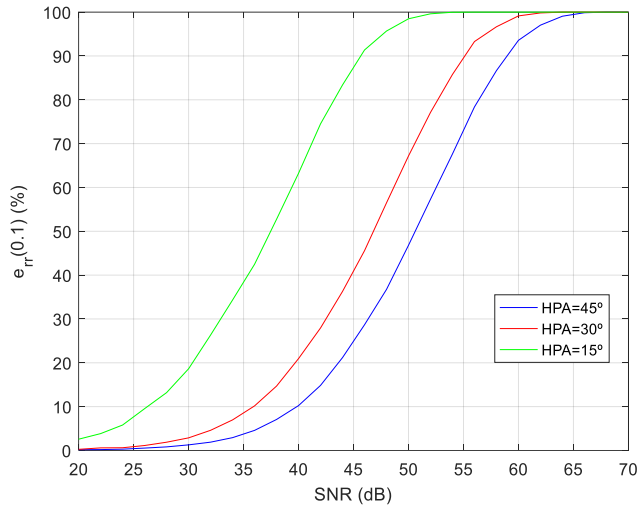

Fig. 8. The positioning error performance as function of SNR, for fixed values of HPA.

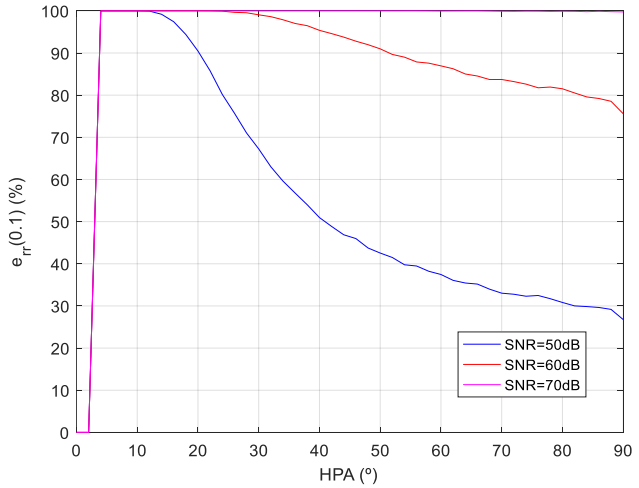

Fig. 9. The positioning error performance as function of HPA, for fixed values of SNR.

D Error Performance using Averaging Techniques

Figure 10 depict the averaging effect on the PE, which shows the error below 10 cm for fixed values of SNR of 30, 40 and 50 dB as function of the number of averaging steps. It can be seen from the Fig 10 that, the error performance increases with the number of averaging steps and SNR. Therefore, it is possible to use averaging to improve PE.

V CONCLUSIONS

This paper presented a feasibility study on the usage of reverse trilateration for position estimation, based on RSS. The system under study, comprised a single Tx and three PDs based Rx. Simulation results disclosed that, the system is very susceptible to the noise, demanding very high SNR in order to achieve low positioning error performance. As a standalone system, the proposed scheme is not feasible. However, considering that RSS can be supported with averaging techniques (such as spread spectrum) able to improve SNR, the proposed system can represent a possible choice for low power and low complexity VLP positioning sensors. System performance analysis disclosed some important results, which could be of interest for other applications, namely: (*i*) the simple estimation equations can be of use to study and optimize transmitter placement in conventional trilateration schemes; and (*ii*) performance based on the probability of error being lower than some predefined value can be taken as a standard approach for performance analysis in VLP systems.

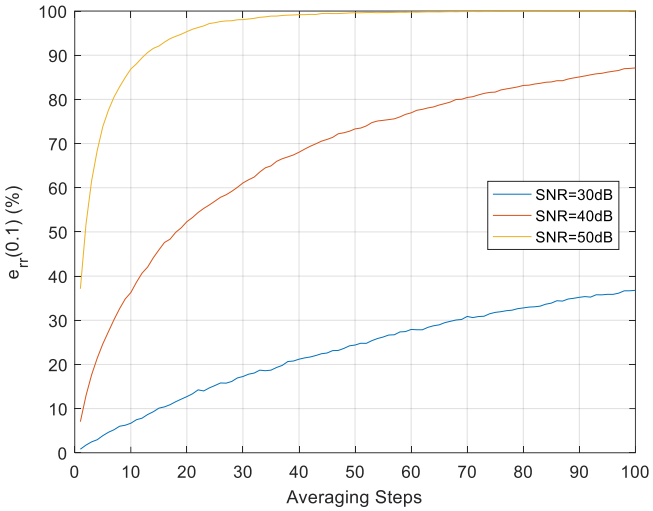

Fig. 10 – Averaging effect on the error performance for a range of SNRs.

ACKNOWLEDGMENT

This work is supported by H2020/MSCA-ITN funding program under the framework of European Training Network on Visible Light Based Interoperability and Networking, project (VisIoN) grant agreement no 764461.

REFERENCES

[1] W. Z . Zhang, M.I.S. Chowdhury and M. Kavehrad, "Asynchronous indoor positioning system based on visible light communication", OptEng., 53(4),2014.

[2] N. Lourenco and M. Siegel, "VLC for indoor positioning: An industrial view on applications", Ch. 12, pp. 373-404, Visible Light Communications: Theory and Applications, Eds. Z. Ghassemlooy, L N Alves, et al, CRC Press, 2017

[3] N. Priyantha, A. Miu, H. Balakrishnan, and S. Teller, "The cricket compass for context-aware mobile applications," 6th ACM Mobicom, July 2001, Rome, Italy.

[4] P. Bahl and V. N. Padmanabhan, "RADAR: An in-building RF-based user location and tracking system," in Proc. IEEE Infocom, 2000, Mar., vol. 2, pp. 775-784.

[5] S. Gezici, Z. Tian, G. B. Giannakis, H. Kobaysahi, A. F. Molisch, H. V. Poor, and Z. Sahinoglu, "Localization via ultra-wideband radios: A look at positioning aspects for future sensor networks," IEEE Signal Process. Mag., vol. 22, no. 4, pp. 77-84, Jul. 2005.

[6] D. J. Ruiz, F. S. Granja, J. C. P. Honorato, and J. I. G. Rosas, " Accurate pedestrian indoor navigation by tightly coupling footmounted IMU and RFID measurements," IEEE Trans. Instrum. Meas., vol. 61, no. 1, pp. 178–189, Jan. 2012.

[7] Y. Po and W. Wenyan, "Efficient particle filter localization algorithm in dense passive RFID tag environment," IEEE Trans. Ind. Electron., vol. 61, no. 10, pp. 5641–5651, Oct. 2014.

[8] H. Liu, H. Darabi, P. Banerjee and J. Liu, "Survey of wireless indoor positioning techniques and systems" IEEE Transactions on Systems, Man, and Cybernetics, Part C: Applications and Reviews, 37(6):1067–1080, 2007.

[9] O. C. Ugweje, "Radio Frequency and Wireless Communications." The Internet Encyclopedia, April 2004. [DOI:10.1002/047148296X.tie151]

[10] B. Praher, K. Straka and G. Steinbichler, "An ultrasound-based system for temperature distribution measurements in injection moulding: system design, simulations and off-line test measurements in water", Measurement Sci. and Tech., Vol. 24, No. 8, 10 July 2013.

[11] D. Dardari, N. Decarli, A. Guerra, F. Guidi, "The future of ultra-wideband localization in RFID", IEEE International Conf. on RFID, May 2016, Orlando, USA.

[12] M. Collotta, G. Pau, T. Timothy, and Ozan K, "Bluetooth 5: a concrete step forward towards the IoT," IEEE Comm., Magaz., journ., November,2017.

[13] Z. Ghassemlooy, L. N. Alves, S. Zvanovec and M. A. Khalighi: Visible Light Communications: Theory and Applications, CRC June 2017.

[14] J. Luo, L. Fan and H. Li, "Indoor Positioning Systems Based on Visible Light Communication: State of the Art," IEEE Commun. Surveys Tuts., vol. 19, no. 4, pp. 2871-2893, 2017.

[15] D. Trong-Hop and Y. Myungsik, "TDOA-based indoor positioning using visible light," Photon . Netw. Commun., vol. 27, no. 2, pp. 80-88, 2014.

[16] L. Seongsu and S. Jung, "Location awareness using angle-of-arrival based circular-pd-array for visible light communication," IEEE AsiaPacific Conference on Communications, pages 480–485, 2012.

[17] Y. Li, Z. Ghassemlooy, X. Tang, B. Lin and Y. Zhang, "A VLC Smartphone Camera based Indoor Positioning System," IEEE Photonics Technology Letters, 30 (13), pp. 1171-1174, May 2018.

[18] T. H. Do and M. Yoo, "An in-depth survey of visible light communication based positioning systems," Sensors (Basel), vol. 16, no. 5, May 2016.

[19] F. I. K. Mousa, H. L. Minh, Z. Ghassemlooy, X. Dai, S. T. Tran, A. C. Boucouvalas and S. K. Liaw, "Indoor localization system utilizing two visible light emitting diodes," Opt. Eng. 55(11), 116114, 2016.

[20] Q. L. Li, J. Y. Wang, T. Huang and Y. Wang, "Three-dimensional indoor visible light positioning system with a single Transmitter and a single tilted Receiver," Opt. Eng. 55(10), 106103, 2016.

[21] T. Huang, X. Gao, S. Li, Q. Li, C. Li, H. Zhu and Y. Wang, "Visible light indoor positioning fashioned with a single tilted optical Rx," in Int. Conf. on Optical Communications and Networks, 2015.

[22] Y. Xu, J. Zhao, J. Shi and Nan Chi, "Reversed Three-Dimensional Visible Light Indoor Positioning Utilizing Annular Rxs with Multi-Photodiodes", MDPI journ., Sensors, August, 2016.

[23] A. Gradim, P. Fonseca, L. N. Alves and R. E. Mohamed, "On the Usage of Machine Learning Techniques to Improve Position Accuracy in Visible Light Positioning Systems," 2018 11th International Symposium on Communication Systems, Networks & Digital Signal Processing (CSNDSP), Budapest, pp. 1-6, 2018

5.3 An Indoor Visible Light Positioning System Using Tilted LEDs with High Accuracy

This section is a version of the published manuscript:

> **N. Chaudhary,** O. I. Younus, L. N. Alves, Z. Ghassemlooy, S. Zvanovec, and H. Le-Minh, 'An Indoor Visible Light Positioning System Using Tilted LEDs with High Accuracy', Sensors, vol. 21, no. 3, p. 920, Jan. 2021.

Connection to my Ph.D. thesis:

The accuracy of the received signal strength-based VLP system in indoor applications is constrained by the tilt angles of transmitters and receivers as well as multipath reflections. Therefore, for the first time, it was shown that tilting the transmitter can be beneficial in VLP systems considering both LOS and NLOS transmission paths. With the transmitters oriented towards the center of the receiving plane (i.e., the pointing center F), the received power level is maximized due to the LOS components on F. It was also proved that, the proposed scheme offers a significant accuracy improvement of up to ~66% compared with a typical non-tilted transmitter VLP at a dedicated location within a room using a low complex linear least square algorithm with polynomial regression. The effect of tilting the transmitter on the lighting uniformity was also investigated and results proved that the uniformity achieved complies with the European Standard EN 12464-1. Furthermore, it was revealed that the accuracy of VLP can be further enhanced with a minimum positioning error of 8 mm by changing the height of F.

sensors

MDPI

Article

An Indoor Visible Light Positioning System Using Tilted LEDs with High Accuracy

Neha Chaudhary [1,*], Othman Isam Younus [2], Luis Nero Alves [1], Zabih Ghassemlooy [2], Stanislav Zvanovec [3] and Hoa Le-Minh [2]

[1] Instituto de Telecomunicações and Departamento de Electrónica, Telecomunicações e Informática, Universidade de Aveiro, 3810-193 Aveiro, Portugal; nero@ua.pt
[2] Optical Communications Research Group, Faculty of Engineering and Environment, Northumbria University, Newcastle upon Tyne NE1 8ST, UK; othman.younus@northumbria.ac.uk (O.I.Y.); z.ghassemlooy@northumbria.ac.uk (Z.G.); hoa.le-minh@northumbria.ac.uk (H.L.-M.)
[3] Department of Electromagnetic Field, Faculty of Electrical Engineering, Czech Technical University in Prague, 16627 Prague, Czech Republic; xzvanove@fel.cvut.cz
* Correspondence: neha.chaudhary@ua.pt

Abstract: The accuracy of the received signal strength-based visible light positioning (VLP) system in indoor applications is constrained by the tilt angles of transmitters (Txs) and receivers as well as multipath reflections. In this paper, for the first time, we show that tilting the Tx can be beneficial in VLP systems considering both line of sight (LoS) and non-line of sight transmission paths. With the Txs oriented towards the center of the receiving plane (i.e., the pointing center F), the received power level is maximized due to the LoS components on F. We also show that the proposed scheme offers a significant accuracy improvement of up to ~66% compared with a typical non-tilted Tx VLP at a dedicated location within a room using a low complex linear least square algorithm with polynomial regression. The effect of tilting the Tx on the lighting uniformity is also investigated and results proved that the uniformity achieved complies with the European Standard EN 12464-1. Furthermore, we show that the accuracy of VLP can be further enhanced with a minimum positioning error of 8 mm by changing the height of F.

Keywords: localization; visible light communication; visible light positioning; received signal strength; linear least square; polynomial regression; Tx's tilting

Citation: Chaudhary, N.; Younus, O.I.; Alves, L.N.; Ghassemlooy, Z.; Zvanovec, S.; Le-Minh, H. An Indoor Visible Light Positioning System Using Tilted LEDs with High Accuracy. *Sensors* **2021**, *21*, 920. https://doi.org/10.3390/s21030920

Received: 10 December 2020
Accepted: 26 January 2021
Published: 29 January 2021

Publisher's Note: MDPI stays neutral with regard to jurisdictional claims in published maps and institutional affiliations.

Copyright: © 2021 by the authors. Licensee MDPI, Basel, Switzerland. This article is an open access article distributed under the terms and conditions of the Creative Commons Attribution (CC BY) license (http://creativecommons.org/licenses/by/4.0/).

1. Introduction

Coronavirus disease 2019 (COVID-19) has had a major impact on society at a global level, where social distancing, monitoring, and tracking has become effective in controlling and reducing the spread of the virus [1]. Precise localization and tracking technologies for use in indoor and outdoor environments will play a crucial role in dealing with COVID-19 and other pandemic outbreaks in the future. Nowadays, indoor positioning has a prominent contribution in day-to-day activities in organizations such as health care centers, airports, shopping malls, manufacturing, underground locations, etc., for the safe operating environments. In indoor environments, both radio frequency (RF) and optical wireless-based technologies could be adopted for localization [2,3]. Although the RF-based global positioning system offers higher penetration rates with reduced accuracy (i.e., in the range of a few meters), it does not work well in indoor environments (and not at all in certain cases such as tunnels, mines, etc.) due to the very weak signal and no direct access to the satellites [4–6]. On the other hand, the light-based system known as a visible light positioning (VLP) system, which uses the light-emitting diodes (LEDs)-based lighting infrastructure, could be used at low cost and high accuracy compared with the RF-based system [7,8].

VLP can be implemented using different techniques. Proximity and scene analysis (i.e., fingerprinting) are considered the simplest methods with relatively low positioning errors ε_p i.e., typically in a range of 10 to 45 cm, depending on the fingerprint database [8–10]. In the scene analysis technique, the estimation process of the relative position can be obtained by comparing the measured value with a pre-measured location of each position and then matching it to determine the real position. However, the measurement can be affected by the distributions of base stations, i.e., transmitters (Txs), shadowing and blocking, as well as the absolute location (i.e., probabilistic and correlation) dependency on pattern recognition techniques [9]. A VLP using two photodiodes (PDs) and an image sensor (IS) was proposed in [7,8,11]. Note, visible light communication (VLC) with IS (composed of a large PD array) naturally fits well with multiple inputs multiple-output systems in indoor and outdoor applications. In IS-based VLP, image-processing techniques can be used to determine the position but at the cost of increased complexity [12]. Note that, in VLP the transmission speeds (i.e., data rates) of the PD and IS are not critical at all since the aim is to achieve positioning with high accuracy [13]. Most research reported on VLP has focused on the investigation of geometrical properties using triangulation/trilateration, fingerprinting, or proximity methods to determine the transmission distance based on establishing a one-to-one relationship between the target location and its received signal strength (RSS). In such works, the analyses were based on the intensity modulation, angle of arrival [9], time of arrival [10], time difference of arrival [14], time of flight (TOF), and direct detection. In VLP systems, linear least square (LLS) or non-linear least square (NLLS) algorithms are often used for the position estimation [15–17].

Despite the fact that the user's mobility can influence the performance of the VLP system, most research reported in the literature has focused primarily on static scenarios. The major issues of shadowing and blocking affecting user's mobility were reported in [18], where the VLC system performance considering the changes in the channel conditions in different indoor scenarios (i.e., a furniture equipped office room, an empty hall, and a corridor) was investigated. It was shown that, the cumulative distribution function (CDF) of the received power distribution differs in the worst case by up to 7% in a furnished office (people density > 0.16 people/m^2). Alternatively, the highest root mean square (RMS) delay spread of 6.5% in comparison with the case with no people was observed for an empty hall. The results also revealed that, the corridor with the maximum RMS delay of 2% at the people density >0.16 people/m^2 is the most robust against the people's movement compared with the other two where the problem of shadowing or blockage could be readily avoided. Another concern with the user's mobility is the processing time required that needs considering with respect to the speed of movement for the receiver (Rx).

In most of the reported methods, the angular dependency was neglected in RSS-based localization with the assumption that, the Rx has a fixed height and is pointing up towards the Txs [19]. However, computational and implementation costs are too high, and the assumptions made may not be valid in real-time application scenarios with mobile Rxs, which needs further investigation. Recent works have focused on the impact of multipath induced reflections on the performance of VLP without considering the tilting angles [20–22], where it was shown that, multipath reflections considerably increase ε_p; whereas in [23], it was shown that, the channel capacity can be significantly improved by carefully selecting the Rx's tilting angle θ_{Rx}. However, the initial research demonstrated that in VLP θ_{Rx} usually results in increased ε_p (i.e., lower accuracy).

The widely used commercially available LED spotlights in building facilitates the concept of using Txs with tilting features. For instance, the impact of the Tx (LED) tilting angle θ_{Tx} on the accuracy of RSS-based VLP was studied in [24], where it was shown that ε_p increased (i.e., in the order of centimeters) with θ_{Tx}. In [25], a 4-LED VLP system using an artificial neural network (ANN) was proposed to improve the positioning accuracy, which is impacted by the random and unknown static Tx tilt angle with a maximum variation of 2°. It was shown that ANN offered improved performance compared

with standard trilateration, achieving localization errors below 1 cm for the line-of-sight (LoS) channel. In Addition, an RSS-based localization algorithm with multidimensional LED array was proposed in [26], where the design of the lamp structure was introduced to exploit the direction of the LED in a LoS environment. The authors showed that, the proposed system achieved a RMS error of 0.04 and 0.06 m in two- and three-dimensional localization, respectively for the LED with a tilt angle of 15°. While in [27], an angle diversity Tx (ADT) together with accelerometers was proposed for uplink three-dimensional localization in a LoS environment. ADT was a combination of 19 or 37 LEDs (LEDs array), which were placed on the ground, and PDs located on the ceiling. The results showed that, an average localization error of less than 0.15 m.

The impact of non-line of sight (NLoS) path in a VLC system deployed in a referenced empty room has been reported in the literature. In [28], the impact of the power levels from NLoS paths on the performance of VLP for different Rx positions and their orientations was reported. It provided a theoretical framework for the design of VLP resource allocation methods to improve the performance of the non-tilted Tx. Channel modeling and its characterisation with the existence of reflections from objects and surfaces were investigated in [29]. Considering the delay spread and the channel gain in a typical room, it was shown that it is not required to consider all objects within rooms [29,30]. Moreover, the use of flexible organic LED-based VLC in indoor environments (i.e., offices, corridors, semi-open corridors in shopping malls, etc.) was investigated in [31], where it was shown that the channel gain in an empty room is higher by 4.8 and 5.2 dB compared with the fully furnished room and a semi-open corridor, respectively [31].

Unlike previous works, in this paper we investigate LED tilting for the first time and show that it can be beneficial in VLPs in improving the positioning accuracy (PA). We show the impact of reflections on the accuracy by means of the received power from both LoS and NLoS transmission paths, the positioning algorithm utilized, and the accuracy of the VLP system for a single PD-based static Rx (i.e., putting the Rx at fixed locations) where the user movement has not been considered. In this approach, the Txs are oriented towards the pointing center F with the (x_F, y_F, z_F) coordinates without violating the acceptable uniformity range of the light distribution in the illuminated region. Note, F is selected at the center of the receiving plane in this work, and alignment is achieved with respect to the Tx normal $\hat{\boldsymbol{t}}_k$.

We investigate the regression, which is fitted with the received power P_R points at various Rx locations for two different scenarios. Note, the Rx locations are within a squared shape region centered at F with a side length D_r. The polynomial regressions (PRs) are fitted with the PR points for the full and half rooms of areas of 6 × 6 and 3 × 3 m², which is termed as scenarios S1 and S2, respectively-. The study is carried out using the LLS algorithm for position estimation, which is a low complexity solution. Hence, we offer a significant accuracy improvement by up to ~66% compared with a link without Tx's tilt. We show ε_p of 1.7, and 1.3 cm for S1 and S2, respectively, and for z_F of 0 m (i.e., the height of F from the floor level). Furthermore, we investigate z_F with respect to ε_p and we show that, the lowest ε_p of 1.3 and 0.8 cm were for S1 and S2, respectively.

The remainder of this paper is structured as follows. Section 2 presents the VLC system model used in the positioning algorithm. The positioning algorithm is briefly explained in Section 3. The results and discussion are included in Section 4. Finally, Section 5 provides the conclusion of the paper.

2. Proposed Visible Light Positioning (VLP) System Model

In RSS-based localization systems, positioning accuracy depends mainly on P_R. For NLoS links, reflection from near and far walls should be considered, which contributes to the degradation of PA. For example, Figure 1 illustrates a system with two Txs aligned with respect to F (i.e., shown as the tilted Tx normal $\hat{\boldsymbol{t}}_k$), which is used to investigate the impact of reflections from walls on the accuracy of VLP). Here, the aim is to maximize P_R from the LoS paths to improve accuracy at F, which is initially set at the center of the re-

ceiving plane (i.e., x_F, y_F, and z_F are all set to zero). The tilting orientation is estimated based on the position of F, which is given by:

$$\hat{\boldsymbol{t}}_k = \frac{\overrightarrow{T_k}}{\left\|\overrightarrow{T_k}\right\|}, \tag{1}$$

where $\overrightarrow{T_k}$ is a vector that represents the difference between the coordinates of the k^{th} Tx and point F (x_F, y_F, z_F), and $\|\cdot\|$ is the Euclidean norm. The tilted irradiance angle $\omega_{k,w}^{\text{tilt}}$ is given by:

$$\cos\left(\omega_{k,w}^{\text{tilt}}\right) = \frac{d_{k,w}.\hat{\boldsymbol{t}}_k}{\left\|d_{k,w}\right\|.\left\|\hat{\boldsymbol{t}}_k\right\|}, \tag{2}$$

where $d_{k,w}$ is the distance between the k^{th} Tx and the reflective area, and $\cdot$ represents the product dot operation.

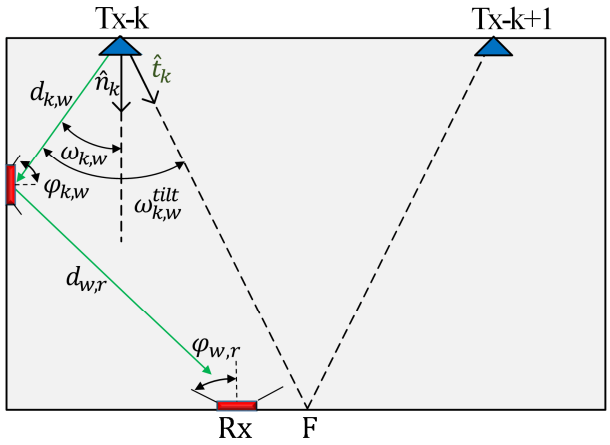

(**a**)

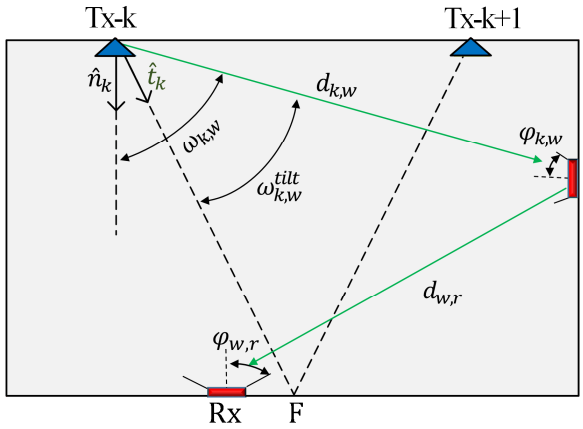

(**b**)

Figure 1. An example of a reflected light ray in case of light-emitting diode (LED) tilt: (**a**) near-wall reflections case, and (**b**) far wall reflections case.

The NLoS power contributions from the near-wall reflections represented by the Tx's cosine terms expressed in (2) can be reduced by tilting the Txs towards F (i.e., $\hat{\boldsymbol{t}}_k$ is directed towards F that implies $\omega_{k,w}^{\text{tilt}} > \omega_{k,w}$, where $\omega_{k,w}$ is the irradiance angle with no tilted Tx, see Figure 1a. Even though the Tx's cosine terms of NLoS signals will increase for the far-wall reflections, which is implied by $\omega_{k,w}^{\text{tilt}} < \omega_{k,w}$, the link experience a higher path loss due to the longer transmission range, see Figure 1b. Having these observations

in mind, we can infer that tilting the Txs can be beneficial in VLP by leveraging the effect of reflections from both near- and far-walls. Under this perspective, it reasonable to explore tilting based on F at the center of the receiving plane and investigate how this can improve PA. These observations remain valid for the entire area of the walls when concerning the first reflection. Higher-order reflections also have an impact on positioning accuracy. However, due to the fact that these higher-order reflections have reduced power levels when compared with the LoS and 1st order case in regions near the center of the room, the previous discussion is still valid, and LoS power can be maximized by tilting towards the center.

Figure 2 shows the geometrical set-up diagram of the proposed indoor VLP system, which is composed of 4 Txs (i.e., LEDs) and an Rx (i.e., a PD) positioned on the ceiling and the floor level, respectively. Each k^{th} Tx has a known set of coordinates (x_k, y_k, z_k), which is associated with the world coordinate system (WCS), with $\hat{\boldsymbol{t}}_k$ of $[\sin\theta_{\text{Tx},k}\cos\alpha_k, \sin\theta_{\text{Tx},k}\sin\alpha_k, -\cos\theta_{\text{Tx},k}]$ where $\theta_{\text{Tx},k}, \alpha_k$ are the tilting and azimuth angles, respectively and k is 1, …, 4. Note that, in this work, as a reference, an empty room is considered to study the impact of Tx's tilting on the positioning accuracy. The proposed system can be utilized for positioning purposes where the positioning accuracy is a major concern. However, if indoor positioning system uses the already existing wireless communication network architectures, then high accuracy may no longer be critical. Therefore, there exists always a trade-off between accuracy and other system requirements including scalability, complexity, coverage, etc.

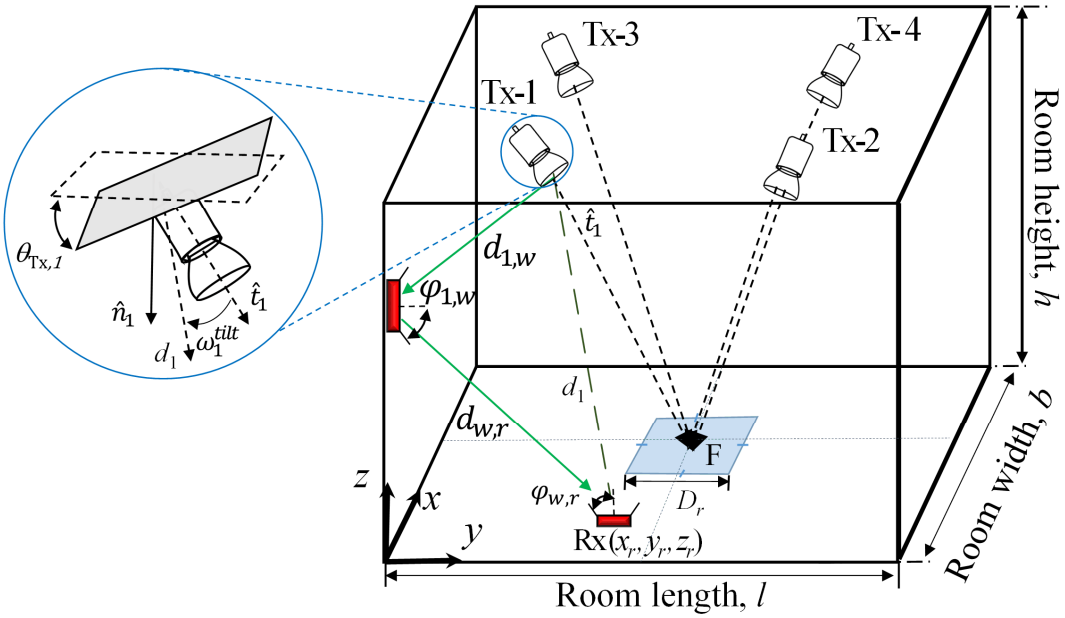

Figure 2. The proposed indoor visible light positioning (VLP) system with the tilted transmitter (Tx).

Each Tx broadcast unique ID information of 2 bits, which is encoded and modulated using on-off keying (OOK), which allows separation at the Rx using a correlation method that can be received at the Rx in advance of location identification, see Figure 3. Considering the 1st order reflections, the received total power is given by:

$$P_R = \sum P_{R-\text{LoS}} + \sum P_{R-\text{NLoS}}, \tag{3}$$

where $P_{R-\text{LoS}}$ and $P_{R-\text{NLoS}}$ represent the received power for LoS and NLoS, respectively. Typically, the signal-to-noise ratio in standard VLC will be high (>20 dB [32]), which would be considered noise-free in common cases). Moreover, noise sources (mostly dominated by the background lights) [32] will have a similar effect on the VLP system

with and without tilting Tx. Thus, a noise-free system is considered in this work. The conventional trilateration technique based on a range of three minimum observation points offers the advantage of simple geometrical solutions [14]. Using the RSS algorithm and 4-Tx (i.e., LEDs), the $P_{R-\mathrm{LoS}}$ for the LoS path is given as [33,34]:

$$\sum P_{R-\mathrm{LoS}} = \sum_{k=1}^{K} C_{\mathrm{o}} P_t \frac{\cos^m\left(\omega_k^{\mathrm{tilt}}\right)\cos(\varphi)}{\|d_k\|^2} T_s(\varphi) g(\varphi), \tag{4}$$

where

$$C_{\mathrm{o}} = \frac{m+1}{2\pi} \mathcal{R}\, A_r, \tag{5}$$

and

$$m = -\frac{\ln(2)}{\ln\left(\cos\left(\Theta_{\frac{1}{2}}\right)\right)}, \tag{6}$$

where K is the total number of Txs, $\Theta_{1/2}$ is the light source irradiance half-power angle, ω_k^{tilt} and φ are the tilted irradiance angle from the k^{th} Tx to the Rx and the receiving incident angle, respectively. d_k is the distance between k^{th} Tx and Rx. A_r and $\mathcal{R}$ are the PD's active area and responsivity, respectively. $T_s(\varphi)$ and $g(\varphi)$ are the gains of the optical filter and the concentrator at the Rx, respectively. Note, $T_s(\varphi)$ and $g(\varphi)$ are set to unity, $\varphi < 90°$ and $d \gg \sqrt{A_r}$.

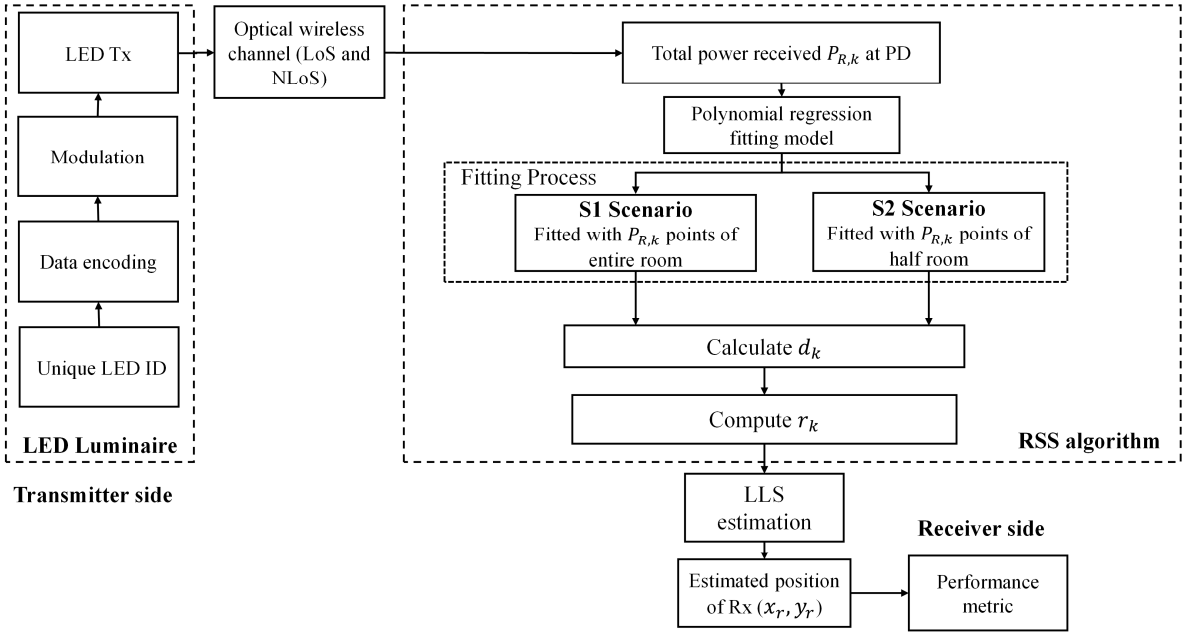

Figure 3. Block diagram of the proposed VLP system.

For the NLoS path and considering only the first-order reflection, the received total power can be expressed as [32]:

$$\sum P_{R-\mathrm{NLoS}} = \sum_{k=1}^{K} \sum_{\mathrm{wall}} \rho C_{\mathrm{o}} P_t A_{\mathrm{ref}} \frac{\cos^m\left(\omega_{k,w}^{\mathrm{tilt}}\right)\cos\left(\varphi_{k,w}\right)}{\pi\left(\left\|d_{k,w}\right\|\left\|d_{w,r}\right\|\right)^2} T_s\left(\varphi_{w,r}\right) g\left(\varphi_{w,r}\right)\cos\left(\omega_{w,r}\right)\cos\left(\varphi_{w,r}\right), \tag{7}$$

where $d_{k,w}$, $\omega_{k,w}^{\mathrm{tilt}}$, and $\varphi_{k,w}$ are the distances, irradiance angle, and the receiving incident angle between the k^{th} Tx and the reflective area, respectively. $d_{w,r}$, $\omega_{w,r}$, and $\varphi_{w,r}$ are the distances, irradiance angle, and the receiving incident angle between the reflective area and the Rx, respectively, see Figure 1a. ρ is the reflection coefficient, which depends

on the material of the reflective surface and A_{ref} is the reflection area. $P_{R-\text{NLoS}}$ for the signals from the NLoS paths is determined based on the Matlab code 3.2 from [32].

Moreover, the uniform distribution of the P_R inside the illuminated zone is essential in indoor environments [16]. The uniformity of light distribution in the room (U) is represented as the ratio of the minimum to maximum power intensity at the receiving plane, which is given by:

$$U = \frac{\min(P_R)}{\max(P_R)}, \tag{8}$$

Here we consider a grid (1 cm resolution) of 3600 Rx positions on the receiving plane, which is associated with WCS of (x_r, y_r, z_r). We have also specified the dedicated region, which is a square shape centered at the point F and located at the receiving plane. The receiving positions are considered inside this region only. All the other key system parameters are given in Table 1.

Table 1. The key system parameters.

Parameter	Symbol	Value
Room size	(l, b, h)	6 × 6 × 3 m^3
The coordinates of		
Tx-1	(x_1, y_1, z_1)	(−1.7 m, −1.7 m, 3 m)
Tx-2	(x_2, y_2, z_2)	(1.7 m, −1.7 m, 3 m)
Tx-3	(x_3, y_3, z_3)	(−1.7 m, 1.7 m, 3 m)
Tx-4	(x_4, y_4, z_4)	(1.7 m, 1.7 m, 3 m)
Transmit power of each Tx	P_t	1 W
Receiver's field of view	FoV	75°
Reflection coefficient	ρ	0.7
Half power angle	HPA	60°
Photodiode area	A_r	10^{-4} m^2
Responsivity	$\mathcal{R}$	1 A/W
Reflection coefficient	ρ	0.7

3. Positioning Algorithm

3.1. Distance Estimation Using Polynomial Regression

The block diagram of the proposed VLP system is shown in Figure 3, in which P_R is processed to estimate the Rx position. Distance estimation is the central feature of the RSS positioning approach, and for LoS paths it is normally deducted from (4), which is estimated as:

$$\|d_k\|^2 = \|r_k\|^2 + h^2 \tag{9}$$

where h is the vertical distance between the Tx and the Rx. The estimated distance between the Rx and the k^{th} Tx can be estimated from (4), which is given by:

$$r_k = \sqrt{\left(\frac{P_t \mathrm{C_o} h^{m+1}}{P_{R-\text{LoS},k}}\right)^{\frac{2}{m+3}} - h^2}, \tag{10}$$

where, $P_{R-\text{LoS},k}$ is the LoS received power at Rx from k^{th} Tx. In NLoS links, this approach results in increased errors due to reflections [35,36], therefore the distance estimation approach using (10) is no longer valid. One possible approach would be to generate a polynomial fitted model for the power and distance relationship as defined by:

$$d_k = a_0 + a_1 P_{R,k} + a_2 \left(P_{R,k}\right)^2 + \cdots + a_j \left(P_{R,k}\right)^j, \tag{11}$$

where a_j is the coefficient of the fitted polynomial at j^{th} degree polynomial and $P_{R,k}$ is the total received power at Rx from k^{th} Tx. Note, d_k is computed using (11), which is then substituted into (9) to determine r_k.

3.2. Linear Least Square (LLS) Estimation

LLS is adopted to analyze the performance of the proposed system by considering the estimated distances of the NLoS paths, which is a low complexity solution as compared with the NLLS algorithm. Following geometric properties, a minimum of 3-Tx located at the center of the circle is required, where the estimated distance is considered as the circle radius. The intersection point of the three circles is considered as the measured position of the Rx. E.g., the k^{th} LED luminaire is positioned at (x_k, y_k, z_k) and the Rx is located at (x_r, y_r, z_r). A closed-form solution using the LLS estimation method is given by:

$$X = (A^T A)^{-1} A^T B \tag{12}$$

where

$$A = \begin{bmatrix} x_2 - x_1 & y_2 - y_1 \\ x_3 - x_1 & y_3 - y_1 \\ x_4 - x_1 & y_4 - y_1 \end{bmatrix}, \; X = \begin{bmatrix} x_r \\ y_r \end{bmatrix} \tag{13}$$

$$B = 0.5 \times \begin{bmatrix} ({r_1}^2 - {r_2}^2) + ({x_2}^2 + {y_2}^2) - ({x_1}^2 + {y_1}^2) \\ ({r_1}^2 - {r_3}^2) + ({x_3}^2 + {y_3}^2) - ({x_1}^2 + {y_1}^2) \\ ({r_1}^2 - {r_4}^2) + ({x_4}^2 + {y_4}^2) - ({x_1}^2 + {y_1}^2) \end{bmatrix}. \tag{14}$$

4. Results and Discussion

4.1. Impact of the Transmitter (Tx) Tilting on the Radiation Pattern

Figure 4a shows the received power distributions for the link (i.e., received signal strength indicator RSSI) with and without the tilting Txs. Note, the Txs are directed towards F following the proposed model in Section 2. As shown in Figure 4b, there is a significant improvement in the power distribution with the tilting Txs (i.e., a much more uniform distribution) around the center of the receiving plane. All the observed tilted Tx normal $\hat{\mathbf{t}}_k$ for 4-Tx are given in Table 2.

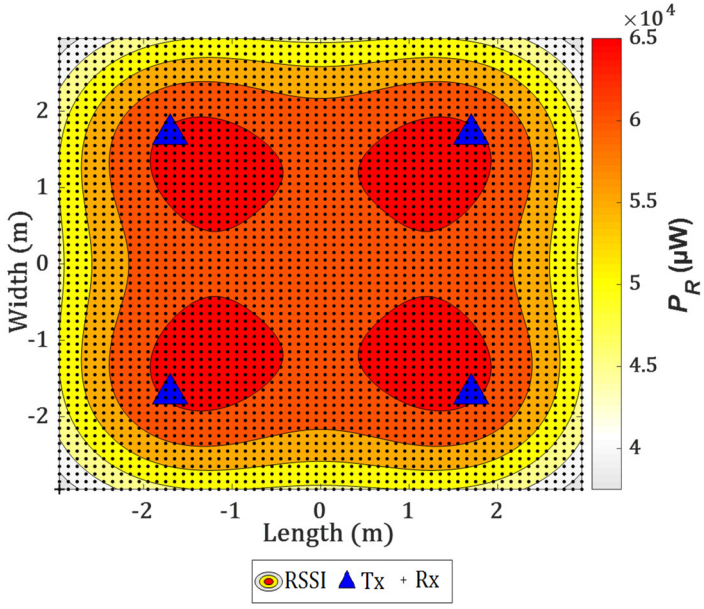

(**a**)

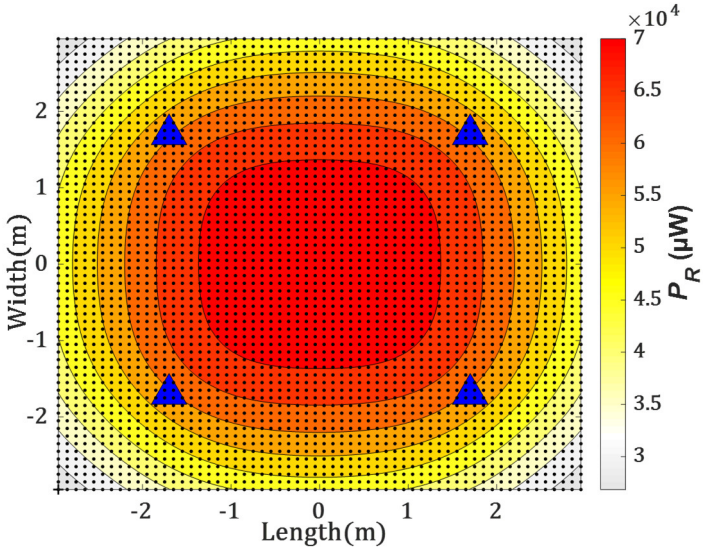

(**b**)

Figure 4. The received power distributions for the proposed system for the Txs with: (**a**) no tilting, and (**b**) tilting.

Table 2. The values of tilted Tx normal for all Txs.

Tx Number	Tilted LED Normal, $\hat{t}_k$
Tx-1	[0.4, 0.4, −0.8]
Tx-2	[−0.4, 0.4, −0.8]
Tx-3	[0.4, −0.4, −0.8]
Tx-4	[−0.4, −0.4, −0.8]

4.2. Polynomial Fitting

With reference to Figure 3, d_k is estimated based on $P_{R,k}$ and the PR (polynomial regression) method as outlined in Section 3.1. The accuracy and precision of fitting are measured by the coefficient of determination R^2, which is a statistical measure of how close the data are to the fitted regression line, and the standard deviation. Note, PR is considered for various data points and categorized into two scenarios S1 and S2 based on the room dimensions. For scenarios S1 and S2, the PRs are fitted with the $P_{R,k}$ points for the full and half rooms of areas of 6 × 6 and 3 × 3 m^2, respectively. The deviation of $P_{R,k}$ points is impacted mainly by the reflections wherein the data near the walls imply a larger estimation error as stated previously in the literature [19,32]. Therefore, 3600 samples (a full room with a 1 cm grid size) are considered for the polynomial fitting for S1, while for S2 we only have considered 900 samples (an inner half room). A stabilized residual sum of squares is achieved with the polynomial order j of 4. The polynomial coefficients of the fitted curve and R^2 are estimated for both S1 and S2.

The polynomial fitted curves for VLP without and with the tilting Txs are illustrated in Figure 5. The green points and blue plots indicate the $P_{R,k}$ points for the full and half rooms, respectively. Figure 5a shows that, the $P_{R,k}$ points span between 0 and 4.2 mW, and are uniformly distributed for both S1 and S2. However, Figure 5b depicts that the $P_{R,k}$ points for S1 are more scattered with a smaller span of 0.5 to 3.2 mW, which corresponds to the corner of the room. In S2, the $P_{R,k}$ points are more focused towards S2 due to tilting of the Tx, thus the fitting data points are considered for S2 only. From the results obtained, both R^2 and the standard deviation are positively affected with tilting of the Tx, i.e., higher R^2 value of 0.98 and lower standard deviation of 0.98 is achieved for the tilted Tx as compared with a lower R^2 value of 0.96 and higher standard deviation of 1.01 in the

case of no tilted Tx, see Figure 5b. Table 3 shows the estimated polynomial coefficients and R^2 values for S2 with and without the tilted Txs.

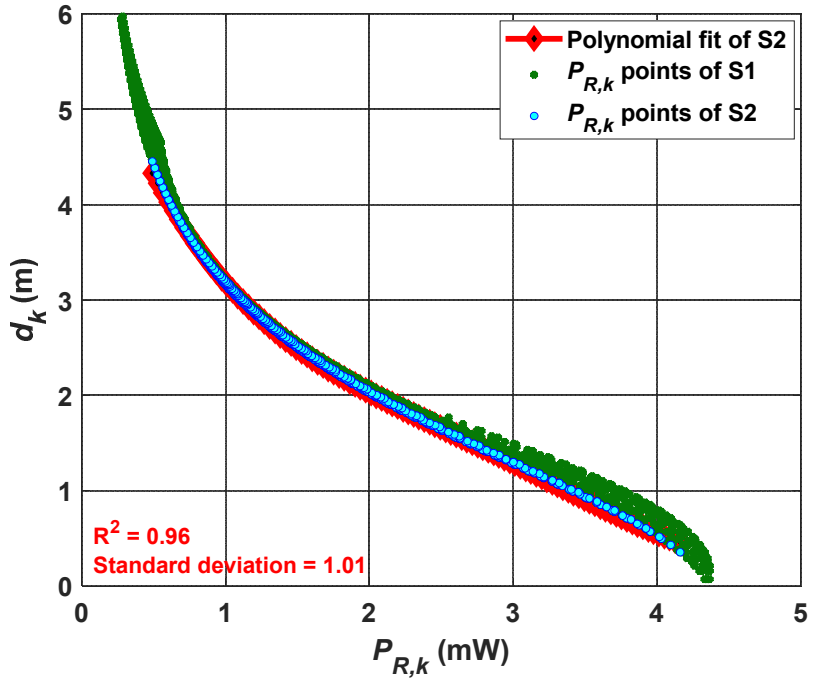

(**a**)

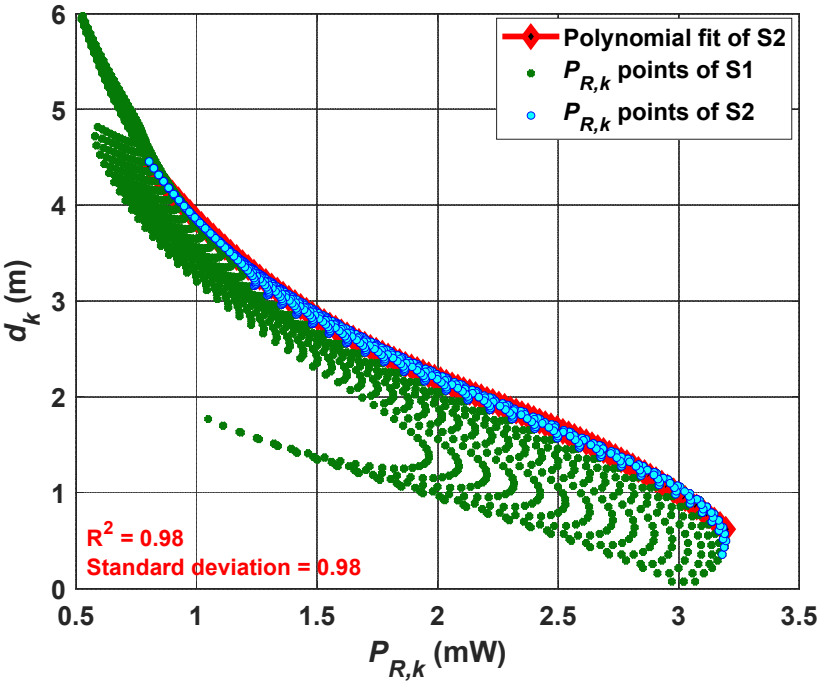

(**b**)

Figure 5. The distance estimation for Tx-k using the polynomial regression (PR) method employed in S2 for the Txs with: (**a**) no tilting, and (**b**) tilting.

Table 3. The coefficients of the polynomial fitted curve for the scenario S2.

Cases	Estimated Polynomial Coefficients (No Units)					R^2
	a_0	a_1	a_2	a_3	a_4	
With tilted Tx	7.38×10^4	-3.60×10^5	2.37×10^4	-6.26×10^2	8.10	0.98
Without tilted Tx	8.86×10^6	9.93×10^5	3.96×10^4	7.35×10^2	7.44	0.96

4.3. Impact of the Tx Tilting and the Altitude of F on VLP

In this section, we investigate ε_p for different values of D_r to realize the impact of tilted Txs near the center of the receiving plane, and further analyze the impact of changing the height of z_F on the positioning accuracy. Figure 6 illustrates Inv(90%) as a function of D_r for S1 and S2 with the LLS algorithm, which is applied for the case with LoS and NLoS paths to estimate the Rx's position, as described in Section 3. The quantile function Inv(χ) is used as a performance metric to observe the confidence interval of ε_p, which is given by:

$$\varepsilon_{p,\chi} = \text{Inv}(\chi) = \text{CDF}^{-1}(\chi) \quad (15)$$

where χ is the percentage of the confidence interval, and CDF represents the cumulative distribution function of ε_p.

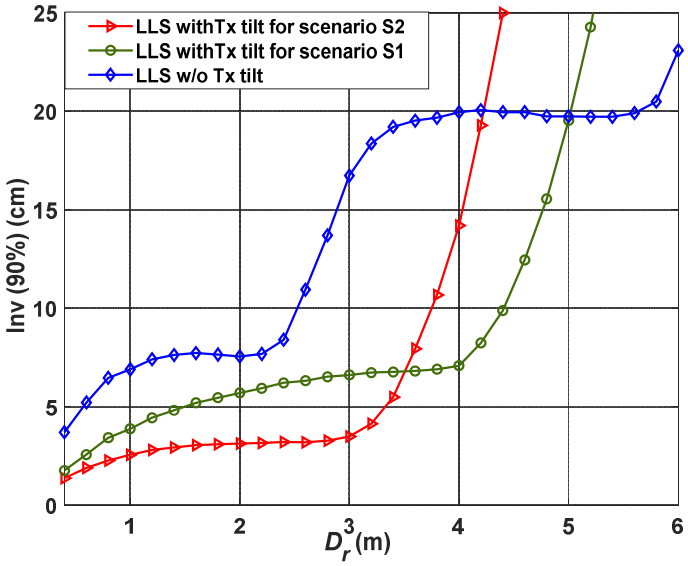

Figure 6. The measured quantile function at χ of 90% for various D_r for linear least square (LLS) with and without the tilted Txs.

To ensure a VLP link with high reliability, we have selected a 90% confidence interval for ε_p to include the majority of the measured points. Note that, the Txs' tilting angle is fixed at the point F for all values of D_r. Moreover, the error can be reduced significantly depending on S1 or S2. For instance, for S1, ε_p values of 1.7 and 3.6 cm are obtained for both tilting and non-tilting scenarios, respectively for D_r of 40 cm. In addition, we have achieved the accuracy improvement of 44, 24, 60, and 64% for D_r of 1, 2, 3, and 4 m, respectively with the maximum accuracy improvement of 66% for D_r of 3.6 m. In addition, for S2, ε_p of 1.3 cm is obtained for the observation area with D_r of 40 cm with the tilted Tx. Hence, the Tx's tilting (LED tilting angle) can improve the positioning accuracy in both S1 and S2 with the same detection area of 5 × 5 m^2 (up to D_r of 5 m) as compared with the case with non-tilting Tx. This could be explained by the fact that, for large observation areas (i.e., large D_r), the CDF of the error becomes affected by the walls and corners of the room, with no improvement in the accuracy. Hence, the NLoS paths become dominant for regions far away from the point F, which degrades the positioning

accuracy. Therefore, the proposed VLP system with the tilted Txs outperforms the system with no tilting Txs for almost the entire room i.e., an area of 5 × 5 m².

We further analyze the impact of changing the height of pointing center F (i.e., z_F) on the positioning accuracy, which is eventually the variation in the Tx's tilting. Figure 7 depict the Inv(90%) as a function of D_r for a range z_F (i.e., −2 to 2 m) with and without the tilting Txs for S1 and S2. Note that, a high negative value of z_F implies that the Tx is pointing vertically downwards towards the Rx. For instance, −∞ for z_F corresponds to the standard non-tilted case and it does not imply reception under the floor. From the Figure 7, it is observed that, (i) ε_p increases and decreases s with the positive and negative values of z_F (i.e., $z_F > 0, < 0$), respectively for both S1 and S2; (ii) the minimum ε_p of 1.3 cm is at z_F of −0.5 m compared with 1.7 cm for z_F of 0 m for S1 with D_r of 40 cm, see Figure 7a; and (iii) the lowest ε_p is achieved at $-2 < z_F < 0$ m depending on the value of D_r. The proposed VLP system can be further improved for the regions with D_r of up to 5.5 m by adjusting the negative value of z_F. For S2, the minimum ε_p of 0.8 cm is observed at z_F of −2 m and D_r of 40 cm compared with 1.3 cm at F (i.e., $z_F = 0$ m), see Figure 7b. However, the case with tilting Txs offers the lowest ε_p for D_r up to 4.36 m.

Finally, Figure 8 shows the uniformity of light distribution U against D_r without and with the tilting Tx and a range of z_F. The dashed line represents the EN 12464-1 European standard of lighting in an indoor environment [37], which defines the minimum acceptable ranges of uniformity of the light distribution. We have shown that the proposed VLP system with the tilting Txs is capable of providing higher uniformity for the entire room for $z_F \leq -1$ m. The uniformity of the VLP system with tilted Tx increases with the decreased value of z_F.

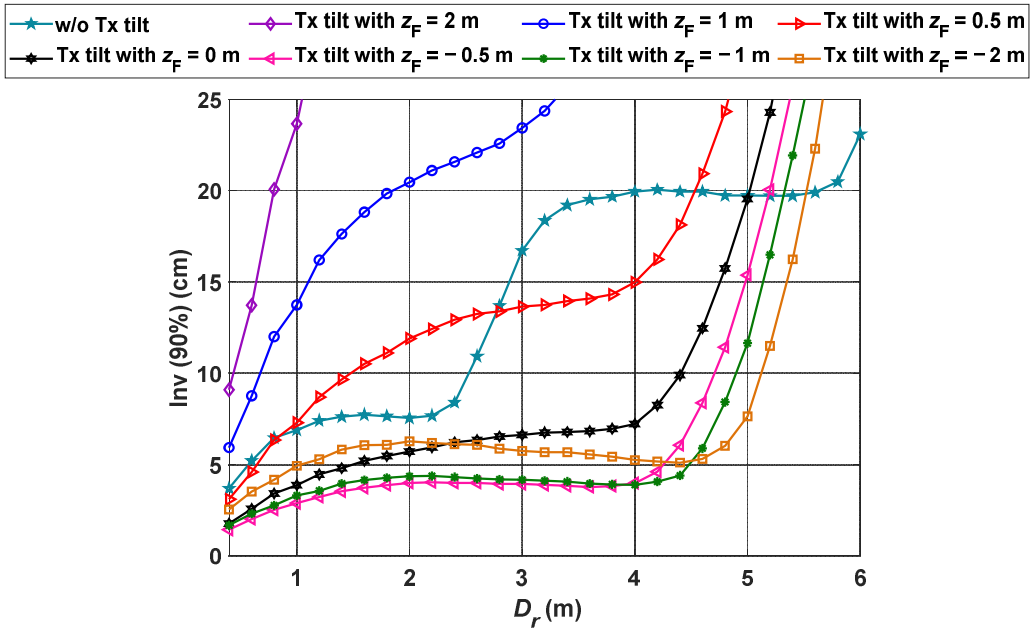

(a)

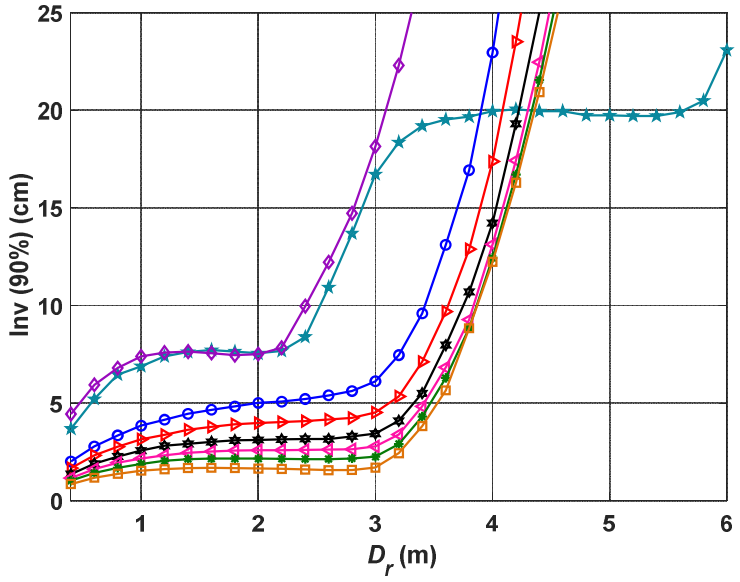

(**b**)

Figure 7. The measured quantile function at χ of 90% for various z_F values for: (**a**) S1, and (**b**) S2.

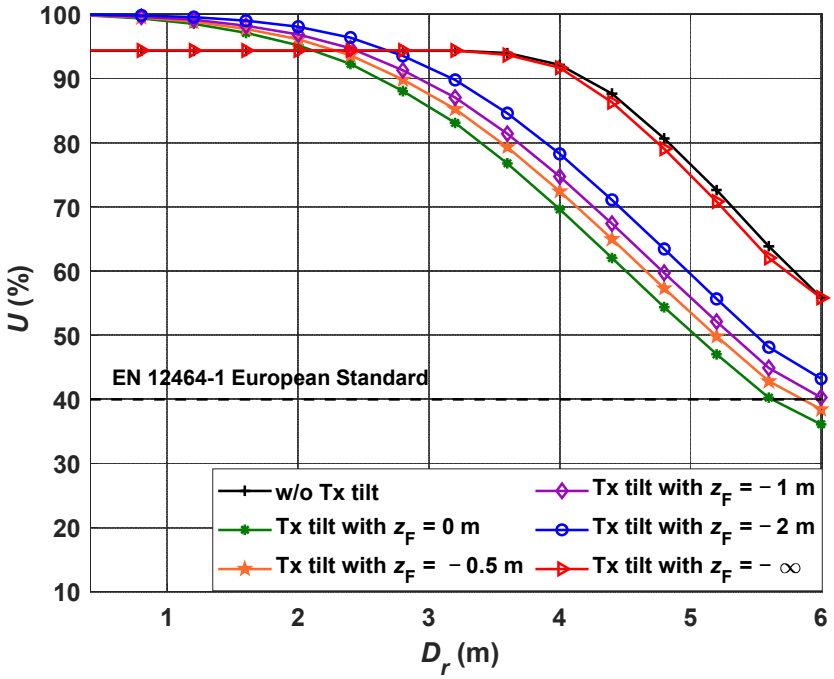

Figure 8. The uniformity of light distribution in different D_r *w/o* and with the tilting Txs.

5. Conclusions

In this paper, a novel approach was proposed to achieve a highly accurate indoor VLP system by considering multipath reflections. Initially, the Tx was tilted towards the center of the receiving plane to achieve higher accuracy by maximizing the received power level due to contributions from the LoS paths at the pointing center F. The positioning error was estimated by using the LLS algorithm with polynomial regression. We investigated the regression fitted with the received power points for two scenarios of S1 and S2. The results showed a significant improvement in the accuracy by up to ~66% compared with a typical non-tilting Tx case. In addition, positioning errors of 1.7, and 1.3 were obtained for the tilted Tx for S1 and S2, respectively at z_F of 0 m. The results also

showed that, the uniformity of the proposed VLP system in line with European Standard EN 12464-1, therefore meeting the uniformity requirement of the visible illumination regions. Furthermore, we improved the accuracy of the proposed VLP system by controlling the height of F by achieving the lowest ε_p of 1.3 and 0.8 cm for S1 and S2, respectively. Ultimately, it was concluded that the proposed VLP system with the tilting Tx outperforms the non-tilted Tx scenario. Likewise, we could gain lower ε_p when considering S2, whereas ε_p will increase with D_r as indicated for S1.

Author Contributions: The contributions of the authors in this paper are the following: conceptualization: N.C., O.I.Y., L.N.A., and Z.G.; investigation: N.C., and O.I.Y.; methodology: N.C., O.I.Y., L.N.A. and Z.G.; project administration: L.N.A., Z.G., and S.Z.; software: N.C., and O.I.Y.; validation: L.N.A., Z.G., S.Z., and H.L.-M. All authors have read and agreed to the published version of the manuscript.

Funding: This research was funded by H2020/MSCA-ITN funding program under the framework of the European Training Network on Visible Light Based Interoperability and Networking, project (VisIoN) grant agreement No 764461. One of the authors (Othman Isam Younus) is funded by the Northumbria University Ph.D. scholarship.

Institutional Review Board Statement: Not applicable.

Informed Consent Statement: Not applicable.

Conflicts of Interest: The authors declare no conflict of interest.

Nomenclature

Short Form	Description
ADT	Angle diversity transmitter
ANN	Artificial neural network
CDF	Cumulative distribution function
IS	Image sensor
LEDs	Light-emitting diodes
LLS	Linear least square
LoS	Line of sight
NLLS	Nonlinear least square
NLoS	Non-line of sight
OOK	On-off keying
PA	Positioning accuracy
PDs	Photodiodes
PR	Polynomial regression
RF	Radio frequency
RMS	Root mean square
RSS	Received signal strength
RSSI	Received signal strength indicator
Rx	Receiver
TOF	Time of flight
Tx	Transmitter
VLC	Visible light communication
VLP	Visible light positioning
WCS	World coordinate system

References

1. Nguyen, C.T.; Saputra, Y.M.; Huynh, N.V.; Nguyen, N.-T.; Khoa, T.V.; Tuan, B.M.; Nguyen, D.N.; Hoang, D.T.; Vu, T.X.; Dutkiewicz, E.; Chatzinotas, S.; Ottersten B. A Comprehensive Survey of Enabling and Emerging Technologies for Social Distancing—Part I: Fundamentals and Enabling Technologies. *IEEE Access* **2020**, *8*, 153479–153507.

2. Luo, J.; Fan, L.; Li, H. Indoor Positioning Systems Based on Visible Light Communication: State of the Art. *IEEE Commun. Surv. Tutor*. **2017**, *19*, 2871–2893.
3. Armstrong, J.; Sekercioglu,Y.A.; Neild, A. Visible Light Positioning: A Roadmap for International Standardization. *IEEE Commun. Mag*. **2013**, *51*, 68–73.
4. Chung, J.; Donahoe, M.; Schmandt, C.; Kim, I.-J.; Razavai, P.; Wiseman, M. Indoor location sensing using geo-magnetism. In Proceedings of the 9th International Conference on Mobile Systems, Applications, and Services, Washington, DC, USA, 29 June–01 July 2011, pp. 141–154.
5. Youssef, M.; Agrawala, A. The Horus WLAN location determination system. In Proceedings of the 3rd International Conference on Mobile Systems, Applications, and Services, Washington, DC, USA, 6–8 June 2005, pp. 205–218.
6. Chen, Y.; Lymberopoulos, D.; Liu, J.; Priyantha, B. FM-based indoor localization. In Proceedings of the 10th International Conference on Mobile Systems, Applications, and Services, Low Wood Bay, Lake District, UK, 26–28 June 2012, pp. 169–182.
7. Elgala, H.; Mesleh, R.; Haas, H. Indoor optical wireless communication: Potential and state-of-the-art. *IEEE Commun. Mag*. **2011**, *49*, 56–62.
8. Maheepala, M.; Kouzani, A.Z.; Joordens, M.A. Light-Based Indoor Positioning Systems: A Review. *IEEE Sens. J*. **2020**, *20*, 3971–3995.
9. Do, T.H.; Yoo, M. An in-Depth Survey of Visible Light Communication Based Positioning Systems. (in eng). *Sensors (Basel)* **2016**, *16*, 678.
10. Chaudhary, N.; Alves, L.N.; Ghassemlooy, Z. Current Trends on Visible Light Positioning Techniques. In Proceedings of the 2019 2nd West Asian Colloquium on Optical Wireless Communications (WACOWC), Teheran, Iran, 27–28 April 2019, pp. 100–105.
11. Lee, J.; Kim, S.; Han, S. 3D Visible Light Indoor Positioning by Bokeh Based Optical Intensity Measurement in Smartphone Camera. *IEEE Access* **2019**, *7*, 91399–91406.
12. Cheng, H.; Xiao, C.; Ji, Y.; Ni, J.; Wang, T. A Single LED Visible Light Positioning System Based on Geometric Features and CMOS Camera. *IEEE Photonics Technol. Lett*. **2020**, *32*, 1097–1100.
13. Younus, O.I.; Hassan, N.B.; Ghassemlooy, Z.; Haigh, P.A.; Zvanovec, S.; Alves, L.N.; Minh, H.L. Data Rate Enhancement in Optical Camera Communications Using an Artificial Neural Network Equaliser. *IEEE Access* **2020**, *8*, 42656–42665
14. Rabadan, J.; Guerra, V.; Guerra, C.; Rufo, J.; Perez-Jimenez, R. A Novel Ranging Technique Based on Optical Camera Communications and Time Difference of Arrival. *Appl. Sci*. **2019**, *9*, 2382.
15. Zhuang, Y.; Hua, L.; Qi, L.; Yang, J.; Cao, P.; Cao, Y.; Wu, Y.; Thompson, J.; Haas, H. A Survey of Positioning Systems Using Visible LED Lights. *IEEE Commun. Surv. Tutor*. **2018**, *20*, 1963–1988.
16. Chaudhary, N.; Alves, L.N.; Ghassemlooy, Z. Impact of Transmitter Positioning Uncertainty on RSS-based Visible Light Positioning Accuracy. In Proceedings of the 12th International Symposium on Communication Systems, Networks & Digital Signal Processing (CSNDSP), Porto, Portugal, 20–22 July 2020.
17. Plets, D.; Almadani, Y.; Bastiaens, S.; Ijaz, M.; Martens, L.; Joseph, W. Efficient 3D trilateration algorithm for visible light positioning. *J. Opt*. **2019**, *21*, 05LT01.
18. Chvojka, P.; Zvanovec, S.; Haigh, P.A.; Ghassemlooy, Z. Channel Characteristics of Visible Light Communications within Dynamic Indoor Environment. *J. Lightwave Technol*. **2015**, *33*, 1719–1725.
19. Naz, A.; Asif, H.M.; Umer, T.; Ayub, S.; Al-Turjman, F. Trilateration-based indoor localization engineering technique for visible light communication system, *Softw. Pract. Exp*. **2020**, 1–14.
20. Gu, W.; Aminikashani, M.; Deng, P.; Kavehrad, M. Impact of Multipath Reflections on the Performance of Indoor Visible Light Positioning Systems. *J. Lightwave Technol*. **2016**, *34*, 2578–2587.
21. Plets, D.; Eryildirim, A.; Bastiaens, S.; Stevens, N.; Martens, L.; Joseph, W. A Performance Comparison of Different Cost Functions for RSS-Based Visible Light Positioning Under the Presence of Reflections. In Proceedings of the 4th ACM Workshop on Visible Light Communication Systems, Snowbird, UT, USA, 16 October 2017.
22. Liu, Y.; Zhang, J.; Liu, Y.; Chen, B.; Liu, S.; Zuo, Y. A new indoor visible light positioning scheme to reduce the influence of reflections. In 17th International Conference on Optical Communications and Networks (ICOCN2018), Zhuhai, China, 16–19 November 2018.
23. Wang, J.-Y.; Li, Q.-L.; Zhu, J.-X.; Wang, Y. Impact of receiver's tilted angle on channel capacity in VLCs. *Electron. Lett*. **2017**, *53*, 421–423.
24. Plets, D.; Bastiaens, S.; Martens, L.; Joseph, W. An Analysis of the Impact of LED Tilt on Visible Light Positioning Accuracy. *Electronics* **2019**, *8*, 389.
25. Raes, W.; Stevens, N. Performance Assessment of Artificial Neural Networks on the RSS-Based Visible Light Positioning Accuracy with Random Transmitter Tilt. In Proceedings of the International Symposium on Communication Systems, Networks and Digital Signal Processing (CSNDSP), Porto, Portugal, 20–22 July 2020.
26. Lixuan, W.; Caili, G.; Luo, P.; Li, Q. Indoor visible light localization algorithm based on received signal strength ratio with multi-directional LED array. In Proceedings of the 2017 IEEE International Conference on Communications Workshops (ICC Workshops), Paris, France, 21–25 May 2017, pp. 138–143.
27. Yin, L.; Wu, X.; Haas, H. Indoor Visible Light Positioning with Angle Diversity Transmitter. In Proceedings of the 2015 IEEE 82nd Vehicular Technology Conference (VTC2015-Fall), Boston, USA, 6–9 September 2015, pp. 1–5.

28. Zhou, B.; Liu, A.; Lau, V. Performance Limits of Visible Light-Based User Position and Orientation Estimation Using Received Signal Strength Under NLOS Propagation. *IEEE Trans. Wirel. Commun*. **2019**, *18*, 5227–5241.
29. Miramirkhani, F.; Uysal, M. Channel Modeling and Characterization for Visible Light Communications. *IEEE Photonics. J.* **2015**, *7*, 1–16.
30. Uysal, M.; Miramirkhani, F.; Narmanlioglu, O.; Baykas, T.; Panayirci, E. IEEE 802.15.7r1 Reference Channel Models for Visible Light Communications. *IEEE Commun. Mag.* **2017**, *55*, 212–217.
31. Chaleshtori, Z.N.; Ghassemlooy, Z.; Eldeeb, H.B.; Uysal, M.; Zvanovec, S. Utilization of an OLED-Based VLC System in Office, Corridor, and Semi-Open Corridor Environments. *Sensors* **2020**, *20*, 6869.
32. Ghassemlooy, Z.; Popoola, W.; Rajbhandari, S. *Optical Wireless Communications: System and Channel Modelling with Matlab®*, 2nd ed.; CRC Press: Boca Raton, FL, USA, 2019.
33. Chaudhary, N.; Alves, L.N.; Ghassemblooy, Z. Feasibility Study of Reverse Trilateration Strategy with a Single Tx for VLP. In Proceedings of the 2019 2nd West Asian Colloquium on Optical Wireless Communications (WACOWC), Teheran, Iran, 27–28 April 2019, pp. 121–126.
34. Younus, O.I.; Minh, H.L.; Dat, P.T.; Yamamoto, N.; Pham, A.T.; Ghassemlooy, Z. Dynamic Physical-Layer Secured Link in a Mobile MIMO VLC System. *IEEE Photonics J*. **2020**, *12*, 1–14
35. Shawky, S.; El-Shimy, M.A.; El-Sahn, Z.A.; Rizk, M.R.M.; Aly, M.H. Improved VLC-based indoor positioning system using a regression approach with conventional RSS techniques InProceedings of the *2017* 13th International Wireless Communications and Mobile Computing Conference (IWCMC), Valencia, Spain, 26–30 June 2017, pp. 904–909.
36. Sun, X.; Duan, J.; Zou, Y.; Shi, A. Impact of multipath effects on theoretical accuracy of TOA-based indoor VLC positioning system. *Photonics Res*. **2015**, *3*, 296–299.
37. De Normalisation, C.E. *EN 12464-1: Light and Lighting-Lighting of Work Places, Part 1: Indoor Work Places*; BSI: London, UK, 2002.

5.4 Impact of Transmitter Positioning and Orientation Uncertainty on RSS-based Visible Light Positioning Accuracy

This section is a version of the published manuscript:

> **N. Chaudhary**, L. N. Alves, and Z. Ghassemlooy, 'Impact of Transmitter Positioning and Orientation Uncertainty on RSS-based Visible Light Positioning Accuracy', Sensors, vol. 21, no. 9, p. 3044, April 2021.

Connection to my Ph.D. thesis:

The impact of transmitter's position and the orientation uncertainty on the accuracy of the VLP system was studied, based on the RSS. There are several constraining factors for RSS-based algorithms, particularly, due to multipath channel characteristics and set-up uncertainties. The impact of transmitter uncertainties on positioning error performance was studied, assuming a statistical modelling of the uncertainties. Simulation results showed that, the transmitter uncertainties have a severe impact on the positioning error, which can be leveraged through the usage of more transmitters. Concerning a smaller transmitter's position uncertainty of 5 cm, the average positioning errors were 23.3, 15.1, and 13.2 cm with the standard deviation values of 6.4, 4.1, and 2.7 cm for 4-, 9- and 16-transmitter cases, respectively. While for a smaller transmitter' orientation uncertainty of 5º, the average positioning errors were 31.9, 20.6, and 17 cm with standard deviation values of 9.2, 6.3, and 3.9 cm for 4-, 9- and 16-transmitter cases, respectively.

sensors

MDPI

Article

Impact of Transmitter Positioning and Orientation Uncertainty on RSS-Based Visible Light Positioning Accuracy †

Neha Chaudhary [1,*], Luis Nero Alves [1] and Zabih Ghassemlooy [2]

[1] Instituto de Telecomunicações and Departamento de Electrónica, Telecomunicações e Informática, Universidade de Aveiro, 3810-193 Aveiro, Portugal; nero@ua.pt
[2] Optical Communications Research Group, Faculty of Engineering and Environment, Northumbria University, Newcastle upon Tyne NE1 8ST, UK; z.ghassemlooy@northumbria.ac.uk
* Correspondence: neha.chaudhary@ua.pt
† Chaudhary, N., Alves, L.N., Ghassemlooy, Z. Impact of transmitter positioning uncertainty on RSS-based visible light positioning accuracy. In Proceedings of the 12th International Symposium on Communication Systems, Networks and Digital Signal Processing (CSNDSP), Porto, Portugal, 20–22 July 2020.

Abstract: This paper present simulation-based results on the impact of transmitter (Tx) position and orientation uncertainty on the accuracy of the visible light positioning (VLP) system based on the received signal strength (RSS). There are several constraining factors for RSS-based algorithms, particularly due to multipath channel characteristics and set-up uncertainties. The impact of Tx uncertainties on positioning error performance is studied, assuming a statistical modelling of the uncertainties. Simulation results show that the Tx uncertainties have a severe impact on the positioning error, which can be leveraged through the usage of more transmitters. Concerning a smaller Tx's position uncertainty of 5 cm, the average positioning errors are 23.3, 15.1, and 13.2 cm with the standard deviation values of 6.4, 4.1, and 2.7 cm for 4-, 9-, and 16-Tx cases, respectively. While for a smaller Tx' orientation uncertainty of 5°, the average positioning errors are 31.9, 20.6, and 17 cm with standard deviation values of 9.2, 6.3, and 3.9 cm for 4-, 9-, and 16-Tx cases, respectively.

Keywords: localization; VLC; visible light positioning; received signal strength; localization algorithm; Tx's uncertainty

check for updates

Citation: Chaudhary, N.; Alves, L.N.; Ghassemlooy, Z. Impact of Transmitter Positioning and Orientation Uncertainty on RSS-Based Visible Light Positioning Accuracy . *Sensors* **2021**, *21*, 3044. https://doi.org/10.3390/s21093044

Academic Editor: Yang Yue

Received: 6 April 2021
Accepted: 24 April 2021
Published: 27 April 2021

Publisher's Note: MDPI stays neutral with regard to jurisdictional claims in published maps and institutional affiliations.

Copyright: © 2021 by the authors. Licensee MDPI, Basel, Switzerland. This article is an open access article distributed under the terms and conditions of the Creative Commons Attribution (CC BY) license (https://creativecommons.org/licenses/by/4.0/).

1. Introduction

The demand for highly precise indoor positioning (IP) systems is growing rapidly due to its potential in the increasingly popular techniques of Internet of Thing (IoT), smart mobile devices, and artificial intelligence. Consequently, IP becomes a promising research domain that is getting wide attention due to its benefits in several working scenarios, such as, industries, health sectors, indoor public locations, and autonomous navigation [1]. The traditional positioning methods, which depend on satellites such as the global positioning system (GPS), is common nowadays for outdoor positioning; however, it is not well-suited for indoor environments. This is because the GPS signals from the satellites suffer from high penetration loss and multipath fading due to building walls. Some other systems also have been proposed for IP, for example, Bluetooth, ultrasound, ultra-wideband (UWB), wireless-Fidelity, radio frequency identification (RFID), and radio-frequency (RF)-based techniques [2–4]. For instance, the UWB technology transmits short RF pulses with a low duty cycle, which provides precise localization and tracking of mobile devices in indoor environments [4]. Despite the advantage of precise localization, the UWB technology is still not perfect for IP systems, and it has not been embraced widely because of its cost, complexity, and need for synchronization between transmitters (Txs) and the targets [5]. Moreover, these RF-based systems may not be suitable in RF restricted areas, such as hospitals due to the RF-induced interference [2].

Another developed technology that makes use of the pre-installed lighting infrastructure is visible light positioning (VLP). VLP is based on visible light communications (VLC), which is license-free, and free from RF induced electromagnetic interference-free, thus making it ideal in many applications including hospitals. In addition, VLC uses the pre-existing light-emitting diodes (LEDs) infrastructure as a Tx which has the ability to provide illuminance and communication simultaneously [6]. VLP is an emerging technology promising high accuracy, high security, low deployment cost, shorter time response, and low relative complexity when compared with RF-based positioning [7].

Existing VLP approaches estimate the position of a receiver (Rx) based on several characteristics of light including received signal strength (RSS) [8], angle of arrival (AOA)/angle difference of arrival (ADOA) [9], image [10], and time of arrival (TOA)/time difference of arrival (TDOA) [11]. It has been established that, VLP based on AOA/ADOA, image, and TOA/TDOA require auxiliary devices to capture angle/image/time. On the contrary, the RSS approach can be achieved by utilizing a single photodiode (PD) without the need of any additional auxiliary devices, which makes the RSS-based approach the most well-known method for VLP [12].

Recent research works have addressed the impact of (*i*) LED power uncertainty [13]; (*ii*) reflections from walls and objects within the transmission paths [14]; and (*iii*) noise on the positioning performance [15]. The multipath channel has a direct influence on the model for the estimation of the received signal power, which has been addressed previously using machine learning algorithms [16]. The Tx and the Rx design specifications, such as the Tx beam width and its tilting angle have been investigated before. For instance, in [13], the impact of LED output power uncertainty on the accuracy of the RSS-based VLP system was explored, with the maximum error of 17 and 40 cm for a tolerance (possible variations) value of 5% and 20%, respectively. The performance analysis of various VLP systems relies on line-of-sight (LOS) transmission path, which can underestimate the achievable error bounds, due to the fact that a real scenario will definitely include non-line of sight (NLOS) paths [14]. Therefore, NLOS transmission paths should not be neglected. In [15], an RSS-based VLP system using received optical power from the emitting LEDs was investigated considering signals from both LOS and NLOS paths. The results revealed that, the positioning accuracy of <10 cm on average can be achieved at a signal-to-noise ratio (SNR) of >12 dB.

The location of the Rx can be estimated by using different estimation methods, such as linear least square (LLS) and non-linear least square (NLLS) [14]. In [17], a polynomial regression-based method was used to investigate the accuracy of an RSS-based VLP system along with LLS and NLLS estimation algorithms. The results revealed that, the positioning error ε_p was <0.6 m by using the regression approach, which is much lower than other traditional methods. In [18], the impact of the Tx's orientation (i.e., the tilting angle) on the positioning accuracy of the RSS-based VLP system was studied. Another estimation method, i.e., normalized least square estimation was utilized to estimate the positioning accuracy. In [19], an artificial neural network (ANN) based 4-LED VLP system was proposed to reduce ε_p for the LOS path, which is affected by the random and unknown static Tx tilt angle with a maximum variation of 2°. It was revealed that ANN achieved localization errors below 1 cm. In general, the positions and orientations of Txs may not be symmetrical, which (*i*) depends on the indoor environments such as museums, galleries, train stations, shopping centers, etc., where lights are pointing in different directions; and (*ii*) can change when replacing lights, carrying out maintenance, etc. Therefore, the random variations in the Tx's orientation will lead to the random errors in VLP systems, which requires further studies. The impact of Tx's position and its orientation uncertainties on the positioning estimation have not yet been systematically explored, which is the objective of this paper.

In this paper, we investigate the impact of Tx's position and its orientation uncertainties on ε_p of the RSS-based VLP system under multipath reflections. The uniform distribution of light inside the illuminated place is a necessity in indoor environments. As a result, lighting uniformity becomes a vital aspect for a well-lit environment. Moreover,

both lighting uniformity and the positioning performance are related to the Tx's positions and the Lambertian half-power angles (HPA). Therefore, in this work we investigate (*i*) how the uniformity of light in the room changes for different HPA and the Tx positions; and (*ii*) the impact of Tx position and its orientation uncertainties on the positioning accuracy considering the optimized Tx positions from a lighting uniformity perspective. This works focused only on the LED uncertainties caused during installation and is an extension of our previous work [20], where the problem of Tx's orientation uncertainty was not considered.

The rest of the paper is organized as follows, Section 2 introduces the set-up of the system and position estimation approaches in detail. The impact of different set-up uncertainties and uniformity are presented in Section 3. In Section 4, a discussion of the simulation results attained is made, followed by the final concluding remarks in Section 5.

2. VLP System Modelling

2.1. Channel Model

Our proposed VLP system is composed of a PD as an Rx, which is placed on the ground and a number of LEDs as the Txs (i.e., 4-, 9-, and 16-LED) that are installed on the ceiling of the room as depicted in Figure 1. The field of view (FOV) and the detection area A_r of the PD are 70° and 10^{-4} m^2, respectively. All Txs are located at the same height h from the ground level and the coordinates of kth Tx ($k = 1, \ldots, K$) is (x_k, y_k, z_k), where K is the total number of Txs. The Rx coordinate is denoted by (x_r, y_r, z_r). The position and orientation of the Txs is best illustrated by the Tx_k, with the coordinate of $(\delta x, \delta y)$ and the angles of α, β, and γ. Both δx and δy, and α, β, and γ, are assumed to be Gaussian variables with $N(0, \sigma^2)$ and $N(0, \zeta^2)$ probability distribution functions, respectively. The distance between the Txs relies on the lighting uniformity considerations that are described in a later section. An empty room is considered as a reference to study the impact of Tx's position and its orientation uncertainty on the positioning accuracy. In this work, both LOS and NLOS transmission paths are assumed between the Txs and the Rx. However, for the NLOS path, we only consider the first reflection due to the fact that the second order reflections have much reduced intensities and therefore can be neglected [21]. Each Tx broadcast a unique 2-bit ID information, which is encoded and modulated using on-off keying (OOK), which allows separation at the Rx using a correlation method that can be received at the Rx in advance of location identification.

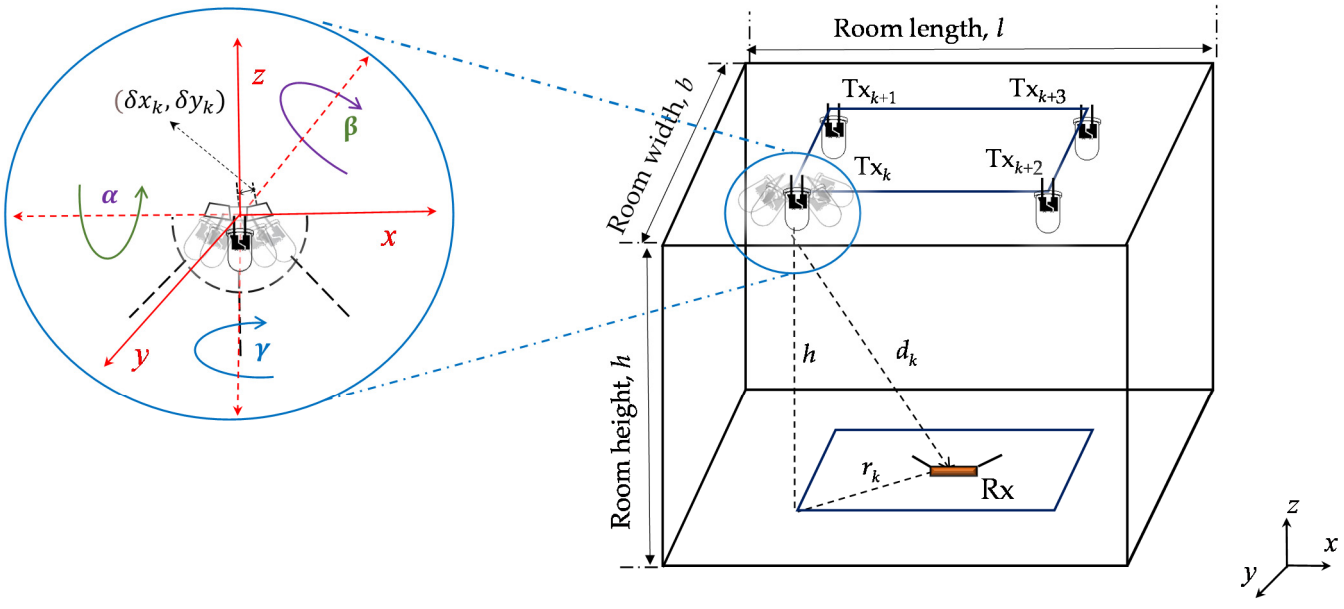

Figure 1. Overview of the simulation set-up.

The total received optical power P_r at the PD comprises the power from the LOS and NLOS paths, as given by:

$$P_r = \sum P_{r(\mathrm{LOS})} + \sum P_{r(\mathrm{NLOS})}, \tag{1}$$

where $P_{r(\mathrm{LOS})}$ and $P_{r(\mathrm{NLOS})}$ represent the received power for LOS and NLOS, respectively. Generally, the SNR will be high (i.e., >20 dB) in standard VLC, which could be considered noise-free in normal cases [22]. Thus, in this study, no actual noise (e.g., shot noise or thermal noise) is considered as a source of "measurement noise", to unambiguously evaluate the effect of the Tx's position and its orientation uncertainty.

2.2. RSS-Based Positioning

Using the RSS algorithm, $P_{r(\mathrm{LOS})}$ for the LOS path can be expressed as [22,23]:

$$\sum P_{r(\mathrm{LOS})} = \sum_{k=1}^{K} P_t \, A_r \mathcal{R} \left(\frac{m+1}{2\pi} \right) \frac{\cos^m(\omega_k) \, cos(\varphi)}{\|d_k\|^2} T_s(\varphi) g(\varphi), \tag{2}$$

where

$$m = -\frac{\ln(2)}{\ln\left(\cos\left(\Theta_{\frac{1}{2}}\right)\right)}, \tag{3}$$

where P_t is the transmit power, d_k is the distance between kth Tx and the Rx, K is the total number of Txs, and $\Theta_{1/2}$ is the light source irradiance half-power angle (HPA) [22]. ω_k and φ are the irradiance angle from the kth Tx to the Rx and the receiving incident angle, respectively. A_r and $\mathcal{R}$ are the PD's active area and responsivity, respectively. $T_s(\varphi)$ and $g(\varphi)$ are the gains of the optical filter and the concentrator at the Rx, respectively. Note, $T_s(\varphi)$ and $g(\varphi)$ are set to unity.

Considering the NLOS path, i.e., the first-order reflection, the total received power can be expressed as [22]:

$$\sum P_{r(\mathrm{NLOS})} = \sum_{k=1}^{K} \sum_{\mathrm{wall}} \rho P_t \, A_r \mathcal{R} \left(\frac{m+1}{2\pi} \right) A_{\mathrm{ref}} \frac{\cos^m(\omega_{k,w}) \, cos(\varphi_{k,w})}{\pi(\|d_{k,w}\| \|d_{w,r}\|)^2} \, T_s(\varphi_{w,r}) \, g(\varphi_{w,r}) \cos(\omega_{w,r}) \cos(\varphi_{w,r}), \tag{4}$$

where $d_{k,w}$, $\varphi_{k,w}$, and $\omega_{k,w}$ are the distances, receiving incident angle, and the irradiance angle between the kth Tx and the reflective area, respectively. $d_{w,r}$, $\varphi_{w,r}$, and $\omega_{w,r}$ are the distances, receiving incident angle, and the irradiance angle between the reflective area and the Rx, respectively, see Figure 2. ρ is the reflection coefficient that relies on the reflective surface material, and A_{ref} is the reflection area. $P_{r(\mathrm{NLOS})}$ for the signals from the NLOS paths is obtained based on Matlab [22]. For each Tx, we integrate (4) over all the walls accompanied by the assumption of a grid area with a resolution A_{ref} of 0.1 m.

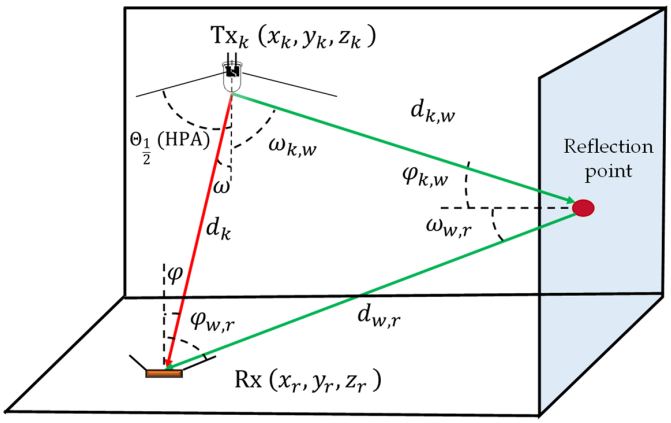

Figure 2. Overview of the visible light channel.

2.3. Distance Estimation Using Polynomial Regression

The block diagram of the proposed VLP system is shown in Figure 3. In the case of LOS, the horizontal distance can be computed as $\|r_k\|^2 = \|d_k\|^2 - h^2$ and therefore can be determined from (2) as given by:

$$r_k = \sqrt{\left(\frac{(m+1)\, A_r \mathcal{R} P_t (h)^{m+1}}{2\pi P_{r(\mathrm{LOS}),k}}\right)^{\frac{2}{m+3}} - h^2}, \tag{5}$$

where h is the vertical distance between the Tx and the Rx. $P_{r(\mathrm{LOS}),k}$ is the LOS received power at the Rx from the kth Tx. In (5), the cosine terms are clearly stated in terms of the set-up geometry, as $h/\|d_k\|$. However, in case of NLOS links, high errors are introduced in the channel due to the presence of reflections [17,24], thus, the above method fails to determine the distance. Another method that can be used is to employ a polynomial fitted model for the power-distance relationship [25]. In this particular case, the relation between d_k and $P_{r,\,k}$ for the kth Tx is represented as:

$$d_k = \alpha_0 + \alpha_1 P_{r,k} + \alpha_2 (P_{r,k})^2 + \ldots + \alpha_s (P_{r,k})^s \tag{6}$$

where $P_{r,\,k}$ is the total received power at the Rx from the kth Tx, and α_s represent the coefficients of the fitted polynomial. Note, d_k is computed using (6), which is later employed to determine r_k.

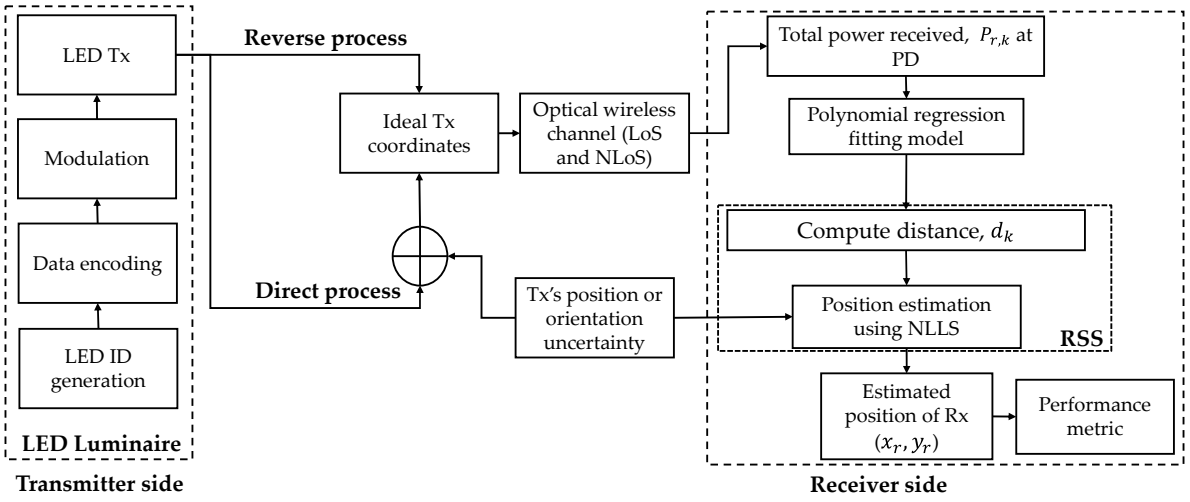

Figure 3. Block diagram of the proposed system.

We estimated the best polynomial fitting using 3600 data points extracted from channel simulation, see Figure 4. Note that, the 3600 data points are considered as 3600 different locations each within the room. The best-fitted solution was exhibited by analyzing the value of R^2 (coefficient of determination) for different orders, and a fourth order polynomial was selected with a value of R^2 of 0.8942. Note, the polynomial fitting is not highly accurate. This is because of the data points considered within the entire room for both LOS and NLOS paths. At the center of the room, the impact of NLOS is negligible when compared to the regions near walls and corners. As such, fitting all the data will be dominated by the data near walls and corners. However, it shows the best fitted solution considering that the data points corresponding to lower received power have higher contributions to the error compared with the data points in the center of the room. The values of polynomial coefficients are listed in Table 1.

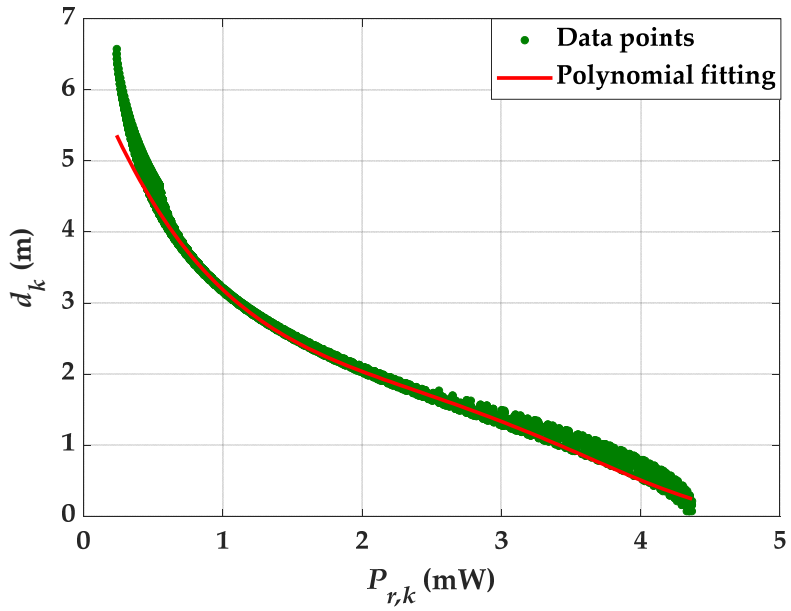

Figure 4. Estimation using the polynomial fitting method.

Table 1. The value of polynomial coefficients for the best polynomial fitting.

Polynomial Coefficient	α_0	α_1	α_2	α_3	α_4
Value	8.85×10^6	-9.93×10^5	3.96×10^4	-7.34×10^2	7.4

2.4. Estimation Using Nonlinear Least Squares

The relation between the Tx coordinates (x_k, y_k) and the Rx coordinates (x_r, y_r) are described using the following equations:

$$\begin{cases} (x_r - x_1)^2 + (y_r - y_1)^2 = {r_1}^2 \\ (x_r - x_2)^2 + (y_r - y_2)^2 = {r_2}^2 \\ \vdots \\ (x_r - x_K)^2 + (y_r - y_K)^2 = {r_K}^2 \end{cases}, \tag{7}$$

where K is the total number of Txs. NLLS estimation can be utilized to estimate the target location, in which the solution can be estimated by attaining $\widetilde{X} = [\tilde{x}, \tilde{y}]$ that minimizes a cost function given by [15]:

$$\widetilde{Q} = \sum_i \left(\sqrt{(x_r - x_k)^2 + (y_r - y_k)^2} - r_k \right)^2. \tag{8}$$

An iterative procedure is utilized to estimate $\widetilde{X}$ by employing the trust-region reflective algorithm [26]. In this algorithm, first, an estimate is introduced as $\widetilde{X}_0$, followed by computing the corresponding cost function $\widetilde{Q}_0$. Next, several points in the neighborhood of $\widetilde{X}_0$ are replaced in (8), and the one that minimizes the cost $\widetilde{Q}_1$ is selected as $\widetilde{X}_1$. The Rx coordinates $\widetilde{X}$ will eventually be obtained following several iterative steps to ensure convergence of $\widetilde{Q}$. In the proposed system, the initial value for $\widetilde{X}_0$ is estimated using a linear least square approach.

2.5. Performance Metrics

ε_p is assumed to be a random variable (as it may rely on the uncertainties, i.e., the Tx's position or its orientation uncertainties, estimation process, or noise); thus, it is reasonable to use the standard statistical analyses to access error performance. Here we use the

probability distribution function (PDF) and the cumulative distribution function (CDF), as a mean to calculate the 95% quantile on ε_p. Hence, the PDF and CDF are composed of the spatial distribution of ε_p within the entire room. The PDF of ε_p is defined as:

$$f_{\varepsilon_p}(p) = \lim_{\substack{N \to \infty \\ \varepsilon \to 0}} \frac{\#\varepsilon_p\left(|\varepsilon_p - p| \leq \varepsilon\right)}{N}, \tag{9}$$

where ε defines an error interval centered around p, and N is the number of samples. The cardinal operator # signifies the counting of occurrences were $|\varepsilon_p\text{-}p| < \varepsilon$. The limiting process is naturally implied by the discrete nature of the simulation. The CDF can be expressed as:

$$F_{\mathrm{CDF}}(p) = \int_0^p f_{\varepsilon_p}(p)dp. \tag{10}$$

Figure 5 depicts the CDF against ε_p for NLLS estimation with and without polynomial regression. The maximum ε_p values estimated by NLLS and NLLS with polynomial regression are 0.6 and 1.57 m, respectively. It is observed that, there is an evident improvement in the positioning accuracy by using NLLS estimation with polynomial regression for power-distance modeling. Therefore, the polynomial regression can improve the accuracy of position estimation without the inclusion of high complexity algorithms. However, there are some limitations of the polynomial regression; for instance, the coefficients of the polynomial model must be provided along with the Tx's positions in practical scenarios. Moreover, the polynomial model can deal with the empty and non-empty rooms with the fixed furniture and objects, but with no user's mobility.

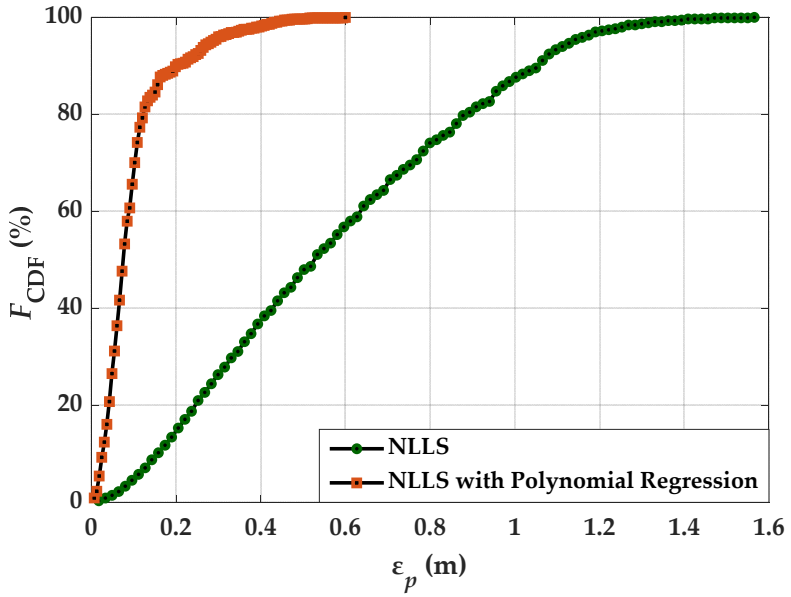

Figure 5. CDF of the ε_p computed by NLLS and NLLS with polynomial regression estimation.

3. Set-Up Uncertainties

The major challenge in studying the Tx's position or orientation uncertainties occurs in simulation, i.e., we must use random Tx positions in order to investigate the uncertainties. This raises the necessity to re-simulate the channel for each iteration (new random TX position). Give that the channel estimation is by itself complex and time-consuming, this problem becomes complex. We have developed two approaches for both Tx's position and its orientation uncertainties to fully analyze the problem, which is termed direct and reverse

processes. The reason for these designations is straightforward. The direct process entails the estimation of the position given the effect of the uncertainties on the channel. It is in this sense, complex and time-consuming. In the reverse process, the channel is assumed fixed and the effects of the Tx uncertainties are coupled directly into the estimation equations, this avoids the channel simulation at each set of newly generated Tx positions.

3.1. Uncertainties of the Tx's Position

For Tx's position uncertainties, in the direct process, we assume that the channel is re-stimulated for each newly generated set of Tx positions. The Tx positions are composed by the ideal position (fixed) and a random perturbation in two-dimensions. While in the reverse process, we assume that the channel is fixed for a set of ideal Tx positions, and the uncertainties are directly coupled into the estimation Equation (7). To illustrate the concept, let us consider one of the terms in (7), in the direct process, the effect of the uncertainties is on the right side of the equation, as follows:

$$(x_r - x_k)^2 + (y_r - y_k)^2 = f_R(x_k + \delta x, y_k + \delta y), \tag{11}$$

where (x_r, y_r) and (x_k, y_k) are the coordinates of the Rx and the Tx (ideal positions), respectively. $(\delta x, \delta y)$ express the uncertainty at the Tx coordinates. Both δx and δy are assumed to be Gaussian variables with $N(0,\ \sigma^2)$. The channel needs to be re-simulated at each iteration in order to obtain f_R.

In the reverse process, it is not required to re-simulate the channel at each iteration as the uncertainties are part of the Tx position, as follows:

$$(x_r - x_k - \delta x)^2 + (y_r - y_k - \delta y)^2 = f_R(x_k, y_k). \tag{12}$$

Subtracting (11) and (12) and extracting the mathematical expectation of both sides gives:

$$U_r(\sigma_r) = E\Big[\delta x^2 + \delta y^2 - 2\delta x(x_r - x_k) - 2\delta y(y_r - y_k)\Big], \tag{13}$$

where σ_r is the Tx's uncertainty of the reverse process. The reverse process has an expectation as stated in (13), which is given by (after solving (13)):

$$U_r(\sigma_r) = 2{\sigma_r}^2. \tag{14}$$

Performing the same analysis for the direct process we have:

$$U_d(\sigma_d) = E[f_R(x_k, y_k) - f_R(x_k + \delta x, y_r + \delta y)]. \tag{15}$$

Here, the value of U_d is estimated using numerical simulation, where σ_d is the Tx's uncertainty of the direct process. Assuming that, the reverse and direct processes are equivalent, the expectation values U_d and U_r must be equal. In this case, it is possible to infer the relation between σ_d and σ_r. This relation can be estimated assuming that the Rx is placed at the center of the room and a single Tx is placed in a uniform grid of positions for the whole room. Using mathematical simulation, we have computed the values of $U_d(\sigma_d)$ for different values of σ_d, see Figure 6. Note, the two processes generate uncertainties, i.e., U_d and U_r and these processes would be equivalent if these uncertainties are the same for certain values of σ_d and σ_r. This indicates that, the uncertainties from the reverse process can be generated with the knowledge of the direct process as given by:

$$\sigma_r^2 = \frac{U_d(\sigma_d)}{2}. \tag{16}$$

Simulating the uncertainty for the reverse process using the correction in (16) provides the same values for the expectation as depicted in Figure 6 (curve labelled U_r).

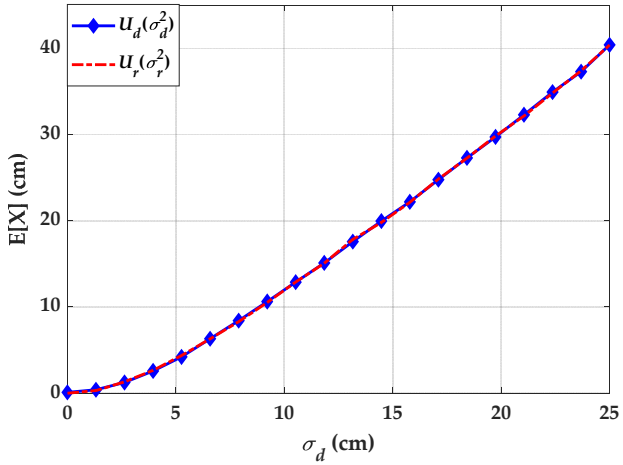

Figure 6. Study on Tx's position uncertainty based on the direct and reverse processes.

3.2. Uncertainties of the Tx's Orientation

The Tx's orientation uncertainties can be treated in a similar fashion as before. There are, however, some aspects that need addressing. In this paper, the Tx' orientation uncertainties are modeled via three random axis-rotations of the Tx's heading vector. Let us consider the kth Tx's heading vector, $\hat{n_k}$, which is given by:

$$\hat{n_k} = R_x(\alpha) \cdot R_y(\beta) \cdot R_z(\gamma) \cdot \hat{n_k^0} = R(\alpha,\ \beta, \gamma) \cdot \hat{n_k^0} \tag{17}$$

where $R_x(\alpha)$, $R_y(\beta)$ and $R_z(\gamma)$ represent the three rotation matrix relative to the x-axis, y-axis, and z-axis, respectively, α, β, and γ are three random angles with probability distribution function $N(0, \zeta^2)$, finally, $\hat{n_k^0}$ represents the unperturbed heading vector of the kth Tx. $R(\alpha,\ \beta, \gamma)$ is a composed rotation matrix. The effect of (17) on the Tx's heading is due to the cosine terms due to the Txs in (2) and (4), showing that a rotation will impact the received signal. The next step resorts to the evaluation of the expectations due to the direct and reverse process. In the direct process, the channel is re-simulated for each random iteration, generating an expectation value, for the kth Tx, which is given by:

$$U_d(\zeta_d) = E[f_R(x_k, y_k) - f_R(x_k, y_r, R(\alpha, \beta, \gamma))]. \tag{18}$$

U_d cannot be cast in a closed-form solution. Instead, we resorted to simulation using the approach described in the previous section, results are depicted in Figure 7.

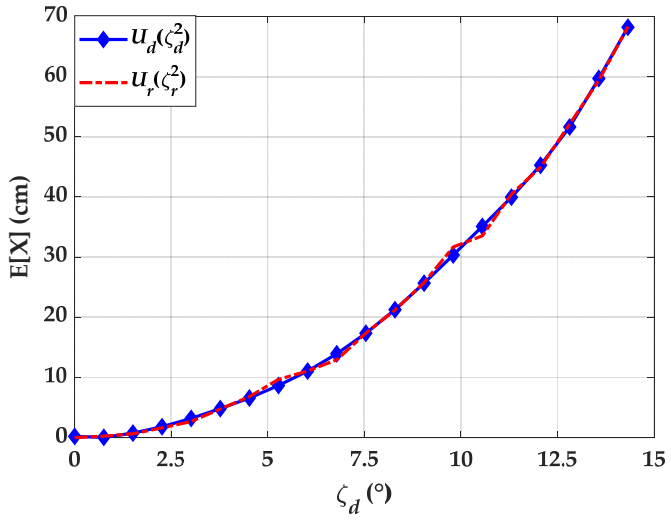

Figure 7. Study on Tx's orientation uncertainty based on the direct and reverse processes.

The expectation of the reverse process reveals some difficulties. The quadratic forms in the left side of (7) are invariant to rotations, which would imply that orientation uncertainties do not affect error performance. Since this is not the case, we approach the problem in a similar manner as in the case of Tx's position uncertainties, that is, assuming that the effect of random headings can be reproduced by affecting the Tx's positions with a random perturbation. Following this approach, the expectation of the reverse process can be cast as:

$$U_r(\zeta_r) = E\left[\delta x^2 + \delta y^2 - 2(x_r - x_k)\delta x - 2(y_r - y_k)\delta y\right] = 2{\zeta_r}^2 \tag{19}$$

where δx and δy are the equivalent position perturbations, which are functions of the random orientation angles α, β, and γ. Equating U_d and U_r, allows to retrieve the correction values for the angle uncertainty, ζ_r as a function of ζ_d. To show that the processes are indeed equivalent, we performed the simulation for U_r, the results are depicted in Figure 7. As it can be seen the two expectations match well and reveal that the effect of orientation uncertainty is worse than the position uncertainty.

3.3. Lighting Uniformity

In the indoor environments, it is essential to uniformly distribute P_r inside the illuminated zone [27]. This constraint is generally assumed in well-lit spaces, where the uniformity of light is linked to the best perception of the objects. The uniform distribution of light in the room, U_l, is represented as the ratio of the minimum to maximum power intensity at the receiving plane, which is given by:

$$U_l = \frac{\min(P_r)}{\max(P_r)}, \tag{20}$$

Lighting uniformity relies on the three factors related to the Txs, i.e., the distance between the Txs, HPA, and the number of Txs. Figure 8 illustrates the lighting uniformity as a function of the number of Txs (i.e., 4 and 9) and for different values of HPA.

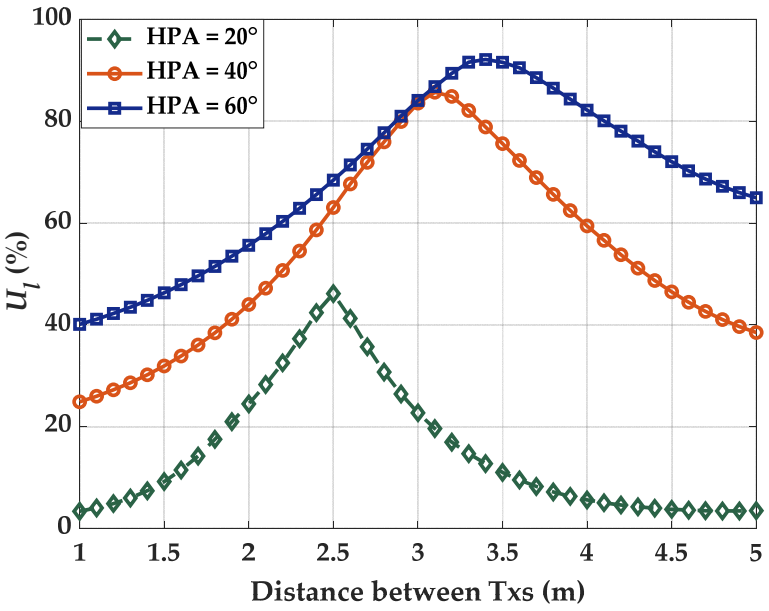

(a)

Figure 8. *Cont.*

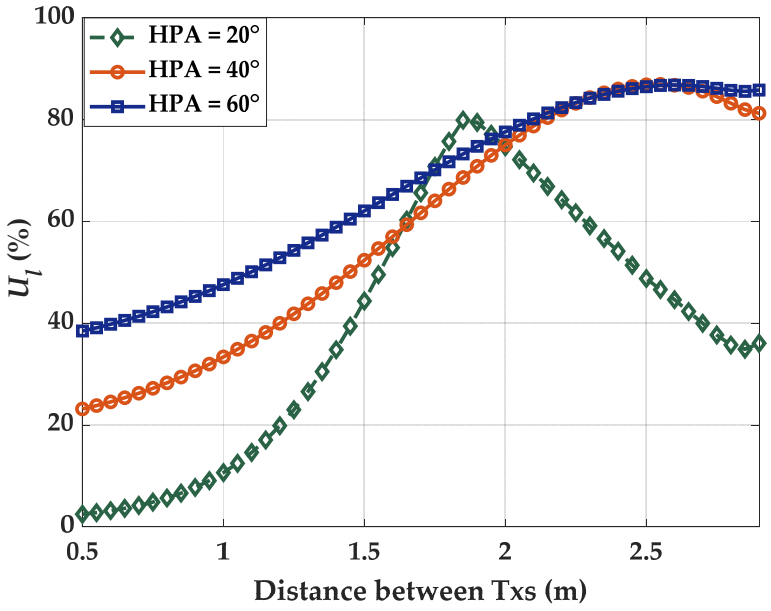

(**b**)

Figure 8. Comparison of uniformity for different HPA and distance between the Txs in case of (**a**) 4-Tx, and (**b**) 9-Tx.

It is noticed from the figure that, a higher number of Txs provide improved uniformity. The maximum uniformity is achieved at distances of 3.4 and 2.6 m for HPA of 60° for 4- and 9-Tx, respectively. It is interesting to notice that, the same factors influence both lighting uniformity and positioning accuracy. It is usually believed that, positioning accuracy can be enhanced with higher uniformity. However, our study reveals that, this is not a general rule, moreover, HPA seems to have a more prominent impact on the positioning accuracy than the uniformity.

4. Simulation Results

In this section, the performance of the proposed VLP system is evaluated by simulation results. We consider the scenario where the LED-based Txs are located on the ceiling of a room of dimension $6 \times 6 \times 3$ m^3, which are assumed to be the same and modelled as pointwise Lambertian sources with order m depending ζ on the value of HPA, see (2). In practical environments also, the square LED placement layout is common. We have considered three different cases of 4-, 9-, and 16-LEDs, which are arranged in a square grid on the ceiling plane. The Rx is located on the ground plane. For all simulation purposes, the resolution of the grid is fixed at 1 cm, which implies that the PD can be placed at 3600 different locations. All the key parameters for the simulation are detailed in Table 2.

Table 2. The key parameters for the indoor VLP system.

Parameter	Value
Room size	$6 \times 6 \times 3$ m^3
Number of LED Txs	4/9/16
Transmit power of each Tx	1 W
Rx's field of view	75°
Reflection coefficient	0.7
Area of PD	10^{-4} m^2
Responsivity of PD	0.5 A/W
Tx elevation	−90°
Tx azimuth	0°
Rx elevation	90°
Rx azimuth	0°

4.1. Positioning Error Dependence on Lighting Uniformity

This section analyses the influence of lighting uniformity and HPA on ε_p. Here, we vary the uniformity between 0.5 and 0.8 in steps of 0.05 and for HPA of 40° and 60°. For this, we first select the values of distance between the Txs according to the results of Figure 8. Following this, we estimate ε_p for each set of conditions using NLLS and the polynomial regression power-distance model. ε_p for different values of uniformity for 4-, 9-, and 16-Tx are illustrated in Figure 9. It is observed that the minimum ε_p is attained for the case of 4-Tx with HPA and uniformity of 60° and 0.65, respectively, whereas, in the case of 9-Tx, the minimum ε_p is achieved with HPA of 60° and uniformity equal to 0.55. For the 16-Tx case, the minimum ε_p is accomplished with an HPA of 40° and with the uniformity of 0.65. It is clear from Figure 9 that, (*i*) low to a moderate value of lighting uniformity can support low ε_p; and (*ii*) an optimal value for the number of Txs and the associated HPA, which do not match the optimal value of lighting uniformity conditions. Under the simulated conditions, the optimal values for the HPA, uniformity, and distance between the Tx based on the lowest ε_p are shown in Table 3.

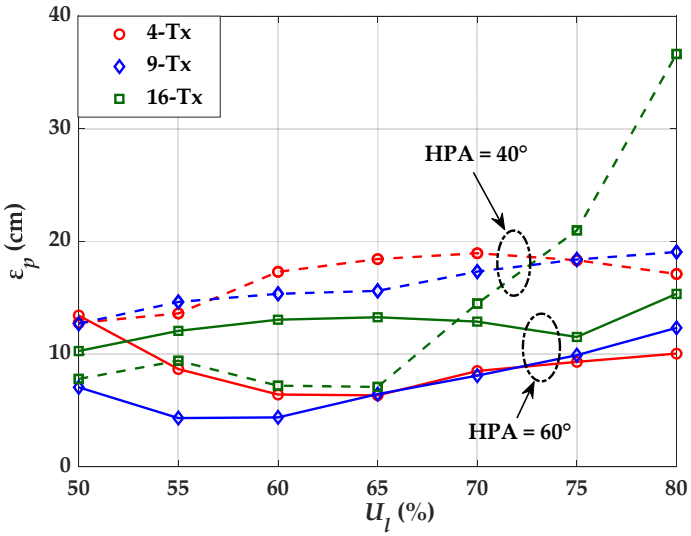

Figure 9. Comparison of ε_p for different Txs and uniformity.

Table 3. The optimized values for all cases of Txs.

Number of Txs	Uniformity	Distance between Txs (m)	HPA (°)
4	0.65	2.4	60
9	0.55	1.3	60
16	0.65	1.34	40

4.2. Impact of Tx's Position and Orientation Uncertainty on Error Performance

In this section, we investigate the impact of Tx's position uncertainties σ and the Tx's orientation uncertainties ζ on the error performance. We follow the same approach that has been described in detail in Section 3.1. The simulation follows the reverse method with 1000 random iterations for each σ value using the adjusted variance values given by (16), where a random displacement vector $(\delta x, \delta y)$ is added in the ideal Tx positions as explained in (11). The quantile function $\mathrm{Q_F}(p)$ is employed as a performance metric considering both, its average and standard deviation, over the 1000 random iterations to obtain the confidence interval of ε_p, which is given by:

$$\mathrm{Q_F}(p) = {F_{\mathrm{CDF}}}^{-1}(p), \tag{21}$$

where p is the percentage of the confidence interval.

Figure 10 illustrates the average and standard deviation of the 95% quantile of ε_p as a function of σ for 4-, 9-, and 16-Tx for the Tx's positioning uncertainty. It is observed that the effect of Tx's position uncertainty, σ, traduces in an increasing error dependence, which is more prominent for set-ups with a lower number of Txs. The standard deviation of the error quantile, i.e., the increasing error also confirms an increasing trend with σ, is more evident for the 4-Tx case. It is noticed that, for σ of 5 cm the average positioning errors are 23.3, 15.1, and 13.2 cm, with the standard deviation values of 6.4, 4.1, and 2.7 cm for 4-, 9-, and 16-Tx cases, respectively. Figure 10 suggests that the error dependence on the Tx's position uncertainty can be lowered by increasing the number of Txs.

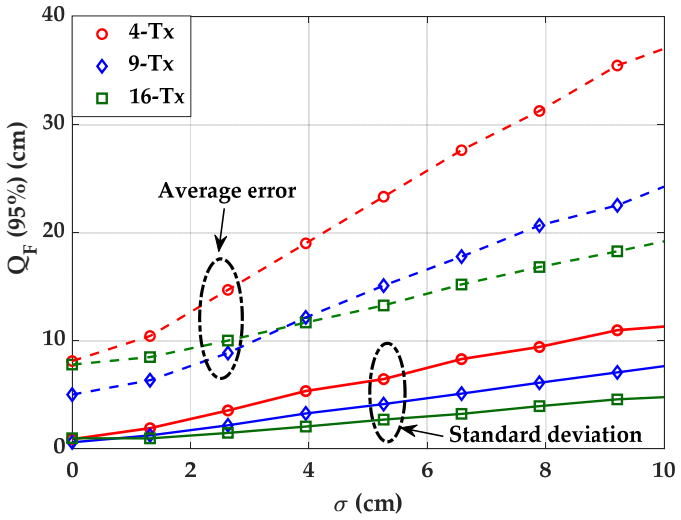

Figure 10. Comparison of positioning error for different Txs and σ.

Figure 11 depicts the average and standard deviation of the 95% quantile of ε_p or as a function of ζ for 4-, 9-, and 16-Tx for the Tx's orientation uncertainty. It is clear from the figure that, alike the case of Tx's position uncertainty, the effect ζ has more significant error dependence for set-ups with a lower number of Txs. It is observed that for ζ of 5°, the average positioning errors are 31.9, 20.6, and 17 cm, with the standard deviation values of 9.2, 6.3, and 3.9 cm for 4-, 9-, and 16-Tx cases, respectively. The increasing error also proves an increasing trend with ζ, therefore, the placement of Tx with the accurate Tx's position and its orientation should be taken into consideration, as the error may rise even with low values of set-up uncertainties.

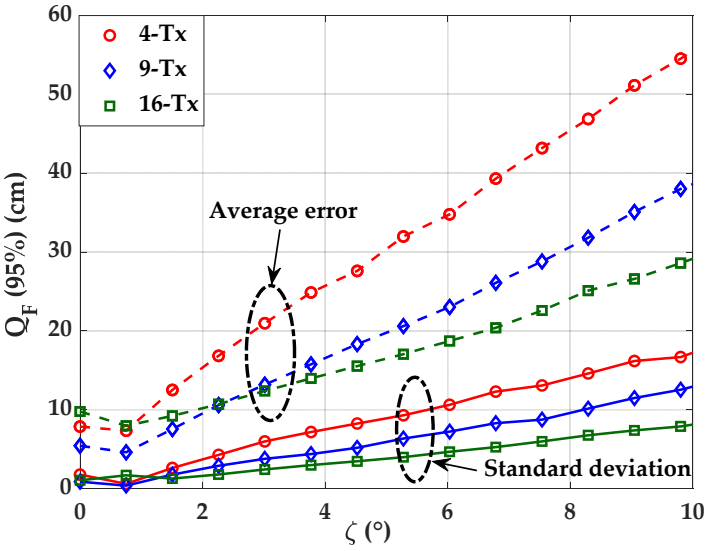

Figure 11. Comparison of positioning error for different Txs and ζ.

5. Conclusions

In this paper, we demonstrated the influence of Tx's position and orientation uncertainty on the performance of VLP systems based on RSS. From the results, we can conclude that light uniformity and Tx's HPA are crucial design parameters for developing an efficient VLP system. The selection of the Tx's HPA as well as the optimum distance between Txs have to be carefully implemented. Moreover, we showed that the best uniformity and optimum error performance were not met for the same conditions, inferring necessary design trade-offs. Furthermore, the effect of error dependence on Tx's position and orientation uncertainty reduced with increasing the number of Txs. In case of square grid Tx placement for a VLP system, the number of Txs can be further explored as an added variable to optimize both light uniformity and error performance, as it reduces the HPA for smaller distances between Txs.

Author Contributions: The contributions of the authors in this paper are the following: conceptualization: N.C. and L.N.A.; investigation: N.C.; methodology: N.C., L.N.A. and Z.G.; project administration: L.N.A. and Z.G.; software: N.C.; validation: L.N.A. and Z.G. All authors have read and agreed to the published version of the manuscript.

Funding: This research was funded by H2020/MSCA-ITN funding program under the framework of the European Training Network on Visible Light Based Interoperability and Networking, project (VisIoN) grant agreement no 764461.

Institutional Review Board Statement: Not applicable.

Informed Consent Statement: Not applicable.

Data Availability Statement: Not applicable.

Acknowledgments: This paper was raised under the frameworks of the COST Action NEWFOCUS (CA19111), supported by COST (European Cooperation in Science and Technology).

Conflicts of Interest: The authors declare no conflict of interest.

Nomenclature

ADOA	Angle difference of arrival
ANN	Artificial neural network
AOA	Angle of arrival
CDF	Cumulative distribution function
FOV	Field of view
GPS	Global positioning system
HPA	Half power angle
IoT	Internet of things
IP	Indoor positioning
LEDs	Light-emitting diodes
LLS	Linear least square
LOS	Line of sight
NLLS	Nonlinear least square
NLOS	Non-line of sight
OOK	On-off keying
PD	Photodiode
PDF	Probability distribution function
PR	Polynomial regression
RF	Radio frequency
RFID	Radio frequency identification
RSS	Received signal strength
Rx	Receiver
SNR	Signal-to-noise ratio

TDOA	Time difference of arrival
TOA	Time of arrival
Tx	Transmitter
UWB	Ultra-wide band
VLC	Visible light communication
VLP	Visible light positioning

References

1. Chaudhary, N.; Alves, L.N.; Ghassemblooy, Z. Current Trends on Visible Light Positioning Techniques. In Proceedings of the 2019 2nd West Asian Colloquium on Optical Wireless Communications (WACOWC), Tehran, Iran, 27–28 April 2019; pp. 100–105.
2. Do, T.-H.; Yoo, M. An In-Depth Survey of Visible Light Communication Based Positioning Systems. *Sensors* **2016**, *16*, 678. [CrossRef] [PubMed]
3. Yassin, A.; Nasser, Y.; Awad, M.; Al-Dubai, A.; Liu, R.; Yuen, C.; Raulefs, R.; Aboutanios, E. Recent Advances in Indoor Localization: A Survey on Theoretical Approaches and Applications. *IEEE Commun. Surv. Tutor.* **2017**, *19*, 1327–1346. [CrossRef]
4. Gezici, S.; Tian, Z.; Giannakis, G.B.; Kobayashi, H.; Molisch, A.F.; Poor, H.V.; Sahinoglu, Z. Localization via Ultra-Wideband Radios: A Look at Positioning Aspects for Future Sensor Networks. *IEEE Signal Process. Mag.* **2005**, *22*, 70–84. [CrossRef]
5. Tariq, Z.B.; Cheema, D.M.; Kamran, M.Z.; Naqvi, I.H. Non-GPS Positioning Systems: A Survey. *ACM Comput. Surv.* **2017**, *50*, 1–34. [CrossRef]
6. Luo, J.; Fan, L.; Li, H. Indoor Positioning Systems Based on Visible Light Communication: State of the Art. *IEEE Commun. Surv. Tutor.* **2017**, *19*, 2871–2893. [CrossRef]
7. Armstrong, J.; Sekercioglu, Y.; Neild, A. Visible Light Positioning: A Roadmap for International Standardization. *IEEE Commun. Mag.* **2013**, *51*, 68–73. [CrossRef]
8. Zhuang, Y.; Wang, Q.; Shi, M.; Cao, P.; Qi, L.; Yang, J. Low-Power Centimeter-Level Localization for Indoor Mobile Robots Based on Ensemble Kalman Smoother Using Received Signal Strength. *IEEE Internet Things J.* **2019**, *6*, 6513–6522. [CrossRef]
9. Zhu, B.; Cheng, J.; Wang, Y.; Yan, J.; Wang, J. Three-Dimensional VLC Positioning Based on Angle Difference of Arrival With Arbitrary Tilting Angle of Receiver. *IEEE J. Sel. Areas Commun.* **2018**, *36*, 8–22. [CrossRef]
10. Xu, J.; Gong, C.; Xu, Z. Experimental Indoor Visible Light Positioning Systems With Centimeter Accuracy Based on a Commercial Smartphone Camera. *IEEE Photonics J.* **2018**, *10*, 1–17. [CrossRef]
11. Naeem, A.; Hassan, N.U.; Pasha, M.A.; Yuen, C.; Sikora, A. Performance Analysis of TDOA-Based Indoor Positioning Systems Using Visible LED Lights. In Proceedings of the 2018 IEEE 4th International Symposium on Wireless Systems within the International Conferences on Intelligent Data Acquisition and Advanced Computing Systems (IDAACS-SWS), Lviv, Ukraine, 20–21 September 2018; pp. 103–107.
12. Xie, C.; Guan, W.; Wu, Y.; Fang, L.; Cai, Y. The LED-ID Detection and Recognition Method Based on Visible Light Positioning Using Proximity Method. *IEEE Photonics J.* **2018**, *10*, 1–16. [CrossRef]
13. Plets, D.; Bastiaens, S.; Stevens, N.; Martens, L.; Joseph, W. Monte-Carlo Simulation of the Impact of LED Power Uncertainty on Visible Light Positioning Accuracy. In Proceedings of the 2018 11th International Symposium on Communication Systems, Networks & Digital Signal Processing (CSNDSP), Budapest, Hungary, 18–20 July 2018; pp. 1–6.
14. Gu, W.; Aminikashani, M.; Deng, P.; Kavehrad, M. Impact of Multipath Reflections on the Performance of Indoor Visible Light Positioning Systems. *J. Light. Technol.* **2016**, *34*, 2578–2587. [CrossRef]
15. Mousa, F.I.K.; Almaadeed, N.; Busawon, K.; Bouridane, A.; Binns, R.; Elliot, I. Indoor Visible Light Communication Localization System Utilizing Received Signal Strength Indication Technique and Trilateration Method. *Opt. Eng.* **2018**, *57*, 1. [CrossRef]
16. Wang, X.; Shen, J. Machine Learning and Its Applications in Visible Light Communication Based Indoor Positioning. In Proceedings of the 2019 International Conference on High Performance Big Data and Intelligent Systems (HPBD&IS), Shenzhen, China, 9–11 May 2019; pp. 274–277.
17. Shawky, S.; El-Shimy, M.A.; El-Sahn, Z.A.; Rizk, M.R.M.; Aly, M.H. Improved VLC-Based Indoor Positioning System Using a Regression Approach with Conventional RSS Techniques. In Proceedings of the 2017 13th International Wireless Communications and Mobile Computing Conference (IWCMC), Valencia, Spain, 26–30 June 2017; pp. 904–909.
18. Plets, D.; Bastiaens, S.; Martens, L.; Joseph, W. An Analysis of the Impact of LED Tilt on Visible Light Positioning Accuracy. *Electronics* **2019**, *8*, 389. [CrossRef]
19. Plets, D.; Bastiaens, S.; Martens, L.; Joseph, W. Performance Assessment of Artificial Neural Networks on the RSS-Based Visible Light Positioning Accuracy with Random Transmitter Tilt. In Proceedings of the CSNDSP, Porto, Portugal, 20–22 July 2020; Volume 8, p. 389.
20. Chaudhary, N.; Alves, L.N.; Ghassemlooy, Z. Impact of Transmitter Positioning Uncertainty on RSS-Based Visible Light Positioning Accuracy. In Proceedings of the 2020 12th International Symposium on Communication Systems, Networks and Digital Signal Processing (CSNDSP), Porto, Portugal, 20 July 2020; pp. 1–6.
21. Shi, G.; Li, Y.; Cheng, W. Accuracy Analysis of Indoor Visible Light Communication Localization System Based on Received Signal Strength in Non-Line-of-Sight Environments by Using Least Squares Method. *Opt. Eng.* **2019**, *58*, 1. [CrossRef]
22. Ghassemblooy, Z.; Popoola, W.; Rajbhandari, S. *Optical Wireless Communications: System and Channel Modelling with Matlab®*; CRC Press: Boca Raton, FL, USA, 2019.

23. Chaudhary, N.; Alves, L.N.; Ghassemblooy, Z. Feasibility Study of Reverse Trilateration Strategy with a Single Tx for VLP. In Proceedings of the 2019 2nd West Asian Colloquium on Optical Wireless Communications (WACOWC), Tehran, Iran, 27–28 April 2019; pp. 121–126.
24. Sun, X.; Duan, J.; Zou, Y.; Shi, A. Impact of Multipath Effects on Theoretical Accuracy of TOA-Based Indoor VLC Positioning System. OSA Publishing: Washington, DC, USA, 2015; Volume 4.
25. Chaudhary, N.; Younus, O.I.; Alves, L.N.; Ghassemlooy, Z.; Zvanovec, S.; Le-Minh, H. An Indoor Visible Light Positioning System Using Tilted LEDs with High Accuracy. *Sensors* **2021**, *21*, 920. [CrossRef] [PubMed]
26. Shiquan, W. Computation of a Trust Region Step. *ACTA Math. Appl. Sin.* **1991**, *7*, 354–362.
27. Hu, Y.; Luo, M.R.; Yang, Y. A Study on Lighting Uniformity for LED Smart Lighting System. In Proceedings of the 2015 12th China International Forum on Solid State Lighting (SSLCHINA), Shenzhen, China, 2–4 November 2015; pp. 127–130.

5.5 Usage of ANNs for Regression Analysis in Visible Light Positioning Systems

This section is a version of the submitted manuscript:

> **N. Chaudhary,** O. I. Younus, L. N. Alves, Z. Ghassemlooy, and S. Zvanovec, 'Usage of ANNs for Regression Analysis in Visible Light Positioning Systems', Sensors, submitted.

Connection to my Ph.D. thesis:

The design aspects of an indoor VLP system were studied that uses an ANN for positioning estimation, considering a multipath channel. The study considered the influence of noise as a performance indicator, for the comparison between different design approaches. Three different ANN algorithms were considered, including LM, BR, and SCG algorithms are explored to minimize the positioning error in the VLP system. The ANN design was optimized based on the number of neurons in the hidden layers, the number of training epochs and the size of the training set. It was shown that, the ANN with Bayesian regularization outperforms the traditional RSS technique using the NLLS estimation for all values of SNR. Furthermore, in the inner region, which includes the area of the receiving plane within the transmitters, the positioning accuracy improved by 43, 55, and 50% for the SNR values of 10, 20, and 30 dB, respectively. In the outer region, which is the remaining area within the room, the positioning accuracy improved by 57, 32, and 6% for the SNR of 10, 20, and 30 dB, respectively. Moreover, the impact of different training dataset sizes in ANN was also analyzed, and it was shown that, the system can achieve a minimum positioning error of 2 cm for 30 dB of SNR using a random selection scheme. Finally, it was observed that positioning error was low even for lower values of SNR, i.e., positioning error values were 2, 11, and 44 cm for the SNR of 30, 20, and 10 dB, respectively.

sensors

MDPI

Article

The Usage of ANN for Regression Analysis in Visible Light Positioning Systems

Neha Chaudhary [1,*], Othman Isam Younus [2], Luis Nero Alves [1], Zabih Ghassemlooy [2], and Stanislav Zvanovec [3]

[1] Instituto de Telecomunicações and Departamento de Electrónica, Telecomunicações e Informática, Universidade de Aveiro, 3810-193 Aveiro, Portugal; nero@ua.pt
[2] Optical Communications Research Group, Faculty of Engineering and Environment, Northumbria University, Newcastle upon Tyne NE1 8ST, U.K; othman.younus@northumbria.ac.uk (O.I.Y); z.ghassemlooy@northumbria.ac.uk (Z.G)
[3] Department of Electromagnetic Field, Faculty of Electrical Engineering, Czech Technical University in Prague, 16627 Prague, Czech Republic; xzvanove@fel.cvut.cz
* Correspondence: neha.chaudhary@ua.pt

Abstract: In this paper, we study the design aspects of an indoor visible light positioning (VLP) system that uses an artificial neural network (ANN) for positioning estimation by considering a multipath channel. Previous results usually rely on the simplistic line of sight model with limited validity. The study considers the influence of noise as a performance indicator for the comparison between different design approaches. Three different ANN algorithms are considered, including Levenberg-Marquardt, Bayesian regularization, and scaled conjugate gradient algorithms, to minimize the positioning error (ε_p) in the VLP system. The ANN design is optimized based on the number of neurons in the hidden layers, the number of training epochs, and the size of the training set. It is shown that, the ANN with Bayesian regularization outperforms the traditional received signal strength (RSS) technique using the non-linear least square estimation for all values of signal to noise ratio (SNR). Furthermore, in the inner region, which includes the area of the receiving plane within the transmitters, the positioning accuracy is improved by 43, 55, and 50 % for the SNR of 10, 20, and 30 dB, respectively. In the outer region, which is the remaining area within the room, the positioning accuracy is improved by 57, 32, and 6 % for the SNR of 10, 20, and 30 dB, respectively. Moreover, we also analyze the impact of different training dataset sizes in ANN, and we show that, it is possible to achieve a minimum ε_p of 2 cm for 30 dB of SNR using a random selection scheme. Finally, it is observed that ε_p is low even for lower values of SNR, i.e., ε_p values are 2, 11, and 44 cm for the SNR of 30, 20, and 10 dB, respectively.

Keywords: Visible light communication (VLC), visible light positioning, multipath reflections, Non-linear least square, artificial neural network (ANN), Bayesian regularization.

Citation: Chaudhary, N.; Younus, O.I.; Alves, L.N.; Ghassemlooy, Z.; Zvanovec, S. An Indoor Visible Light Positioning System Using Tilted LEDs with High Accuracy. *Sensors* **2022**, *21*, x. https://doi.org/10.3390/xxxxx

Academic editor:
Received: XXXX
Accepted: XXXX
Published: date

Publisher's Note: MDPI stays neutral with regard to jurisdictional claims in published maps and institutional affiliations.

Copyright: © 2021 by the authors. Submitted for possible open access publication under the terms and conditions of the Creative Commons Attribution (CC BY) license (http://creativecommons.org/licenses/by/4.0/).

1. Introduction

The necessity for indoor location-based services has been growing over the past decades because of its significance in the development of various applications, such as smart home appliances, robots, supermarkets, shopping malls, hospitals, etc. Various conventional positioning techniques are based on radio frequency (RF) technologies; for instance, the global positioning system has been used in outdoor environments. However, in indoor environments, it suffers from multipath-induced fading, which can affect the accuracy of the position estimation significantly [1,2]. A number of RF-based positioning systems have also been introduced including Bluetooth [3], ultrasound [4], wireless local area network [5], ultra-wide band [5], and RF identification [6].

Light-emitting diodes (LEDs)-based visible light communication (VLC) systems have been introduced in recent years, which have shown great potential in achieving high-

precision indoor positioning due to the use of optical signals. These systems are known as visible light positioning (VLP), which allows the usage of pre-installed LED luminaries as transmitters (Txs) in indoor environments [7]. VLP systems are considered as an emerging and cost-effective solution compared with other technologies. VLP also leverages the use of well-developed algorithms, which have been developed for other technologies [8], including the angle of arrival (AOA), time of arrival (TOA), proximity, scene analysis, and received signal strength (RSS) [9]. RSS, AOA, and TOA have been explored in VLP systems with the positioning error ε_p of 10 to 40 centimeters [10]. RSS-based positioning systems are much simpler for implementation compared with TOA and AOA-based positioning systems due to the fact that, they do not need highly accurate transceiver synchronization or a receiver (Rx) with efficient detection of the incidence angle [11]. Therefore, most of the previous studies have been focused on RSS-based VLP systems [12–16], where the strength of the received power is used to estimate the Rx's position. Numerous research works have reported ε_p close to 1 cm in the past three years [15,17,18]. The relatively simpler algorithms, such as proximity and scene analysis, trade simplicity with the accuracy, are most appropriate for low accuracy systems.

Different estimation approaches have been used to estimate the Rx's position. For instance, in [19], two conventional methods relying on linear least squares (LLS) and nonlinear least squares (NLLS) were used for the position estimation. However, NLLS and LLS achieved the minimum ε_p values of 46.42 and 55.89 cm, respectively. An efficient RSS-based VLP algorithm was proposed in [20] to estimate the three- dimensional location of an Rx, combining two-dimensional trilateration with the NLLS. The computational time for NLLS is limited to approximately 17 ms, which is further reduced to less than 2 ms using a fast search algorithm.

Recently, an artificial neural network (ANN) has been utilized in RSS-based positioning systems. In [21], both RSS and ANN methods were proposed to achieve an accurate indoor VLP system with a diffuse optical channel. An accuracy of 6.4 cm was achieved with the averaged ε_p being ~13 times smaller than RSS-based positioning system. In addition, a low-cost indoor VLP system was proposed using a machine learning algorithm in [6], which was achieved ε_p of 3.7 cm with a height tolerance of 15 cm in line of sight (LoS) environment. In [22], a new 2-D ANN-based VLP system was proposed, where the LEDs were grouped into blocks, and the block coordinates were encoded using undersampled modulation. A camera was used as an Rx to decode the block coordinate, and the system achieved a mean ε_p of 1.5 cm in LoS channel. In [23], a VLP system based on the RSS and a deep ANN-based Bayesian regularization VLP system was proposed, where only the LoS transmission was considered). The results showed that, using only 20 training points a minimum ε_p of 3.4 cm was achieved. In [24], an ANN-based approach was proposed exploiting the distortions caused by inaccurate modeling (i.e., phase and intensity models) in both phase difference of arrival (PDOA) and RSS-based positioning systems. The pre-trained models were applied to the ANN-based VLP system for reduced complexity and enhanced robustness, showing an ε_p of 12 cm in an indoor LoS channel.

However, in many previous works, the effects of noise and multipath were not fully and consistently considered. For example, the works reported in [23,24] considered only LoS paths in the analysis of positioning performance without taking into account the multipath nature of the channel. Note, for systems using Txs and Rxs with a wide beam and a field of view (FOV), respectively the impact of multipath reflections is inevitable and therefore must be considered as was reported in [19]. The results showed that, ε_p values of 0.4 and 46.4 cm were achieved for the entire room without and with multipath reflections, respectively. Moreover, the impact of noise was investigated in [25], but the considered signal-to-noise ratio (SNR) was very high (i.e., 30 dB). Alternatively, in [26] the nonline of sight (NLoS) was considered under a very low power noise level (i.e., -140 to -180 dBm), where the minimum ε_p of 0.05 cm was achieved by analytically solving Lambertian transmission equation group. In [27], both multipath reflections and the impact of

noise were considered, where ε_p of 28 cm was achieved but at a high SNR of 30 dB. Therefore, the impact of multipath reflections should be considered as it severely reduces the accuracy of the VLP system. Although the influence of NLOS on the system performance has been studied extensively and reported in the literature [28,25,29,30], but not much has been done on the power distance relation, which is more complex. For regression analysis and position estimation, several machine learning approaches can be used.

The aim of this work is to investigate the utilization of ANN for regression analysis in the VLP system. A comprehensive study is done about the optimization of an ANN for VLP systems and a complete assessment of its performance. The error performance of the proposed system is evaluated by considering the noise over a wide range of SNR. For that, three different ANN algorithms, including Levenberg-Marquardt, Bayesian regularization, and scaled conjugate gradient, are explored to minimize ε_p of the proposed VLP system. The error performance is analyzed and compared with the traditional RSS technique, which uses an NLLS algorithm along with a polynomial regression model [30]. Firstly, the proposed ANN is optimized based on the number of neurons in the hidden layers (HLs) and the number of training epochs. Finally, we analyze the noise performance of the proposed system in comparison with the traditional approaches. We show that, the ANN with Bayesian regularization outperforms the traditional RSS technique using NLLS for a wide range of SNR. Moreover, we also analyze the impact of different training dataset sizes when training the neural network. We also observed an improvement in the positioning accuracy for the inner region by 43, 55, and 50% compared to 57, 32, and 6% in the outer region for the SNR values of 10, 20, and 30 dB, respectively.

The main contribution of this work is the performance evaluation and the design process of already existing ANN algorithms in the VLP systems considering multipath channel, which has not been reported previously. In addition, we have optimized the proposed ANN model based on different parameters, such as the number of neurons in the hidden layers, the number of training epochs, and the size of the training set, which is proven to improve the positioning accuracy of the VLP system.

The rest of the paper is organized as follows; Section 2 presents the system model, the positioning algorithms, and the polynomial regression approach in detail. The ANN used for position estimation and different training algorithms are presented in Section 3. In Section 4, simulation results are discussed in detail, and finally, Section 5 concludes the paper.

2. VLP System Modelling

2.1. System Model

The proposed system consists of a standard empty room with several LED-based Txs and a single photodiode (PD)-based Rx which is facing upwards, as depicted in Fig. 1. The Txs and Rxs are placed on the ceiling and floor levels at heights, h_t, and h_r of 3 and 0 m, respectively from the ground. In the channel, we consider signals from both LoS and NLoS transmission paths. Note, for the NLOS we have limited the reflections to the 1st order due (*i*) simplicity sake [31]; and (*ii*) the containing most of the transmit power [32]. In this work, we have adopted a simple Lambertian model with v of 1 [33].

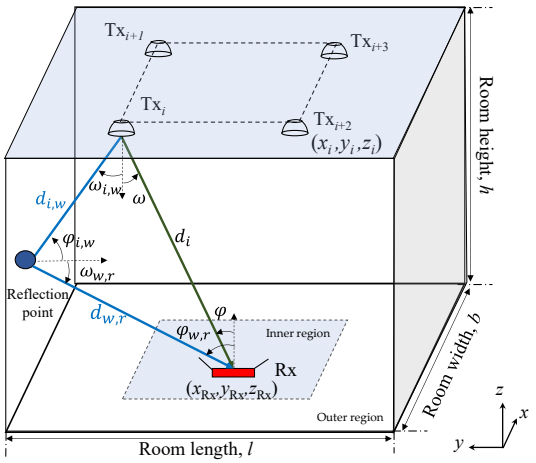

Figure 1. A VLP system with system configuration.

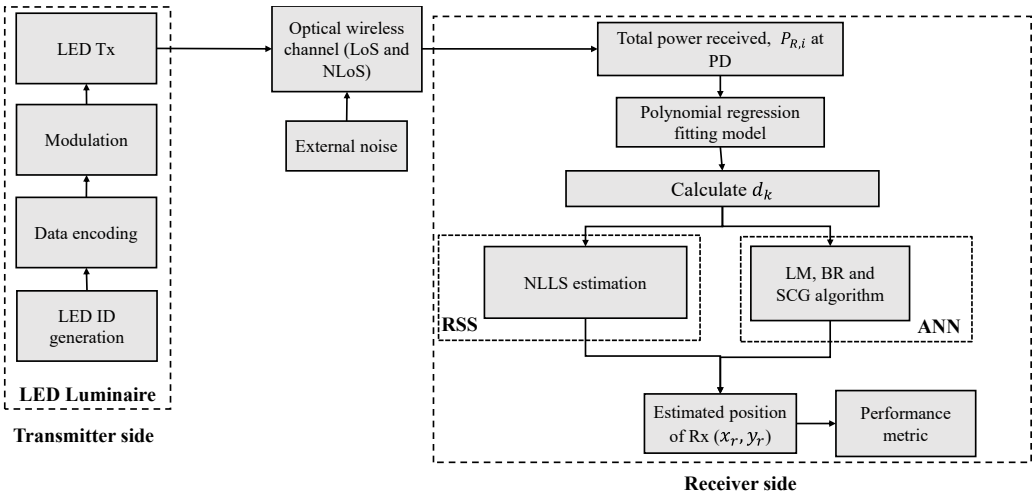

Figure 2. Block diagram of the proposed system.

The block diagram of the proposed scheme is depicted in Fig. 2. We have not considered the synchronization issue and have assumed that each Tx transmits unique ID information, which is encoded and modulated in the on-off keying (OOK) signal format, and at the Rx the received power $P_{R,i}$ due to each Tx is determined using correlation methods, which is given by [30]:

$$P_{R,i} = \sum P_{\mathrm{LoS},i} + \sum P_{\mathrm{NLoS},i} + n_G, \tag{1}$$

where $P_{\mathrm{LoS},i}$ and $P_{\mathrm{NLoS},i}$ are the received power from the i^{th} Tx due to LoS and NLoS paths, respectively, and n_G is the additive white Gaussian noise power with a zero mean and variance σ^2 i.e., $N(0, \sigma^2)$, which arise from the thermal noise, and dark current, signal, and background radiation-induced shot noises. Note, in VLC systems, the latter is the dominant noise source.

Fig. 3 depicts the received power distribution for LoS, NLoS, and LoS with NLoS transmission paths. As illustrated in Fig. 3 (a), for the LoS the power is the highest directly beneath the Txs. The power decreases gradually with the user moving towards the corners and walls of the room. Fig. 3(b) shows that, for the NLoS paths, power distributions are the highest along the walls, thus resulting in a slight rise in the total power received at the Rx near the walls. Fig. 3(c) depicts the total power at Rx from both LoS and NLoS paths showing higher peak and average power level compared to Figs. 3(a) and (b). Note that, the received power from the NLoS paths leads to the overestimation of the transmission

distances and therefore further degrades the positioning accuracy in the localization process.

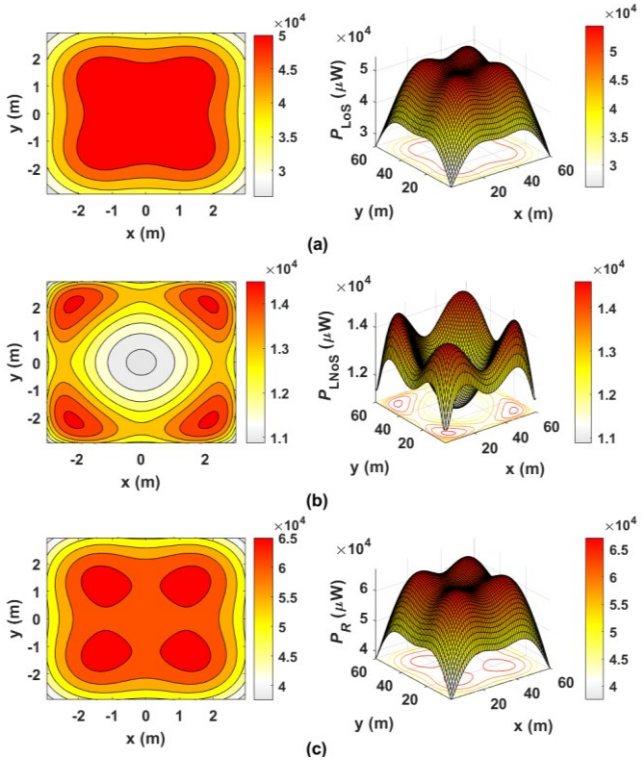

Figure 3. The received power distributions for the proposed system for: (a) LoS, (b) NLoS, and (c) LoS and NLoS links.

The received power from LoS path can be expressed as [34]:

$$\sum P_{\mathrm{LoS},i} = \sum_{i=1}^{I} \frac{m+1}{2\pi} \mathcal{R} A_r P_{t,i} \frac{\cos^m(\omega_i)\cos(\varphi)}{\|d_i\|^2} T_s(\varphi) g(\varphi), \tag{2}$$

where d_i is the distance between the i^{th} Tx and the Rx, ω_i is the irradiance angle from the i^{th} Tx to the Rx, φ, and $\mathcal{R}$ are the incident angle and PD responsivity, respectively. $P_{t,i}$ is the transmit power from the i^{th} Tx and A_r is the area of the PD. $T_s(\varphi)$ and $g(\varphi)$ are the transmittance function and the concentrator gain of the Rx, respectively that are considered to be unity for simplicity's sake. Lambertian order is given by:

$$v = -\frac{\ln(2)}{\ln(\cos(\mathrm{HPA}))}, \tag{3}$$

where HPA refers to the half-power angle for the light source. The RSS algorithm incorporates a distance estimation step based on the total received power $P_{R,i}$, where the distance between the i^{th} Tx and the Rx is estimated as:

$$d_i = \sqrt{r_i^2 + h^2}, \tag{4}$$

where r_i is the horizontal distance from the i^{th} Tx to the Rx and h is the difference in height between the Tx and Rx, i.e., ($h_t - h_r$). The received power from the 1st order reflection is given by [35]:

$$\sum P_{\mathrm{NLoS},i} = \sum_{i=1}^{I} \sum_{\text{wall}} \left(\frac{m+1}{2\pi^2}\right) \rho \mathcal{R} A_r P_{t,i} A_{\text{ref}} \frac{\cos^m(\omega_{i,w})\cos(\varphi_{i,w})}{\|d_{i,w}\|^2 \|d_{w,r}\|^2} \times \cos(\omega_{w,r}) \cos(\varphi_{w,r}) T_s(\varphi_{w,r}) g(\varphi_{w,r}), \tag{5}$$

where $d_{i,w}$, $\varphi_{i,w}$, and $\omega_{k,w}$ are the distances, receiving incident angle, and the irradiance angle between the i^{th} Tx and the reflective area, respectively. $d_{w,r}$, $\varphi_{w,r}$, and $\omega_{w,r}$ are the distances, receiving incident angle, and irradiance angle between the reflective area and the Rx, respectively. ρ is the reflectance factor of the reflecting surfaces and A_{ref} is the reflectance area. For the NLoS case, a significant error may occur when calculating the distance due to the existence of reflections, as noted in (5). Therefore, a polynomial fitted model is introduced to express the relation between $P_{R,i}$ and the total distance from i^{th} Tx and the Rx [35,36], which is given by:

$$d_i(P_{R,i}) = a_0 + a_1 P_{R,i} + a_2 \left(P_{R,i}\right)^2 + \cdots + a_g \left(P_{R,i}\right)^g, \quad (6)$$

where $a_0 \ldots a_g$ are the coefficients of the polynomial model for a g^{th} order polynomial.

2.2. Estimation Algorithms

In the case of LLS, a_g values are initially estimated based on the fitting process for the given values of d_i and $P_{R,i}$. These values are then utilized for estimation of d_i and substitution in (4) to determine r_i for each Tx. Note that, LLS is used to find a coarse estimate of the Rx's position, which is given by [19]:

$$\hat{X} = \begin{bmatrix} \hat{x}_{\text{Rx}} \\ \hat{y}_{\text{Rx}} \end{bmatrix} = (A^T A)^{-1} A^T B, \quad (7)$$

where $[\hat{x}_{\text{Rx}}, \hat{y}_{\text{Rx}}]$ is the estimated position of the Rx, and A and B are given as:

$$A = \begin{bmatrix} x_2 - x_1 & y_2 - y_1 \\ \vdots & \vdots \\ x_I - x_1 & y_I - y_1 \end{bmatrix}, \quad B = 0.5 \times \begin{bmatrix} (r_1^2 - r_2^2) + (x_2^2 + y_2^2) - (x_1^2 + y_1^2) \\ \vdots \\ (r_1^2 - r_I^2) + (x_I^2 + y_I^2) - (x_1^2 + y_1^2) \end{bmatrix}. \quad (8)$$

However, the LLS estimation solution may not offer a high positioning accuracy [19]. This is especially true for the positions close to the walls and corners, where the signal power levels from the NLoS paths are higher. The NLLS estimation can be utilized as an alternative approach for position estimation, which minimizes the approximation error attained from LLS estimation [29]. The trust region algorithm is employed to solve the unrestricted optimization problem to realize the 3D positioning [12]. The estimated location is found at the minimum of the averaged squared error $\tilde{C}$, which is given by:

$$\tilde{C} = \sum_{i=1}^{I} \left(\sqrt{(\tilde{x}_{\text{Rx}} - x_i)^2 + (\tilde{y}_{\text{Rx}} - y_i)^2} - r_i \right)^2, \quad (9)$$

where $\tilde{x}_{\text{Rx}}$ and $\tilde{y}_{\text{Rx}}$ are the estimated position of the Rx. r_i is computed from (4) and (6). In this work, we consider NLLS with a polynomial fitted model for the distance as the baseline for performance comparison.

3. The Concept of Neural Network

3.1. Use of ANN for Regression

Even with the power versus the distance relation for NLoS described in (6), the room morphology (corners, walls, furniture, etc.) changes a great deal, thus making it difficult to infer an approximate model, which is applicable for every scenario. As a result, using ANN is advantageous since it is trained using $P_{R,i}$ from each Tx and the transmission distance. The regression analysis is useful to model the relationship between a dependent variable and one or more independent variables (i.e., the input values in the model). One of the possible solutions for any type of regression problem is the ANN. The ANN is inspired by the process of the human brain and therefore, is composed of neurons that work in parallel. Each neuron is capable of performing a simple mathematical operation individually [37]. Collectively, the neurons can evaluate complex problems, emulating most

of the functions and providing precise solutions. The ANN is an interconnected network of processing elements (neurons) and it includes two different phases: (*i*) the training phase - where the ANN estimates an input-output map based on the training data set. During this training phase, the neuron weights are continuously adapted to minimize the error between the estimated output and the training data vectors. The process terminates when the required performance is achieved, or the complete training set is used; and (*ii*) the operation phase - where the ANN is employed to perform estimates based on the input data alone. The ANN structure consists of at least three layers; a single input layer consisting of γ_N, one or several hidden layers (HL), and a single output layer, see Fig. 4(a). These layers are linked together based on a collection of connected units or nodes, called the artificial neurons. The importance of these neurons is defined based on their weights and the learning process.

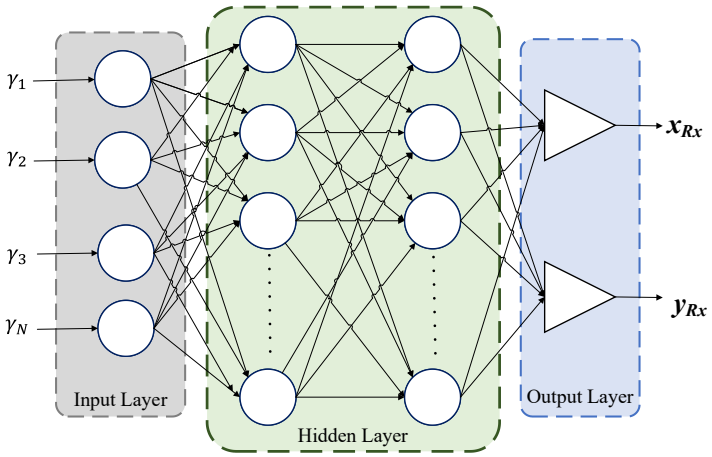

(**a**)

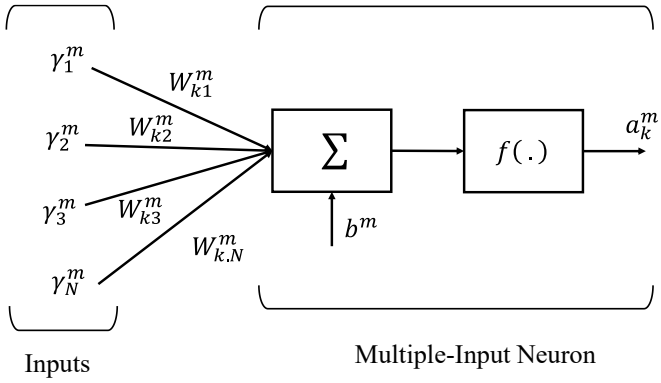

(**b**)

Figure 4. The artificial neural network with: (a) a basic structure, and (b) a structure of k^{th} neuron with N inputs in the layer m.

The weight W_{kn}^m has the capability to acquire and store experimental knowledge, where k, n, and m represent the number of neurons, inputs, and layers, respectively. These are also known as the synaptic weights because their principle is like the synapses present in biological brains. It relates the n^{th} input to the k^{th} neuron. Note, the number of neurons in the hidden layer controls the weights and the bias in the network. Each neuron can be biased with a value b^m as depicted in Fig. 4(b). For HLs, a sigmoid transfer function is used as an activation function that applies thresholding to the input data and produces outputs as a continuous value between zero and one, while the output layer employs a linear transfer function. The performance of an ANN algorithm is measured by the mean square error, which can be expressed as a function of $F(p_k^m)$ as:

$$F(p_k^m) = e_k^m = \|t_k^m - a_k^m\|_2, \tag{10}$$

where p_k is the vector containing all of the network weights and biases for the k^{th} neuron (i.e., $p_k = [W_k, b_k]$), and a_k^m is the network output of the k^{th} neuron for the m^{th} layer and t_k^m is the target output of the k^{th} neuron for the m^{th} layer. The weights and the bias are updated by the backpropagation method [37] as:

$$W_{k,n+1}^m = W_{k,n}^m - Gs^m(a_k^{m-1})^T \tag{11}$$

$$b_{k,n+1}^m = b_{k,n}^m - Gs^m, \tag{12}$$

where G is the learning rate, $m = 0,1,\dots,M-1$, M is the number of layers in the network, and $(.)^T$ is the transpose. $b_{k,n}^m$ is the bias vector. γ_{kn}^m is the input vector, $n = 0,1,\dots,N$, and N is the total number of inputs in the network. s^m is the sensitivity matrix, which is evaluated from the least mean square error function, $\hat{F}(p_k^m)$ for various values of j, wherein j is defined in the matrix form as $\gamma_k W_k + b_k$.

The ANN structure in the proposed study is composed of four layers: an input layer, two hidden layers (HLs), and an output layer. Each layer has a different number of neurons, with the input and output layers having four and two neurons, respectively. The estimated x and y position coordinates are represented by the output neurons. The estimated distances from each Tx are applied to the input layer with the help of (6).

In this work, we have investigated the number of hidden layers (HLs) and have determined that a simple ANN with only one hidden layer would not provide the desired results i.e., high positioning errors. Using two hidden layers provided a more effective framework for achieving improved performance. Therefore, based on our preliminary research, we limited the number of hidden layers to two. The neurons in the HLs are activated using a Sigmoid transfer function, which thresholds the input data and outputs a continuous value between zero and one. A linear transfer function is used in the output layer. All notations utilized in the paper are indicated in Table 1 in the appendix.

Following that, we have adopted a few well-known training algorithms and used them to analyze the positioning error of the proposed system. For this investigation, we have used the default values of Matlab's fitnet tool to fix the parameters such as the learning rate. Note that, other parameters such as the number of neurons in HLs or the activation functions could also be optimized based on the topology of the HLs. Since Sigmoid and linear activation functions have been shown to perform well in regression tasks [38], therefore, they are used in the hidden and output layers, respectively. Having selected Bayesian regularization as the optimal learning algorithm, we then optimized the learning phase using the number of epochs and size of the training set.

3.2. ANN Training Methods

The network records the trained information in W_{kn}^m and b^m. Note, the ANN can be trained in supervised and unsupervised modes, where the former offers higher reliability compared with the latter; thus, it is adopted in this work as explained in the following subsections.

3.2.1. Levenberg-Marquardt Algorithm

Levenberg-Marquardt (LM) algorithm is employed to solve the NLLS problems. By leveraging the most used optimization algorithms (i.e., Gauss-Newton algorithm, and the steepest descent algorithm), the LM algorithm can avoid some problems, such as over-parameterization, local minima, and non-existence of the inverse matrix [39]. Moreover, it inherits the speed advantage of Gauss-Newton algorithm and the stability of the steepest descent algorithm. The updated rule of weights and biases, i.e., p_k is given by:

$$p_{k+1} = p_k - [J_k^T J_k + \mu_k \mathrm{I}]^{-1} - J_k e_k, \tag{13}$$

where J_k is Jacobian matrix of the function, $F(p_k)$, and $\mu_k \geq 0$ is a scalar, and I is the identity matrix.

3.2.2. Bayesian Regularization Algorithm

Bayesian regularization (BR) is an algorithm that updates the values of weight and bias in accordance with LM optimization. In this algorithm, firstly, a linear combination of the squared errors and the weights are minimized and then, the linear combination is modified with the aim of obtaining a network with good generalization qualities [37]. In BR, the mean squared error function can be defined as:

$$F(p_k) = \beta E_D + \alpha E_W, \tag{14}$$

where E_D is the squared error, E_W is the sum of squared weights, which penalizes large weights in reaching a better generalization and smoother mapping, α, and β are the regularization parameters (or objective functions), which are given as:

$$\alpha = \frac{\gamma_e}{2E_W(p_k)}, \beta = \frac{N_{wb} - \gamma_e}{2E_D(p_k).}, \tag{15}$$

where $\gamma_e = N - 2\alpha \mathrm{tr}(H^{-1})$ is called the effective number of parameters, $H = \nabla^2 F(p_k)$ is Hessian matrix, N_{wb} is the total number of parameters (weights and biases) of the network, $\mathrm{tr}(H^{-1})$ is the trace of the inverse of Hessian matrix. Note, the 2nd term in (15) is known as the weight decay, and therefore small values of W would reduce the overfitting of the model.

3.2.3. Scaled Conjugate Gradient Algorithm

Most of the conjugate gradient algorithms use a line search for each iteration, thus making them computationally complex. Therefore, to address this we have adopted the scaled conjugate gradient (SCG) algorithm developed by Moller [40]. SCG is based on conjugate directions without performing line search, with reduced computational complexity. The SCG algorithm, which is a scaled conjugate gradient method for updating the weight and bias values, is robust and does not depend on the user-defined parameters given that the step size is a function of quadratic approximation of the error [40]. Different approaches are used for estimating the step size, which is given by:

$$\xi_k = \frac{\mu_k}{\delta_k} = \frac{-\bar{p}_k^T E'_{qw}(p_k)}{\bar{p}_k^T \bar{s}_k + \lambda_k |\bar{p}_k|^2}, \tag{16}$$

where $E'_{qw}(p_k)$ is the quadratic approximation of the error function, $F(p_k)$. $\bar{p}_1, \bar{p}_2, \ldots . \bar{p}_k$ is the set of non-zero weight vectors, and $\bar{s}_k$ is the second-order information. λ_k is the scaler to be updated such that:

$$\lambda_k = 2\left(\lambda_k - \frac{\delta_k}{|\bar{p}_k|^2}\right). \tag{17}$$

If $\Delta_k > 0.75$, then $\lambda_k = \lambda_k/4$, and if $\Delta_k < 0.25$ then $\lambda_k = \lambda_k + \delta_k(1 - \Delta_k)/|\bar{p}_k|^2$. Δ_k is a comparison parameter given by:

$$\Delta_k = \frac{2\delta_k[F(p_k) - F(p_k + \xi_k \bar{p}_k)]}{\mu_k^2}. \tag{18}$$

4. Results and Discussion

The proposed system adopted in section 2 is implemented in the simulation environment using MATLAB. Both NLLS and different ANN algorithms are applied to the proposed VLP system, and the performance of all algorithms is compared. The ANN structure is composed of 4 layers, which include an input layer, two HLs, and an output layer. The number of neurons in each layer is variable, with 4 and 2 neurons in the input and output layers, respectively. The latter represents the estimated x and y position

coordinates. Using (6), the calculated distances from each Tx are fed to the input layer. A sigmoid transfer function is used as the activation function for the neurons in the HLs, which threshold the input data and provides the output as a continuous value between zero and one. The output layer employs a linear transfer function.

Besides, the proposed positioning process includes (*i*) the total received power computed at the Rx; (*ii*) the polynomial regression model used to determine the power distance relation, and the distance from each Tx to the Rx; (*iii*) the computed distance is used as the input to the NN algorithm for training purpose; and (*iv*) the position is estimated as the output of the ANN algorithm. Furthermore, for the real implementation, the use of these algorithms would imply two phases: the training phase, where previously collected data will be used for training the ANN; and the stand-alone phase, where the trained ANN with fixed weights will be used in the hardware for position estimation.

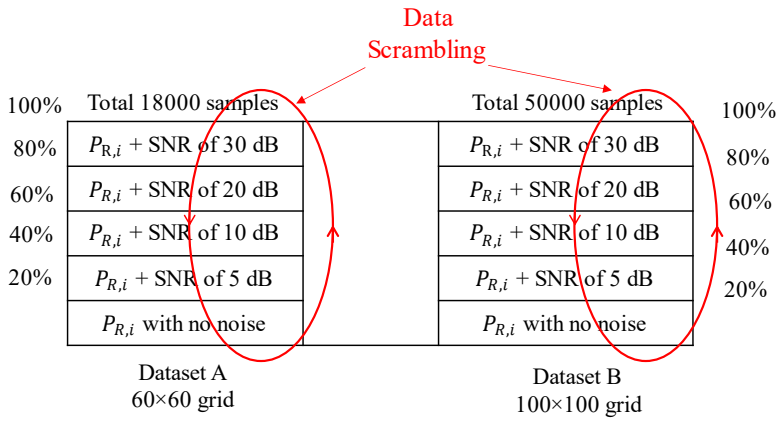

Figure 5. Total dataset samples considered for the proposed ANN.

In this study, two datasets are considered for training, testing, and validation of the ANN as depicted in Fig. 5. These datasets are composed of the received power information for a given grid of Rxs with different noise power levels (according to the SNR).

Table 2. The key system parameters.

Parameter	Value
Room size	6 × 6 × 3 m^3
Locations of the Txs	
$(x_1,\ y_1,\ z_1)$,	(-1.7, -1.7, 3),
$(x_2,\ y_2,\ z_2)$	(-1.7, 1.7, 3),
$(x_3,\ y_3,\ z_3)$,	(1.7, -1.7, 3),
$(x_4,\ y_4,\ z_4)$	(1.7, 1.7, 3)
Area of PD	10^{-4} m^2
Half-power angle (HPA)	70°
Responsivity of PD	0.5 A/W
Field of view (FOV)	75°
Transmitted power	1 W
Reflection coefficient	0.7
Activation function	Sigmoid, linear
Number of neurons in the input layer	4
Number of neurons in the hidden layer	2-36
Number of neurons in the output layer	2
Number of hidden layers	2
Percentage of train to test	0.8

Note, (*i*) the data samples are randomly scrambled; and (*ii*) different datasets are used to avoid biasing of the training process, that is, ANN optimization is done using a single dataset while for the verification and testing another dataset is adopted. Therefore, 80% of dataset A and 20% of dataset B are used for training and for testing and validation, respectively. Data scrambling is used to feed the data randomly to the inputs of the neural network for training the network, see Fig. 5. We consider a grid (1 cm resolution) of 3600 Rx's positions on the receiving plane, which is divided into two regions, i.e., the inner region where the received power is more uniform and includes the area of the receiving plane within the Txs (LEDs), and the outer region representing the remaining area near the walls and corners as depicted in Fig. 1. All the other key system parameters are given in Table 2.

4.1. VLP Error Performance

Generally, RSS-based positioning algorithms are susceptible to the ambient induced shot noise, thus leading to increased ε_p. In this work, we consider the impact of noise, which is modelled as Gaussian with $N(0, \sigma^2)$, on the performance of VLP. A total of 1000 iterations are performed in this simulation to gain some statistical significance. The performance evaluation of the VLP system is provided in terms of the Quantile function Q, which is a valid performance metric to show the level of accuracy. The measurement of the confidence interval of ε_p is carried out through the performance metrics of the Q, which is given by [30]:

$$Q(\eta) = \mathrm{CDF}^{-1}(\eta), \tag{19}$$

where CDF represents the cumulative distribution function of ε_p, and η is the percentage of the confidence interval.

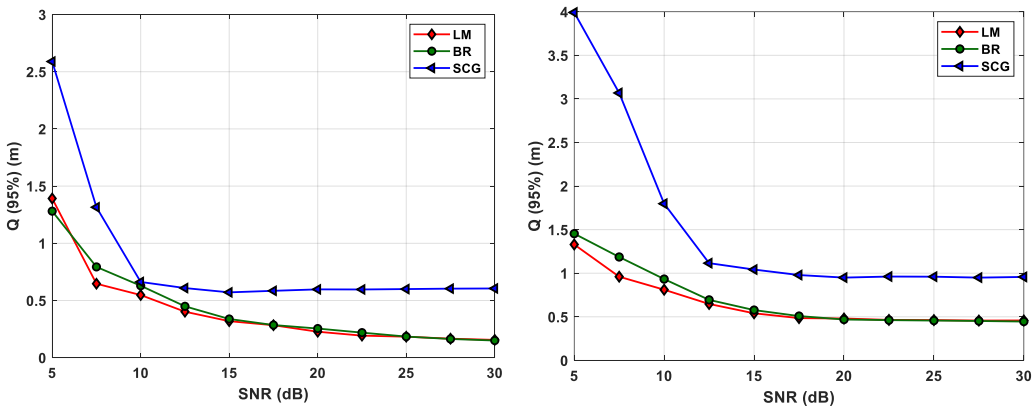

Figure 6. The measured 95% quantile function for different ANN algorithms for: (a) the inner, and (b) the outer regions.

Figure. 6 shows the measured $Q(95\%)$ as a function of the SNR for different ANN algorithms in both inner and outer regions. It is observed that, LM and BR outperform SCG in both regions. For instance, in the inner region at the SNR of 10 dB, $\varepsilon_{p-\min}$ are 54, 62, and 66 cm for LM, BR, and SCG, respectively, which increases to 80, 95, and 170 cm, respectively for the outer region. Note, the SNR thresholds for the inner and outer regions are 10 and 15 dB, respectively, where beyond these values, the positioning errors remain almost constant at the lowest levels. Note that, we have considered the average SNR values in the analysis. The decreasing trend in the positioning error is justified by the increase of SNR. For high values of SNR, the effect of noise on the estimated position is reduced. On the contrary, for the small values of SNR, the randomness of the input data leads to overfitting, thus making the estimated error larger. To improve the proposed VLP system,

we further investigate the impact of ANN algorithms, the number of neurons in the HLs, and the epochs in the following sections.

4.2. Selection of the Training Algorithm and Number of Neurons in the HL

The number of neurons in the HL and different training methods are investigated in this subsection to determine the optimum algorithm based on $\varepsilon_{p-\min}$. The accuracy of the inner region is higher than the outer region due to more reflections being considered in the corners of the room. Therefore, we have only considered the inner region for the selection of the number of neurons in both HLs. As depicted in Fig. 6, both LM and BR have lower ε_p compared with SCG, therefore, are considered for further analysis. Next, we investigate a different number of neurons in the HL and the training for an ideal scenario (i.e., no noise).

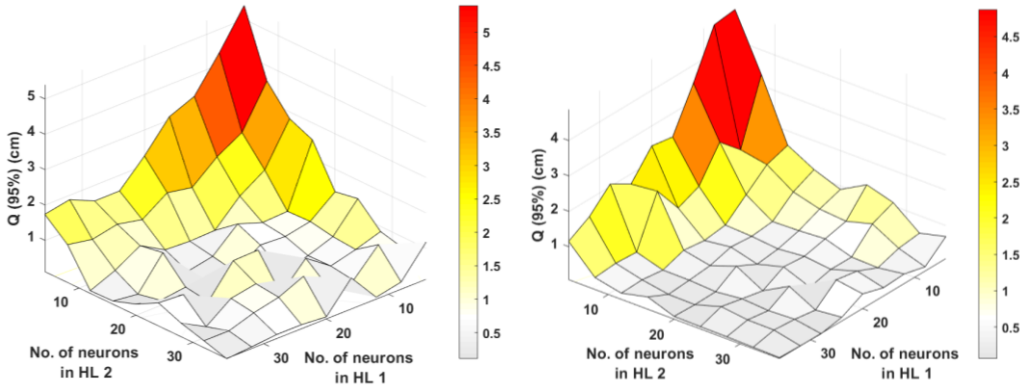

(**a**) (**b**)

Figure 7. The positioning error for the inner region for different training methods of ANN: (a) LM, and (b) BR.

Table 3. Comparison of $\varepsilon_{p-\min}$ for different training algorithms.

Algorithms	ε_p (cm)	Neurons in HL 1	Neurons in HL 2
LM	0.11	36	36
BR	0.06	32	28

Fig. 7 shows the surface plots for Q of 95% for the different number of neurons for LM and BR. As depicted in Fig. 7, ε_{p-min} are 0.11 and 0.06 cm for (*i*) LM with 36 neurons each in the HLs of 1 and 2; and (*ii*) BR with 32 and 28 neurons in HLs 1 and 2, respectively. Based on ε_{p-min} the number of neurons in the HL is selected for LM and BR as detailed in Table 3. Note, the training performance is compared for 1000 epochs between LM and BR with the total computation times are 22 and ~10 minutes, respectively, which is achieved using CPU Intel (R) Core (TM) i9-9900K CPU @ 3.60GHz, 3600 MHz, 8 Core PC, having 16 Logical Processors and 32 GB RAM. The epochs represent the number of times the ANN algorithm will run over the full training dataset. BR offers a faster training phase, and therefore, is selected for further investigation of the impact of a different number of epochs.

4.3. Impact of Epochs and Noise Performance an the VLP System

Firstly, the effect of epochs in the proposed VLP system is observed, where we investigate different epoch values their impacts on the error performance. Fig. 8 depicts the Q(95%) as a function of SNR for epochs of 500, 1000, and 3000 for inner and outer regions. We can see that, for the inner and outer regions, the epoch of 3000 offers the lowest Q for all values of SNR, therefore, it is considered further analysis with the noise. This shows

that BR is strongly affected by the number of training epochs, with a larger number of epochs resulting in more tuned network weights.

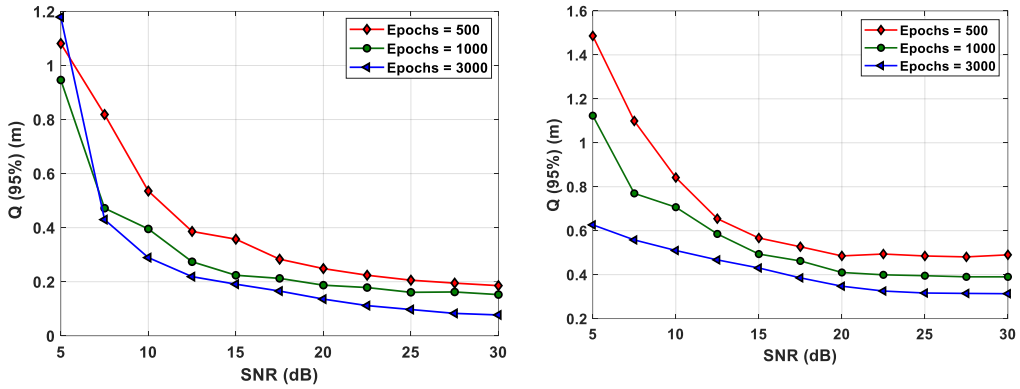

Figure 8. The measured 95% quantile function for various number of epochs for BR in the: (a) inner, and (b) outer regions.

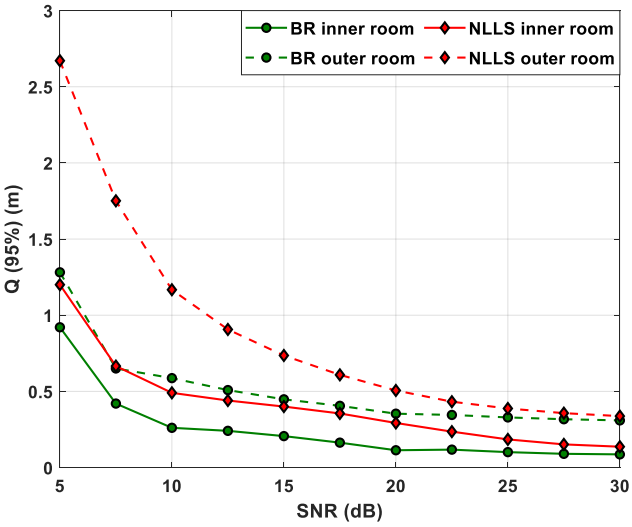

Figure 9. The measured 95% quantile function for NLLS and BR.

Fig. 9 depicts the $Q(95\%)$ as the function of SNR for the BR-based ANN algorithm and with RSS, as well as for the inner and outer regions and for the epochs of 3000. Results show that NLLS is more prone to the effect of noise and proximity from walls and corners than BR. This can be explained by the ability of the ANN to better estimate the positions near the walls than NLLS and the inherent immunity to the noise. As shown, ε_p is reduced significantly using ANN. For instance, at the SNR of 30 dB and for the inner region $\varepsilon_{p-\min}$ are 8 and 13 cm for BR and NLLS, respectively. Moreover, in the inner region, the accuracy improvement values of 46, 58, and 38% are observed for the SNR values of 10, 20, and 30 dB, respectively. While in the case of the outer region, the accuracy improvements of 50, 30, and 9% are observed for the SNR values of 10, 20, and 30 dB, respectively. Therefore, the BR outperforms the traditional NLLS for the SNR range of 5 – 30 dB.

Fig. 10 depicts the error distribution plots using Bayesian Regularization algorithm for different ranges of SNR. It can be observed that the positioning error ε_p decreases by increasing the SNR values. Therefore, we can clearly see the impact of noise in these error plots. The main observations are detailed in Table 4.

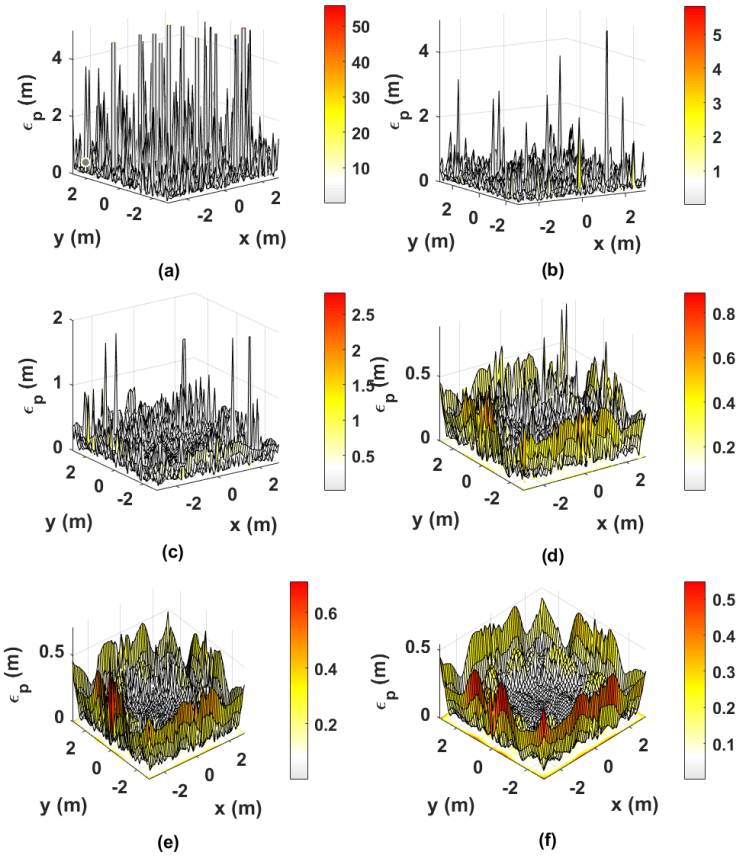

Figure 10. Different error distribution plots using BR algorithm for SNR value: (a) 5 dB, (b) 10 dB, (c) 15 dB, (d) 20 dB, (e) 25 dB, and (f) 30 dB.

Table 4. Final observations of the comparison of BR and traditional RSS with NLLS algorithms.

	BR	**RSS with NLLS**
Max. P_R (μW)	6.7×10^4	6.7×10^4
Min. P_R (μW)	3.6×10^4	3.6×10^4
Max. ε_p at 20 dB (m)	0.89	1.29
Min. ε_p at 20 dB (m)	16×10^{-4}	18×10^{-4}
Max. ε_p at 25 dB (m)	0.71	0.72
Min. ε_p at 25 dB (m)	6.1×10^{-4}	15×10^{-4}
Max. ε_p at 30 dB (m)	0.54	0.67
Min. ε_p at 30 dB (m)	5.4×10^{-4}	4.6×10^{-4}

4.4. Impact of Different Training Dataset Sizes on the VLP System

Furthermore, we analyze the impact of different training dataset sizes denoted by I_n on the Q. For this, we have considered two training scenarios: the random selection (RS), and the uniform selection (US). In the former, the original dataset A is down-sampled from the original 18,000 samples to 9000, 4500, 2250, and 1125 datasets. While, in the latter, the grid size is down-sampled from the original 60×60 samples to the aforementioned sizes. By doing so, we aim to show if the system performance depends on the selection of training dataset samples. Here, we have only generated results for considering only the data from the inner region.

Fig. 11 shows the error performance versus the SNR for a range of I_n and for both RS and US scenarios. For the RS scenario, the $\varepsilon_{p-\min}$ values are 2, 11, and 44 cm for the SNR values of 30, 20, and 10 dB, respectively with a lower I_n of 9000 compared to 15, 22, and 44

cm for the US scenario with a higher I_n of 18000. Results show that, the US scenario conducts to larger errors, this is because we are sampling the grid resolution. This may conduct to overfitting problems. With the RS scenario, the accuracy improves for high SNR values showing that there is an optimum size for the training dataset. This can be attributed to the fact that the original grid resolution is fixed, leading to less probability of overfitting. Therefore, considering the original dataset provides improved results. Hence, the proper selection of the training dataset sizes is also essential to properly design the system.

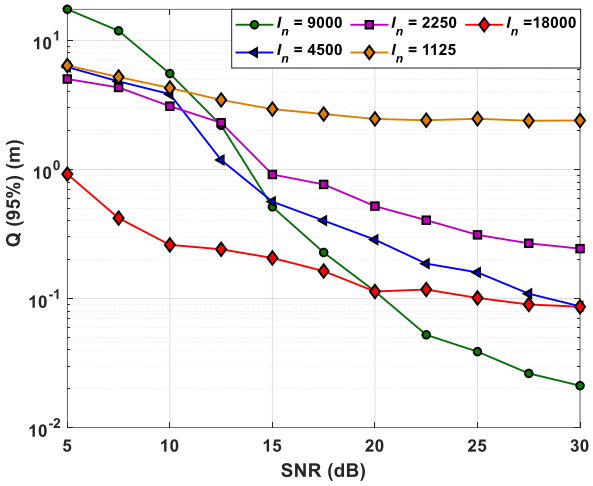

(**a**)

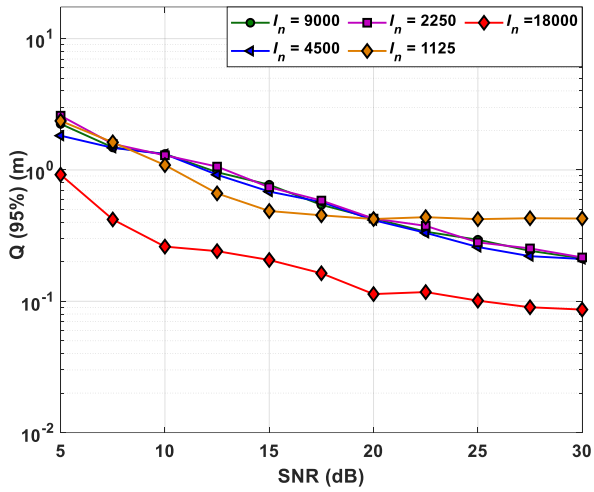

(**b**)

Figure 11. The measured 95% quantile function for a different number of samples in the input with: (a) RS, and (b) US.

5. Conclusions

An indoor VLP system using an artificial neural network for positioning estimation in the presence of both line-of-sight and non-line-of-sight multipath signals was analyzed. In order to implement a realistic scenario, we studied the influence of noise in the proposed system. Three different ANN algorithms of Levenberg-Marquardt, Bayesian regularization, and scaled conjugate gradient algorithms were explored for minimizing the positioning error. The optimization of ANN was done based on the number of neurons in the hidden layers and the number of training epochs. We showed that, the ANN with Bayesian regularization outperforms the traditional RSS technique using NLLS for the SNR range of 5 – 30 dB. We also observed an improvement in the positioning accuracy for the inner region by 43, 55, and 50% compared to 57, 32, and 6% in the outer region for the

SNR of 10, 20, and 30 dB, respectively. We further studied the impact of different training dataset sizes for training the neural network. It is concluded that, ANN is an efficient method that allows to achieve a minimum positioning error of 2 cm for 30 dB of SNR with a random selection of training dataset sizes. Finally, we observed that the positioning error is low even for a lower range of SNR, i.e., positioning error values of 2, 11, and 44 cm for the SNR of 30, 20, and 10 dB, respectively. In our future work, we will be developing an experimental test-bed for verification of the simulated results.

Author Contributions: The contributions of the authors in this paper are the following: conceptualization: N.C., O.I.Y., L.N.A., and Z.G.; investigation: N.C., and O.I.Y.; methodology: N.C., O.I.Y., L.N.A. and Z.G.; project administration: L.N.A., Z.G., and S.Z.; software: N.C., and O.I.Y.; validation: L.N.A., Z.G., and S.Z. All authors have read and agreed to the published version of the manuscript.

Funding: This work was supported by H2020/MSCA-ITN funding program under the framework of European Training Network on Visible Light Based Interoperability and Networking, project (VisIoN) grant agreement no 764461, Northumbria University Ph.D. Scholarship, EU COST Action NEWFOCUS CA19111.

Institutional Review Board Statement: Not applicable.

Informed Consent Statement: Not applicable.

Conflicts of Interest: The authors declare no conflict of interest.

Appendix A

Table 1. List of notations used in this paper.

Notation	Definition
ε_p	Positioning error
h_t	Height of the Tx
h_r	Height of the Rx
m	Lambertian mode
$P_{R,i}$	Total received power from the i^{th} Tx
$P_{LoS,i}$	Received power from the i^{th} Tx due to the path loss
$P_{NLoS,i}$	Received power from i^{th} Tx due to NLoS path
n_G	Additive white Gaussian noise
d_i	Distance between the i^{th} Tx and the Rx
ω_i	The irradiance angle from the i^{th} Tx to the Rx
φ	Incident angle
$\mathcal{R}$	Photodiode responsivity
$P_{t,i}$	Transmitted power from the i^{th} Tx
$T_s(\varphi)$	Transmittance function
$g(\varphi)$	Concentrator gain of the Rx
A_r	Area of the photodetector
r_i	The horizontal distance from the Tx to the Rx
h	The difference in height between the Tx and Rx, i.e., ($h_t - h_r$)
$d_{i,w}$, $\varphi_{i,w}$, $\omega_{k,w}$	The distances, receiving incident angle, and the irradiance angle between the i^{th} Tx and the reflective area, respectively
$d_{w,r}$, $\varphi_{w,r}$, $\omega_{w,r}$	The distances, receiving incident angle, and the irradiance angle between the reflective area and the Rx, respectively

ρ	The reflectance factor depending on the material of the reflective surface
A_{ref}	Reflectance area
$a_0 \ldots a_g$	Coefficients of the polynomial model for the g^{th} order polynomial
$[\hat{x}_{\text{Rx}}, \hat{y}_{\text{Rx}}]$	The estimated position of the Rx
$\tilde{C}$	Averaged squared error
$\tilde{x}_{\text{Rx}}$, $\tilde{y}_{\text{Rx}}$	The estimated position of the Rx.
W_{kn}^{m}	Weight
p_k	The vector containing all the network weights and biases for the k^{th} neuron, i.e., $p_k = [W_k, b_k]$
a_k	The network output for the k^{th} neuron
t_k	The target output of the network for the k^{th} neuron
G	Learning rate
M	Maximum number of layers
b	Bias vector
m	Number of layers
k	Number of neurons
γ	Input vector,
N	Total number of inputs
n	Number of inputs
e_k	Error matrix
$\mathbf{s}$	Sensitivity matrix
$\hat{F}(p_k^m)$	Least mean square error function
$F(p_k^m)$	Mean square error
J_k	Jacobian matrix
μ_k	A scalar
I	Identity matrix
E_D	Squared error
E_W	Sum of squared weights
α, β	Regularization parameters
γ_e	Effective number of parameters
H	Hessian matrix
N_{wb}	Total number of parameters (weights and biases) of the network
$\text{tr}(H^{-1})$	The trace of the inverse of Hessian matrix
$E'_{qw}(p_k)$	Quadratic approximation of the error function, $F(p_k)$
$\bar{p}_1, \bar{p}_2, \ldots . \bar{p}_k$	The set of non-zero weight vectors
$\bar{s}_k$	Second-order information
λ_k	A Scalar
Δ_k	Comparison parameter
η	Percentage of the confidence interval
Q	Quantile function
$\varepsilon_{p-\min}$	Minimum positioning error

ξ_k	Step size

References

1. Kaplan, E.D.; C. J. Hegarty *Understanding GPS : Principles and Applications*; Boston : Artech House, 1996;
2. Zhuang, Y.; El-Sheimy, N. Tightly-Coupled Integration of WiFi and MEMS Sensors on Handheld Devices for Indoor Pedestrian Navigation. *IEEE Sensors Journal* **2016**, *16*, 224–234, doi:10.1109/JSEN.2015.2477444.
3. Nieminen, J.; Gomez, C.; Isomaki, M.; Savolainen, T.; Patil, B.; Shelby, Z.; Xi, M.; Oller, J. Networking Solutions for Connecting Bluetooth Low Energy Enabled Machines to the Internet of Things. *IEEE Network* **2014**, *28*, 83–90, doi:10.1109/MNET.2014.6963809.
4. Priyantha, N.B.; Miu, A.K.L.; Balakrishnan, H.; Teller, S. The Cricket Compass for Context-Aware Mobile Applications. In Proceedings of the Proceedings of the 7th Annual International Conference on Mobile Computing and Networking; Association for Computing Machinery: New York, NY, USA, 2001; pp. 1–14.
5. Liu, H.; Darabi, H.; Banerjee, P.; Liu, J. Survey of Wireless Indoor Positioning Techniques and Systems. *IEEE Transactions on Systems, Man and Cybernetics Part C: Applications and Reviews* **2007**, *37*, 1067–1080, doi:10.1109/TSMCC.2007.905750.
6. Hsu, C.-W.; Liu, S.; Lu, F.; Chow, C.-W.; Yeh, C.-H.; Chang, G.-K. Accurate Indoor Visible Light Positioning System Utilizing Machine Learning Technique with Height Tolerance. *2018 Optical Fiber Communications Conference and Exposition (OFC)* **2018**, *1*, M2K.2, doi:10.1364/ofc.2018.m2k.2.
7. Hassan, N.U.L.; Adeel Pasha, M.; Naeem, A.; Jadoon, T.M. Indoor Positioning Using Visible LED Lights: A Survey. *ACM Transactions on Sensor Networks* **2015**, *11*, 1–30, doi:10.1145/0000000.000000.
8. Do, T.-H.; Yoo, M. An In-Depth Survey of Visible Light Communication Based Positioning Systems. *Sensors* **2016**, *16*, 678, doi:10.3390/s16050678.
9. Yassin, A.; Nasser, Y.; Awad, M.; Al-Dubai, A.; Liu, R.; Yuen, C.; Raulefs, R.; Aboutanios, E. Recent Advances in Indoor Localization: A Survey on Theoretical Approaches and Applications. *IEEE Communications Surveys and Tutorials* **2017**, *19*, 1327–1346, doi:10.1109/COMST.2016.2632427.
10. Luo, J.; Fan, L.; Li, H. Indoor Positioning Systems Based on Visible Light Communication: State of the Art. *IEEE Commun. Surv. Tutorials* **2017**, *19*, 2871–2893, doi:10.1109/COMST.2017.2743228.
11. Wang, K.; Nirmalathas, A.; Lim, C.; Skafidas, E. Optical Wireless-Based Indoor Localization System Employing a Single-Channel Imaging Receiver. *JOURNAL OF LIGHTWAVE TECHNOLOGY* **2016**, *34*, 9.
12. Kim, H.S.; Kim, D.R.; Yang, S.H.; Son, Y.H.; Han, S.K. An Indoor Visible Light Communication Positioning System Using a RF Carrier Allocation Technique. *Journal of Lightwave Technology* **2013**, *31*, 134–144, doi:10.1109/JLT.2012.2225826.
13. Zheng, H.; Xu, Z.; Yu, C.; Gurusamy, M. Indoor Three-Dimensional Positioning Based on Visible Light Communication Using Hamming Filter. *Optics InfoBase Conference Papers* **2016**, *2016*, 4–6, doi:10.1364/sppcom.2016.spm4e.3.
14. Xiang Liu, X.L.; Aiying Yang, A.Y.; Yu Wang, Y.W.; and Lihui Feng, and L.F. Combination of Light-Emitting Diode Positioning Identification and Time-Division Multiplexing Scheme for Indoor Location-Based Service. *Chinese Optics Letters* **2015**, *13*, 120601–120606, doi:10.3788/col201513.120601.
15. Do, T.H.; Yoo, M. An In-Depth Survey of Visible Light Communication Based Positioning Systems. *Sensors (Switzerland)* **2016**, *16*, doi:10.3390/s16050678.
16. Chaudhary, N.; Alves, L.N.; Ghassemblooy, Z. Current Trends on Visible Light Positioning Techniques. *2019 2nd West Asian Colloquium on Optical Wireless Communications (WACOWC)* **2019**, 100–105, doi:10.1109/wacowc.2019.8770211.
17. Li, D.; Gong, C.; Xu, Z. A RSSI-Based Indoor Visible Light Positioning Approach. *2016 10th International Symposium on Communication Systems, Networks and Digital Signal Processing, CSNDSP 2016* **2016**, 1–6, doi:10.1109/CSNDSP.2016.7574003.

18. Zhuang, Y.; Wang, Q.; Shi, M.; Cao, P.; Qi, L.; Yang, J. Low-Power Centimeter-Level Localization for Indoor Mobile Robots Based on Ensemble Kalman Smoother Using Received Signal Strength. *IEEE Internet of Things Journal* **2019**, *PP*, 1–1, doi:10.1109/JIOT.2019.2907707.
19. Gu, W.; Aminikashani, M.; Deng, P.; Kavehrad, M. Impact of Multipath Reflections on the Performance of Indoor Visible Light Positioning Systems. *Journal of Lightwave Technology* **2016**, *34*, 2578–2587, doi:10.1109/JLT.2016.2541659.
20. Plets, D.; Almadani, Y.; Bastiaens, S.; Ijaz, M.; Martens, L.; Joseph, W. Efficient 3D Trilateration Algorithm for Visible Light Positioning. *J. Opt.* **2019**, *21*, 05LT01, doi:10.1088/2040-8986/ab1389.
21. Heqing Huang, H.H.; Aiying Yang, A.Y.; Lihui Feng, L.F.; Guoqiang Ni, G.N.; and Peng Guo, and P.G. Artificial Neural-Network-Based Visible Light Positioning Algorithm with a Diffuse Optical Channel. *Chinese Optics Letters* **2017**, *15*, 050601–050605, doi:10.3788/col201715.050601.
22. Lin, B.; Guo, Q.; Lin, C.; Tang, X.; Zhou, Z.; Ghassemlooy, Z. Experimental Demonstration of an Indoor Positioning System Based on Artificial Neural Network. *Opt. Eng.* **2019**, *58*, 1, doi:10.1117/1.OE.58.1.016104.
23. Zhang, H.; Cui, J.; Feng, L.; Yang, A.; Lv, H.; Lin, B.; Huang, H. High-Precision Indoor Visible Light Positioning Using Deep Neural Network Based on the Bayesian Regularization With Sparse Training Point. *IEEE Photonics J.* **2019**, *11*, 1–10, doi:10.1109/JPHOT.2019.2912156.
24. Zhang, S.; Du, P.; Chen, C.; Zhong, W.-D.; Alphones, A. Robust 3D Indoor VLP System Based on ANN Using Hybrid RSS/PDOA. *IEEE Access* **2019**, *7*, 47769–47780, doi:10.1109/ACCESS.2019.2909761.
25. Zhang, W.; Kavehrad, M. A 2-D Indoor Localization System Based on Visible Light LED. In Proceedings of the 2012 IEEE Photonics Society Summer Topical Meeting Series; IEEE: Seattle, WA, USA, July 2012; pp. 80–81.
26. Zhou, Z. Indoor Positioning Algorithm Using Light-Emitting Diode Visible Light Communications. *Opt. Eng* **2012**, *51*, 085009, doi:10.1117/1.OE.51.8.085009.
27. Aminikashani, M.; Gu, W.; Kavehrad, M. Indoor Location Estimation with Optical-Based OFDM Communications. *arXiv:1506.07571 [cs, math]* **2015**.
28. Gu, W.; Aminikashani, M.; Deng, P.; Kavehrad, M. Impact of Multipath Reflections on the Performance of Indoor Visible Light Positioning Systems. *J. Lightwave Technol.* **2016**, *34*, 2578–2587, doi:10.1109/JLT.2016.2541659.
29. Chaudhary, N.; Alves, L.N.; Ghassemlooy, Z. Impact of Transmitter Positioning and Orientation Uncertainty on RSS-Based Visible Light Positioning Accuracy. *Sensors* **2021**, *21*, 3044, doi:10.3390/s21093044.
30. Chaudhary, N.; Younus, O.I.; Alves, L.N.; Ghassemlooy, Z.; Zvanovec, S.; Le-Minh, H. An Indoor Visible Light Positioning System Using Tilted LEDs with High Accuracy. *Sensors* **2021**, *21*, 920, doi:10.3390/s21030920.
31. Komine, T.; Nakagawa, M. Fundamental Analysis for Visible-Light Communication System Using LED Lights. *IEEE Transactions on Consumer Electronics* **2004**, *50*, 100–107, doi:10.1109/TCE.2004.1277847.
32. Pandey, O.J.; Sharan, R.; Hegde, R.M. Localization in Wireless Sensor Networks Using Visible Light in Non-Line of Sight Conditions. *Wireless Pers Commun* **2017**, *97*, 6519–6539, doi:10.1007/s11277-017-4853-4.
33. Uysal, M.; Baykas, T.; Jungnickel, V. IEEE 802.11bb Reference Channel Models for Indoor Environments. **2018**, 60.
34. Chaudhary, N.; Alves, L.N.; Ghassemblooy, Z. Feasibility Study of Reverse Trilateration Strategy with a Single Tx for VLP. *2019 2nd West Asian Colloquium on Optical Wireless Communications (WACOWC)* **2019**, 121–126, doi:10.1109/wacowc.2019.8770213.
35. Shawky, S.; El-Shimy, M.A.; El-Sahn, Z.A.; Rizk, M.R.M.; Aly, M.H. Improved VLC-Based Indoor Positioning System Using a Regression Approach with Conventional RSS Techniques. *2017 13th International Wireless Communications and Mobile Computing Conference, IWCMC 2017* **2017**, 904–909, doi:10.1109/IWCMC.2017.7986406.

36. Chaudhary, N.; Alves, L.N.; Ghassemlooy, Z. Impact of Transmitter Positioning Uncertainty on RSS-Based Visible Light Positioning Accuracy. In Proceedings of the 12th IEEE/IET International Symposium on Communication Systems, Networks and Digital Signal Processing- CSNDSP; 2020.
37. Hagan, M.T.; Demuth, H.B.; Beale, and M. *Neural Network Design*; PWS Publishing Co.: USA, 1997;
38. Nwankpa, C.; Ijomah, W.; Gachagan, A.; Marshall, S. Activation Functions: Comparison of Trends in Practice and Research for Deep Learning. *arXiv:1811.03378 [cs]* **2018**.
39. Lera, G.; Pinzolas, M. Neighborhood Based Levenberg-Marquardt Algorithm for Neural Network Training. *IEEE Transactions on Neural Networks* **2002**, *13*, 1200–1203, doi:10.1109/TNN.2002.1031951.
40. Møller, M.F. A Scaled Conjugate Gradient Algorithm for Fast Supervised Learning. *Neural Networks* **1993**, *6*, 525–533, doi:10.1016/S0893-6080(05)80056-5.

Publisher's Note: MDPI stays neutral with regard to jurisdictional claims in published maps and institutional affiliations.

© 2022 by the authors. Submitted for possible open access publication under the terms and conditions of the Creative Commons Attribution (CC BY) license (http://creativecommons.org/licenses/by/4.0/)...

5.6 A Visible Light Positioning System based on Support Vector Machines

This section is a version of the published manuscript:

> **N. Chaudhary**, O. I. Younus, Z. N. Chaleshtori, L. N. Alves, Z. Ghassemlooy, and S. Zvanovec, 'A Visible Light Positioning System based on Support Vector Machines', in *2021 IEEE 32nd Annual International Symposium on Personal, Indoor and Mobile Radio Communications (PIMRC)*, Helsinki, Finland, Sep. 2021, pp. 1–6.

Connection to my Ph.D. thesis:

A new indoor visible light positioning algorithm based on SVM, and polynomial regression was proposed. Two different multipath environments of an empty room and a furnished room were considered. The algorithm started by addressing the received power distance relation, considering polynomial regression models fitted to the specific areas of the room. In the second stage, an SVM was used to classify the best-fitted polynomial, which was used with nonlinear least squares to estimate the position of the receiver. The results showed that, in an empty room, the positioning accuracy improvement for positioning errors of 2.5 cm are 36.1, 58.3, and 72.2 % for three different scenarios according to the regions' distribution in the room. For the furnished room, the positioning accuracy improvement of 214, 170, and 100 % were observed for positioning error of 0.1, 0.2, and 0.3 m, respectively.

2021 IEEE 32nd Annual International Symposium on Personal, Indoor and Mobile Radio Communications (PIMRC) | 978-1-7281-7586-7/21/$31.00 ©2021 IEEE | DOI: 10.1109/PIMRC50174.2021.9569249

A Visible Light Positioning System based on Support Vector Machines

Neha Chaudhary[1], Othman Isam Younus[2], Zahra Nazari Chaleshtori[3], Luis Nero Alves[1], Zabih Ghassemlooy[2], and Stanislav Zvanovec[3]

[1] *Instituto de Telecomunicações and Departamento de Electrónica, Telecomunicações e Informática, Universidade de Aveiro*, 3810-193 Aveiro, Portugal.

[2] *Optical Communications Research Group, Faculty of Engineering and Environment, Northumbria University*, Newcastle upon Tyne NE1 8ST, U.K.

[3] *Department of Electromagnetic Field, Faculty of Electrical Engineering, Czech Technical University in Prague*, Prague 16627, Czech Republic.

Corresponding author: Neha Chaudhary (e-mail: neha.chaudhary@ua.pt)

***Abstract*— In this work, a new indoor visible light positioning algorithm is proposed based on support vector machines (SVM) and polynomial regression. Two different multipath environments of an empty room and a furnished room are considered. The algorithm starts by addressing the received power distance relation, considering polynomial regression models fitted to the specific areas of the room. In the second stage, an SVM is used to classify the best-fitted polynomial, which is used with nonlinear least squares to estimate the position of the receiver. The results show that, in an empty room, the positioning accuracy improvement for the positioning error, ε_p of 2.5 cm are 36.1, 58.3, and 72.2 % for three different scenarios according to the regions' distribution in the room. For the furnished room, a positioning relative accuracy improvement of 214, 170, and 100 % is observed for ε_p of 0.1, 0.2, and 0.3 m, respectively.**

Keywords—VLC, visible light positioning, polynomial regression, SVM, RSS.

I INTRODUCTION

Indoor positioning system (IPS) with high precision and low cost has become one of the most exciting features of next-generation indoor optical wireless communication systems [1]. A number of potential applications include object tracking or human tracking, industrial manufacturing, and robot control and navigation [2], [3]. Several technologies have been exploited for IPS purposes, for instance, Wi-Fi [4], ultrasound [5], radio frequency identification [6], ultra-wideband [7], Bluetooth [8], amongst others. The radio frequency (RF)-based approaches suffer from the influence of reflections, which may severely affect positioning accuracy (PA) [3]. Besides them, visible light positioning (VLP) acquires special attention due to the advantages introduced by the light-emitting diodes (LEDs), i.e., low-cost, ubiquitous in living infrastructures, longer lifetimes, and energy efficiency [9], [10]. In VLP systems, LEDs are used as a transmitter (Tx) beacon. The receivers (Rxs) may come with different varieties, either using photodiodes (PDs) or image sensors (IS) [11], [12]. Different algorithms have been utilized for estimating location, such as, received signal strength (RSS), time of arrival, angle of arrival, amongst others [13]–[15]. Amongst these algorithms, RSS is typically used in VLP, where a PD is utilized to measure the strength of the received information from multiple LEDs. After that, the position is estimated based on the trilateration or the triangulation approaches, where the intersection of multiple circles is obtained based on the inferred distance between the Rx and the Txs [16], [17].

Recently, the use of machine learning in RSS-based VLP systems has been explored in [18]. The authors proposed the usage of K-Means clustering algorithm to achieve a 0.31 m of PA for a room of dimension 4.3×4×4 m^3. Moreover, a PA of 3.65 cm along with a height tolerance of 15 cm was achieved using a backpropagation algorithm -for an indoor VLP system in [19]. Additionally, an innovative solution was proposed for indoor positioning based on the dual-function machine learning algorithms that contain machine learning classification and machine learning regression functions. in [20]. Classification algorithms, such as, random forest and support vector machines (SVM) were used for obtaining the highest PA of 8.6 and 10.2 cm, respectively. The results showed that, SVM is the optimal solution for VLP systems with a low positioning error ε_p.

The previous works focused mainly on a simple line of sight (LoS) channel model, making it straightforward to estimate the received optical power P_r as a function of the distance d. The influence of non-line of sight (NLoS) paths in a VLC system implemented in a referenced empty room has been described in the literature. For instance, in [21], the impact of multipath reflections on the indoor VLP system was studied. The results proved that, the minimum ε_p achieved were 46.4 and 0.4 cm with and without multipath reflections, respectively. Therefore, reflections play an important role in estimating the PA, which needs considering. Estimating the received power versus the distance for the case of a multipath channel is a complex task, which depends strongly on the presence of corners, walls, and furniture within a room [21]. A new VLP system was proposed in [22], where a polynomial regression-based approach was utilized to improve the PA of the proposed system. Polynomial regression appears as a method to establish the relation between P_r and d, suitable for multipath environments. The results showed that, the minimum ε_p achieved was 0.6 m by employing a nonlinear least square (NLLS) with the polynomial regression model. Another VLP system was introduced in [23], where the LEDs

978-1-7281-7586-7/21/$31.00 ©2021 IEEE

Authorized licensed use limited to: b-on: UNIVERSIDADE DE AVEIRO. Downloaded on February 17,2022 at 21:40:18 UTC from IEEE Xplore. Restrictions apply.

were tilted towards the center of the room, thus resulting in higher PA. The same polynomial regression approach was used along with a low complexity linear least squares (LLS) method, which showed a PA improvement of ~66%. In addition, by changing the polynomial fitting depending on the regions (i.e., inner region or the entire space) of the room, the PA was further enhanced. These results suggest that, the accuracy of the polynomial regression model depends on the specific area within the room.

In this work, a new indoor VLP system is proposed based on the polynomial regression and SVM. Two different environments are considered an empty room and a furnished room, where multipath channels are considered and estimated using OpticStudio® software. In both environments, the total room area is divided into different regions, such as, corners, the middle area of the room, regions near the walls, or depending on furniture layout, thus creating four different scenarios. At a second stage, polynomial fitting is carried out for these different regions and the position is estimated for the entire room using the polynomial regression approach. Finally, SVM is employed to perform the classification and select the best region based on the lowest ε_p.

The rest of the paper is organized as follows, Section II presents the system set-up for both empty room and furnished room environments and the computed received power in detail. The polynomial fitting, positioning algorithm, and SVM are explained in Section III. Results and discussion are done in Section IV, followed by the final concluding remarks in Section V.

II VLP System Modelling

In this work, two different environments are considered, i.e., empty room and furnished room. In both environments, the proposed VLP system consists of several LEDs as the Txs, and a single PD-based Rx. All Txs are installed at the same height h_k from the ground level. The coordinates of k^{th} Tx (k = 1, …, K) is (x_k, y_k, z_k), where K is the total number of Txs. While the Rx with the coordinate (x_r, y_r, z_r) is placed at h_r above the ground level. The system is modelled by employing a non-sequential ray-tracing feature of OpticStudio® for estimating P_r at the Rx and the path lengths in a complex 3D environment. Then, the channel characteristics are processed using Matlab® for the position estimation. In the case of an empty room environment, a referenced empty room is considered to analyze the performance of the system. In the case of a furnished room, a usual office room is considered with several furniture and static users inside the room. The dimensions of both empty and furnished rooms are identical, i.e., 6 × 6 × 3 m^3. Fig. 1 depicts both empty and furnished room environments.

Each Tx broadcast a unique 2-bit ID information that is encoded and in the on-off keying (OOK) format, which arrives at the Rx before the location identification, thus allowing separation at the Rx using a correlation method [22]. $P_{r,k}$ at the Rx from the k^{th} Tx will be a combination of power from both LoS and NLoS paths and can be expressed as:

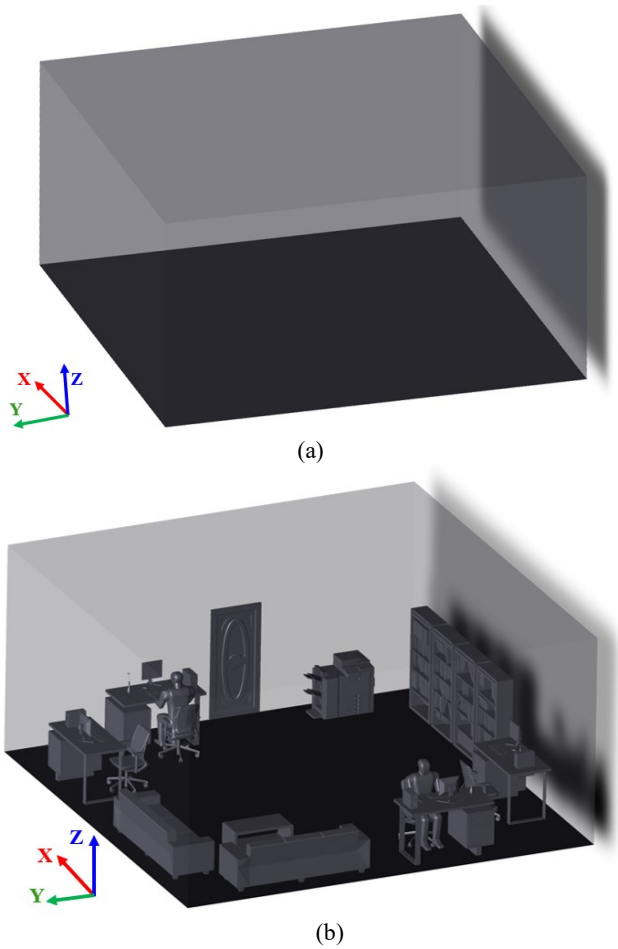

Fig. 1. System configuration for: (a) empty room, and (b) furnished room.

$$P_{r,k} = \sum P_{r,k(\text{LoS})} + \sum P_{r,k(\text{NLoS})}, \quad (1)$$

where $P_{r,k(\text{LoS})}$ and $P_{r,k(\text{NLoS})}$ represents the received power for LoS and NLoS at the k^{th} Tx, respectively. The values of $P_{r,k}$ are computed using OpticStudio®.

III VLP Algorithm

In our work, the position estimation of the Rx includes three major stages (*i*) the receiving plane of the entire room is distributed into different regions, and the data from $P_{r,k}$ is used for polynomial fitting. A polynomial model is inferred based on P_r and d; (*ii*) these polynomial models are used to estimate the position for the entire room by using RSS algorithm; and (*iii*) SVM is employed for classification, to obtain the solution with the minimum ε_p. The major stages are explained in more detail next subsections.

3.1 RSS polynomial model

For the polynomial fitting, firstly the room is divided into different regions, where d_k and $P_{r,k}$ are computed. The shape and the area of each region needs to be selected prior to the system deployment. After that, a polynomial regression method is used for polynomial fitting for each region. This allows inferring a polynomial dependent on different parts of the room. The room division strategy considers the influence

Authorized licensed use limited to: b-on: UNIVERSIDADE DE AVEIRO. Downloaded on February 17,2022 at 21:40:18 UTC from IEEE Xplore. Restrictions apply.

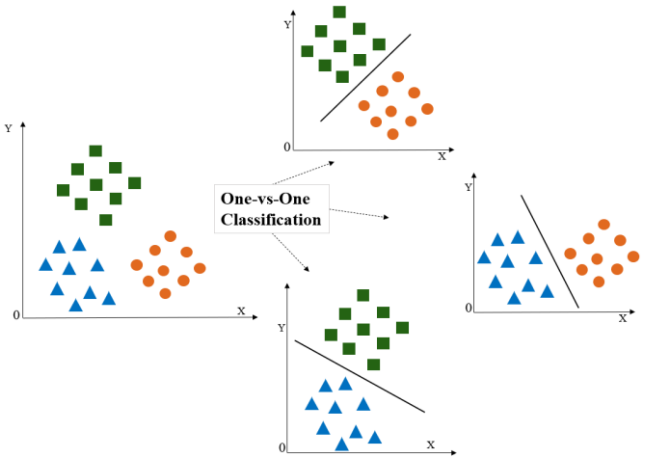

Fig. 2. The schematic diagram of one-vs-one multiclass SVM.

of reflection on P_r, as such, the areas near the corners or walls should have polynomial models different from the areas at the center of the room, where the impact of reflections is much less. The polynomial model is given by:

$$d_k = \alpha_0 + \alpha_1 P_{r,k} + \alpha_2 \left(P_{r,k}\right)^2 + \cdots + \alpha_s \left(P_{r,k}\right)^s, \quad (2)$$

where $\alpha_0 \ldots \alpha_s$ represent the coefficients of the fitted polynomial obtained using the linear least-squares method.

The next step consists of converting d_k computed with (2) in the distance projection in the horizontal plane. The horizontal distance from k^{th} Tx to the Rx r_k is given by:

$$\|r_k\|^2 = \|d_k\|^2 - h^2 , \quad (3)$$

where h is the vertical distance between k^{th} Tx and the Rx. Note, the value of h for all Txs is the same in this work since all the Txs are placed at the same height from the ground. The next step is to employ NLLS estimation method.

3.2 Nonlinear least square estimation

In this work, the target location is estimated using the NLLS approximation, in which the estimated solution is achieved with $\tilde{X} = [\tilde{x}, \tilde{y}]$, which minimizes the cost function represented as:

$$\tilde{Q} = \sum_i \left(\sqrt{(x_r - x_k)^2 + (y_r - y_k)^2} - r_k\right)^2. \quad (4)$$

The value of $\tilde{X}$ is estimated iteratively by employing the LLS and trust-region reflective algorithm [24]. Primarily, the value of $\tilde{X}_0$ is initiated from LLS, followed by computing the corresponding $\tilde{Q}_0$. Then, the consecutive points in the neighborhood of $\tilde{X}_0$ are replaced in (4), and where the value the minimum $\tilde{Q}_1$ is achieved the corresponding value of $\tilde{X}_1$ is selected. The coordinates of the Rx represented by $\tilde{X}$ will eventually be obtained with several iterative steps to ensure convergence of $\tilde{Q}$.

3.3 Support vector machines

SVM is a supervised machine learning algorithm utilized for solving classification and regression problems. SVM classifies data by achieving the best hyperplane that distinguishes all data points of one class from those of another class. The best hyperplane is the one with the largest margin between two (different) classes. Although SVMs were originally developed for binary class classification, they can be extended to multiclass classification. The multiclass problem is split into multiple binary classification cases, also known as one-vs-one classification, as depicted in Fig. 2.

TABLE I. SYSTEM PARAMETERS

Room size	
Empty room	6× 6× 3 m^3
Furnished room	6× 6× 3 m^3
Tx and Rx	
Number of LED-based Txs K	4
Transmitters x_k, y_k locations in meter	(1.5, 1.5), (1.5, 4.5), (4.5, 1.5), and (4.5, 4.5).
Tx model [28]	Cree Xlamp MC-E
LED-based optical power	11 W
Beam angle-based Tx	120°
PD Rx dimension	1 cm^2
PD field of view (FOV)	85°
Reflection specification	
Type of reflections	Purely diffuse [25]
Number of reflections	3
Material reflectance	Wavelength-dependent [26]
Wall coating material	Plaster [26]
Number of rays	10^4
Scatter fraction	1
Chair, sofa	Leather [25]
Human clothes	Cotton [25]
Plant	Plant [25]
Desk, bookshelf, book	Pinewood [25]
PC, printer	Black gloss paint [25]

In one-vs-one classification, a series of classifiers are employed to each pair of classes, with the most frequent class identifier [27]. SVMs also need the training of different classifiers using the data from each pair of classes. The number of classifiers N_c required for one-vs-one multiclass classification can be retrieved by [27]:

$$N_c = \frac{\eta \times (\eta - 1)}{2}, \quad (5)$$

where η represents the number of classes. In this work, the SVM is used to classify the minimum ε_p based on different regions, so the number of classes is given by the number of regions.

For non-linear problems, the training data is not linearly separable in the original input space. Therefore, mapping of the original input space into a high-dimensional space is done using a concept called kernel trick [27]. In this algorithm, N training samples are considered. Each sample is indicated by (u_i, p_i), where u_i corresponds to the attribute set for the i^{th} sample (i = 1, 2, …, N), and p_i correspond to the i^{th} label. The SVM classifier can be defined as:

$$f(u) = \sum_{i,j=1}^{N} \alpha_i p_i G\left(u_i, u_j\right) + b, \quad (6)$$

where α_i is Lagrange multiplier, and b is the bias term. $G\left(u_i, u_j\right)$ is the kernel function, and u_j is any data point in the

Authorized licensed use limited to: b-on: UNIVERSIDADE DE AVEIRO. Downloaded on February 17,2022 at 21:40:18 UTC from IEEE Xplore. Restrictions apply.

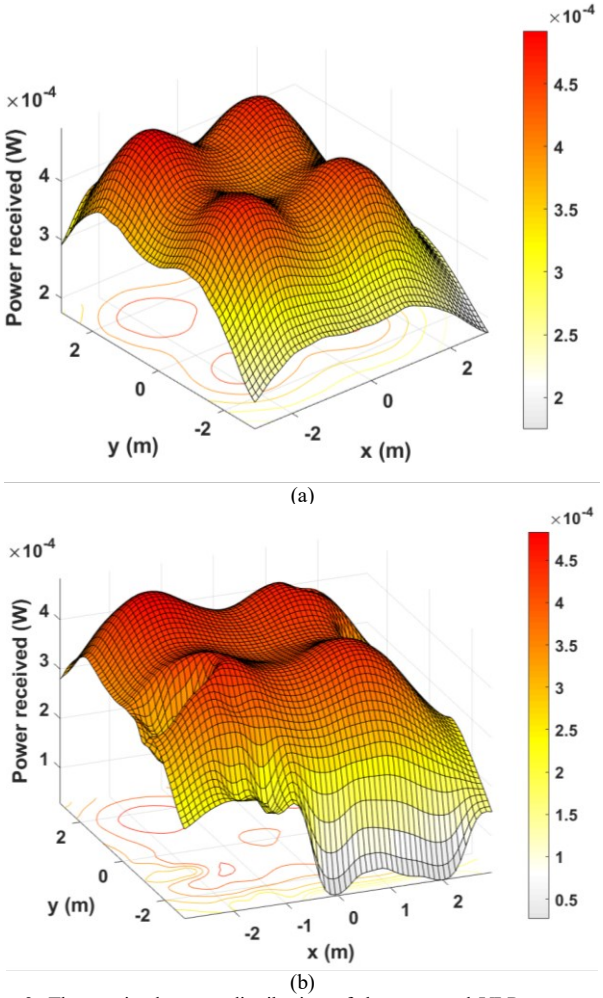

Fig. 3. The received power distribution of the proposed VLP system: (a) empty room, and (b) furnished room.

sample. In this work, the polynomial kernel is used, which is given by:

$$G(u_i, u_j) = (u_i^{\mathrm{T}}.u_j + c)^d, \quad (7)$$

where c is the constant, T represents the transpose, and d is the degree of the polynomial [27]. Lagrange multipliers are obtained using the convex quadratic optimization algorithms [24].

IV. Results and Discussion

4.1 System setup

The simulation setup is composed of two different environments i.e., a referenced empty room and a furnished room. Four Txs are symmetrically placed on the ceiling at the height h_k of 3 m while the Rx is placed at the height h_r of 0.8 m above the ground level. The modelling of the proposed system is done based on the specifications of the Txs and the Rx, the characteristics of CAD models of each object within the environment, the type of surface material (wall, floor, ceiling, and objects where the value of reflectance is wavelength-dependent), and the number of emitted rays [28]. All other system parameters are provided in Table I.

The Txs are assumed to be Lambertian radiators with Lambertian order of 1, and optical power of each Tx is 11 W.

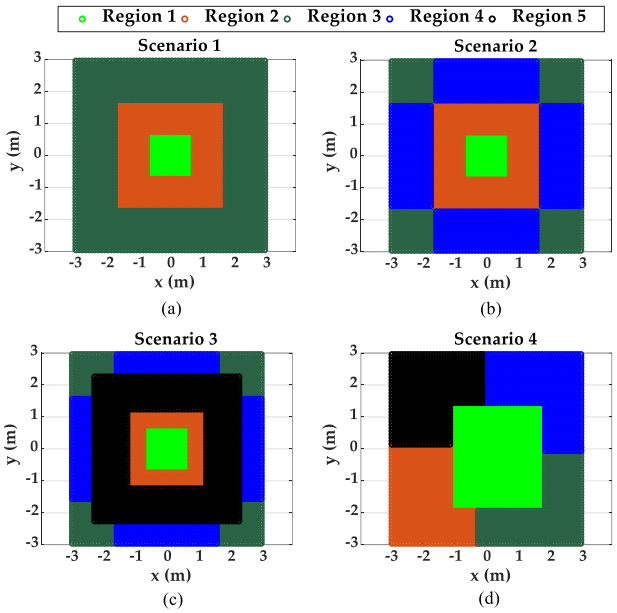

Fig. 4. Different scenarios according to the regions: (a) Scenario 1 for empty room with 3 regions, (b) Scenario 2 for empty room with 4 regions, (c) Scenario 3 for empty room with 5 regions, and (d) Scenario 4 for a furnished room with 5 regions.

The Rx's field of view (FOV) is 85°. A grid of 1 cm resolution is considered on the receiving plane, which includes 3600 Rx's positions. The cubic SVM algorithm is used in this work, where 3600 samples are considered for training the network. To prevent overfitting, a cross-validation process is applied to the SVM algorithm, in which the data set is partitioned into 5 folds and the accuracy is measured for each fold.

4.2 Power distribution for both environments

The distribution of received power for both empty room and furnished room environment are shown in Fig. 3. In the case of an empty room, the received power is uniformly distributed around the center of the receiving plane, being lower at the corners and the area near the walls due to the reflections, see Fig. 3(a). In the case of furnished room, P_r is lower for the regions with furniture due to the presence of thereflections from objects, walls, and other furniture. Moreover, P_r is minimum near the bookshelf as can be seen in Fig. 3(b) (please refer to Fig 1(b) for comparison).

4.3 Simulated scenarios for both environments

The receiving plane is divided into different regions and different scenarios are made for both empty and furnished rooms. The four different scenarios are illustrated in Fig. 4. Scenarios 1, 2, and 3 consider the empty room, while scenario 4 is for the furnished room.

In scenario 1, the first region is the area near the centre of the room, where P_r is more uniform. The second region is the area between the center of the receiving plane and the area near the walls of the room. The third region is the area near the walls of the room as depicted in Fig. 4(a). While in scenario 2, the third region includes only the corners of the room, where the multipath reflections will be high and the fourth region includes the area near the walls except the corners, see Fig. 4(b). In case of scenario 3, the fifth region is the area of the receiving plane just below the LEDs as shown in Fig. 4(c). On

Authorized licensed use limited to: b-on: UNIVERSIDADE DE AVEIRO. Downloaded on February 17,2022 at 21:40:18 UTC from IEEE Xplore. Restrictions apply.

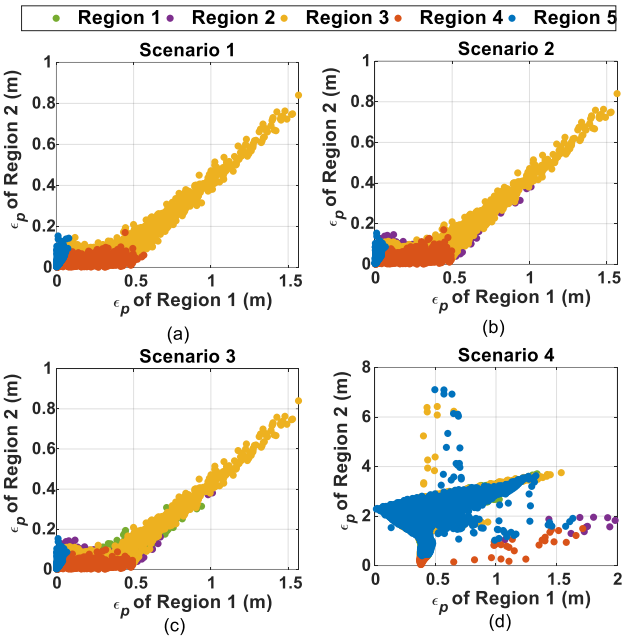

Fig. 5. Data used for: (a) Scenario 1 for empty room with 3 regions, (b) Scenario 2 for empty room with 4 regions, (c) Scenario 3 for empty room with 5 regions, and (d) Scenario 4 for furnished room with 5 regions.

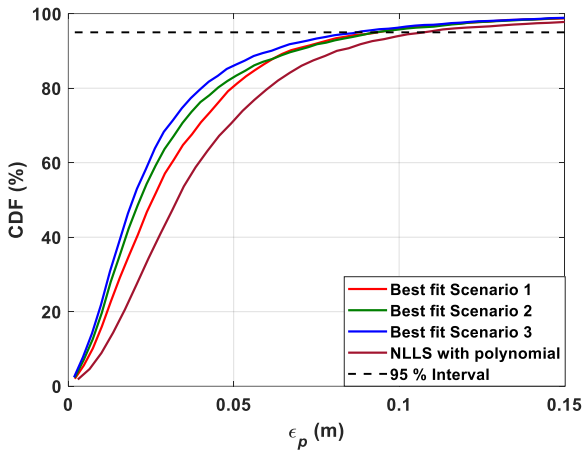

Fig. 6. Comparison of SVM with different scenarios and normal NLLS with polynomial for empty room environment.

the other hand, for the room with furniture, the regions are considered according to the distribution of furniture as presented in Fig. 4(d). Note, region 1 is the empty area of the furnished room, see Fig. 1(b).

After estimating ε_p for each scenario based on different regions, SVM is used for classification to obtain the lowest ε_p based on the errors attained from each region. Fig. 5 depicts data scatter plots showing how data (ε_p in different regions) spreads for different regions (clustered data can be adequately classified, while spread data can represent classification challenges). Fig. 5(a, b, and c) shows the data used for training the SVM for an empty room. For instance, Fig. 5(a) shows three different colour of data which represents three different regions and used as three different classes. Similarly, Fig. 5(b, and c) also represents the data of scenario 2 and scenario 3 with 4 and 5 classes which will be used for classification. We can also observe from Fig. 5(d), that the data is more dispersed

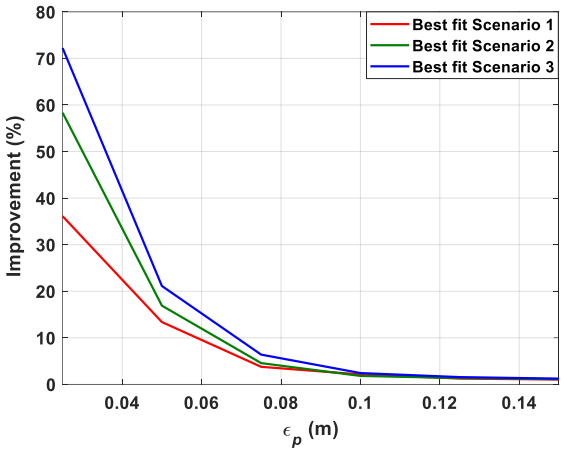

Fig. 7. Improvement of VLP system with different scenarios for empty room environment.

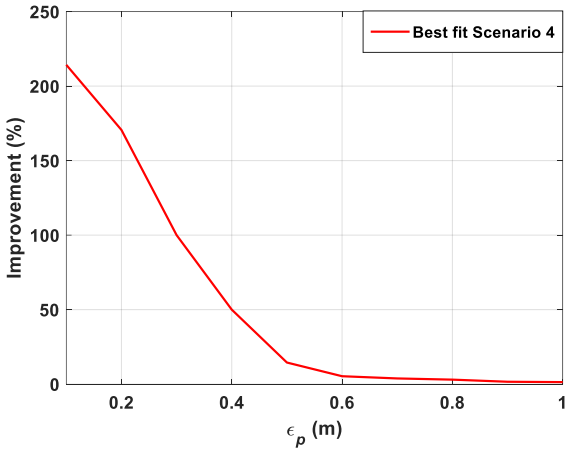

Fig. 8. Improvement of VLP system with different scenarios for furnished room environment.

in a furnished room due to the reflections from objects and furniture.

4.4 Positioning error performance of VLP

Fig. 6 depicts the CDF plots for the empty room, where ε_p of different scenarios is obtained by means of SVM and the NLLS with the polynomial fitting using the data points of the entire room. We have selected a 95% confidence interval for ε_p to include the majority of the measured points to ensure a VLP link with high reliability. As can be seen from Fig. 6, scenario 3 displays the best profile for the entire room. At the 95% interval limit, ε_p values are 9, 9, 8, and 11 cm for scenarios 1, 2, 3, and NLLS with polynomial, respectively.

Next, we measured the improvement of PA by using SVM with relation to the NLLS for the different scenarios. Fig. 7 illustrates the improvement of the VLP system for scenarios 1-3 for an empty room. We can see that, the best PA is achieved in scenario 3. It was revealed that, the PA improvement for ε_p of 2.5 cm are 36.1, 58.3, and 72.2 % for scenario 1, 2, and 3, respectively. Whereas the improvement of 13.3, 16.9, and 21.1 % are observed for ε_p of 5 cm for scenario 1, 2, and 3, respectively. Similarly, Fig. 8 depicts the accuracy improvement of a furnished room for a range of ε_p, higher accuracy improvement is achieved at lower values of ε_p i.e., < 0.4 m. Although the improvement in the furnished

Authorized licensed use limited to: b-on: UNIVERSIDADE DE AVEIRO. Downloaded on February 17,2022 at 21:40:18 UTC from IEEE Xplore. Restrictions apply.

case is high, the achieved precision is very low (i.e, higher ε_p). The reason for the high error in this scenario, is the presence of the reflections from objects, walls, and other furniture, as well as the failure to find suitable polynomial models for regions near the furniture.

V. Conclusions

This paper proposed a new indoor VLP system based on the polynomial regression and SVM. Achieved results showed that, the use of SVM allows for an accurate classification of the polynomial model, hence, improving the accuracy of the system. Tests done in a furnished environment revealed that, the presence of furniture makes the task of inferring suitable polynomial models difficult and conditions the overall accuracy of the system. Nevertheless, due to the simplicity of the approach and its feasibility for implementation, the proposed methods seem suitable for applications demanding coarse positioning accuracies, such as positioning in large shopping areas.

Acknowledgment

This work is supported by the European Union's Horizon 2020 research and innovation programme under the Marie Sklodowska-Curie grant agreement no. 764461 (VisIoN). It is also supported by Northumbria University Ph.D. Scholarship, and CTU project SGS20/166/OHK3/3T/13. It is also based upon work from COST Action CA19111 NEWFOCUS, supported by COST (European Cooperation in Science and Technology).

References

[1] J. Armstrong, Y. Sekercioglu, and A. Neild, 'Visible light positioning: a roadmap for international standardization', *IEEE Commun. Mag.*, vol. 51, no. 12, pp. 68–73, Dec. 2013.

[2] N. Chaudhary, L. N. Alves, and Z. Ghassemblooy, 'Current Trends on Visible Light Positioning Techniques', in *2019 2nd West Asian Colloquium on Optical Wireless Communications (WACOWC)*, Tehran, Iran, Apr. 2019, pp. 100–105.

[3] T.-H. Do and M. Yoo, 'An in-Depth Survey of Visible Light Communication Based Positioning Systems', *Sensors*, vol. 16, no. 5, p. 678, May 2016, doi: 10.3390/s16050678.

[4] A. Poulose, J. Kim, and D. S. Han, 'A Sensor Fusion Framework for Indoor Localization Using Smartphone Sensors and Wi-Fi RSSI Measurements', *Applied Sciences*, vol. 9, no. 20, p. 4379, Oct. 2019.

[5] J. Rabadan, V. Guerra, R. Rodríguez, J. Rufo, M. Luna-Rivera, and R. Perez-Jimenez, 'Hybrid Visible Light and Ultrasound-Based Sensor for Distance Estimation', *Sensors*, vol. 17, no. 2, p. 330, Feb. 2017, doi: 10.3390/s17020330.

[6] H. Zou, L. Xie, Q.-S. Jia, and H. Wang, 'Platform and Algorithm Development for a RFID-Based Indoor Positioning System', *Un. Sys.*, vol. 02, no. 03, pp. 279–291, Jul. 2014, doi: 10.1142/S2301385014400068.

[7] M. J. Kuhn, J. Turnmire, M. R. Mahfouz, and A. E. Fathy, 'Adaptive leading-edge detection in UWB indoor localization', in *2010 IEEE Radio and Wireless Symposium (RWS)*, New Orleans, LA, USA, Jan. 2010, pp. 268–271. doi: 10.1109/RWS.2010.5434259.

[8] Y. Zhuang, J. Yang, Y. Li, L. Qi, and N. El-Sheimy, 'Smartphone-Based Indoor Localization with Bluetooth Low Energy Beacons', *Sensors*, vol. 16, no. 5, p. 596, Apr. 2016, doi: 10.3390/s16050596.

[9] Y. Zhuang *et al.*, 'A Survey of Positioning Systems Using Visible LED Lights', *IEEE Commun. Surv. Tutorials*, vol. 20, no. 3, pp. 1963–1988, 2018, doi: 10.1109/COMST.2018.2806558.

[10] J. Luo, L. Fan, and H. Li, 'Indoor Positioning Systems Based on Visible Light Communication: State of the Art', *IEEE Commun. Surv. Tutorials*, vol. 19, no. 4, pp. 2871–2893, 2017, doi: 10.1109/COMST.2017.2743228.

[11] N. Chaudhary, L. N. Alves, and Z. Ghassemblooy, 'Feasibility Study of Reverse Trilateration Strategy with a Single Tx for VLP', in *2019 2nd West Asian Colloquium on Optical Wireless Communications (WACOWC)*, Tehran, Iran, Apr. 2019, pp. 121–126. doi: 10.1109/WACOWC.2019.8770213.

[12] S. Zhang, P. Du, C. Chen, and W.-D. Zhong, '3D Indoor Visible Light Positioning System using RSS ratio with Neural Network', in *2018 23rd Opto-Electronics and Communications Conference (OECC)*, Jeju Island, Korea (South), Jul. 2018, pp. 1–2. doi: 10.1109/OECC.2018.8729887.

[13] R. Zhang, W.-D. Zhong, K. Qian, and D. Wu, 'Image Sensor Based Visible Light Positioning System with Improved Positioning Algorithm', *IEEE Access*, pp. 1–1, 2017, doi: 10.1109/ACCESS.2017.2693299.

[14] B. Lin, Q. Guo, C. Lin, X. Tang, Z. Zhou, and Z. Ghassemlooy, 'Experimental demonstration of an indoor positioning system based on artificial neural network', *Opt. Eng.*, vol. 58, no. 01, p. 1, Jan. 2019, doi: 10.1117/1.OE.58.1.016104.

[15] S.-H. Yang, H.-S. Kim, Y.-H. Son, and S.-K. Han, 'Three-Dimensional Visible Light Indoor Localization Using AOA and RSS With Multiple Optical Receivers', *J. Lightwave Technol.*, vol. 32, no. 14, pp. 2480–2485, Jul. 2014, doi: 10.1109/JLT.2014.2327623.

[16] A.-C. Anastou, K. K. Delibasis, A.-A. A. Boulogeorgos, H. G. Sandalidis, A. Vavoulas, and S. K. Tasoulis, 'A Low Complexity Indoor Visible Light Positioning Method', vol. 9, p. 16, 2021.

[17] N. Chaudhary, L. N. Alves, and Z. Ghassemlooy, 'Impact of Transmitter Positioning Uncertainty on RSS-based Visible Light Positioning Accuracy', in *2020 12th International Symposium on Communication Systems, Networks and Digital Signal Processing (CSNDSP)*, Porto, Portugal, Jul. 2020, pp. 1–6.

[18] M. Saadi, T. Ahmad, Y. Zhao, and L. Wuttisttikulkij, 'An LED Based Indoor Localization System Using k-Means Clustering', in *2016 15th IEEE International Conference on Machine Learning and Applications (ICMLA)*, Anaheim, CA, USA, Dec. 2016, pp. 246–252. doi: 10.1109/ICMLA.2016.0048.

[19] C.-W. Hsu, S. Liu, F. Lu, C.-W. Chow, C.-H. Yeh, and G.-K. Chang, 'Accurate Indoor Visible Light Positioning System utilizing Machine Learning Technique with Height Tolerance', in *Optical Fiber Communication Conference*, San Diego, California, 2018, p. M2K.2. doi: 10.1364/OFC.2018.M2K.2.

[20] H. Tran and C. Ha, 'Improved Visible Light-Based Indoor Positioning System Using Machine Learning Classification and Regression', *Applied Sciences*, vol. 9, no. 6, p. 1048, Mar. 2019.

[21] W. Gu, M. Aminikashani, P. Deng, and M. Kavehrad, 'Impact of Multipath Reflections on the Performance of Indoor Visible Light Positioning Systems', *J. Lightwave Technol.*, vol. 34, no. 10, pp. 2578–2587, May 2016, doi: 10.1109/JLT.2016.2541659.

[22] N. Chaudhary, L. N. Alves, and Z. Ghassemlooy, 'Impact of Transmitter Positioning and Orientation Uncertainty on RSS-Based Visible Light Positioning Accuracy', *Sensors*, vol. 21, no. 9, p. 3044, Apr. 2021, doi: 10.3390/s21093044.

[23] N. Chaudhary, O. I. Younus, L. N. Alves, Z. Ghassemlooy, S. Zvanovec, and H. Le-Minh, 'An Indoor Visible Light Positioning System Using Tilted LEDs with High Accuracy', *Sensors*, vol. 21, no. 3, p. 920, Jan. 2021, doi: 10.3390/s21030920.

[24] W. Shiquan and W. Fang, 'Computation of a trust region step', *Acta Mathematicae Applicatae Sinica*, no. 7, pp. 354–362, Oct. 1991, doi: 10.1007/BF02009686.

[25] Z. Nazari Chaleshtori, Z. Ghassemlooy, H. B. Eldeeb, M. Uysal, and S. Zvanovec, 'Utilization of an OLED-Based VLC System in Office, Corridor, and Semi-Open Corridor Environments', *Sensors*, vol. 20, no. 23, p. 6869, Dec. 2020, doi: 10.3390/s20236869.

[26] F. Miramirkhani and M. Uysal, 'Channel Modeling and Characterization for Visible Light Communications', *IEEE Photonics J.*, vol. 7, no. 6, pp. 1–16, Dec. 2015, doi: 10.1109/JPHOT.2015.2504238.

[27] 'Chamasemani and Singh - 2011 - Multi-class Support Vector Machine (SVM) Classifie.pdf'.

[28] M. Uysal, T. Baykas, and V. Jungnickel, 'IEEE 802.11bb Reference Channel Models for Indoor Environments', p. 60, 2018.

Authorized licensed use limited to: b-on: UNIVERSIDADE DE AVEIRO. Downloaded on February 17,2022 at 21:40:18 UTC from IEEE Xplore. Restrictions apply.

5.7 A Convolutional Neural Network-based Visible Light Positioning System using Rolling Shutter Cameras

This section is a version of the submitted manuscript:

> **N. Chaudhary**, C. J. Verdu, P. Fonseca, L. N. Alves, R. P. Jimenez, and Z. Ghassemlooy, 'A Convolutional Neural Network-based Visible Light Positioning System using Rolling Shutter Cameras', Optics Express, submitted.

Connection to my Ph.D. thesis:

A new visible light positioning system based on CNN was proposed in which LEDs were used as transmitters and a rolling shutter camera is used as receiver. A detection algorithm named SSD was used which relies on CNN (i.e, MobileNet or ResNet) for classification as well as position estimation of each LED in the image. Additionally, a PnP problem algorithm was employed to estimate the receiver position. The system was validated using a real-world size test setup containing eight LED luminaries. The obtained results showed that the maximum average root mean square positioning error achieved is 4.67 and 5.27 cm with SSD MobileNet and SSD ResNet models, respectively. The validation results show that the system can process 67 images per second, allowing real-time positioning.

A Convolutional Neural Network-based Visible Light Positioning System using a Rolling Shutter Camera

Neha Chaudhary,[1,*] Cristo Jurado-Verdu,[2] Pedro Fonseca,[1] Luis Nero Alves,[1] Rafael Perez-Jimenez,[2] and Zabih Ghassemlooy,[3]

[1] *Instituto de Telecomunicações and Departamento de Electrónica, Telecomunicações e Informática, Universidade de Aveiro, 3810-193 Aveiro, Portugal*

[2] *Institute for Technological Development and Innovation in Communications (IDeTIC), Universidad de Las Palmas de Gran Canaria (ULPGC), 35017 Las Palmas de Gran Canaria, Canary Islands, Spain*

[3] *Optical Communications Research Group, Faculty of Engineering and Environment, Northumbria University, Newcastle upon Tyne NE1 8ST, UK.*

**neha.chaudhary@ua.pt*

Abstract: In this work, we propose a new visible light positioning system-based on convolutional neural networks (CNN) in which light-emitting diodes (LEDs) are used as transmitters and a rolling shutter camera is used as the receiver. A detection algorithm named single shot detector (SSD) is used, which relies on CNN (i.e, MobileNet or ResNet) for classification as well as position estimation of each LED in the image. Additionally, a perspective-n-point problem algorithm is employed to estimate the receiver's position. The system is validated using a real-world size test setup containing eight LED luminaries. The obtained results show that the maximum average root mean square positioning errors achieved are 4.67 and 5.27 cm with SSD MobileNet and SSD ResNet models, respectively. The validation results show that the system can process 67 images per second, allowing real-time positioning.

© 2022 Optical Society of America under the terms of the OSA Open Access Publishing Agreement

I. Introduction

Indoor positioning systems (IPSs) have gained increasing attention from the academic and industrial communities with numerous applications, including pedestrian navigation, asset tracking, and autonomous robot guidance [1]. IPS has already generated revenues of USD 6.54 billion in 2020 and has a target to hit USD 35.65 Billion by 2028 [2]. Moreover, the IPS are used widely in smart factories to improve efficiency. For instance, intelligent transport vehicles are necessary to navigate through their environments and avoid collisions. A precise positioning plays a key role in promoting industrial automation. Despite the fact that a Global positioning system (GPS) provides exceptional performance in outdoor localization, it is unreliable for indoor localizations due to signal attenuation or signal blockage, and multipath issues [3], therefore, the need for indoor localization services is increasing.

In recent years, various IPS solutions, such as, WiFi-based, infrared, and Ultra-Wideband (UWB) have been developed [1], [4], [5]. The visible light positioning (VLP) technology is another promising technique that can be considered an alternative or integrated technology to radio waves, in which the pre-existing LED infrastructure is used as transmitter (Tx) beacons to provide illumination and communication simultaneously [6]. In addition to offering high bandwidth, high security, high-speed data transmission, and low implementation costs, LEDs are also energy-efficient and provide long service life [6], [7].

There are two major types of VLP devices based on the type of detector used at the receiver (Rx) side: photodiode (PD) [8], [9] and image sensor (IS) [10], [11]. For mobile terminals, PDs do not provide an ideal positioning device. The primary reason is that PD-based positioning will result in large errors due to the angle measurement, variation in light intensity, and received

signal strength measurement. Furthermore, the positioning accuracy is compromised by diffuse reflections of the light signal. Alternatively, IS-based VLP is better suited for navigating within indoor environments. In addition, IS-based VLP can easily be implemented or integrated with the current mobile terminals and mobile devices due to the widely used complementary metal-oxide semiconductor (CMOS) sensor cameras [10].

The recent advances in VLP include the deployment of artificial neural networks (ANNs). For instance, in [12], both received signal strength (RSS) and ANN methods were proposed to achieve an accurate indoor VLP system in a diffuse optical channel. An accuracy of 6.39 cm was achieved with the averaged positioning error ε_p being ~13 times smaller than RSS-based positioning systems. In addition, a low-cost indoor VLP system was proposed using a backpropagation algorithm in [13], in which ε_p of 3.65 cm was achieved with a height tolerance of 15 cm.

Another prominent technology, i.e., deep learning (DL) is a subfield of machine learning approach that outperforms traditional methods in a wide range of applications and has been extensively employed in estimating position [14]. For instance, in [15], supervised learning was used to train the angle of arrival information from the training locations using a deep convolutional neural network (CNN). In [16], two multilayer perceptron (MLP) and CNN based deep ANN models were used for efficient mapping of the instantaneous received signal to noise ratio (SNR) with the user three-dimensional (3D) position and user equipment (UE) orientation for joint estimation of user 3D position and orientation of UE with unknown emission power. The results revealed that the average ε_p were 10.53 and 13.04 cm for CNN and MLP, respectively. [17] describes a new VLP indoor localization technique based on a CNN-based algorithm with handover probability analysis. The algorithm was categorized into two modes: offline and online. Firstly, the algorithm was trained utilizing a dataset of received VLC signal and data generated from the smart device in the offline mode. Secondly, users assessed their position in the online mode based on the received VLC signal. The simulation results revealed that the average ε_p achieved was 4.31 cm for the proposed algorithm.

In this paper, we propose a new indoor VLP system based on CNN and optical camera communication (OCC). A single shot detector (SSD) algorithm is used, which relies on CNN (i.e., MobileNet or ResNet) for classification as well as position estimation of each LED in the image. Firstly, the LEDs are intensity modulated with on-off keying (OOK) with a unique symbol period to ease their recognition. A dataset is created in which images are acquired by a CMOS camera and the classification and position of each visible LED in that image are labeled. The SSD model is trained by using the dataset, and object detection is done. Finally, the Rx position is estimated by using the pinhole camera model concept where three OpenCV algorithms are employed.

The rest of this paper is organized as follows. The proposed system model is detailed in section II. In section III, a detailed explanation of SSD is given and the process of generation of the dataset is described. Finally, Section IV presents the experiment setup and results of the proposed system, followed by the conclusion.

II. System Model

The geometrical set-up diagram of our proposed VLP system is depicted in Fig. 1, in which a total K number of Txs (i.e., LEDs) and one Rx (i.e., a CMOS camera) are positioned on the ceiling and at the floor level, respectively. Each k^{th} Tx has a known set of coordinates (x_k, y_k, z_k) and (u_k, v_k), which is relative to the world coordinate system (WCS) and the image coordinate system (ICS), respectively, where $k = 1,...,K$. In addition, let (x_{Rx}, y_{Rx}, z_{Rx}) be the unknown position (coordinate) of the camera-based Rx, respectively.

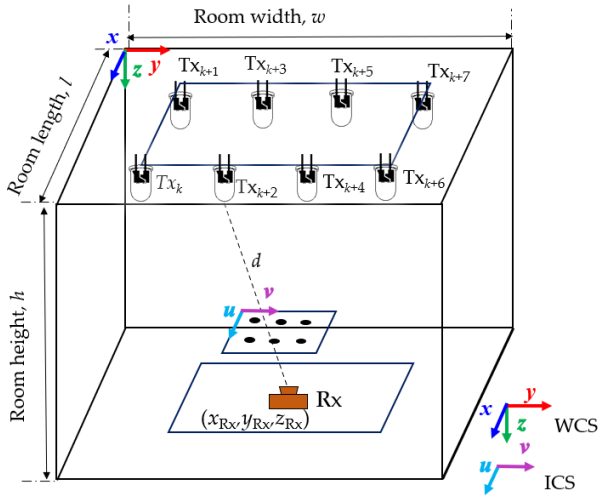

Fig. 1. Proposed indoor VLP system.

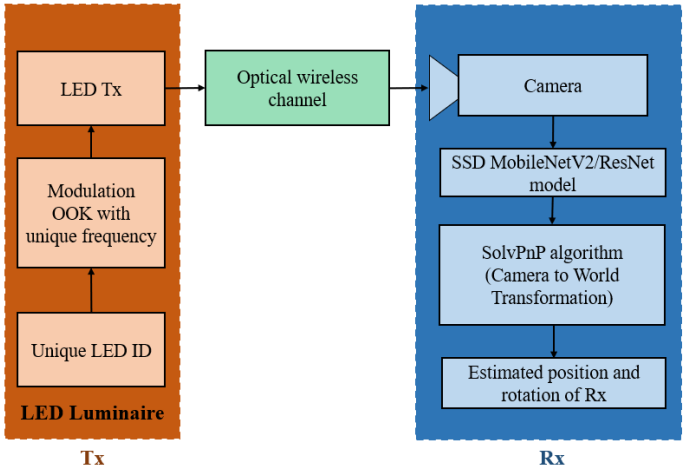

Fig. 2. Block diagram of the proposed indoor VLP system.

Figure. 2 illustrates the system block diagram, which is composed of the three main blocks, i.e., the Tx, a channel, and the Rx. The LED identity code is in the OOK format with the unique frequency for each Tx, which is high enough that human eyes cannot perceive any fluctuation in the light intensity - essentially flicker-free transmission. Since we are interested in using the LED for general-purpose illumination, their time-averaged luminous intensity is ideally constant and equal among them. At the Rx, an image is acquired using a CMOS camera whose exposure time is set to its minimum possible value. After that, the captured image is applied to the trained CNN-SSD model for the classification and detection of LEDs (i.e., recognition of LED-ID and their positions in the captured image domain). The detected LED-ID is further used to determine the location of LEDs in WCS, which were already stored in the database. Next, the SolvePnP algorithm and WCS are adopted to the detected LED position in the image domain and for estimating the Rx's position, respectively for the camera to world transformation, which finds the pose (i.e., position and orientation) of the Rx.

2.1 Proposed VLP system

The proposed SSD-VLP system is primarily comprised of two key procedures: LED-ID identification and the positioning algorithm. The former is accomplished by utilizing the CMOS IS's rolling shutter mechanism. Note, in CMOS -based camera the scanning of the scene is

sequential, and the IS camera exposes the image sensor row by row of pixels. This results in an image that consists of bright and dark stripes, while the LED is turning on and off throughout the exposure time. The length of the stripes is determined by the relation between the symbol duration and the row sampling time, both temporal quantities. The signal should be recovered within the region-of-interest (ROI) where the SNR is optimal. However, as the distance between the LEDs and the camera increases, the projection of the LEDs in the image will decrease, resulting in fewer stripes. In the second key procedure, i.e., the positioning algorithm, the camera position is made up of six degrees of freedom (i.e., 3D rotation - *x*, *y,* and *z* and 3D rotation - roll, pitch, and yaw). Therefore, at least three image points and their corresponding WCS information are necessary to estimate the position of the Rx. Already a number of solutions are available to solve this perspective-n-point (PnP) problem [18]. In the proposed system, we consider the open-source implementation present in the OpenCV computer vision library, the solvePnP function, using the solver presented in [19], [20]. This SolvePnP algorithm outputs the rotation and translation vectors, which is further used to obtain the rotation matrix. Consequently, the Rodrigues algorithm is employed for determining the rotation matrix from the rotation vector [21]. As a final step, the position of the Rx is estimated using a rotation matrix and the translation vector. Additionally, we use the RQDecomp3x3 algorithm [22] to compute the orientation of the Rx.

III. SSD-CNN

3.1 SSD model and training

SSD is an object detection model that uses feed-forward convolutional networks to generate a set of fixed-size bounding boxes and scores that indicate the presence of an object class instance in each box. Following this, an additional non-maximum suppression step is performed to detect final objects [23]. In SSD, only a single shot is required to detect multiple objects within the image. As illustrated in Fig. 3, the SSD object detection model comprises of two main blocks: (*i*) a feature extractor block; and (*ii*) an extra feature block in which convolutional filters are applied for object detection. The model adopted in this work is the pre-trained *SSD_MobileNet_v2_COCO* and *SSD_ResNet50_v1_COCO*, which embeds all the enumerated features are available in [24].

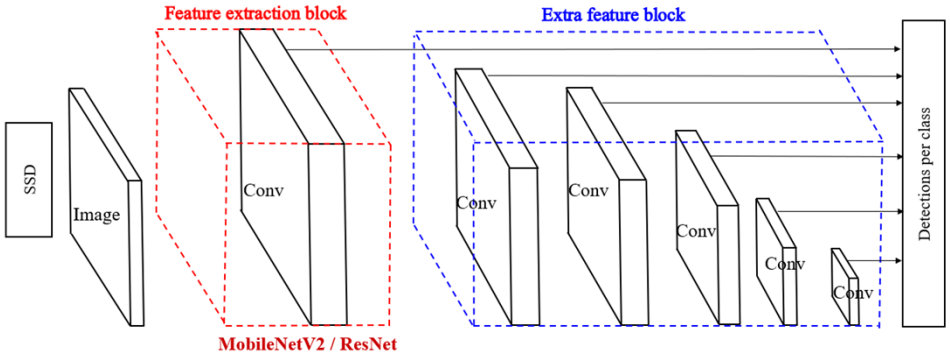

Fig. 3. SSD network structure of the proposed indoor VLP system.

In the proposed system, two different models are used for feature maps extraction, i.e., MobileNetV2 [25] and ResNet [26] for high-quality image classification, which we will call the feature extractor network (in our case, it is either MobileNetV2 or ResNet) that will be explained later in this section. The most significant difference between training an SSD and a traditional detector (such as, region-based CNNs, i.e., R-CNNs), is that the ground truth information must be assigned to specific outputs in a fixed set of detector outputs. After the assignment, the loss function and backpropagation are employed end-to-end.

Matching strategy: The predictions of SSD are categorized as positive or negative matches. SSD considers the positive matches only for the calculation of localization cost (i.e.,

the boundary box mismatch). It is measured by the intersection over union (IoU) parameter, which is the ratio between the intersected area over the joined area for two regions. The match is positive if the corresponding default boundary box (not the predicted boundary box) has an IoU > 0.5 with the ground truth, otherwise, it is negative. Once the positive matches have been identified, the cost is calculated using the predicted boundary boxes. This matching strategy encourages each prediction to predict shapes closer to the corresponding default box. As a result, our training predictions are more stable and diverse.

Training objective: The objective of SSD training is derived from the MultiBox [27] objective, but is extended to process multiple object categories. Let $x_{ij}^{p} = \{1,0\}$ be an indicator for matching the i^{th} default box to the j^{th} ground box of the category p. In the matching strategy above, we can have $\sum_i x_{ij}^{p} \geq 1$. The overall objective loss function is defined as a weighted sum of both localization loss L_{loc} and confidence loss L_{conf}, which is defined as:

$$L(x,c,l,g) = \frac{1}{N}(L_{\text{conf}}(x,c) + \alpha L_{\text{loc}}(x,l,g)), \tag{1}$$

where N is the number of positive matches, and α is the weight for the localization loss. For $N = 0$, the loss is set to 0. The localization loss is the Smooth L_1 loss [28] between the ground truth g and the predicted boundary box l parameters. As mentioned earlier, SSD only considers predictions from the positive matches, and therefore, negative matches can be ignored. Similar to Faster R-CNN [29], we regress to offsets for the center (cx; cy) of the default bounding box d and for its width w and height h. The L_{loc} and L_{conf} are computed as:

$$L_{\text{loc}}(x,l,g) = \sum_{i \in Pos}^{N} \sum_{m \in \{cx,cy,w,h\}} x_{ij}^{k} \text{smooth}_{\text{L1}}\left(l_i^m - \hat{g}_j^m\right)$$

$$\hat{g}_j^{cx} = \frac{\left(g_j^{cx} - d_i^{cx}\right)}{d_i^w} \qquad \hat{g}_j^{cy} = \frac{\left(g_j^{cy} - d_i^{cy}\right)}{d_i^h} \tag{2}$$

$$\hat{g}_j^w = \log\left(\frac{\left(g_j^w\right)}{d_i^w}\right) \qquad \hat{g}_j^h = \log\left(\frac{\left(g_j^h\right)}{d_i^h}\right).$$

The confidence loss is the loss of making a class prediction. Note, for the matching with (*i*) positive prediction, a loss is incurred according to the confidence score of the class corresponding to the prediction; and (*ii*) negative prediction, the loss is incurred according to the confidence score of the class "0" (i.e., the class "0" indicates that no object being detected). The confidence loss is computed as the softmax loss over multiple classes confidences c (class score). The softmax loss consists of Softmax activation combined with a cross-entropy loss. The Softmax activation function provides a probability for each class, and the summation of these probabilities adds up to unity. The Cross entropy loss is the result of summing the negative logarithm of probabilities as given by:

$$L_{\text{conf}}(x,c) = -\sum_{i \in Pos}^{N} x_{ij}^{p} \log\left(\hat{c}_i^p\right) - \sum_{i \in Neg} \log\left(\hat{c}_i^0\right), \tag{3}$$

where $\hat{c}_i^p = \frac{\exp\left(c_i^p\right)}{\sum_p \exp\left(c_i^p\right)}$ and the α is set to 1 by cross-validation.

3.2 ResNet

ResNet is a type of neural network that consists of sequences of convolutions bypassed by skip connections, thus allowing the model to learn residual values within the convolutional layers [30]. The ResNet-50 model presented in [26] incorporates 16 bottleneck blocks and 50 layers with trainable parameters, including a convolutional layer following the input and output layers.

3.3 MobileNetV2

MobileNetV2 uses a depthwise convolutional layer [25]. The number of input channels in the depthwise convolution layer equals the number of filter channels. This layer reduces the total number of parameters to a minimum because this depthwise convolutional layer split the computation of convolution into two separable steps, resulting in the reduction of the number of kernel's parameters [31]. MobileNet v2 introduces a new layer called 1 × 1 convolution layer, whose purpose is to increase the number of channels in the data prior to depthwise convolution. A depthwise convolution layer followed by a 1 × 1 convolution layer is referred to as the pointwise/projection layer. The projection layer projects data with a high number of channels into the output with a much lower number of channels. The residual connection works similarly to ResNet to add gradients in MobileNetV2. ReLU6 is used to prevent too many activations.

3.4 Dataset generation

As a prerequisite to the implementation of the VLP system based on the SSD algorithm, it is necessary to train the algorithm by creating a labeled dataset consisting of images like test images and their annotations. A series of steps are followed to generate the training dataset. Firstly, images are captured by a CMOS camera, which is then converted to the grayscale followed by the smoothing process (median blur). After that, an adaptive threshold and two sequential morphological operations (erosion and dilation) are employed to allow bright stripes standing out from the background. Afterward, the borders of the bright stripes are detected using contour detection. By combining contours that are close together, which represent stripes of a single LED, a bounding box is generated for each LED in the image adapted to its dimensions. This dataset is available online as well as in [32]. The overall procedure, which is also illustrated in Fig. 4, is repeated for all images for labeling. In this work, the dataset (images and annotations) used for the training and testing are detailed in the next section.

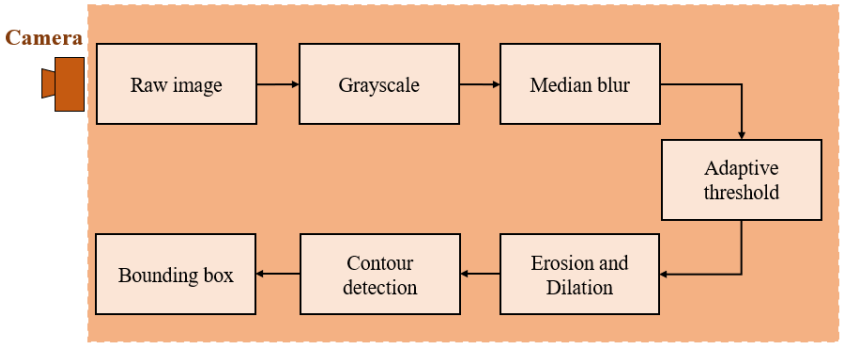

Fig. 4 Procedure of detecting ROI and creating bounding box (labeling).

IV. Experiments and Results

4.1 Experimental Setup

The experimental setup for our SSD-VLP model is depicted in Fig. 5 (a), which is used for the performance evaluation and dataset generation of the proposed system. The setup consists of eight LEDs intensity modulated with data at frequencies in the range of 1 -to 4.5kHz with a 500 Hz interval, see Fig. 5(b). Each LED employs a DLA G2 lamp from Tridonic, with a nominal power of 18 W and a diameter of 15 cm. The point with coordinates (0,0,0) corresponds to the bottom left corner of the room as depicted in Fig. 5. The CMOS camera (Rx) used in this experiment is Raspberry Pi Camera module v2, which is kept at a height of 25.6 cm above the ground level. All key system parameters are detailed in Table I.

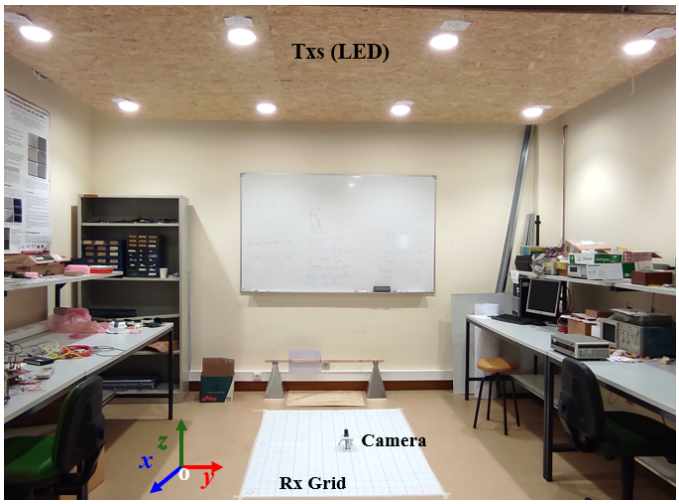

(a)

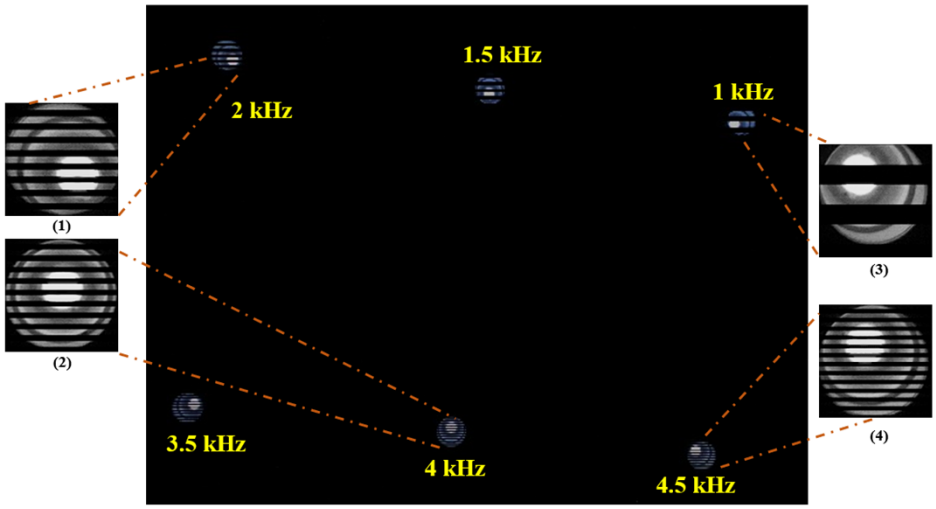

(b)

Fig. 5 Experimental setup of the proposed system: (a) experimental set-up, and (b) the image captured with different symbol periods for: (1) 2kHz, (2) 4 kHz, (3) 1 kHz, and (4) 4.5 kHz.

The images of the Txs were acquired in RAW format with a resolution of 3264 × 2464 pixels and with the exposure time set to 28 μs. In this work, firstly 495 images were taken (with 10 degrees of rotation between each one), and then, horizontal, and vertical flip augmentation was used to artificially expand the size of the training datasets to improve the performance and ability of the models to generalize. In the present study, we are not using any other augmentation scale, such as, rotation or skewness augmentation, because it may change the virtual symbol band stripes, which may result in misclassification of LED-IDs. Therefore, a total of 1980 images are collected for training and testing, where 80% of the total images were selected for training, and the remaining 20% were considered for testing, which is widely used in the literature to validate the performance of the model with images not seen by the model before. Both SSD MobileNetV2 and SSD ResNet were trained with 10,000 iterations.

TABLE I. The key system parameters.

Parameter	Value
Room size (w,l,h)	4.2 × 2.7 × 2.71 m^3
Tx specification	
Hardware	Tridonic DLA G2 lamp
Locations of the Txs	
(x_1, y_1, z_1),	(0.330, 0.485, 2.710) m,
(x_2, y_2, z_2)	(1.523,0.485,2.710) m,
(x_3, y_3, z_3),	(2.713,0.485,2.710) m,
(x_4, y_4, z_4),	(2.908,0.492,2.710) m,
(x_5, y_5, z_5),	(0.335,2.080,2.710) m,
(x_6, y_6, z_6),	(1.528,2.087,2.710) m,
(x_7, y_7, z_7),	(2.713,2.081,2.710) m,
(x_8, y_8, z_8),	(2.908,2.085,2.710) m,
Tx diameter	15 cm
Tx power	18 W
Rx specification	
Hardware	Raspberry Pi Camera Module V2
Image resolution	3264 × 2464 pixels
Exposure time	28 µs
Focal length (f)	3.04 mm
Rx's field of view (FoV)	62.2 degrees (horizontal), 48.8 degrees (vertical)
Sensor image area	3.68 × 2.76 mm^2
Focal ratio (F-Stop)	2
Frame rate	15 fps
SSD specification	
Number of classes	8
Number of epochs	10,000
Batch size	4
Augmentation	Horizontal and vertical flip

4.2 Positioning error performance

Average precision (AP) is one of the most popular metrics to evaluate the accuracy of object detection methods like Faster R-CNN and SSD. It is calculated as the AP value for recall values ranging from 0 to 1 AP indicates retrieval performance based on recall and precision in ranked results, with a higher AP value showing better object detection. The precision refers to the percentage of correctly identified objects compared with the total number of boxes detected. The recall index measures the percentage of targets that are labeled as true targets considering the actual number of targets. The precision, recall, and AP can be computed as:

$$R_n = \frac{\mathrm{TP}}{\mathrm{TP} + \mathrm{FN}}, \tag{5}$$

$$P_n = \frac{\mathrm{TP}}{\mathrm{TP} + \mathrm{FP}}, \tag{6}$$

$$\mathrm{AP} = \sum_n (R_n - R_{n-1}) P_n, \tag{7}$$

where TP, and FN and FP are the true positive, false negative, and false positive, respectively. P_n and R_n denote the precision and recall, respectively at the n^{th} threshold. Another important metric is the IoU parameter, which is the ratio between the intersected area over the joined area

for two regions. Moreover, mean AP (mAP) is used as the evaluation performance metric for multiclass object detection, which is computed by the mean of AP values overall classes, as given by:

$$\text{mAP} = \frac{1}{N}\sum_{i=1}^{N} \text{AP}_i. \tag{8}$$

In the validation dataset, mAP values of 0.99 and 0.81 were obtained for the IoU threshold of 0.5 for SSD MobileNetV2 and SSD ResNet Algorithm, respectively. The number of trainable parameters for MobilenetV2 and ResNet are 3.4 million [31]and 23 million [31], respectively. The reason behind the reduction in the number of parameters between both models is that the MobileNetV2 replaces the convolutional layers of ResNet with depthwise separable convolutional layers, which split the computation of convolution into two separable steps reducing the number of kernel's parameters [31]. Therefore, the time taken to train the MobilenetV2 is half than ResNet. To assess how successfully the training is proceeding, we have used the loss value. The loss for the model is the number of incorrect predictions on the training samples. In the case of a perfect prediction by the model, the loss value is zero; otherwise, the loss is greater. The objective of training a model is to obtain weights and biases that are associated with low losses across all data. Different loss profiles as a function of epochs from SSD Mobilenet and SSD ResNet are illustrated in Fig. 6. Both models are trained for 10,000 epochs, the total training loss is almost stable at this point. The SSD MobileNet and SSD ResNet model achieved total losses (including both localization and classification) of 0.024 and 0.032, respectively at epochs values of 10,000.

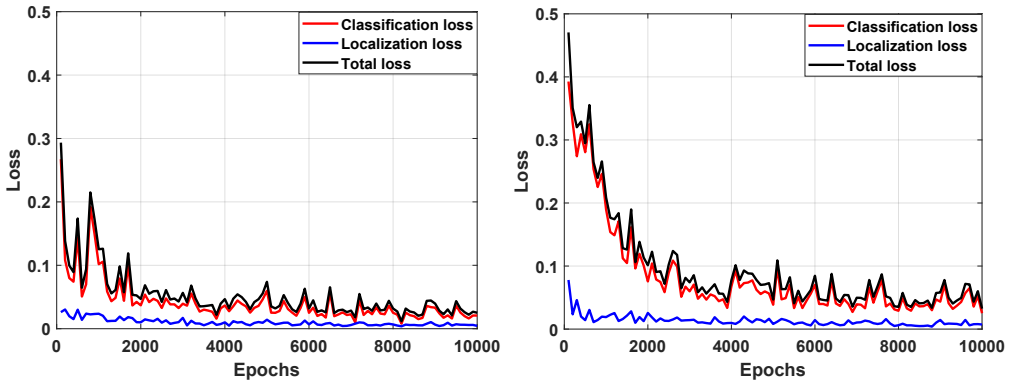

(a) (b)

Fig. 6. Training losses of SSD with: (a) MobileNetV2, and (b) ResNet.

We have defined four different regularly spaced points on the floor level following successful training and application of the proposed SSD-VLP system to be able to analyse ε_p. A set of 65 images were taken at each point (i.e., the camera is rotated from 0 to 320º and images are taken at interval of 5º (which is 65 images) per each location) for the evaluation purpose. Therefore, a total of 260 images were given used for evaluation. Fig. 7(a, and b) shows the real and estimated positions of the SSD MobileNetV2- and SSD ResNet-based VLP systems, whereas Fig. 8(a, and b) depicts the histogram of the error values for both algorithms, where the root mean square of ε_p for SSD MobileNetV2 and SSD ResNet are 4.67 and 5.27 cm, respectively.

Fig. 9 present the cumulative distribution function (CDF) of ε_p resulting from the proposed SSD MobileNetV2 and SSD ResNet models. The ε_p achieved at the 95% confidence interval are 9.11 and 10.24 cm for SSD MobileNetV2 and SSD ResNet, respectively. The computational time is depended on the hardware used, the process data size, and the complexity of the algorithm. We evaluated the time-cost of the proposed SSD-VLP system with the input image size of 3264 × 2464 pixels. The average processing time of proposed SSD MobileNetV2 and

SSD ResNet models achieved are 14.9 and 15 ms, respectively using CPU Intel (R) Core (TM) i9-9900K CPU @ 3.60GHz, 3600 MHz with NVIDIA GeForce RTX 2060, 8 Core PC, having 16 Logical Processors and 32 GB RAM.

Note that, the results presented here are not compared with other data due to (*i*) not using the same hardwares; and (*ii*) SSD-CNN is being used for the first time in indoor VLP with experimental validation. However, there are some reported works based on simulation, for example, [16], where the average positioning error were 10.53 and 13.04 cm for CNN and MLP, but the dataset used were huge (dataset of size 10^5).

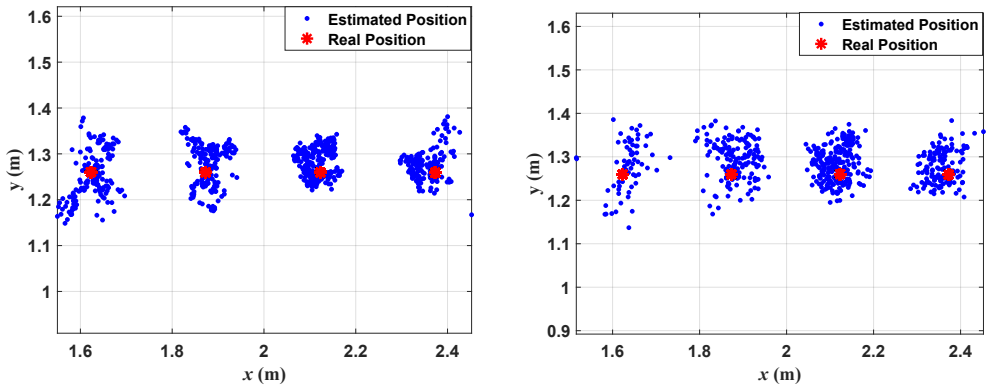

(a) (b)

Fig. 7. 2D Error plots of SSD with: (a) MobileNetV2, and (b) ResNet.

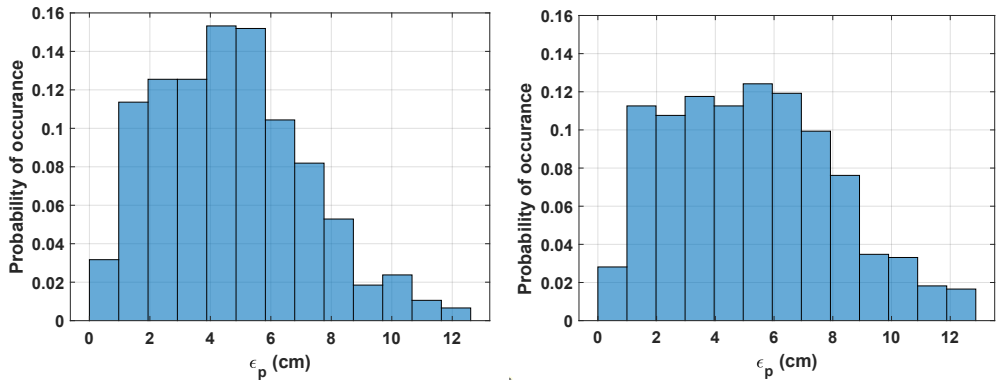

(a) (b)

Fig. 8 Histogram of SSD with: (a) MobileNetV2, and (b) ResNet.

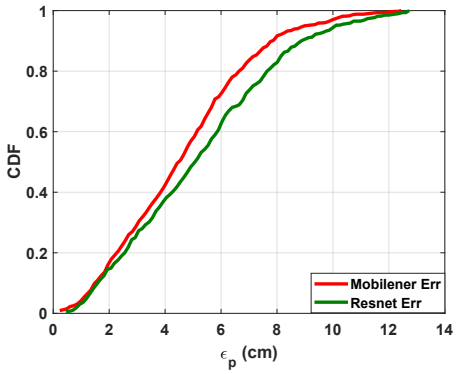

Fig. 9 CDF plot for positioning error, ε_p from SSD with MobileNetV2 and SSD ResNet.

V. Conclusion

In this work, we proposed an indoor VLP system based on CNN and a rolling shutter camera. Initially, the LEDs were modulated with OOK with a unique symbol period to ease their recognition. A dataset was created in which images were acquired by the CMOS camera and the classification and position of each visible LED in that image were labelled. A perspective-n-point problem algorithm was employed to estimate the receiver position. The system was validated using a real-world size test setup containing eight LEDs. The obtained results showed that the maximum average root mean square positioning error achieved were 4.67 and 5.27 cm with SSD MobileNet and SSD ResNet models, respectively. The validation's results revealed that the system can process 67 images per second, allowing real-time positioning.

Acknowledgments

This work is supported by the European Union's Horizon 2020 research and innovation programme under the Marie Sklodowska-Curie grant agreement no. 764461 (VisIoN). It is also supported by EU COST Action CA19111 NEWFOCUS.

Disclosures

The authors declare no conflicts of interest.

References

[1] T.-H. Do and M. Yoo, 'An in-Depth Survey of Visible Light Communication Based Positioning Systems', *Sensors*, vol. 16, no. 5, p. 678, May 2016, doi: 10.3390/s16050678.

[2] Vantage Market Research, 'Indoor Positioning and Navigation System Market', Dec. 2021. [Online]. Available: https://www.vantagemarketresearch.com/industry-report/indoor-positioning-and-navigation-system-market-0158

[3] A. S. Paul and E. A. Wan, 'RSSI-Based Indoor Localization and Tracking Using Sigma-Point Kalman Smoothers', *IEEE J. Sel. Top. Signal Process.*, vol. 3, no. 5, pp. 860–873, Oct. 2009, doi: 10.1109/JSTSP.2009.2032309.

[4] N. Chaudhary, L. N. Alves, and Z. Ghassemlooy, 'Current Trends on Visible Light Positioning Techniques', in *2019 2nd West Asian Colloquium on Optical Wireless Communications (WACOWC)*, Tehran, Iran, Apr. 2019, pp. 100–105. doi: 10.1109/WACOWC.2019.8770211.

[5] A. B. M. M. Rahman, T. Li, and Y. Wang, 'Recent Advances in Indoor Localization via Visible Lights: A Survey', *Sensors*, vol. 20, no. 5, p. 1382, Mar. 2020, doi: 10.3390/s20051382.

[6] Z. Ghassemlooy, L. N. Alves, S. Zvanovec, and M.-A. Khalighi, *Visible Light Communications: Theory and Applications.* CRC Press, 2017. doi: 10.1201/9781315367330-3.

[7] J. Luo, L. Fan, and H. Li, 'Indoor Positioning Systems Based on Visible Light Communication: State of the Art', *IEEE Commun. Surv. Tutorials*, vol. 19, no. 4, pp. 2871–2893, 2017, doi: 10.1109/COMST.2017.2743228.

[8] N. Chaudhary, L. N. Alves, and Z. Ghassemlooy, 'Impact of Transmitter Positioning Uncertainty on RSS-based Visible Light Positioning Accuracy', in *2020 12th International Symposium on Communication Systems, Networks and Digital Signal Processing (CSNDSP)*, Porto, Portugal, Jul. 2020, pp. 1–6. doi: 10.1109/CSNDSP49049.2020.9249532.

[9] N. Chaudhary, L. N. Alves, and Z. Ghassemlooy, 'Impact of Transmitter Positioning and Orientation Uncertainty on RSS-Based Visible Light Positioning Accuracy', *Sensors*, vol. 21, no. 9, p. 3044, Apr. 2021, doi: 10.3390/s21093044.

[10] P. Lin *et al.*, 'Real-time visible light positioning supporting fast moving speed', *Opt. Express*, vol. 28, no. 10, p. 14503, May 2020, doi: 10.1364/OE.390781.

[11] Y. Zhuang *et al.*, 'A Survey of Positioning Systems Using Visible LED Lights', *IEEE Commun. Surv. Tutorials*, vol. 20, no. 3, pp. 1963–1988, 2018, doi: 10.1109/COMST.2018.2806558.

[12] H. H. Heqing Huang, A. Y. Aiying Yang, L. F. Lihui Feng, G. N. Guoqiang Ni, and and P. G. and Peng Guo, 'Artificial neural-network-based visible light positioning algorithm with a diffuse optical channel', *Chinese Optics Letters*, vol. 15, no. 5, pp. 050601–050605, 2017, doi: 10.3788/col201715.050601.

[13] C.-W. Hsu, S. Liu, F. Lu, C.-W. Chow, C.-H. Yeh, and G.-K. Chang, 'Accurate Indoor Visible Light Positioning System utilizing Machine Learning Technique with Height Tolerance', in *Optical Fiber Communication Conference*, San Diego, California, 2018, p. M2K.2. doi: 10.1364/OFC.2018.M2K.2.

[14] A. Kendall, M. Grimes, and R. Cipolla, 'PoseNet: A Convolutional Network for Real-Time 6-DOF Camera Relocalization', in *2015 IEEE International Conference on Computer Vision (ICCV)*, Santiago, Chile, Dec. 2015, pp. 2938–2946. doi: 10.1109/ICCV.2015.336.

[15] X. Wang, X. Wang, and S. Mao, 'CiFi: Deep convolutional neural networks for indoor localization with 5 GHz Wi-Fi', in *2017 IEEE International Conference on Communications (ICC)*, Paris, France, May 2017, pp. 1–6. doi: 10.1109/ICC.2017.7997235.

[16] M. A. Arfaoui *et al.*, 'Invoking Deep Learning for Joint Estimation of Indoor LiFi User Position and Orientation', p. 17, 2020.

[17] S. M. Sheikholeslami, F. Fazel, J. Abouei, and K. N. Plataniotis, 'Sub-Decimeter VLC 3D Indoor Localization With Handover Probability Analysis', *IEEE Access*, vol. 9, pp. 122236–122253, 2021, doi: 10.1109/ACCESS.2021.3108173.

[18] M. A. Fischler and R. C. Bolles, 'Random sample consensus: a paradigm for model fitting with applications to image analysis and automated cartography', *Commun. ACM*, vol. 24, no. 6, pp. 381–395, Jun. 1981, doi: 10.1145/358669.358692.

[19] G. Terzakis and M. Lourakis, 'A Consistently Fast and Globally Optimal Solution to the Perspective-n-Point Problem', in *Computer Vision – ECCV 2020*, vol. 12346, Cham: Springer International Publishing, 2020, pp. 478–494. doi: 10.1007/978-3-030-58452-8_28.

[20] 'Opencv: Camera calibration and 3d Reconstruction.' [Online]. Available: https://docs.opencv.org/3.4/d9/d0c/group__calib3d.html#ga549c2075fac14829ff4a58bc931c033d

[21] 'Opencv: Camera calibration and 3d Reconstruction.' [Online]. Available: https://docs.opencv.org/3.4/d9/d0c/group__calib3d.html#ga61585db663d9da06b68e70cfbf6a1eac

[22] 'Opencv: Camera calibration and 3d Reconstruction.' [Online]. Available: https://docs.opencv.org/3.4/d9/d0c/group__calib3d.html#ga1aaacb6224ec7b99d34866f8f9baac83

[23] W. Liu *et al.*, 'SSD: Single Shot MultiBox Detector', *arXiv:1512.02325 [cs]*, vol. 9905, pp. 21–37, 2016, doi: 10.1007/978-3-319-46448-0_2.

[24] https://github.com/tensorflow/models/blob/master/research/object_detection/g3doc/tf2_detection_zoo.md

[25] M. Sandler, A. Howard, M. Zhu, A. Zhmoginov, and L.-C. Chen, 'MobileNetV2: Inverted Residuals and Linear Bottlenecks', *arXiv:1801.04381 [cs]*, Mar. 2019, Accessed: Jan. 03, 2022. [Online]. Available: http://arxiv.org/abs/1801.04381

[26] R. Maisano, V. Tomaselli, A. Capra, F. Longo, and A. Puliafito, 'Reducing Complexity of 3D Indoor Object Detection', in *2018 IEEE 4th International Forum on Research and Technology for Society and Industry (RTSI)*, Palermo, Sep. 2018, pp. 1–6. doi: 10.1109/RTSI.2018.8548514.

[27] D. Erhan, C. Szegedy, A. Toshev, and D. Anguelov, 'Scalable Object Detection Using Deep Neural Networks', in *2014 IEEE Conference on Computer Vision and Pattern Recognition*, Columbus, OH, USA, Jun. 2014, pp. 2155–2162. doi: 10.1109/CVPR.2014.276.

[28] R. Girshick, 'Fast R-CNN', *arXiv:1504.08083 [cs]*, Sep. 2015, Accessed: Jan. 03, 2022. [Online]. Available: http://arxiv.org/abs/1504.08083

[29] S. Ren, K. He, R. Girshick, and J. Sun, 'Faster R-CNN: Towards Real-Time Object Detection with Region Proposal Networks', *arXiv:1506.01497 [cs]*, Jan. 2016, Accessed: Jan. 03, 2022. [Online]. Available: http://arxiv.org/abs/1506.01497

[30] K. He, X. Zhang, S. Ren, and J. Sun, 'Deep Residual Learning for Image Recognition', *arXiv:1512.03385 [cs]*, Dec. 2015, Accessed: Jan. 03, 2022. [Online]. Available: http://arxiv.org/abs/1512.03385

[31] N. Reddy, A. Rattani, and R. Derakhshani, 'Comparison of Deep Learning Models for Biometric-based Mobile User Authentication', in *2018 IEEE 9th International Conference on Biometrics Theory, Applications and Systems (BTAS)*, Redondo Beach, CA, USA, Oct. 2018, pp. 1–6. doi: 10.1109/BTAS.2018.8698586.

[32] https://www.kaggle.com/celsopereira1/visible-light-positioning-dataset

Chapter 6: Conclusions and Future Work

This chapter summarizes the major contributions of this work to the VLC based indoor localization. Firstly, the thesis begins with an analysis of the objectives underlying the development of this thesis, supported by the experimental results presented in this thesis. Additionally, there is a discussion of how this work may lead to new research directions.

6.1 Conclusions

This thesis focused on the topics of VLP systems by addressing the key challenges and proposing novel analytical and experimental solutions. The result of this work has been a glimpse into some possible solutions for VLP, which are essential for its implementation. Firstly, the transmitter tilting was analyzed, and determined that the accuracy of the RSS-based VLP system in indoor applications was limited by the tilt angles of transmitters and receivers as well as multipath reflections. Therefore, a new indoor VLP system was proposed in section 5.3, and it was shown that tilting the transmitter could improve the positioning accuracy of the VLP system. For that, the transmitter was tilted towards the center of the receiving plane to achieve higher accuracy by maximizing the received power level due to contributions from the LOS paths at the pointing center F. The positioning error was estimated by using the LLS algorithm with polynomial regression. The results showed a significant improvement in the accuracy by up to ~66% compared with a typical non-tilting transmitter case. The results also showed that, the uniformity of the proposed VLP system in line with European Standard EN 12464-1, therefore meeting the uniformity requirement of the visible illumination regions. Ultimately, it was concluded that the proposed VLP system with the tilting transmitter outperforms the non-tilted transmitter scenario.

After that, the influence of transmitter's position and orientation uncertainty on the performance of VLP systems based on RSS was demonstrated in section 5.4. From the results, it was concluded that light uniformity and transmitter's HPA are crucial design parameters for developing an efficient VLP system. The selection of the transmitter's HPA as well as the optimum distance between transmitters needs to be carefully implemented. Moreover, it was shown that the best uniformity and optimum error performance were not met for the same conditions, inferring necessary design trade-offs. Furthermore, the effect of error dependence on transmitter's position and orientation uncertainty reduced with increasing the number of transmitters. In the case of square grid transmitter placement for a VLP system, the number of transmitters can be further

explored as an added variable to optimize both light uniformity and error performance, as it reduces the HPA for smaller distances between transmitters.

ANNs have been attracting a lot of attention regarding the solution of regression problems. Therefore, a comprehensive study was done about the optimization of an ANN for VLP systems and a complete assessment of its performance (see section 5.5). For that, an indoor VLP system using an ANN for positioning estimation in the presence of both LOS and non-line-of-sight multipath signals was analysed. Three different ANN algorithms of Levenberg-Marquardt, Bayesian regularization, and scaled conjugate gradient algorithms were explored for minimizing the positioning error. The optimization of ANN was done based on the number of neurons in the hidden layers and the number of training epochs. The results showed that, the ANN with Bayesian regularization outperforms the traditional RSS technique using NLLS for the SNR range of 5 – 30 dB.

Next, a new indoor VLP system based on the polynomial regression and SVM was proposed in section 5.6. Achieved results showed that the use of SVM allows for accurate classification of the polynomial model, hence, improving the accuracy of the system. Tests performed in a furnished environment revealed that, the presence of furniture makes the task of inferring suitable polynomial models difficult and constrains the overall accuracy of the system. Nevertheless, due to the simplicity of the approach and its feasibility for implementation, the proposed methods seem suitable for applications demanding coarse positioning accuracies, such as positioning in large shopping areas. Finally, an indoor VLP system based on CNN and a rolling shutter camera were proposed and demonstrated experimentally, see section 5.7. In this work, a dataset was created in which images were acquired by the CMOS camera and the classification and position of each visible LED in that image were labelled. The system was validated using a real-world size test setup containing eight LEDs. It is realized from the validation results that the system can process 67 images per second, allowing real-time positioning.

6.2 Future works

During the research carried out for this thesis, additional opportunities and areas for further investigation were identified. The following recommendations are made for future works:

1. There is presently no robust and comprehensive set of international standards that cover all aspects of VLP systems. In addition to specifying how LED addresses and LED IDs should be coded, the standards also need to detail the complete architecture to achieve the global position of the receiver based on its local position. For future applications, an

international standard need to be designed quickly. Furthermore, the standard should be sufficiently flexible to facilitate future modifications and extensions.

2. A tracking system may be more suitable for moving objects since positioning systems can only provide disconnected positioning results. According to the literature, many existing positioning systems are not tracking-capable. Therefore, it will be interesting to add tracking capabilities to existing positioning systems.
3. A further challenge to implement the smartphones as a receiver is synchronizing the inertial sensors with the camera frame. The sensor and camera frame generally use different clocks, which leads to inaccuracy. Different sensor types can also lead to time delays. In order to be able to estimate motion more accurately, the time offsets between sensors and cameras must be estimated.
4. The ability for a system to perform both positioning as well as communication would be appreciated. However, this may require the intelligent design of the structural frame. For instance, the headers of the frame can be used for positioning. But then, modulation in such systems would also be an issue. Due to the high data rate requirement for communication, the VLC signal might be affected by intersymbol interference, which might result in positioning inaccuracy. Considering that most of the current positioning systems are designed exclusively for positioning, so integrating positioning with communication in a system is a challenge.
5. The outdoor VLP is both fascinating and challenging. However, there are still many difficulties in locating objects using PDs in the outdoor environment. However, using a camera may become a possible method for outdoor localization in the future, as well as a research topic in the short term.
6. Most existing studies on VLP systems do not take into account fundamental techniques such as modulation and multiplexing. Although these techniques are crucial to any system, there exists an open issue as to whether there can be a new modulation technique to eliminate flickering or a new multiplexing technique to reduce the positioning latency.
7. There are still several unresolved issues regarding indoor localization using cameras that require further research. For instance, research areas might include investigating techniques for camera calibration to optimize the focal length of the lens or reduce lens distortion.

8. The smartphones are often equipped with low-cost sensors that are prone to a variety of systematic errors, non-negligible misalignments between sensor axes, and different sensitivity along various sensor axes. It is necessary to model and compensate for these errors (calibrate) through a real-time or off-line process.
9. Additional sensors that complement VLP should be explored. Inertial measurement unit sensors have gained attention in the recent years, and its use may even become more useful in the future, if more research is done on it.

References

[1] Vantage Market Research, 'Indoor Positioning and Navigation System Market', Dec. 2021. [Online]. Available: https://www.vantagemarketresearch.com/industry-report/indoor-positioning-and-navigation-system-market-0158

[2] N. B. Priyantha, A. K. L. Miu, H. Balakrishnan, and S. Teller, 'The cricket compass for context-aware mobile applications', in *Proceedings of the 7th annual international conference on Mobile computing and networking - MobiCom '01*, Rome, Italy, 2001, pp. 1–14. doi: 10.1145/381677.381679.

[3] P. Bahl and V. N. Padmanabhan, 'RADAR: An in-building RF-based user location and tracking system', *Proceedings - IEEE INFOCOM*, vol. 2, pp. 775–784, 2000, doi: 10.1109/infcom.2000.832252.

[4] S. Gezici *et al.*, 'Localization via ultra-wideband radios: A look at positioning aspects of future sensor networks', *IEEE Signal Processing Magazine*, vol. 22, no. 4, pp. 70–84, 2005, doi: 10.1109/MSP.2005.1458289.

[5] H. M. Hussien, Y. N. Shiferaw, and N. B. Teshale, 'Survey on indoor positioning techniques and systems', *Lecture Notes of the Institute for Computer Sciences, Social-Informatics and Telecommunications Engineering, LNICST*, vol. 244, no. 6, pp. 46–55, 2018, doi: 10.1007/978-3-319-95153-9_5.

[6] S. Gezici *et al.*, 'Localization via ultra-wideband radios: a look at positioning aspects for future sensor networks', *IEEE Signal Process. Mag.*, vol. 22, no. 4, pp. 70–84, Jul. 2005, doi: 10.1109/MSP.2005.1458289.

[7] Z. B. Tariq, D. M. Cheema, M. Z. Kamran, and I. H. Naqvi, 'Non-GPS Positioning Systems: A Survey', *ACM Comput. Surv.*, vol. 50, no. 4, pp. 1–34, Nov. 2017, doi: 10.1145/3098207.

[8] T. Cunliffe, *Celestial Navigation*, 3rd, revised ed. Wiley Nautical, 2012.

[9] P. Ball, 'An astrolabe for the people', *Nature*, vol. 452, no. 7187, pp. 534–534, Apr. 2008, doi: 10.1038/452534b.

[10] J. Luo, L. Fan, and H. Li, 'Indoor Positioning Systems Based on Visible Light Communication: State of the Art', *IEEE Commun. Surv. Tutorials*, vol. 19, no. 4, pp. 2871–2893, 2017, doi: 10.1109/COMST.2017.2743228.

[11] A. Arafa, S. Dalmiya, R. Klukas, and J. F. Holzman, 'Angle-of-arrival reception for optical wireless location technology', *Opt. Express*, vol. 23, no. 6, p. 7755, Mar. 2015, doi: 10.1364/OE.23.007755.

[12] T. H. Do and M. Yoo, 'TDOA-based indoor positioning using visible light', *Photonic Network Communications*, vol. 27, no. 2, pp. 80–88, 2014, doi: 10.1007/s11107-014-0428-4.

[13] D. Karunatilaka, F. Zafar, V. Kalavally, and R. Parthiban, 'LED Based Indoor Visible Light Communications: State of the Art', *IEEE Commun. Surv. Tutorials*, vol. 17, no. 3, pp. 1649–1678, 2015, doi: 10.1109/COMST.2015.2417576.

[14] 'Google Scholar'. https://scholar.google.com/ (accessed Jan. 31, 2022).

[15] N. U. Hassan, A. Naeem, M. A. Pasha, T. Jadoon, and C. Yuen, 'Indoor Positioning Using Visible LED Lights: A Survey', *ACM Comput. Surv.*, vol. 48, no. 2, pp. 1–32, Nov. 2015, doi: 10.1145/2835376.

[16] T.-H. Do and M. Yoo, 'An in-Depth Survey of Visible Light Communication Based Positioning Systems', *Sensors*, vol. 16, no. 5, p. 678, May 2016, doi: 10.3390/s16050678.

[17] W. Zhang and M. Kavehrad, 'Comparison of VLC-based indoor positioning techniques', San Francisco, California, USA, Jan. 2013, p. 86450M. doi: 10.1117/12.2001569.

[18] N. Chaudhary, L. N. Alves, and Z. Ghassemlooy, 'Current Trends on Visible Light Positioning Techniques', in *2019 2nd West Asian Colloquium on Optical Wireless Communications (WACOWC)*, Tehran, Iran, Apr. 2019, pp. 100–105. doi: 10.1109/WACOWC.2019.8770211.

[19] H. S. Kim, D. R. Kim, S. H. Yang, Y. H. Son, and S. K. Han, 'Indoor positioning system based on carrier allocation visible light communication', *Optics InfoBase Conference Papers*, vol. 1, no. September, pp. 787–789, 2011, doi: 10.1109/IQEC-CLEO.2011.6193741.

[20] S. Shawky, M. A. El-Shimy, Z. A. El-Sahn, M. R. M. Rizk, and M. H. Aly, 'Improved VLC-based indoor positioning system using a regression approach with conventional RSS techniques', in *2017*

13th International Wireless Communications and Mobile Computing Conference (IWCMC), Valencia, Spain, Jun. 2017, pp. 904–909. doi: 10.1109/IWCMC.2017.7986406.

[21] D. Plets, Y. Almadani, S. Bastiaens, M. Ijaz, L. Martens, and W. Joseph, 'Efficient 3D trilateration algorithm for visible light positioning', *J. Opt.*, vol. 21, no. 5, p. 05LT01, May 2019, doi: 10.1088/2040-8986/ab1389.

[22] Y. Zhuang *et al.*, 'A Survey of Positioning Systems Using Visible LED Lights', *IEEE Commun. Surv. Tutorials*, vol. 20, no. 3, pp. 1963–1988, 2018, doi: 10.1109/COMST.2018.2806558.

[23] T. Akiyama, M. Sugimoto, and H. Hashizume, 'Time-of-arrival-based smartphone localization using visible light communication', *2017 International Conference on Indoor Positioning and Indoor Navigation, IPIN 2017*, vol. 2017-Janua, pp. 1–7, 2017, doi: 10.1109/IPIN.2017.8115904.

[24] C. Amini, A. Taherpour, T. Khattab, and S. Gazor, 'On the more accurate channel model and positioning based on time-of-arrival for visible light localization', *Optical Engineering*, vol. 56, no. 1, p. 016110, 2017, doi: 10.1117/1.oe.56.1.016110.

[25] B. Bai, G. Chen, Z. Xu, and Y. Fan, 'Visible light positioning based on LED traffic light and photodiode', *IEEE Vehicular Technology Conference*, 2011, doi: 10.1109/VETECF.2011.6092849.

[26] S. Y. Jung, S. Hann, and C. S. Park, 'TDOA-based optical wireless indoor localization using LED ceiling lamps', *IEEE Transactions on Consumer Electronics*, vol. 57, no. 4, pp. 1592–1597, 2011, doi: 10.1109/TCE.2011.6131130.

[27] Y. Kim, Y. Shin, and M. Yoo, 'VLC-TDOA using sinusodial pilot signal', *2013 International Conference on IT Convergence and Security, ICITCS 2013*, pp. 1–3, 2013, doi: 10.1109/ICITCS.2013.6717899.

[28] J. H. Y. Nah, R. Parthiban, and M. H. Jaward, 'Visible light communications localization using TDOA-based coherent heterodyne detection', *4th International Conference on Photonics, ICP 2013 - Conference Proceeding*, pp. 247–249, 2013, doi: 10.1109/ICP.2013.6687128.

[29] T. H. Do, J. Hwang, and M. Yoo, 'TDoA based indoor visible light positioning systems', *International Conference on Ubiquitous and Future Networks, ICUFN*, pp. 456–458, 2013, doi: 10.1109/ICUFN.2013.6614860.

[30] C. Huang and X. Zhang, 'Impact and feasibility of darklight LED on indoor visible light positioning system', *2017 IEEE 17th International Conference on Ubiquitous Wireless Broadband, ICUWB 2017 - Proceedings*, vol. 2018-Janua, pp. 1–5, 2017, doi: 10.1109/ICUWB.2017.8250973.

[31] A. Naz, N. U. Hassan, M. A. Pasha, H. Asif, T. M. Jadoon, and C. Yuen, 'Single LED ceiling lamp based indoor positioning system', *IEEE World Forum on Internet of Things, WF-IoT 2018 - Proceedings*, vol. 2018-Janua, pp. 682–687, 2018, doi: 10.1109/WF-IoT.2018.8355186.

[32] A. Naeem, N. U. Hassan, M. A. Pasha, C. Yuen, and A. Sikora, 'Performance analysis of TDOA-based indoor positioning systems using visible LED Lights', *Proceedings of the 2018 IEEE 4th International Symposium on Wireless Systems within the International Conferences on Intelligent Data Acquisition and Advanced Computing Systems, IDAACS-SWS 2018*, pp. 103–107, 2018, doi: 10.1109/IDAACS-SWS.2018.8525567.

[33] P. Du, S. Zhang, C. Chen, A. Alphones, and W. De Zhong, 'Demonstration of a low-complexity indoor visible light positioning system using an enhanced tdoa scheme', *IEEE Photonics Journal*, vol. 10, no. 4, pp. 1–10, 2018, doi: 10.1109/JPHOT.2018.2841831.

[34] T. Q. Wang, Y. A. Sekercioglu, A. Neild, and J. Armstrong, 'Position accuracy of time-of-arrival based ranging using visible light with application in indoor localization systems', *Journal of Lightwave Technology*, vol. 31, no. 20, pp. 3302–3308, 2013, doi: 10.1109/JLT.2013.2281592.

[35] H. Zhao and J. Wang, 'A Novel Three-Dimensional Algorithm Based on Practical Indoor Visible Light Positioning', *IEEE Photonics Journal*, vol. 11, no. 3, pp. 1–1, 2019, doi: 10.1109/JPHOT.2019.2911738.

[36] M. H. Bergen, F. S. Schaal, R. Klukas, J. Cheng, and J. F. Holzman, 'Toward the implementation of a universal angle-based optical indoor positioning system', *Frontiers of Optoelectronics*, vol. 11, no. 2, pp. 116–127, 2018, doi: 10.1007/s12200-018-0806-0.

[37] S. Cincotta, C. He, A. Neild, and J. Armstrong, 'Indoor Visible Light Positioning: Overcoming the Practical Limitations of the Quadrant Angular Diversity Aperture Receiver (QADA) by Using the Two-Stage QADA-Plus Receiver', *Sensors (Basel, Switzerland)*, vol. 19, no. 4, 2019, doi: 10.3390/s19040956.

[38] S. Cincotta, C. He, A. Neild, and J. Armstrong, 'High angular resolution visible light positioning using a quadrant photodiode angular diversity aperture receiver (QADA)', *Optics Express*, vol. 26, no. 7, p. 9230, 2018, doi: 10.1364/oe.26.009230.
[39] Y. S. Erogluy, I. Guvency, N. Palay, and M. Yukselz, 'AOA-based localization and tracking in multi-element VLC systems', *2015 IEEE 16th Annual Wireless and Microwave Technology Conference, WAMICON 2015*, pp. 1–5, 2015, doi: 10.1109/WAMICON.2015.7120424.
[40] T. Huang *et al.*, 'Visible light indoor positioning fashioned with a single tilted optical receiver', *ICOCN 2015 - 14th International Conference on Optical Communications and Networks, Proceedings*, pp. 1–4, 2015, doi: 10.1109/ICOCN.2015.7203770.
[41] Y. U. Lee, 'Short-range visible light positioning based on angle of arrival for smart indoor service', *Journal of Electrical Engineering and Technology*, vol. 13, no. 3, pp. 1363–1370, 2018, doi: 10.5370/JEET.2018.13.3.1363.
[42] Y. U. Lee and S. M. Lee, 'Random distributed angle-of-arrival parameter estimation technique for visible light positioning', *2015 38th International Conference on Telecommunications and Signal Processing, TSP 2015*, pp. 467–471, 2015, doi: 10.1109/TSP.2015.7296306.
[43] Q.-L. Li, J.-Y. Wang, T. Huang, and Y. Wang, 'Three-dimensional indoor visible light positioning system with a single transmitter and a single tilted receiver', *Optical Engineering*, vol. 55, no. 10, p. 106103, 2016, doi: 10.1117/1.oe.55.10.106103.
[44] C. Sertthin, T. Fujii, O. Takyu, Y. Umeda, and T. Ohtsuki, 'On physical layer simulation model for 6-axis sensor assisted VLC based positioning system', *GLOBECOM - IEEE Global Telecommunications Conference*, 2011, doi: 10.1109/GLOCOM.2011.6134119.
[45] H. Steendam, 'A 3-D Positioning Algorithm for AOA-Based VLP with an Aperture-Based Receiver', *IEEE Journal on Selected Areas in Communications*, vol. 36, no. 1, pp. 23–33, 2018, doi: 10.1109/JSAC.2017.2774478.
[46] H. Steendam, T. Q. Wang, and J. Armstrong, 'Cramer-Rao bound for indoor visible light positioning using an aperture-based angular-diversity receiver', *2016 IEEE International Conference on Communications, ICC 2016*, pp. 0–5, 2016, doi: 10.1109/ICC.2016.7510822.
[47] H. Steendam, T. Q. Wang, and J. Armstrong, 'Cramer-Rao bound for AOA-based VLP with an aperture-based receiver', *IEEE International Conference on Communications*, pp. 1–6, 2017, doi: 10.1109/ICC.2017.7996691.
[48] M. Vieira, R. Costa, A. Pereira, and P. Fonseca, 'A Validation Framework for Visible Light Positioning in Mobile Robotics', *Proceedings - 2016 International Conference on Autonomous Robot Systems and Competitions, ICARSC 2016*, pp. 47–52, 2016, doi: 10.1109/ICARSC.2016.25.
[49] J. Yan and B. Zhu, 'A visible light communication indoor localization algorithm in rotated environments', *IEEE CITS 2016 - 2016 International Conference on Computer, Information and Telecommunication Systems*, pp. 1–4, 2016, doi: 10.1109/CITS.2016.7546430.
[50] B. Zhu, J. Cheng, Y. Wang, J. Yan, and J. Wang, 'Three-Dimensional VLC Positioning Based on Angle Difference of Arrival with Arbitrary Tilting Angle of Receiver', *IEEE Journal on Selected Areas in Communications*, vol. 36, no. 1, pp. 8–22, 2018, doi: 10.1109/JSAC.2017.2774435.
[51] B. Zhu, Z. Zhu, Y. Wang, and J. Cheng, 'Optimal Optical Omnidirectional Angle-of-Arrival Estimator With Complementary Photodiodes', *Journal of Lightwave Technology*, vol. PP, no. c, pp. 1–1, 2019, doi: 10.1109/jlt.2019.2907969.
[52] Z. Zhu, B. Zhu, Y. Wang, Z. Shi, and Y. Jiang, 'Angle-of-Arrival Estimator for Light Signals Based on Optimized Photodiode Array', *2019 International Conference on Computing, Networking and Communications, ICNC 2019*, pp. 62–66, 2019, doi: 10.1109/ICCNC.2019.8685534.
[53] J. Yan, B. Zhu, L. Chen, J. Wang, and J. Liu, 'Error Analysis on Indoor Localization with Visible Light Communication', *Remote Sensing*, vol. 11, no. 4, p. 427, 2019, doi: 10.3390/rs11040427.
[54] Y.-S. Kuo, P. Pannuto, K.-J. Hsiao, and P. Dutta, 'Luxapose:Indoor Positioning with Mobile Phones and Visible Light', *Proceedings of the 20th annual international conference on Mobile computing and networking - MobiCom '14*, pp. 447–458, 2014, doi: 10.1145/2639108.2639109.
[55] L. Yin, X. Wu, and H. Haas, 'Indoor visible light positioning with angle diversity transmitter', *2015 IEEE 82nd Vehicular Technology Conference, VTC Fall 2015 - Proceedings*, pp. 1–5, 2015, doi: 10.1109/VTCFall.2015.7390984.

[56] S. Cincotta, A. Neild, C. He, and J. Armstrong, 'Visible light positioning using an aperture and a quadrant photodiode', *2017 IEEE Globecom Workshops, GC Wkshps 2017 - Proceedings*, vol. 2017, pp. 1–6, 2017, doi: 10.1109/GLOCOMW.2017.8269150.
[57] S. Bastiaens and H. Steendam, 'Coarse estimation of the incident angle for VLP with an aperture-based receiver', *2017 14th Workshop on Positioning, Navigation and Communications, WPNC 2017*, pp. 1–6, 2017, doi: 10.1109/WPNC.2017.8250050.
[58] T. Tanaka and S. Haruyama, 'New position detection method using image sensor and visible light LEDs', *2009 2nd International Conference on Machine Vision, ICMV 2009*, pp. 150–153, 2009, doi: 10.1109/ICMV.2009.44.
[59] C. Zhang and X. Zhang, 'Pulsar: Towards Ubiquitous Visible Light Localization', 2017.
[60] C. Sertthin and E. Tsuji, 'A Switching Estimated Receiver Position Scheme For Visible Light Based Indoor Positioning System', 2009.
[61] H. Hosseinianfar and M. Brandt-Pearce, 'Performance Limits for Fingerprinting-Based Indoor Optical Communication Positioning Systems Exploiting Multipath Reflections', *IEEE Photonics J.*, vol. 12, no. 4, pp. 1–16, Aug. 2020, doi: 10.1109/JPHOT.2020.2991472.
[62] Z. Sheng, W. De Zhong, D. Pengfei, C. Chen, and D. Wu, 'PDOA based indoor visible light positioning system without local oscillators in receiver', *2017 Conference on Lasers and Electro-Optics Pacific Rim, CLEO-PR 2017*, vol. 2017-Janua, no. July, pp. 1–3, 2017, doi: 10.1109/CLEOPR.2017.8119047.
[63] S. Zhang, W. De Zhong, P. Du, and C. Chen, 'Experimental Demonstration of Indoor Sub-Decimeter Accuracy VLP System Using Differential PDOA', *IEEE Photonics Technology Letters*, vol. 30, no. 19, pp. 1703–1706, 2018, doi: 10.1109/LPT.2018.2866402.
[64] K. Aalimahmoodi, A. Gholami, and Z. Ghassemlooy, 'Impact of Camera Parameters on the OCC based Indoor Positioning System', *2019 2nd West Asian Colloquium on Optical Wireless Communications (WACOWC)*, pp. 96–99, 2019, doi: 10.1109/wacowc.2019.8770205.
[65] B. Lin, Q. Guo, C. Lin, X. Tang, Z. Zhou, and Z. Ghassemlooy, 'Experimental demonstration of an indoor positioning system based on artificial neural network', *Opt. Eng.*, vol. 58, no. 01, p. 1, Jan. 2019, doi: 10.1117/1.OE.58.1.016104.
[66] B. Zhang, M. Zhang, Z. Ghassemlooy, D. Han, and P. Yu, 'A Visible Light Positioning System with a Novel Positioning Algorithm and Two LEDs', in *2019 24th OptoElectronics and Communications Conference (OECC) and 2019 International Conference on Photonics in Switching and Computing (PSC)*, Fukuoka, Japan, Jul. 2019, pp. 1–3. doi: 10.23919/PS.2019.8818035.
[67] Y. Yang, C. Li, R. Bao, C. Guo, C. Feng, and J. Cheng, 'A Multi-Angle Camera Assisted Received Signal Strength Algorithm for Visible Light Positioning', *J. Lightwave Technol.*, pp. 1–1, 2021, doi: 10.1109/JLT.2021.3117408.
[68] C. Qin and X. Zhan, 'VLIP: Tightly coupled visible-light/inertial positioning system to cope with intermittent outage', *IEEE Photonics Technology Letters*, vol. 31, no. 2, pp. 129–132, 2015, doi: 10.1109/LPT.2018.2883345.
[69] W. Guan, L. Huang, B. Hussain, and C. Patrick Yue, 'Robust Robotic Localization using Visible Light Positioning and Inertial Fusion', *IEEE Sensors J.*, pp. 1–1, 2021, doi: 10.1109/JSEN.2021.3053342.
[70] Z. Li, L. Feng, and A. Yang, 'Fusion based on visible light positioning and inertial navigation using extended kalman filters', *Sensors (Switzerland)*, vol. 17, no. 5, 2017, doi: 10.3390/s17051093.
[71] Q. Wang *et al.*, 'Light positioning: A high-accuracy visible light indoor positioning system based on attitude identification and propagation model', *International Journal of Distributed Sensor Networks*, vol. 14, no. 2, 2018, doi: 10.1177/1550147718758263.
[72] C. F. O. R. Papers, 'Location-based information transmission systems using visible light communications', no. October 2012, pp. 433–434, 2015, doi: 10.1002/ett.
[73] Y.-L. Wei, C.-J. Huang, H.-M. Tsai, and K. C.-J. Lin, 'CELLI: Indoor Positioning Using Polarized Sweeping Light Beams', *ACM MobiSys*, pp. 136–147, 2017, doi: 10.1145/3081333.3081352.
[74] S. Kumar and R. M. Hegde, 'Multi-sensor data fusion methods for indoor localization under collinear ambiguity', *Pervasive and Mobile Computing*, vol. 30, pp. 18–31, 2016, doi: 10.1016/j.pmcj.2015.09.001.

[75] R. Zhang, W. De Zhong, D. Wu, and Q. Kemao, ‘A novel sensor fusion based indoor visible light positioning system’, *2016 IEEE Globecom Workshops, GC Wkshps 2016 - Proceedings*, pp. 0–5, 2016, doi: 10.1109/GLOCOMW.2016.7848823.
[76] M. Saadi, T. Ahmad, Y. Zhao, and L. Wuttisttikulkij, ‘An LED Based Indoor Localization System Using k-Means Clustering’, *2016 15th IEEE International Conference on Machine Learning and Applications (ICMLA)*, pp. 246–252, 2016, doi: 10.1109/ICMLA.2016.0048.
[77] Z. Zhang, H. Chen, X. Hong, and J. Chen, ‘Accuracy Enhancement of Indoor Visible Light Positioning using Point-Wise Reinforcement Learning’, *2019 Optical Fiber Communications Conference and Exhibition (OFC)*, vol. 2, no. 3, p. Th3I.3, 2019, doi: 10.1364/ofc.2019.th3i.3.
[78] H. Tran and C. Ha, ‘Improved Visible Light-Based Indoor Positioning System Using Machine Learning Classification and Regression’, *Applied Sciences*, vol. 9, no. 6, p. 1048, 2019, doi: 10.3390/app9061048.
[79] X. Wang and J. Shen, ‘Machine Learning and its Applications in Visible Light Communication Based Indoor Positioning’, in *2019 International Conference on High Performance Big Data and Intelligent Systems (HPBD&IS)*, Shenzhen, China, May 2019, pp. 274–277. doi: 10.1109/HPBDIS.2019.8735490.
[80] Y. Chen, W. Guan, J. Li, and H. Song, ‘Indoor Real-Time 3-D Visible Light Positioning System Using Fingerprinting and Extreme Learning Machine’, *IEEE Access*, vol. 8, pp. 13875–13886, 2020, doi: 10.1109/ACCESS.2019.2961939.
[81] H. Tran and C. Ha, ‘Improved Visible Light-Based Indoor Positioning System Using Machine Learning Classification and Regression’, *Applied Sciences*, vol. 9, no. 6, p. 1048, Mar. 2019, doi: 10.3390/app9061048.
[82] C.-W. Hsu, S. Liu, F. Lu, C.-W. Chow, C.-H. Yeh, and G.-K. Chang, ‘Accurate Indoor Visible Light Positioning System utilizing Machine Learning Technique with Height Tolerance’, in *Optical Fiber Communication Conference*, San Diego, California, 2018, p. M2K.2. doi: 10.1364/OFC.2018.M2K.2.
[83] H. H. Heqing Huang, A. Y. Aiying Yang, L. F. Lihui Feng, G. N. Guoqiang Ni, and and P. G. and Peng Guo, ‘Artificial neural-network-based visible light positioning algorithm with a diffuse optical channel’, *Chinese Optics Letters*, vol. 15, no. 5, pp. 050601–050605, 2017, doi: 10.3788/col201715.050601.
[84] C.-W. Hsu, S. Liu, F. Lu, C.-W. Chow, C.-H. Yeh, and G.-K. Chang, ‘Accurate Indoor Visible Light Positioning System utilizing Machine Learning Technique with Height Tolerance’, *2018 Optical Fiber Communications Conference and Exposition (OFC)*, vol. 1, no. c, p. M2K.2, 2018, doi: 10.1364/ofc.2018.m2k.2.
[85] H. Zhang *et al.*, ‘High-Precision Indoor Visible Light Positioning Using Deep Neural Network Based on the Bayesian Regularization With Sparse Training Point’, *IEEE Photonics J.*, vol. 11, no. 3, pp. 1–10, Jun. 2019, doi: 10.1109/JPHOT.2019.2912156.
[86] S. Zhang, P. Du, C. Chen, W.-D. Zhong, and A. Alphones, ‘Robust 3D Indoor VLP System Based on ANN Using Hybrid RSS/PDOA’, *IEEE Access*, vol. 7, pp. 47769–47780, 2019, doi: 10.1109/ACCESS.2019.2909761.
[87] A. Kendall, M. Grimes, and R. Cipolla, ‘PoseNet: A Convolutional Network for Real-Time 6-DOF Camera Relocalization’, in *2015 IEEE International Conference on Computer Vision (ICCV)*, Santiago, Chile, Dec. 2015, pp. 2938–2946. doi: 10.1109/ICCV.2015.336.
[88] M. A. Arfaoui *et al.*, ‘Invoking Deep Learning for Joint Estimation of Indoor LiFi User Position and Orientation’, p. 17, 2020.
[89] S. M. Sheikholeslami, F. Fazel, J. Abouei, and K. N. Plataniotis, ‘Sub-Decimeter VLC 3D Indoor Localization With Handover Probability Analysis’, *IEEE Access*, vol. 9, pp. 122236–122253, 2021, doi: 10.1109/ACCESS.2021.3108173.
[90] G. Pau, M. Collotta, V. Maniscalco, and K. K. R. Choo, ‘A fuzzy-PSO system for indoor localization based on visible light communications’, *Soft Computing*, pp. 1–11, 2018, doi: 10.1007/s00500-018-3212-z.
[91] B. Zhou, A. Liu, and V. Lau, ‘Robust Visible Light-Based Positioning under Unknown User Device Orientation Angle’, *2018, 12th International Conference on Signal Processing and Communication Systems, ICSPCS 2018 - Proceedings*, no. October, 2019, doi: 10.1109/ICSPCS.2018.8631727.

[92] B. Zhou, V. Lau, Q. Chen, and Y. Cao, 'Simultaneous Positioning and Orientating for Visible Light Communications: Algorithm Design and Performance Analysis', *IEEE Transactions on Vehicular Technology*, vol. 67, no. 12, pp. 11790–11804, 2018, doi: 10.1109/TVT.2018.2875044.
[93] E. Kazikli and S. Gezici, 'Hybrid TDOA/RSS based localization for visible light systems', *Digital Signal Processing: A Review Journal*, vol. 86, pp. 19–28, 2019, doi: 10.1016/j.dsp.2018.12.001.
[94] Q. Peng, W. Guan, Y. Wu, Y. Cai, C. Xie, and P. Wang, 'Three-dimensional high-precision indoor positioning strategy using Tabu search based on visible light communication', *Optical Engineering*, vol. 57, no. 01, p. 1, 2018, doi: 10.1117/1.oe.57.1.016101.
[95] B. Chen, J. Jiang, W. Guan, S. Wen, J. Li, and Y. Chen, 'Performance comparison and analysis on different optimization models for high-precision three-dimensional visible light positioning', *Optical Engineering*, vol. 57, no. 12, p. 1, 2018, doi: 10.1117/1.oe.57.12.125101.
[96] M. Vieira, M. A. Vieira, P. Louro, P. Vieira, and A. Fantoni, 'Fine-grained indoor localization: optical sensing and detection', no. May 2018, p. 18, 2018, doi: 10.1117/12.2306497.
[97] M. Vieira, M. A. Vieira, P. Louro, A. Fantoni, and P. Vieira, 'Visible light communication technology for fine-grained indoor localization', no. May, p. 9, 2018, doi: 10.1117/12.2287462.
[98] M. Vieira, M. A. Vieira, P. Louro, and P. Vieira, 'Light-emitting diodes aided indoor localization using visible light communication technology', *Optical Engineering*, vol. 57, no. 08, p. 1, 2018, doi: 10.1117/1.oe.57.8.087105.
[99] S. W. Ho, A. A. Saed, L. Lai, and C. W. Sung, 'Coding and Bounds for Channel Estimation in Visible Light Communications and Positioning', *IEEE Journal on Selected Areas in Communications*, vol. 36, no. 1, pp. 34–44, 2018, doi: 10.1109/JSAC.2017.2774718.
[100] Z. Ghassemlooy, W. Popoola, and S. Rajbhandari, *Optical wireless communications: system and channel modelling with MATLAB*. Boca Raton, Fla.: CRC Press, 2013.
[101] Z. Ghassemlooy, L. N. Alves, S. Zvanovec, and M.-A. Khalighi, *Visible Light Communications: Theory and Applications*. CRC Press, 2017. doi: 10.1201/9781315367330-3.
[102] P. H. Pathak, X. Feng, P. Hu, and P. Mohapatra, 'Visible Light Communication, Networking, and Sensing: A Survey, Potential and Challenges', *IEEE Commun. Surv. Tutorials*, vol. 17, no. 4, pp. 2047–2077, 2015, doi: 10.1109/COMST.2015.2476474.
[103] M. Ayyash *et al.*, 'Coexistence of WiFi and LiFi toward 5G: concepts, opportunities, and challenges', *IEEE Commun. Mag.*, vol. 54, no. 2, pp. 64–71, Feb. 2016, doi: 10.1109/MCOM.2016.7402263.
[104] H. Elgala, R. Mesleh, and H. Haas, 'Indoor optical wireless communication: potential and state-of-the-art', *IEEE Commun. Mag.*, vol. 49, no. 9, pp. 56–62, Sep. 2011, doi: 10.1109/MCOM.2011.6011734.
[105] M. Figueiredo, L. N. Alves, and C. Ribeiro, 'Lighting the Wireless World: The Promise and Challenges of Visible Light Communication', *IEEE Consumer Electron. Mag.*, vol. 6, no. 4, pp. 28–37, Oct. 2017, doi: 10.1109/MCE.2017.2714721.
[106] T. Komine and M. Nakagawa, 'Fundamental analysis for visible-light communication system using LED lights', *IEEE Trans. Consumer Electron.*, vol. 50, no. 1, pp. 100–107, Feb. 2004, doi: 10.1109/TCE.2004.1277847.
[107] N. Chaudhary, L. N. Alves, and Z. Ghassemblooy, 'Feasibility Study of Reverse Trilateration Strategy with a Single Tx for VLP', *2019 2nd West Asian Colloquium on Optical Wireless Communications (WACOWC)*, pp. 121–126, 2019, doi: 10.1109/wacowc.2019.8770213.
[108] N. Chaudhary, L. N. Alves, and Z. Ghassemlooy, 'Impact of Transmitter Positioning and Orientation Uncertainty on RSS-Based Visible Light Positioning Accuracy', *Sensors*, vol. 21, no. 9, p. 3044, Apr. 2021, doi: 10.3390/s21093044.
[109] Z. Ghassemlooy, W. Popoola, and S.Rajbhandari, *Optical Wireless Communications System and Channel Modelling with MATLAB®, Second Edition*. CRC Press, 2019. doi: 10.1201/9781315151724.
[110] Md. Shahjalal, Md. T. Hossan, Moh. K. Hasan, M. Z. Chowdhury, N. T. Le, and Y. M. Jang, 'An Implementation Approach and Performance Analysis of Image Sensor Based Multilateral Indoor Localization and Navigation System', *Wireless Communications and Mobile Computing*, vol. 2018, pp. 1–13, Oct. 2018, doi: 10.1155/2018/7680780.

[111] J. Gu, Y. Hitomi, T. Mitsunaga, and S. Nayar, 'Coded rolling shutter photography: Flexible space-time sampling', in *2010 IEEE International Conference on Computational Photography (ICCP)*, Cambridge, MA, USA, Mar. 2010, pp. 1–8. doi: 10.1109/ICCPHOT.2010.5585094.
[112] T. Nguyen, A. Islam, T. Hossan, and Y. M. Jang, 'Current Status and Performance Analysis of Optical Camera Communication Technologies for 5G Networks', *IEEE Access*, vol. 5, pp. 4574–4594, 2017, doi: 10.1109/ACCESS.2017.2681110.
[113] N. T. Le, M. S. Ifthekhar, Y. M. Jang, and N. Saha, 'Survey on optical camera communications: challenges and opportunities', *IET Optoelectronics*, vol. 9, no. 5, pp. 172–183, Oct. 2015, doi: 10.1049/iet-opt.2014.0151.
[114] N.-T. Le, 'Invisible watermarking optical camera communication and compatibility issues of IEEE 802.15.7r1 specification', *Optics Communications*, vol. 390, pp. 144–155, May 2017, doi: 10.1016/j.optcom.2016.12.073.
[115] Y. Goto *et al.*, 'A New Automotive VLC System Using Optical Communication Image Sensor', *IEEE Photonics J.*, vol. 8, no. 3, pp. 1–17, Jun. 2016, doi: 10.1109/JPHOT.2016.2555582.
[116] Z. Mei, N. Chen, and L. Yao, 'Analysis of pixel circuits in CMOS image sensors', China, China, Apr. 2015, p. 952226. doi: 10.1117/12.2180432.
[117] P. Luo, T. Jiang, P. A. Haigh, Z. Ghassemlooy, and S. Zvanovec, 'Undersampled Pulse Width Modulation for Optical Camera Communications', in *2018 IEEE International Conference on Communications Workshops (ICC Workshops)*, Kansas City, MO, USA, May 2018, pp. 1–6. doi: 10.1109/ICCW.2018.8403732.
[118] M. Afzalan and F. Jazizadeh, 'Indoor Positioning Based on Visible Light Communication: A Performance-based Survey of Real-world Prototypes', *ACM Comput. Surv.*, vol. 52, no. 2, pp. 1–36, May 2019, doi: 10.1145/3299769.
[119] J. Beysens, Q. Wang, A. Galisteo, D. Giustiniano, and S. Pollin, 'A Cell-Free Networking System With Visible Light', *IEEE/ACM Trans. Networking*, vol. 28, no. 2, pp. 461–476, Apr. 2020, doi: 10.1109/TNET.2020.2966322.
[120] 'Opencv: Camera calibration and 3d Reconstruction.' [Online]. Available: https://docs.opencv.org/3.4/d9/d0c/group__calib3d.html#ga549c2075fac14829ff4a58bc931c033d
[121] 'Camera Calibration and 3d Reconstruction — OpenCV 2.4.13.7 documentation'. [Online]. Available: https://docs.opencv.org/2.4/modules/calib3d/doc/camera_calibration_and_3d_reconstruction.html
[122] W. Gu, M. Aminikashani, P. Deng, and M. Kavehrad, 'Impact of Multipath Reflections on the Performance of Indoor Visible Light Positioning Systems', *Journal of Lightwave Technology*, vol. 34, no. 10, pp. 2578–2587, 2016, doi: 10.1109/JLT.2016.2541659.
[123] W. Shiquan and W. Fang, 'Computation of a trust region step', *Acta Mathematicae Applicatae Sinica*, no. 7, pp. 354–362, Oct. 1991, doi: 10.1007/BF02009686.
[124] Chamasemani and Singh - 2011 - Multi-class Support Vector Machine (SVM) Classifier.pdf.
[125] M. T. Hagan, H. B. Demuth, and and M. Beale, *Neural network design*. USA: PWS Publishing Co., 1997.
[126] C. Nwankpa, W. Ijomah, A. Gachagan, and S. Marshall, 'Activation Functions: Comparison of trends in Practice and Research for Deep Learning', *arXiv:1811.03378 [cs]*, Nov. 2018, Accessed: Sep. 21, 2021. [Online]. Available: http://arxiv.org/abs/1811.03378
[127] N. Chaudhary, O. I. Younus, L. N. Alves, Z. Ghassemlooy, S. Zvanovec, and H. Le-Minh, 'An Indoor Visible Light Positioning System Using Tilted LEDs with High Accuracy', *Sensors*, vol. 21, no. 3, p. 920, Jan. 2021, doi: 10.3390/s21030920.
[128] G. Lera and M. Pinzolas, 'Neighborhood based Levenberg-Marquardt algorithm for neural network training', *IEEE Transactions on Neural Networks*, vol. 13, no. 5, pp. 1200–1203, 2002, doi: 10.1109/TNN.2002.1031951.
[129] M. F. Møller, 'A scaled conjugate gradient algorithm for fast supervised learning', *Neural Networks*, vol. 6, no. 4, pp. 525–533, 1993, doi: 10.1016/S0893-6080(05)80056-5.
[130] W. Liu *et al.*, 'SSD: Single Shot MultiBox Detector', *arXiv:1512.02325 [cs]*, vol. 9905, pp. 21–37, 2016, doi: 10.1007/978-3-319-46448-0_2.

[131] M. Sandler, A. Howard, M. Zhu, A. Zhmoginov, and L.-C. Chen, 'MobileNetV2: Inverted Residuals and Linear Bottlenecks', *arXiv:1801.04381 [cs]*, Mar. 2019, Accessed: Jan. 03, 2022. [Online]. Available: http://arxiv.org/abs/1801.04381

[132] R. Maisano, V. Tomaselli, A. Capra, F. Longo, and A. Puliafito, 'Reducing Complexity of 3D Indoor Object Detection', in *2018 IEEE 4th International Forum on Research and Technology for Society and Industry (RTSI)*, Palermo, Sep. 2018, pp. 1–6. doi: 10.1109/RTSI.2018.8548514.

[133] J. Redmon, S. Divvala, R. Girshick, and A. Farhadi, 'You Only Look Once: Unified, Real-Time Object Detection', in *2016 IEEE Conference on Computer Vision and Pattern Recognition (CVPR)*, Las Vegas, NV, USA, Jun. 2016, pp. 779–788. doi: 10.1109/CVPR.2016.91.

[134] S. Ren, K. He, R. Girshick, and J. Sun, 'Faster R-CNN: Towards Real-Time Object Detection with Region Proposal Networks', *arXiv:1506.01497 [cs]*, Jan. 2016, Accessed: Jan. 03, 2022. [Online]. Available: http://arxiv.org/abs/1506.01497

[135] D. Erhan, C. Szegedy, A. Toshev, and D. Anguelov, 'Scalable Object Detection Using Deep Neural Networks', in *2014 IEEE Conference on Computer Vision and Pattern Recognition*, Columbus, OH, USA, Jun. 2014, pp. 2155–2162. doi: 10.1109/CVPR.2014.276.

[136] R. Girshick, 'Fast R-CNN', *arXiv:1504.08083 [cs]*, Sep. 2015, Accessed: Jan. 03, 2022. [Online]. Available: http://arxiv.org/abs/1504.08083

[137] W. Liu *et al.*, 'SSD: Single Shot MultiBox Detector', *arXiv:1512.02325 [cs]*, vol. 9905, pp. 21–37, 2016, doi: 10.1007/978-3-319-46448-0_2.

[138] K. He, X. Zhang, S. Ren, and J. Sun, 'Deep Residual Learning for Image Recognition', *arXiv:1512.03385 [cs]*, Dec. 2015, Accessed: Jan. 03, 2022. [Online]. Available: http://arxiv.org/abs/1512.03385